Mechanical Characterisation of Novel Polyethylene-based Nanocomposites

by

Abdulaziz Alghamdi

Thesis submitted to the University of Nottingham for the degree of Doctor of Philosophy

July 2014

Dedicated to my parents, my wife and my children

Abstract

Polymer-based nanocomposites are of significant current research interest owing to their outstanding mechanical properties, light weight, processability and low cost. They are also increasingly being considered for a range of industrial applications, including packaging, fuel tanks, gas barriers and high performance films. Ultra-high molecular weight polyethylene (UHMWPE) is already used in various applications, such as lightweight body armour because of its high impact resistance with light weight and total joint replacement due to its high wear resistance. However, a broader use of UHMWPE is limited by the complexity and cost of the manufacturing process, which can be attributed to its high viscosity at processing temperatures. The processability of UHMWPE can be improved by blending with a compatible, lower molecular weight polymer, however, this inevitably results in a reduction in some of the useful properties, such as impact resistance. In this work the potential of adding nano-fillers to such blends to create a range of nanocomposite polymers with the advantages of easy processability and enhanced properties is investigated.

The overall aim of this research was to investigate the effect of processing method, strain rate, nanoparticle type and content on the morphological, thermal and mechanical properties of a family of novel polyethylene-based nanocomposites. Polymer nanocomposites of blended UHMWPE and high density polyethylene (HDPE) reinforced with carbon black (CB), carbon nanotubes (CNTs) or inorganic clay were prepared using conventional processing techniques. After initial experiments into the effects of processing parameters, two sets of processing parameters were selected that gave different blend morphology in order to investigate the effect of this on the blend properties and nanofiller dispersion. Characterization of the pure, blended and nanocomposite materials was achieved by the application of combination of experimental techniques. Tensile testing was carried out to characterise the effect of processing method, strain rate, ambient temperature, nanoparticle type and content on the stress-strain behaviour and also to study heat generation during plastic deformation at high strain rates. Depth sensing indentation (DSI) tests were carried out to characterise the effect of

processing method, ambient temperature, nanoparticle type and content on the near-surface properties of the materials at a micro-scale under a more complex state of stress that more closely approximates that seen in impact applications. The creep behaviour of the materials was investigated at macro and micro scales at various ambient temperatures. This is important as a weakness of UHMWPE is poor creep resistance and it would be extremely useful if blending or the addition of nanofillers could improve this. A phenomenological model was used to analyse the creep data as this can be usefully used to predict creep performance in service and to aid understanding of the creep phenomena in these materials.

The results included in this work are summarised below. Firstly, it was seen that processing parameters had a significant effect on the morphology of the blends, which in turn affected the blend properties and the dispersion of nanoparticles in the blend. Secondly, it was seen that heat generation during plastic deformation of the polyethylene blends and nanocomposites was significantly dependent on morphology, strain rate, nanoparticle type and content. Furthermore, this temperature increase strongly affected the material properties at high strain rates, which is an important consideration if these materials are to be used in high strain rate applications, e.g. as replacement for UHMWPE in helmets and body armour. Thirdly, the macro and micro viscoelastic behaviour of the materials was strongly dependent on the morphology, nanoparticle type and content. A significant increase in creep resistance compared with UHMWPE could be engineered by a careful selection of blend and nanoparticle type and weight fraction.

It can be seen, therefore, that a new class of cheap and easy processable polymer nanocomposites have been characterised that can give a range of property sets dependent on the blend processing and nanofiller type and weight fraction. Although certain compromises in property sets are unavoidable, e.g. it is difficult to engineer maximum creep and impact resistance in the same material, this ability to tailor properties could potentially increase the range of applications for these materials and enable better product design.

Publications

1. C. V. GORWADE, **A. S. ALGHAMDI**, I. A. ASHCROFT, V. V. SILBERSCHMIDT, M. SONG, **(2012)**. Finite element analysis of the high strain rate testing of polymeric materials. *Journal of Physics*, 382, pp. 012043, doi:10.1088/1742-6596/382/1/012043.

2. **A. S. ALGHAMDI**, I. A. ASHCROFT and M. SONG, **(2013)** Mechanical characterisation of novel polyethylene nanocomposites by nanoindentation *In:* 6th International Conference on Computational Methods and Experiments in Materials Characterisation, Siena, Italy, 4-6 June 2013, WIT Press, ISSN: 1743-3533, doi:10.2495/MC130081.

3. **A. S. ALGHAMDI**, I. A. ASHCROFT, M. SONG and D. CAI, **(2013)**. Morphology and Strain Rate Effects on Heat Generation during the Plastic Deformation of Polyethylene/carbon black Nanocomposites*, Polymer Testing*, 32 (6), pp. 1105-1113.

4. I. A. ASHCROFT, C. V. GORWADE, **A.S. ALGHAMDI**, V. V. SILBERSCHMIDT, M. SONG, **(2013)**. Thermo-Mechanical Investigation of Ultra-High Molecular Weight Polyethylene for High Strain-Rate Applications, *Key Engineering Materials*, 577, pp. 493-496.

5. **A.S. ALGHAMDI**, I. A. ASHCROFT, M. SONG and D. CAI, **(2013)**. Nanoparticle Type Effects on Heat Generation during the Plastic Deformation of Polyethylene Nanocomposites, *Polymer Testing*, 32, pp. 1502-1510.

6. **A.S. ALGHAMDI**, I. A. ASHCROFT and M. SONG, **(2014)**. Creep resistance of novel polyethylene/carbon black nanocomposites, International Journal of Materials Science and Engineering, 2 (1), pp. 1-5.

7. **A.S. ALGHAMDI**, I. A. ASHCROFT and M. SONG, **(2014)**. Nanoindentation behaviour of polyethylene nanocomposites at high temperature, Computational Methods and Experimental Measurements (CMEM), In press.

8. **A.S. ALGHAMDI**, I. A. ASHCROFT and M. SONG, **(2014)**. Creep resistance of polyethylene nanocomposites, Drafting in progress.

Acknowledgement

I'd like to thank my supervisors Prof. Ian A. Ashcroft and Prof. Mo Song from Materials Department, Loughborough University for their supervision, recommendations and encouragement throughout this research; in particular, Prof. Ian A Ashcroft for his support and guidance over the last three years. His constructive criticism, invaluable scientific input and patience helped me go through hard times in this study.

Special thanks must go to Dr. Dongyu Cai who supplied most the raw materials and who helped me during materials processing.

I'd like to extend my gratitude to Mr. Andy Sandaver from Wolfson School in Loughborough University for his assistance, support and patience through the experimental work I've done during the first two years of my research at Loughborough University.

Obviously, I'd like to thank my family for all the support and encouragement I've had throughout my study.

Contents

List of Figures

List of Tables

Symbols

n	Degree of Polymerisation
F	Force
σ	Stress
ε	Strain
σ_E	Engineering Stress
ε_E	Engineering Strain
σ_T	True Stress
ε_T	True Strain
A_0	Original Cross-Sectional Area
L_0	Original Length
S	Stiffness
E	Elastic Modulus
T_g	Glass Transition Temperature
$\dot{\varepsilon}$	Strain Rate
δL	Change in the Length
$\dot{\varepsilon_s}$	Steady State Creep Rate
$\dot{\varepsilon_B}$	Creep Rate of Burger's Viscoelastic Model
T	Temperature
P	Load
P_m	Mean Pressure
$F(t)$	Instantaneous Load
$A(t)$	Instantaneous Cross-Sectional Area
A	Power Law Constant
m	Curve Fitting Constant
α	Curve Fitting Constant
k	Dimensionless Constant to Calculate the Indentation Creep Strain Rate
ϵ	Constant Related to Geometry of Indenter
η	Viscous Parameter
E_M	Elastic Modulus of Maxwell Spring
η_M	Viscosity of Maxwell Dashpot
E_K	Elastic Modulus of Kelvin Spring
η_K	Viscosity of Kelvin Dashpot
τ	Retardation Time
h_{max}	Indentation Depth at Maximum Load
h_f	Final Indentation Depth after Unloading
h_c	Indentation Contact Depth

h_p	Indentation Plastic Depth
h_i	Indentation Initial Penetration Depth
Δh	Change of depth during the dwell period
P_i	Indentation Initial Contact Load
A_c	Indentation Contact Area
$\dot{\varepsilon}_1$	Indentation Creep Strain Rate
H	Indentation Hardness
E_r	Reduced Modulus
E_s	Elastic Modulus of Sample from Indentation Test
E_i	Elastic Modulus of Indenter
ν	Poisson’s Ratio

Acronyms

PE	Polyethylene
UHMWPE	Ultra-High Molecular Weight Polyethylene
HDPE	High Density Polyethylene
LDPE	Low Density Polyethylene
LLDPE	Linear Low Density Polyethylene
LMWPE	Low Molecular Weight Polyethylene
PET	Polyethylene Terephthalate
MAE	Quaternary Tallow Ammonium Chloride
U75H25	75 wt. % UHMWPE-25 wt. % HDPE Blend
M1	Processing Method Number One
M2	Processing Method Number Two
CNTs	Carbon Nanotubes
CB	Carbon Black
SWNTs	Single-Walled Nanotubes
MWNTs	Multi-Walled Nanotubes
CNFs	Carbon Nanofibres
SiO_2	Silicon Dioxide
TiO_2	Titanium Dioxide
B-TCP	Tricalcium Phosphate
DSI	Depth Sensing Indentation
SEM	Scanning Electron Microscope
TEM	Transmission Electron Microscope
AFM	Atomic Force Microscope
XRD	X-Ray Diffraction
DSC	Differential Scanning Calorimetry
TGA	Thermogravimetric Analysis
DMA	Dynamic Mechanical Analysis
DMTA	Dynamic Mechanical Thermal Analysis
SANS	Small-Angle Neutron Scattering

WAXD	Wide Angle X-ray Diffraction
CVD	Chemical Vapour Deposition
DAF	Diamond Area Function
1D	One Dimensional
2D	Two Dimensional
3D	Three Dimensional

Chapter 1
Introduction

1.1 Background

Polymer-based nanocomposites of current academic interest and are finding an increasing range of industrial applications, making them the most widely commercialised class of nanocomposites (Bogue 2011). These materials have at least one phase with at least one dimension of less than 100 nm. The transition from microparticles to nanoparticles can lead to a dramatic change in the physical properties owing to the large surface area to volume ratio. These changes can potentially affect chemical and physical interactions (Hussain et al. 2006). The incorporation of a low volume fraction of nanoparticles can lead to a significant improvement in polymer properties, such as tensile strength, elastic modulus, wear and scratch resistance, electrical and thermal conductivity, thermal and flammability resistance and impact strength (Alexandre et al. 2002; Ray and Okamoto 2003; Yusoh et al. 2010; Wang et al. 2010). In addition, many polymer nanocomposites can be fabricated and processed using methods similar to those used for standard polymers, which is important from an economic manufacturing point of view. In many cases a significant reduction in cost can be obtained by enhancing the properties of a cheap polymer using inexpensive nanofiller to match the properties of a more expensive polymer (Alexandre and Dubois 2000). For example, 1Kg of carbon black (CB) or clay cost only 1.8 and 6 British Pound, respectively (Cabot Corporation 2007; Elementis Specialties Inc. 2010).

In recent years, researchers have focussed on the synthesis of new nanocomposites, starting from careful materials selection and process control by either the direct use of an existing technique or by modified and adapted techniques. Various types of nanofillers have been used in polymer-based nanocomposite fabrication, such as; exfoliated clay, modified carbon nanotubes and graphene (Paul and Robeson 2008; Rahmat and Hubert 2011; Shokrieh et al 2013).

However, achieving the uniform dispersion of the nanoparticles is still an important scientific and technological challenge in nanocomposite fabrication. The filler-filler and filler-matrix interactions are also important factors affecting the material properties. These factors are highly dependent on the processing method, the polymer matrix and the nanofiller type and content.

Ultra-high molecular weight polyethylene (UHMWPE) is a high performance thermoplastic with outstanding mechanical properties, such as high wear resistance (wear rate of 400 $mm^3/10^6$ cycles), chemical resistance (>95% residual strength after 100h in acids), yield strength (39-48 MPa) and high impact strength (>1076 J/m of notch), which provide not only practical benefits but are also scientific interest (Kelly 2002; Lucas et al. 2011; Lim et al. 2005). UHMWPE is used in personal armour protection, commercially known as Dyneema or Spectra, and joint replacements (Xu and Tangpong 2013). However, its extremely high molecular weight, and subsequent high viscosity, raises difficulties in processing using standard techniques, such as twin screw extrusion and injection moulding (Sui et al. 2009; Lucas et al. 2011). Reducing the viscosity of UHMWPE is an effective method of avoiding these processing difficulties. Blending UHMWPE with other polymers that have lower viscosity, such as high density polyethylene (HDPE), can therefore be used to improve processability. Compared with UHMWPE, HDPE has a similar chemical structure but with lower molecular weight (0.05-0.25 $\times10^6$g/mole), relatively low cost, better creep resistance and good processability, however, it exhibits lower wear resistance (wear rate of 100 $mm^3/10^6$ cycles), yield strength (22-31 MPa) and impact strength (21-214 J/m of notch) than UHMWPE (Kelly 2002; Fouad and Elleithy 2011). This reduction in performance on adding HDPE to UHMWPE can potentially be mitigated, whilst retaining the improved processability, by the addition of nano-reinforcement, which has been shown to improve the mechanical performance of polyethylene (Tang et al. 2003; Zoo et al. 2004; Xue et al. 2006; Kontou and Niaounakis 2006; Kanagaraj et al. 2007; Sui et al. 2009; Stoeffler et al. 2011; Chen et al. 2012; Ren et al. 2012; Zhenhua and Yunxuan 2012; Khasraghi and Rezaei 2013).

In the polymer matrix, the nanoparticle structure can be classified as one-dimensional (1D, eg. nanotubes), two dimensional (2D, eg. nanoclay platelet) or three-dimensional (3D, eg, carbon black nanoparticle) (Schmidt et al. 2002). Various studies have been carried out to investigate the effect of such nanoparticle structure, content, dispersion, interfacial strength, strain rate and processing method on the mechanical performance of polyethylene nanocomposites for various applications (Tang et al. 2003; Zoo et al. 2004; Xue et al. 2006; Kontou and Niaounakis 2006; Kanagaraj et al. 2007; Sui et al. 2009; Stoeffler et al. 2011; Chen et al. 2012; Ren et al. 2012; Zhenhua and Yunxuan 2012; Khasraghi and Rezaei 2013; Jouni et al. 2013). Additionally, in applications that involve plastic deformation and high strain rates, such as impact, nanoparticle geometry may potentially affect internal heat generation, and consequently the mechanical properties of the materials. It is known that plastic work at high strain rates can be transformed partly into heat, which can lead to a significant temperature increase. Therefore, the behaviour of many materials can be affected by thermal softening when testing at high strain rates (Koenen 1992; Mason et al. 1994; Rittel 1999; McNally et al. 2003; Longère and Dragon 2008; Kuriyagawa and Nitta 2011; Shen et al. 2011). In a uniaxial tension test, heterogeneous deformation in the necking region can result in the localised generation of heat (Kuriyagawa and Nitta 2011). The necking mechanism in polymers is extremely complicated and the existence of nanofiller reinforcement increases this complexity. The effect of heat generation on the polymer properties can be influenced by several factors, such as the polymer matrix (glassy or rubbery), molecular weight, interfacial strength for filled polymer, filler type or shape and strain rate. Conflicting results have been reported on the dependence of heat generation on strain rate in glassy polymer nanocomposites. McNally et al. (2003) investigated heat generation during the uniaxial tensile testing of polyamide-12 and a polyamide-12/MAE synthetic clay nanocomposite. They found that the measured temperature was independent of strain rate in the range tested (50-200 mm/min crosshead speed) but highly dependent on the presence of the nanofiller. The presence of a synthetic clay in the polymer was seen to increase the temperature at failure and elongation at break by 47°C and 500% respectively. It was proposed that this was because the temperature increased above the glass transition temperature (T_g) in the polyamide-12/MAE (30°C), hence, changing the behaviour from glassy polymer to elastomeric. Shen et al. (2011), however, found that strain rate had some influence on the strain hardening behaviour of a PET (polyethylene terephthalate)-clay nanocomposite, which is a glassy polymer with T_g around 70°C. This was attributed to a possible increase in temperature at higher strain rates. The dependence of heat generation on strain rate, however, has not been investigated to date for rubbery (over T_g values) polymer nanocomposites. This could potentially provide clear relationships between heat generation, strain rate and nanofiller due to the large strains to failure in these materials.

In the present work, the effects of material morphology, nanofiller content, dispersion and the strain rate on temperature changes during the tensile testing of polyethylene-based nanocomposites were investigated. This is important when evaluating the use of such materials in applications involving high strain rates, such as impact protection equipment. Moreover, to date, no work has been reported on the effect of nanoparticle structure on the heat generation during plastic deformation of polyethylene nanocomposites and the effect of this heat generation on the mechanical properties. Therefore, three different types of nanoparticle (carbon nanotube, carbon black and inorganic clay platelet) were embedded separately into a UHMWPE/HDPE blend to form nanocomposites using in-house processing methods. The effect of nanoparticle structure on the heat generation during plastic deformation was then investigated using a high sensitivity thermal camera simultaneously with tensile tests, with the spatial and temporal temperature variations recorded along with the stress-strain behaviour. It is also important to evaluate the properties of these materials at high temperatures for use in a particular environment. Moreover, the combination of the temperature increase during deformation and environment may adversely change the mechanical properties of the materials. The correlation between morphology, volume fraction of nanofiller and the creep resistance are also investigated. The creep response was analysed using a standard viscoelastic model, Burger's model.

Depth sensing indentation (DSI) or nanoindentation is an advanced experimental technique, which is capable of providing valuable information about the spatially resolved properties of solid polymers, such as indentation elastic modulus, indentation hardness and viscoelastic and viscoplastic behaviour (Fischer-Cripps 2002). Recently, this technique has become increasingly popular in the investigation of the micro-scale properties of polymer nanocomposites and their correlation to the nanoparticle loading (Aldousiri et al. 2011; Yusoh et al. 2010; Wang et al. 2010; Sreekanth and Kanagaraj 2013). However, the nanoindentation technique to date has been limited to investigating the properties of polymers at room temperature, whereas the properties of many engineering polymers are significantly affected by temperature within their service range. Recent developments in nanoindentation instruments have increased their capability to perform nanomechanical testing at elevated temperatures. Therefore, for better understanding of the spatially resolved properties of polymers in various environments and temperatures ranges and to meet environmental and commercial concerns, some researchers have used the nanoindentation technique at high temperature to perform a reliable measurement of the temperature-dependent properties (Seltzer et al. 2011; Fulcher et al. 2010; Lu et al. 2010). It is important to investigate the temperature-dependent properties of materials at their service temperature to avoid unexpected behaviour or failure. To date, no work has been carried out to investigate the spatially resolved properties of polyethylene-based nanocomposites at elevated temperatures. Therefore, in this work, the dependence of the spatially resolved properties of polyethylene-based nanocomposites on temperature was investigated. Properties investigated include the indentation hardness, elastic modulus and creep behaviour. The correlation between the indentation properties of polyethylene-based nanocomposites and nanoparticle loading at various temperatures was also evaluated. In addition, the dispersion of carbon nanotube

(CNT), carbon black (CB) and inorganic nanoclay in the UHMWPE/HDPE blend manufactured using two different mixing methods was evaluated by DSI.

1.2 Aim and Objectives

The main aim of this research is to characterise the mechanical properties of novel polyethylene-based nanocomposites that may be used to replace an existing material (UHMWPE) with similar or better properties at a low cost and improved processability. This aim will be achieved through the following major objectives:

- To develop a processing method that can be used to improve the miscibility of the blended materials and the dispersion of nanoparticles.
- To understand the effects of processing method parameters on the morphology, crystallinity, nanofiller dispersion and mechanical properties of polyethylene-based nanocomposites.
- To investigate the effects of processing method, nanoparticle addition and strain rate on heat generation during the plastic deformation of polyethylene-based nanocomposites, and consequently the effect of the increased temperature on the mechanical properties.
- To study the effects of nanoparticle type and geometry on heat generation during the plastic deformation of polyethylene-based nanocomposites, and consequently the effect of the increased temperature on the mechanical properties.
- To investigate the effects of ambient temperature increase on the stress-strain and viscoelastic behaviour of polyethylene-based nanocomposites.
- To analyse the effect of processing method and nanoparticle addition on the viscoelastic behaviour of UHMWPE/HDPE blend and polyethylene-based nanocomposites.
- To characterise the effect of ambient temperature increase on the micro-scale properties of polyethylene-based nanocomposites.

- To evaluate the processing method and the distribution of nanoparticles in the polymer matrix using the DSI technique.

1.3 Research Methodology

The work contained within this thesis details the experimental mechanical characterisation of a number of in-house processed polyethylene-based nanocomposite materials. The methodology can be represented by five main steps, as follows:

- Material processing and preparation
- Microstructural and morphological characterisation
- Macro-scale mechanical characterisation
- Depth sensing indentation investigations
- Thermal analysis

Material processing and preparation: The polyethylene powders were mixed with pre-treated CNT, CB or clay nanoparticles for better dispersion. The mixed materials were then blended in a twin-screw extruder using two different processing methods to produce nanocomposite pellets. The pellets were melted under specific temperature and pressure conditions to form a compression moulded plaque. The plaque was solidified under pressure using water cooling. Finally, the specimens were cut from the plaque into appropriate geometries for various tests.

Microstructural and morphological characterisation: In order to evaluate the processing method and nanofiller loading effects on the microstructure of the polymer-based nanocomposites before and after deformation, the specimens were investigated using standard techniques such as scanning electron microscopy (SEM), transmission electron microscopy (TEM), atomic force microscopy (AFM) and X-ray diffraction (XRD). The main key factors in this step were the dispersion of nanoparticles after processing and the formation of micro-cracks after deformation. The fracture surfaces were also investigated to evaluate filler-matrix interaction and crack formation.

Macro-scale mechanical characterisation: In some applications that involve plastic deformation and high strain rate, processing parameters and nanofiller can potentially affect internal heat generation, and consequently the material properties. Therefore, the effects of processing method, nanoparticle volume fraction and type and strain rate on the heat generation during plastic deformation were investigated using a high sensitivity thermal camera applied simultaneously with a tensile test. In addition, the effects of processing method and nanoparticle volume fraction and type on the viscoelastic behaviour of the polyethylene-based nanocomposites were investigated.

Depth sensing indentation investigations: DSI tests were carried out to investigate the effects of processing method, nanoparticle addition and ambient temperature on the micro-scale mechanical properties of the polymer-based nanocomposites. These include indentation hardness, indentation elastic modulus and creep behaviour. The DSI technique was also used to evaluate the distribution of the nanoparticles in the polymer matrix, which can enhance the microstructure analysis presented in the second step.

Thermal analysis: DSC, TGA and infrared thermography were used to investigate the effect of processing and nanoparticle addition on the material crystallinity, degradation temperature and internal heat generation in the material, respectively. The results were used to describe the correlation between thermal and mechanical properties of polyethylene-based nanocomposites. In addition, the effect of ambient temperature on the mechanical properties of the material was studied and the critical softening temperature was determined.

1.4 Thesis Organisation

The thesis contains nine further chapters. A brief description of each chapter is given here.

Chapter 2 contains a review of the literature concerning polymer-based nanocomposites and their mechanical properties and deformation mechanisms.

The chapter is divided into eight parts. It starts with information about polymers and their classification and structure. Then, the difference between composites and blends is discussed followed by a description of polymer nanocomposites and their processing and characterisation techniques. The next part discusses the polyethylene types, blends, nanocomposites and some nanoparticles that can be used with polyethylene. The next part discusses the mechanical properties of polymers, which includes the analysis of stress-strain behaviour, the effect of strain rate and temperature on the mechanical properties of polymers. The mechanical deformation of semi-crystalline polymers is also discussed. This includes both time independent and time dependent deformation. The time dependent behaviour of polymers is also analysed using various constitutive models. The final part discusses the use of nanoindentation techniques to evaluate the micro-scale properties of polymers and polymer-based nanocomposites.

Chapter 3 describes the experimental methods, including the materials used, how they were processed and the characterisation techniques applied.

Chapter 4 describes the effect of the specified processing method and strain rate on the mechanical properties of polyethylene blends using tensile testing and DSI. The temperature increase during plastic deformation and its effect on the mechanical properties of polyethylene blends is also discussed. The dependency of the micro-scale properties on processing method from DSI tests is also included in this chapter.

Chapter 5 provides the results of the investigation of dispersion of the nanoparticles into the polyethylene matrix using SEM, TEM, XRD and DSI techniques.

Chapter 6 provides the results from the investigation of the effect of nanoparticle geometry and volume fraction on the bulk mechanical properties of the polyethylene-based nanocomposites. This includes their correlation with heat generation during plastic deformation, the effect of processing method and strain rate on the heat generation during plastic deformation and the effect of nanoparticle loading and processing method on viscoelastic behaviour.

Chapter 7 describes the effect of nanoparticle loading and processing method on the micro-scale properties of polyethylene-based nanocomposites from DSI tests.

Chapter 8 describes the relationship between the ambient temperature and the mechanical properties of the polyethylene-based nanocomposites. The effect of nanoparticle addition on the thermal degradation of polyethylene-based nanocomposites is also discussed and the effect of temperature on the DSI properties of polyethylene-based nanocomposites is presented.

Chapter 9 presents a discussion of the experimental findings from the previous chapters.

Chapter 10 covers the final conclusions of this research and recommendations for future work are made.

Chapter 2
Literature Review

2.1 Introduction

This chapter presents a review of the literature concerning polymer-based nanocomposites and their processing methods. This includes classification, types of nanoparticle used with polyethylene and the effect of nanoparticle addition on mechanical properties.

The chapter starts with an introduction to polymers and their classification and structure. Polymer blends and polymer composites that can be used to provide new materials with desired properties are then discussed. The next section focuses on polyethylene based materials, including blends, nanocomposites, nanoparticles used with polyethylene and processing methods. A review of the mechanical properties of polymers, such as toughness (area under stress-strain curve), strength, elongation, hardness, elastic modulus, yielding and elastic, plastic and viscoelastic behaviour is presented next. The effects of strain rate, temperature and reinforcement on the deformation mechanism are important factors for the selection of the material for specific application and they are also discussed. The deformation mechanisms of the semi-crystalline polymers when subjected to tensile loading are rather complex and the various attempts that have been published to describe the microstructural changes during deformation of semi-crystalline polymers are discussed. The review then covers the mechanical behaviour of polymers, how this is tested and how it can be modelled. Finally, the findings of the literature review are summarised and conclusions are drawn.

2.2 Polymers

The rapid increase in demand for polymers for advanced applications has attracted researchers in both academia and industry to improve their properties (Zoo et al. 2004; Durmus et al. 2008). Polymers can be classified to be within one of three major classes: elastomers, thermoplastics or thermosets. A polymer is a macromolecule that consists of several structural repeating units (monomers) connected by “covalent bonds”. The structure of the macromolecular chain can be linear, branched, cross-linked or entangled, while they are linked together either physically, as in thermoplastic materials, or chemically, as in thermoset materials. The physical interactions between chains are called “secondary bonds”, which consist of London dispersive forces, hydrogen and dipole bonding (Thomas 2007). Macromolecules may be aligned linearly to form crystalline regions, however, thermoplastics such as polyethylene also contain amorphous areas with randomly oriented molecules between the crystalline regions; therefore they are known as semi-crystalline materials (Ehrenstein 2001). Generally, crystalline polymers have better mechanical properties than amorphous polymers, for example increased stiffness, toughness and impact resistance (Allcock et al. 2003).

Polyethylene (PE) based polymers, such as ultra high molecular weight polyethylene (UHMWPE) and high density polyethylene (HDPE), have been widely used in various applications due to their outstanding mechanical properties, for example impact strength (> 1076 J/m of notch) and wear resistance (wear rate of 400 $mm^3/10^6$ cycles). UHMWPE also has excellent chemical resistance (>95% residual strength after 100h in acids) (Kelly 2002; Lucas et al. 2011; Lim et al. 2005) whilst HDPE has better processability and creep resistance (Xue et al. 2006; Sui et al. 2009). A major area of interest for research and development in the last three decades has been polymer blends (Robenson 2007). Blends can be used to produce materials with tailored properties for a particular application or to enhance manufacturability. For example, blending UHMWPE with other polyethylene types that have lower viscosity, such as HDPE, can be used to improve the processability of UHMWPE and enhance its creep resistance (Xue et al. 2006; Sui et al. 2009). However, a reduction in some of the original polymer properties might occur due to the change in the polymer microstructure. This can potentially be mitigated by addition of a third phase or reinforcement such a nanofiller.

In recent years, nanotechnology has developed nano-sized fillers that have at least one dimension in the range 1- 100 nm. Nanocomposite material can be produced by embedding the nanoparticles in the polymer matrix, which can improve the mechanical properties in a way that cannot be achieved using micro-particles. For example, the addition of CNTs into a UHMWPE/HDPE blend matrix showed significant improvement in the wear performance (Xue et al. 2006). Generally, the polyethylene matrix, processing method, nanoparticle type, volume fraction of nanofiller, and interfacial region are the most important factors affecting mechanical properties of the nanocomposite. In the next section a more detailed introduction to the types of various polymers and their morphology is given.

2.3 Crystallinity in Polymers

Polymers are composed of long chain molecules that tend to fold to create crystalline lamellae. These can form a nucleation site for crystal growth, resulting in the formation of a spherulite. This often has a circular shape, with a diameter in the range of 2 to 20 µm. The spherulite consists of both crystalline and amorphous regions, as shown in Figure 2.1. Polymers can hence be categorised into three different types depending upon their structure: Crystalline polymers, amorphous polymers, and Semi-Crystalline polymers. The latter consisting of lamellar crystals separated by amorphous phases (Ramanathan e al. 2011; Thomas 2007). The thickness of the lamellae is in the range of 2 to 20 nm. The crystallinity, or non-crystallinity, of a polymer can be observed using X-ray diffraction (XRD), for which many polymers will yield a diffraction pattern that will indicate a crystalline, or even semi-crystalline, structure. An alternative method is Differential Scanning Calorimetry (DSC), where analysis of the exothermic crystallisation peak or the endothermic melting peak can be used to determine the degree of crystallinity in the material. The physical properties of the polymer can be changed by allowing a crystal structure to form; most notably the thermal properties of the polymer are affected in such a way that more energy is required to melt the polymer compared to an amorphous state. The degree of crystallinity and the size of the spherulite can have a significant influence on the mechanical properties of a semi-crystalline polymer. These properties include elastic modulus, yield stress, strength and fracture, with a higher degree of crystallinity leading to an increase in stiffness and reduction in ductility (Dusunceli and Colak 2008).

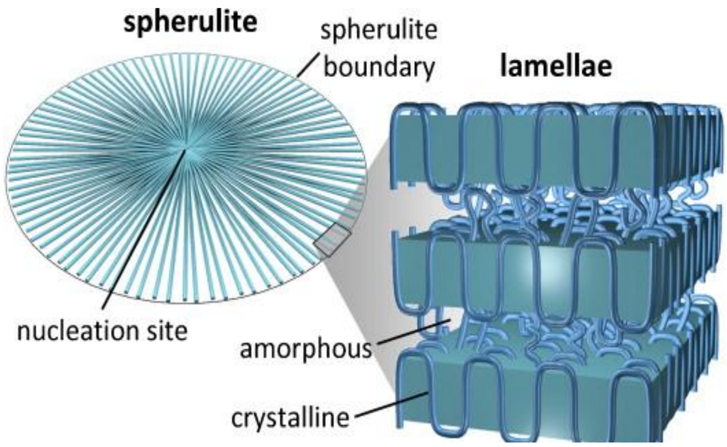

Figure 2.1: Features of semi-crystalline polymer crystals (Ramanathan et al. 2011).

2.4 Composite Materials

Composite materials usually consist of two or more chemically and physically different phases on a microscopic scale. The main difference between composites and blends is that the two main constituents in the composites can be easily distinguished whereas this is not the case for most blends. In composites, stiffer and stronger reinforcements are usually embedded in a continuous phase, which is known as the matrix. The matrix can be polymer, metal or ceramic. Each class of material has specific mechanical properties, e.g. ceramics are strong, brittle, insulating and creep and chemically resistant; metals are ductile and conductive; polymers are insulating, tough, ductile, rubbery, flexible, chemical and wear resistant. The combination of different classes can result in a composite with more desirable behaviour than that seen in the individual components. The reinforcements can be protected by the matrix phase, which distributes the stresses and supports the reinforcement. Due to chemical interaction or processing effects, an additional phase (Interphase) might appear between the embedded reinforcement and the matrix, as shown in Figure 2.2. However, poor interaction between matrix and filler can also occur, for example the embedding of a polar filler into a nonpolar matrix. This can affect the failure mechanisms, failure propagation, and stress-strain behaviour. The dispersion and the distribution of the reinforcement can also play an important role in determining the mechanical properties of the composites. A more homogenous material tends to have better mechanical properties and less probability of failure (Thomas et al. 2012; Thomas 2007).

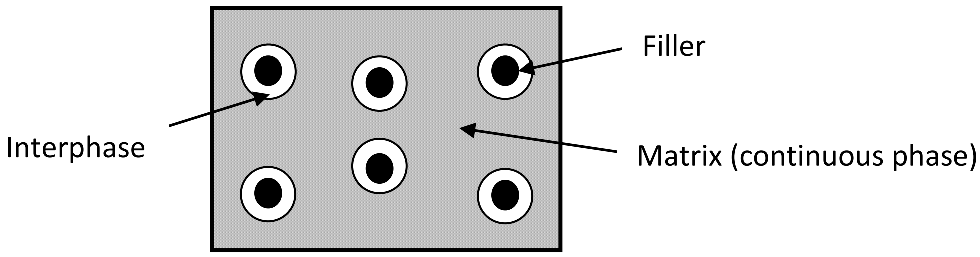

Figure 2.2: Phases in nanocomposite material.

2.5 Polymer Nanocomposites

Polymer-based materials are the most widely commercialised type of nanocomposite (Bogue 2011). The incorporation of nanoparticles into a polymer matrix can result in a nanocomposite material with improved mechanical properties compared to the original polymer. Several types of nanoparticle material can be added to the polymer matrix. These include fibre or tube shaped nanofillers, such as carbon nanotubes (CNTs), plate-like nanoparticles such as clay and three dimensional nanoparticles such as carbon black (CB) (Ajayan et al. 2003).

Polymer/clay nanocomposites were the first nanocomposite materials used in commercial applications. In the late 1980s, the Toyota Company developed a new timing belt cover material with enhanced heat resistance and dimension stability. The material consisted of nylon-6 with the incorporation of layered silicate (nanoclay). Later, CNTs were discovered (Iijima 1991) and extensive work has since been carried out to characterise their properties (Dresselhaus et al. 1996; Saito et al. 1998; Harris 1999). The outstanding mechanical, electrical and thermal properties of CNTs prompted researchers to incorporate them in a wide range of polymer matrices (Qian et al 2000; Yuen et al. 2007; Xu et al. 2006; Chang et al. 2005).

Several review papers have been written on the mechanical properties of polymer nanocomposites (Crosby et al. 2007; Tjong 2006; Balazs et al. 2006; Mayes 2005; Jordan et al. 2005). These papers indicate that the incorporation of nanoparticles into a polymer matrix can enhance the properties for a wide range of polymers. Also, they state that the polymer matrix, nanoparticle, interfacial region, dispersion and distribution are important factors in determining the nanocomposite properties.

2.6 Polymer Nanocomposites Processing Techniques

The first step in polymer nanocomposite development is the material selection, which strongly depends on the material property requirements of the final product. After that, a number of factors should be considered before processing, which can directly affect the processing techniques. The viscosity, or the resistance to flow under applied load, is a fundamental factor during the processing of polymer nanocomposites, particularly in melt processing. The addition of reinforcement into a molten polymer or blend matrix usually causes an increase in viscosity. The use of conventional processing techniques, such as extrusion, injection or compression moulding, can be a particular challenge for a high viscosity polymer or blend (Thomas 2007).

Polymer nanocomposites can be processed using a wide range of techniques, including solvent processing, *in situ* polymerisation and melt (or direct) processing. In solvent processing, the polymer is dissolved in an appropriate solvent to form a suspension of polymer particles in the solvent, and then the reinforcement is added. The dispersion of the reinforcement in the solution, particle wetting and drying are key factors for the properties of the final material. In *in situ* polymerization, a liquid monomer can be mixed with the nanoparticles (reaction mixture) and then polymerized. The reaction mixture consists of a low density solution of reactants, liquid monomers, and components of the reaction of the monomers. Additional chemicals may be used to control the polymer structure, such as an initiator for addition polymerisation, catalysts or cross-linking chemicals. This technique has some advantages compared to the solvent process. Although, the particle in the monomer solution can be characterised by similar methods as solvent processing such as particle wetting, dispersion or equilibrium settling, usually little drying is required and there is less volume change during the process. Notably, cross-linked and thermoset resins can only be processed using *in situ* polymerisation because they are intractable in melt or solvent processing. The third processing technique for nanocomposites is melt (or direct) processing, which is usually applied to high viscosity materials, such as thermoplastics. The nanoparticles are added and mixed with the polymer or blend matrix in a sufficiently melted state. Processing temperature, time and mixing are important factors during the processing of a high viscosity polymer. Exceeding the average melting temperature for polymer crystals is not sufficient to separate the atoms in the chain from the crystal. Also, longer chains may need additional energy to disrupt and separate from the crystals. Thus, to achieve a practical processing viscosity a higher temperature is required, regardless of the processing time. An appropriate cooling rate is also an important factor in crystal formation; a higher cooling rate will result in less perfect crystals with more defects (disrupted crystals). Another important factor that affects the melting process is the mixing, which is a challenging aspect of processing. Good mixing can be achieved by a combination of suitable starting conditions and distribution of shear force (Thomas 2007).

In the current work, melt processing was used to mix the UHMWPE with the HDPE and the nanoparticles using a temperature close to the decomposition temperature.

2.7 Characterisation Techniques for Polymer Nanocomposites

Numerous characterisation techniques can be used to ascertain the mechanical properties of polymer nanocomposites. Polymer nanocomposites can be characterised according to their morphologies using techniques such as scanning electron microscope (SEM), transmission electron microscope (TEM), X-ray diffraction (XRD), Raman spectroscopy, and atomic force microscope (AFM). Thermal properties can be analysed using techniques such as thermogravimetric analysis (TGA), differential scanning calorimetry (DSC), dynamic mechanical analysis (DMA) and infrared thermography. Other properties, such as mechanical performance, rheology and tribology, can be evaluated using techniques such as tensile and creep testing, rheometer, wear and scratch testing (Mittal 2012). For example, Xue et al. (2006) performed wear tests to investigate the effect of CNT addition on the performance of a UHMWPE/HDPE blend. A load of 21.2 N was applied to a stainless steel ball with a diameter of 12.7mm, which rotated around its vertical axis with a speed of 28.2 mm/s and duration time of 60 hours. The results showed that the incorporation of up to 2 wt. % CNTs into the blend matrix can significantly improve the wear resistance compared to pure UHMWPE. However, SEM characterisation indicated that large CNT agglomerations formed in the blend matrix. Zoo et al. (2004) evaluated the effect of reinforcing a UHMWPE matrix with CNTs on the tribological performance. A Ball-on-disc type test was used and the results showed significant improvement in the wear properties by adding up to 0.5 wt. % CNT to the UHMWPE matrix.

Stoeffler et al. (2011) used a standard tensile testing machine to study the effect of clay on the mechanical properties of nanocomposites based on HDPE, LDPE and LLDPE. It was found that LLDPE/clay nanocomposites exhibited a significant increase in tensile modulus and tensile strength compared to neat LLDPE. Similar results were obtained by Pöllänen et al. (2013) after testing the mechanical properties of HDPE/modified clay nanocomposites.

In this study, various techniques were applied to characterise the effect of processing method, nanoparticle type, dispersion, strain rate and temperature on the properties of polyethylene-based nanocomposites. These techniques are discussed in the experimental methods in Chapter 3.

2.8 Polyethylene (PE)

Polyethylene is the most widely used of polymers and classified as a thermoplastic material, which means it can be melted and shaped into a new form (recycled) (Kurtz 2004). It is chemically synthesized by combining ethylene monomers to form long chains. The ethylene molecule (C_2H_4) consists of two carbon atoms connected together by a double bond and a pair of hydrogen atoms attached to each carbon, thus:

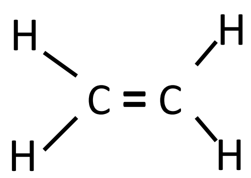

Figure 2.3: Chemical structure of ethylene molecule.

Polyethylene is produced through polymerization of ethylene to form repeating units as shown in Figure 2.4.

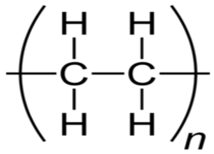

Figure 2.4: Chemical structure of polyethylene.

n in Figure 2.4 represents the degree of polymerisation (the number of ethylene monomers polymerised to form the chain). Typically, the degree of polymerisation varies between 100 and 250,000 or more, therefore molecular weight varies from 1400 to more than 3,500,000 (Peacock 2000). Commercially, the degree of polymerisation of polyethylene is more than 1000 for most available products and polyethylene is the least costly synthetic polymer (Malpass 2010).

Polyethylene molecules can be branched to various degrees and many types of polyethylene exist, with different properties due to differences in chain structure, crystallinity and density level. The overall density of a polyethylene resin can be increased by raising the degree of crystallinity. Generally, a high density of polyethylene indicates a low branch concentration (Peacock 2000). The glass transition temperature of polyethylene is a round – 120°C (Nielson 1974), and the melting point is approximately 140°C.

2.8.1 Classification of Polyethylene

As discussed, the mechanical properties of polyethylene depend significantly on parameters such as molecular weight, crystallinity (or amorphous content), chain branching, and processing. Polyethylene can be classified into different types based on density and molecular weight. The most important polyethylene types are:

- Low Density Polyethylene (LDPE)
- Linear Low Density Polyethylene (LLDPE)
- High Density Polyethylene (HDPE)

- Ultra High Molecular Weight Polyethylene (UHMWPE)

The latter two types of polyethylene will be discussed below in more detail as they are of direct relevance to the current work.

2.8.1.1 High Density Polyethylene (HDPE)

High density polyethylene (HDPE) is widely used in industry, such as in tribological applications in the automotive industry, pressure pipes and low speed bearings (Sahebian et al. 2007; Guermazi et al. 2009; Anderson 1982). HDPE consists of molecules that are linear with little branching. This linearity leads to the development of high degrees of crystallinity. Thus, the characteristics of this type of polyethylene include a relatively high modulus (600 – 1400 MPa), low moisture permeability, high strength, good chemical resistance, high abrasion resistance, good creep resistance and high environmental stress crack resistance. Moreover, HDPE has a low glass transition temperature, $T_g < -100°C$ which makes it suitable for low temperature applications, such as containers (Ehrenstein 2001; Peacock 2000). HDPE has a similar chemical structure to UHMWPE (discussed later) with lower production costs, higher creep resistance and good processability, and thus it can be a candidate polyethylene additive to enhance the processability of UHMWPE in a blending process (Fouad and Elleithy 2011).

2.8.1.2 Ultra-High Molecular Weight Polyethylene (UHMWPE)

Since the 1950s, ultra high molecular weight polyethylene (UHMWPE) has been used in industrial applications, for instance in linings for coal chutes and trucks and sidings for ships (Kurtz 2004). It possesses some outstanding material properties, such as impact, abrasion, wear and chemical resistance as well as a greater capacity for absorbing the kinetic energy of a projectile than other polyethylene types and a low coefficient of friction (Lucas et al. 2011; Lim et al. 2005; Kelly 2002). UHMWPE has also been used as a biomaterial, for example in orthopaedics for the bearing surface in joint replacement components (Westby and Backman 2010; Havelin et al.

2009; Kurtz 2004; Baker et al. 2000). Also, owing to its high resistance to projectile impact, UHMWPE has been used in armour applications, such as personal protection and vehicle armour (Gellert et al. 1998; Deng et al 1996; Prevorsek et al. 1994). UHMWPE has a degree of crystallinity between 39 - 75%, as determined by differential scanning calorimetry (DSC) and the glass transition temperature, T_g, is -122 ± 2°C, as measured using dynamic mechanical analysis (DMA) (Kurtz 2004; Ho et al. 2003). The mechanical properties of UHMWPE are influenced by the degree of crystallinity, the amount of chain entanglement, crosslinks between the crystalline regions and the orientation of the crystallites.

Owing to its extremely high molecular weight, usually between 2 and 6 million, and subsequent high viscosity at elevated temperatures, it is difficult to process UHMWPE using standard techniques, such as twin screw extrusion, injection moulding and compression moulding (Chen et al. 2008). Also, there is an inherent weakness in some properties of UHMWPE, such as creep and fatigue resistance (Tang et al. 2002). Reducing the viscosity of UHMWPE is an effective method of avoiding these processing difficulties. However, although the viscosity can be reduced to improve processability by blending UHMWPE with a polymer that has shorter chains, the properties of the final material will be affected (Galetz et al. 2007; Lim et al. 2005). UHMWPE can be combined with low molecular weight polyethylene (LMWPE), which has a low viscosity, to produce a high molecular weight fibre (Bin et al. 2001). Recently, adding high density polyethylene (HDPE) and nanofillers to pure UHMWPE has received attention due to the improvement in certain mechanical properties for these new materials, such as creep, impact and wear resistance (Lucas et al. 2011; Abadi et al. 2010; Wood et al. 2010; Sui et al. 2009; Xue et al. 2006).

2.8.2 Polyethylene Blends

Polymers have been synthesized since the 1930s, however, there is increasing demand for materials with high mechanical properties, therefore, polymer blends and composites have been developed to provide polymer based materials with enhanced properties. The ability to combine existing polyethylene materials into new blends using conventional processing methods has the advantage of reduced research and development cost compared to the production of a completely new polymer type. Also, owing to the fast growth of processing techniques and the emergence of nanotechnology, polyethylene blends and composites can quickly respond to meet application requirements. Various polyethylene blends can be found, dependent on their composition type and phase behaviour, especially miscibility (homogeneous and stable) and crystallinity, which are important factors that can significantly affect the mechanical properties (Robenson 2007). Table 2.1 shows examples of typical polyethylene blends and their applications, which are reflected in the variations in the resulting mechanical properties. Polyethylene blends can be classified as miscible blends, which exhibit properties similar to a single phase material or immiscible blends, which separate into different phases. Miscibility depends on processing temperature, molecular structure and blend composition. In previous studies, the miscibility of polyethylene blends has been investigated using three different methods (1) DSC combined with TEM (Hill et al. 1992; Hill et al. 1993; Hill et al. 1997; Morgan et al. 1999). If the result showed only one melting peak in the DSC plot and one group of morphology in TEM, the blends were considered as miscible. For two melting peaks and two groups of crystal structure, the blends were considered as immiscible. (2) Rheology method (Chen et al. 2013; Li et al. 2011; Hameed and Hussein 2002; Hussein 2003; Hameed and Hussein 2004; Hussein and Williams 2004), which is based on the dynamic viscosity and viscosity of the blends at zero shear rate. The blends were considered miscible when the two parameters show a linear relationship, otherwise the blends are considered immiscible. (3) Small-angle neutron scattering (SANS) can used to measure the interaction energies of the blend, which can be used to determine the solubility parameters that control the miscibility (Wignall et al. 1995; Alamo et al. 1997; Wignall 2000).

These studies concluded that the branch density and branch type are important factors to control miscibility. The miscibility decreases with increasing branch content or branch length. An increase in the molecular weight of the polyethylene can also reduce the blend miscibility. The blends become more miscible with increasing melt temperature and increasing in linear polyethylene content. Melt processing is an effective method for polyethylene blending. Many researchers have applied this method to prepare polyethylene blends or polyethylene nanocomposites using various mixing conditions (Xue et al. 2006; Deshmane et al. 2007; Liang et al. 2008; Durmus et al. 2008; Lucas et al. 2011; Stoeffler et al. 2011; Pöllänen et al. 2013; Valdes et al. 2013).

Table 2.1: Examples of typical polyethylene blends and their applications.

Polymer 1	Polymer 2	Applications	Reference
HDPE	LDPE	Toughened HDPE with improved processing, especially melt strength; HDPE and LDPE are immiscible	Nwabunma & Kyu 2008
HDPE	LLDPE	Improve rheology for extrusion, rigidity and impact resistance	Nwabunma & Kyu 2008
UHMWPE	HDPE	Improve processability, yield stress and elastic modulus	Khasraghi & Rezaei 2013
UHMWPE	HDPE	Improve processability, improve creep	Xue et al. 2006
HDPE	UHMWPE	Improve wear resistance, improve impact and tensile properties	Lucas et al. 2011

2.8.3 Nanoparticle Materials

When nanoparticles are dispersed in a polymer matrix, the resulting material is known as a polymer nanocomposite. Although, these polymers generally have relatively low concentrations of fillers, e.g. 0.5 – 3 wt. %, the final mechanical, morphological, electrical and thermal properties can be significantly improved. There are a number of different materials that can be used as filler particles; organic or inorganic, natural or synthetic with a wide range of material compositions and structures (Akovali 2001). The reinforcing characteristics of a filler depend on various criteria, such as the particle geometry, the particle size and aspect ratio, the specific area (surface area to volume ratio), the interaction between matrix and fillers, the dispersion, and orientation. All these criteria have a great influence on the polymer nanocomposite properties (Leblance 2010; Laine 2001).

In terms of geometry, nanoparticle materials can be classified as follows. 1D (or fibrous material), with a diameter in the nanometre scale, as shown in Figure 2.5a. For example, carbon nanotubes (CNTs), which can be classified into single-walled nanotubes (SWNTs) with a diameter of 1-2 nm, multi-walled nanotubes (MWNTs) with outer diameter 3-10 nm and carbon nanofibres (CNFs). These particles possess an elongated structure. 2D (or layered material), with one dimension in the nanometre scale and possessing a platelet-like structure, as shown in Figure 2.5b. Layered silicate or nanoclays eg. Montmorillonites, are a good example of this type of nanoparticle. Figure 2.5c shows a 3D (or equi-axed) nanoparticle, which has all three dimensions in the nanometre scale. For example, spherical silica particles (SiO_2), nanocrystals, gold, carbon black (CB), rubber particles and titanium oxide (TiO_2) (Schmidt et al 2002; Lee et al. 2005; Todorov et al. 2009).

The quality of the interface between the matrix and filler in the nanocomposite is very important. The matrix phase provides load transfer to the filler material and protects it against abrasion and damage (Akovali 2001). Poor interaction between matrix and filler can mean that the load is not completely transferred to the particles, which will affect the strength of the polymer composite, which might even be less than that of the neat polymer matrix (Liang et al. 2008). On the other hand, a strong bond between the filler and matrix can result in increased yield strength of the material (Wu et al. 2002). Nanoparticles lead to a large interfacial area in the nanocomposite; hence a great challenge in developing polymer nanocomposite is to control the interface (Ajayan et al 2003).

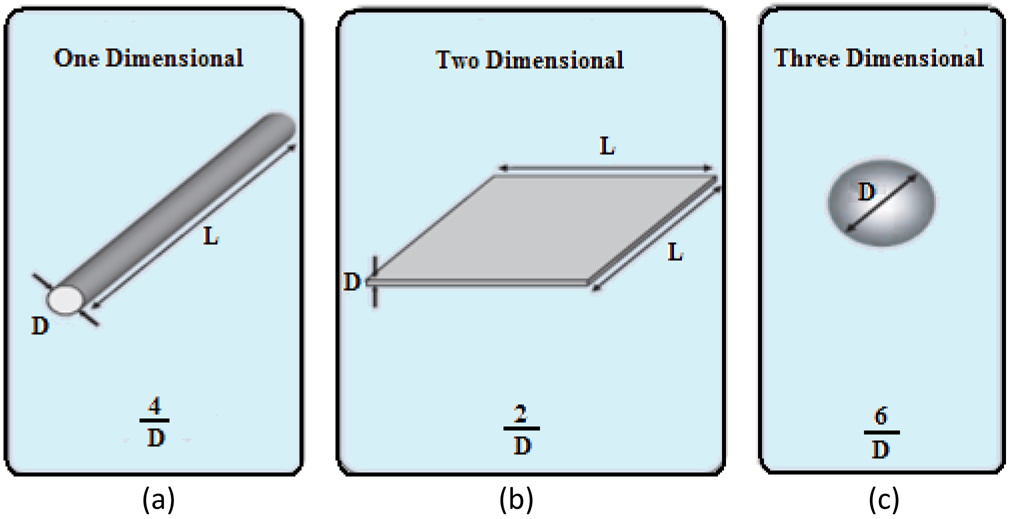

Figure 2.5: Common geometries of nanoparticles and their respective surface area to volume ratios: (a) one dimensional shape, 1D, (b) two dimensional shape, 2D and (c) three dimensional shape, 3D (Reproduced from (Hussain et al. 2006)).

Achieving a good dispersion of nanofillers into the polymer matrix is a key challenge to achieve the desired properties. It is extremely difficult to disperse the nanoparticles uniformly in the polymer matrix due to the Van der Waal forces between particles and the high surface energy. Large agglomerations of nanoparticles can be viewed as defects inside the matrix, which negatively affects the mechanical properties. Various studies have been carried out to investigate the effect of such nanoparticle structure, content, dispersion and interfacial strength on the mechanical performance of polyethylene nanocomposites for various applications (Tang et al. 2003; Zoo 2004; Xue et al. 2006; Kontou and Niaounakis 2006; Kanagaraj et al. 2007; Sui et al. 2009; Abadi et al. 2010; Wood et al. 2010; Stoeffler et al. 2011; Ren et al. 2012; Zhenhua and Yunxuan 2012; Chen et al. 2012). Table 2.2 summarise the effect of the addition of a nanofiller on the mechanical properties of a number of UHMWPE/HDPE based blends. It can be seen that the incorporation of nanofiller can enhance some properties, whilst a reduction in other properties can also occur.

Table 2.2: Examples of UHMWPE/HDPE nanocomposites and their properties from literature.

Polymer1	Polymer2	Reinforcement	Findings	Reference
80 wt. % UHMWPE	20 wt. % HDPE	MWCNT (0.2 – 2 wt. %)	Improvement in wear resistance and reduction in creep resistance	Xue et al. 2006
60 wt. % UHMWPE	40 wt. % HDPE	CNT (1 wt. %)	Improve processability, yield stress and elastic modulus Reduction in tensile strength and elongation at break	Khasraghi & Rezaei 2013
80 wt. % UHMWPE	20 wt. % HDPE	β-TCP (5, 10, 15, 20%)	Increasing in elastic modulus and a reduction in the elongation at yield	Abadi et al. 2010
60 wt. % UHMWPE	40 wt. % HDPE	CNF (0.5, 1, 3 wt. %)	Improvement in processability but reduction in wear properties	Wood et al. 2010

2.8.3.1 Carbon Black Nanocomposites

Carbon black (CB) can be employed as reinforcing to improve dimensional stability, to prolong the lifetime of rubber, colour material and affect conductivity. It is formed by the incomplete combustion of organic materials (hydrocarbon materials) where carbon is the essential element of their composition. The shape of CB particles is spherical or near-spherical, as shown in Figure 2.5c and depends on the production process, which can be furnace black, channel black, thermal black or lamp black. However, the particles are rarely found as individual, but commonly as aggregates of coalesced particles except in the case of thermal black which exist as separate spheres.

Commercially, the furnace process is the most important as it can produce large quantities with different particle size by controlling the combustion ratio. In this process, the combustion ratio i.e. the ratio of total air present to air needed for complete combustion, is the most important factor which will affect the particle size. Small particles, with high surface area to volume ratio, can be produced by using a high combustion ratio. The particle size affects the price of the CB, the particles with small diameter being more expensive. Interactions between CB and other substances occur by means of their surface, hence, surface properties, such as morphology and the localised presence of noncarbon materials, as well as the surface area, are important characteristics (Donnet et al. 1976; Huang 2002).

The rubber industry is one of the most important applications of CB as a reinforcing agent. Generally, CB is used to reinforce elastomers to enhance mechanical properties such as modulus, hardness, tensile strength, and abrasion resistance. However, Cotten and Boonstra (1967) pointed out that the addition of CB to rubber causes a significant decrease in the compression stress relaxation rate. Furthermore, Payne (1965) stated that for reinforcing elastomers, CB has little influence on the temperature-frequency relationship of the dynamic modulus. In addition, the glass transition temperature T_g cannot be changed by CB loading (Kraus 1970). Thus, geometry parameters of CB such as surface morphology and interactions between the CB and the polymer are the most important factors that can influence the mechanical properties of the composite.

Although, the conductivity of composites can be enhanced by the incorporation of CB into the polymer matrix (Huang 2002; Mamunya 2001; Khare et al. 2000; Zois et al. 2001), some mechanical properties such as elongation and impact strength may decrease, which means the composite becomes more brittle. Therefore, mechanical properties of polymer composites such as polyethylene-CB are important issues that need to be investigated. Recently, researchers (Liang et al. 2009; Yuan et al. 2010) have investigated the influence of CB content on the mechanical properties of low density polyethylene (LDPE), linear low density polyethylene (LLDPE) and high density polyethylene (HDPE). The tensile fracture strength and the tensile elongation at break increased significantly by the addition of less than 5% weight fraction of CB. On the other hand, the impact strength decreased with increasing volume fraction of CB. Therefore, choosing the appropriate loading of CB and improving the CB-matrix interaction are important to enhance the mechanical properties of the polymer composite. In addition, other mechanical properties such as the viscoelastic behaviour of polyethylene-CB nanocomposites need to be investigated, as discussed in Chapters 6 and 7.

2.8.3.2 Carbon Nanotube Nanocomposites

In recent years, carbon nanotubes have received great interest from many researchers due to their wide range of applications, such as biological, applications requiring good thermal and electrical conductivity, catalyst support, air and water filtration, electronics fabrication and energy storage. Nanotubes can be classified as 1D nanofillers that have cylindrical shaped molecules with the outer diameter of a single tube spanning from less than one nanometre to around 10 nanometres and with lengths between a few hundred nanometres to several microns (Advani 2007; Peng-Cheng et al. 2010).

Dependent on the fabrication conditions, there are two types of CNT. The first type is the single-walled carbon nanotube (SWCNT), which consists of one cylindrical layer of graphite. The second type, the multi-walled carbon nanotube (MWCNT), consists of two or more cylindrical shells of graphite bonded via van der Waals forces. The different types of CNT have different specific surface areas and conductivity and hence they are more suitable for different applications. Due to the possibility of slip between the layers of MWCNTs, SWCNTs are much stronger (Advani 2007; Lordi et al. 2000).

Carbon nanotubes can be synthesised using various methods, such as high temperature evaporation using arc-discharge, laser ablation, and various chemical vapour deposition (CVD) and catalytic growth processes. A high energy source, a carbon feed, and transition metal catalysts are required in all methods. The final, product differs greatly with regard to size, aspect ratio, entanglement, orientation, purity, surface chemistry, and straightness. All these can be considered as key factors in choosing the CNT and processing method for a specific application (Advani 2007; Lordi et al. 2000).

Carbon nanotubes have extremely high mechanical properties, e.g. 1.2 TPa Young's modulus and 50-200 GPa tensile strength (Qian et al. 2002). However, to utilise these properties, processing is a key challenge that affects the properties of the composite material. Single or twin screw extruders are the most popular equipment for processing, usually with high shear mixing rates. The processing usually starts by feeding pellets containing clustered CNTs into the extruder hopper. Then, a screw rotates at high speed creating a high shear flow which exfoliates the CNT clusters and mixes them uniformly within the resin. The high shear forces can be used to decrease the areas of CNT aggregates and improve the CNT dispersion, which is especially important with materials of high viscosity, such as UHMWPE (Advani 2007; McNally et al. 2005; Thostenson et al. 2002). When successful, the contact area between the CNTs and the polymer matrix (interfacial region) will be large, which can improve load distribution. However, homogenous dispersion, orientation, and interfacial bonding are still the major difficulties in processing CNT nanocomposites (Rahmat and Hubert 2011; Lordi et al. 2000; Lau et al. 2003).

Three different types of interaction can be found in polyethylene/carbon nanotube nanocomposites. The interaction between CNT shells in MWCNTs (Yu et al. 2000), the interaction between different nanotubes in a bundle (Qian et al. 2003) and the interaction between the CNT and the polymer matrix (Haghighatpanah and Bolton 2013; Yang et al. 2007; Li et al. 2011). However, the performance of nanocomposites is affected by the polymer-CNT interaction more than the other types (Rahmat and Hubert 2011).

Rahmat and Hubert (2011) classified the interactions between CNTs and the polymer matrix into two categories. Covalent interaction, where the CNT is chemically bonded to the polymer chains using functionalization techniques and non-covalent interaction, where mechanical interaction is employed, such as bridging, which occur when two or more CNTs interact with a polymer chain; wrapping, which occur when a polymer chain backbone wraps around a CNT. Increasing the volume fraction of the CNT can lead to an increase in a specific type of interaction area. The wrapping interaction is considered to occur between polyethylene (non-polar) and the unmodified CNT used in this study. The polyethylene-CNT interaction, the dispersion and the volume fraction of CNTs are all important factors which can affect the mechanical properties of the nanocomposites. These factors are described in detail in Chapters 6 and 7.

2.8.3.3 Nanoclay Nanocomposites

Nanoclays, which consist of layered silicates, are the most widely investigated nanoparticles in polymer matrices. Nanoclays can be classified as montmorillonite, bentonite, kaolinite, hectorite or halloysite. The structure of the clay consists of a number of layers. For example, montmorillonite consists of octahedral alumina layers and tetrahedral silicate layers to form stacked platelets. The platelet thickness is several nanometres and the lateral dimension can be several microns. Layered silicates are hydrophilic materials; therefore to become compatible with polymers, they can be modified organically to form hydrophobic silicates (organoclay) (Ray and Okamoto 2003).

The structure of polymer-clay nanocomposites can be classified morphologically into intercalated or exfoliated (delaminated), as shown in Figure 2.6. In an intercalated structure, organic material infiltrates between the layers, which make them slightly separated but with a well defined spatial relationship. On the other hand, exfoliated structures consist of clay layers which are completely separated and distributed throughout the organic matrix. Several factors should be considered in the fabrication of intercalated and exfoliated structures. These factors include the polarity of the host matrix, the exchange capacity of the clay, and the chemical nature of the interlayer cations.

The addition of high modulus nanofillers to a lower modulus polymer produces a polymer nanocomposite with higher modulus than the neat polymer (Ajayan et al. 2003). For example, it has been shown that the reinforcement of nano-clay into polymer matrices, such as HDPE and polypropylene resulted in improvements in the elastic modulus and tensile strength, even at low filler loadings, due to the high surface to volume ratio of clay layers and the high quality of the interface between clay and polymer matrix (Advani 2007). The exfoliation and dispersion of clay platelets in the polymer matrix are important issues to achieve the desired mechanical properties, especially for a non-polar matrix such as polyethylene (Durmus et al. 2007). Poor interaction between clay nanoparticle and polymer matrix as well as poor dispersion can reduce the mechanical properties of the nanocomposites such as the strain to failure and impact strength (Durmus et al. 2007; Tjong et al. 2002). These effects are discussed in detail in Chapters 6 and 7.

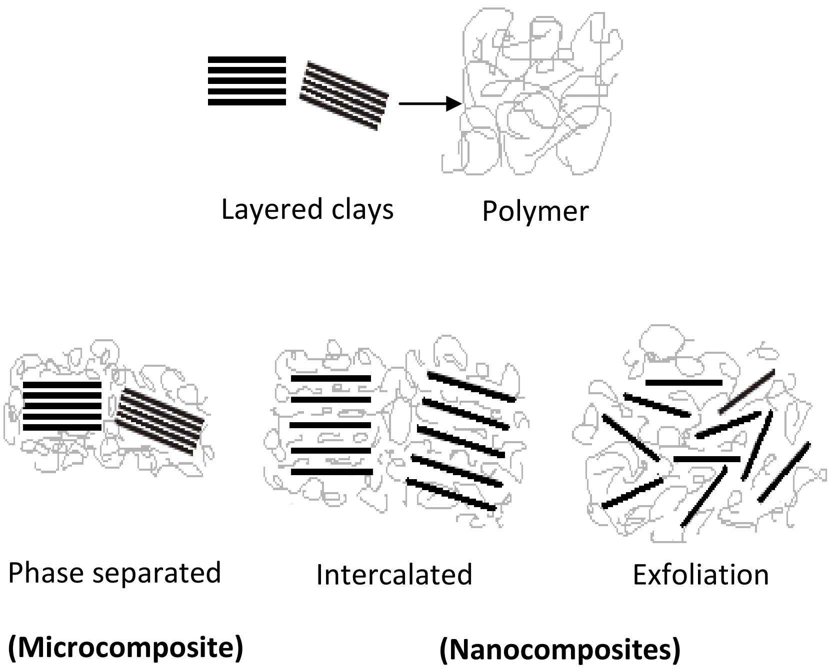

Figure 2.6: The structure of polymer-clay microcomposites and nanocomposites.

2.8.4 Effect of Interfacial Interaction

Novel properties can be achieved by applying process methods that lead to control of the interfacial area, interaction, particle distribution and particle dispersion. The interfacial region has considerable influence on the behaviour of the mechanical properties of polymeric composites. This factor should be properly considered to achieve the desired mechanical properties; otherwise nanofillers may negatively affect the final properties. For example, McNally et al. (2005) pointed out that the reduction in the mechanical properties of PE-(0.1-10 wt. %) CNT is related to the interfacial interaction between the CNTs and PE matrix and not to the maximum volume fraction of nanoparticles. Deshmane et al. (2007) investigated the effect of clay addition on the impact toughness of polyethylene and polypropylene (PP). They found an increase in the impact strength of PP-clay nanocomposites, while a reduction in the impact strength for PE-clay was seen. This was attributed to the strong PP-clay interfacial interaction and weak PE-clay interaction. Stoeffler et al. (2011) pointed out that the type of polyethylene can significantly affect crack propagation in PE-clay composites during deformation. It was seen that the initiation of voids through debonding at the HDPE/clay interface lead to crack formation and propagation. For LDPE-clay and LLDPE-clay composites, however, it was noted that shear banding induced deformation of the clay micro-particles lead to reorganisation of the clay and the formation of micro-cracks.

There is very little or no interaction between non-polar polymers such as polyethylene and polar nanoparticles. This difference in polarity can increase the difficulties of achieving a good exfoliation and dispersion of the nanoparticles into the non-polar matrix (Rahmat and Hubert 2011; Durmus et al. 2007).

2.9 Mechanical Properties of Polymers

In order to ensure that a material is appropriate for a specific application, a number of mechanical properties should be evaluated. The mechanical properties derive from the deformation mechanisms of the material. The stress-strain relationship of a material will provide valuable information about its mechanical properties. The tensile test is one of the most important tests of a materials mechanical response. Various mechanical properties can be obtained from the stress - strain curve, which will be reviewed in this section.

2.9.1 Stress-Strain Behaviour for Polymers

The determination of the relationship between stress and strain behaviour is an extremely important measurement of the mechanical properties of a material and is used to derive constitutive models of the materials mechanical behaviour. In a tensile test, the specimen is subjected to a tensile force that causes deformation in the direction of loading. Engineering stress (σ_E) is defined as the force (F) divided by the original cross-sectional area (A_0), as shown in the following equation:

$$\sigma_E = \frac{F}{A_o} \quad (2.1)$$

Engineering strain (ε, dimensionless) is defined as the change in the length of the sample divided by the original length of the sample, as shown in Equation 2.2:

$$\varepsilon_E = \frac{\delta L}{L_0} \quad (2.2)$$

Engineering stress and strain are applicable when the extension that the material undergoes is very much less than the original length of the sample ($\delta L \ll L_0$). When this not the case, true stress and strain should be used.

The true stress (σ_T) is defined as the instantaneous load (F(t)) divided by instantaneous cross-sectional area (A(t)). The true strain (ε_T) is defined as the rate of instantaneous increase divided by the instantaneous gauge length.

Figure 2.7 shows a typical engineering-stress vs. engineering-strain curve for a semi-crystalline polymer under tensile loading, with images of the sample at different stages (Kuriyagawa and Nitta 2011). Elastic modulus can be obtained from the slope of the elastic part, however, in polymeric materials visco-elastic i.e. rate dependent deformation takes place, which often controlled by the amorphous phase (Humbert et al. 2009). This means that the modulus is strain rate dependent, as discussed in more detail in the next section. The yield stress is the stress at which plastic deformation occurs. Plastic deformation occurs due to the failure of the weak bonds between the molecular chains in thermoplastic materials. In most semi-crystalline polymers whitening can be observed during the plastic deformation, which is caused by the reflection of light during the formation of voids, cracks and crazing. Yielding can be affected by temperature, strain rate and physical properties such as crystallinity, molecular weight and cross-linking (Swallowe 1999; Hillmansen et al. 2000). Beyond the yield point, necking occurs, Parts (b and c) in Figure 2.7, where the spherulitic structure transforms to a fibril structure (Ward and Sweeny

2004). At the end of the neck forming phase (d), neck propagation, or cold drawing, occurs where the molecules align in the direction of loading. Once necking is complete (e), strain hardening starts, where the stress increases until fracture.

Polyethylene is a viscoelastic material, and therefore test conditions such as temperature and strain rate can cause significant variations in the mechanical properties (Merah et al. 2006; Seguela et al. 1994, 1990). The incorporation of reinforcement materials can influence the effect of temperature and strain rate on the material behaviour due to the large difference in properties between the filler and the matrix, such as strength and stiffness. The filler-matrix interaction can also be an important factor in performance at high temperatures or strain rates.

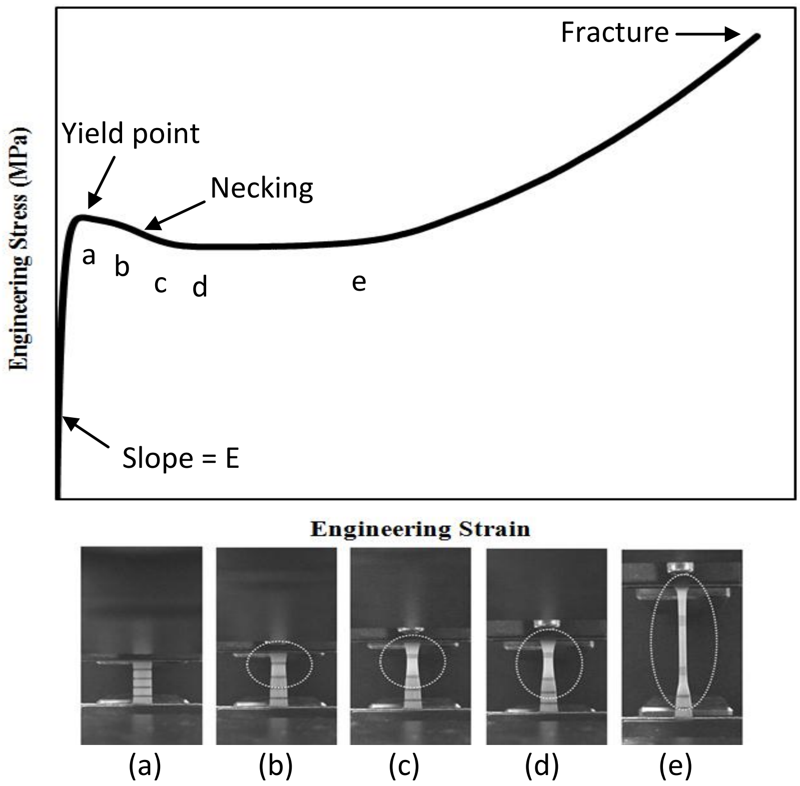

Figure 2.7: Stress vs. strain curve for PE (Kuriyagawa and Nitta 2011).

2.9.2 Strain Rate Effects

The mechanical properties of most materials, particularly polymers, can be affected by strain rate ($\dot{\varepsilon}$). Elastic modulus and yield stress of a polymer can increase with increasing strain rate. Plastic work at high strain rates can be transformed partly into heat, which can lead to a significant temperature increase. At low strain rates, deformation can be assumed to be isothermal and the heat generated transfers into the surrounding atmosphere. However, at very high strain rates, the deformation can be considered to be adiabatic and the heat loss cannot maintain the sample at ambient temperature. The increase in the sample temperature (from adiabatic heat) can lead to thermal softening in the stress-strain behaviour of polymers and a subsequent reduction in mechanical properties such as toughness and strength (Swallowe 1999).

Various studies have indicated that the behaviour of polymers can be affected by thermal softening when testing at high strain rates (Koenen 1992; Mason et al. 1994; Rittel 1999; Longère and Dragon 2008; Kuriyagawa and Nitta 2011; Wang et al. 2010; Wang et al. 2013). However, only a limited number of investigations have indicated that the heat generation effects may increase when testing polymer-based nanocomposites at high strain rates (McNally et al. 2003; Tulsyan 2010; Shen et al. 2011). In a uniaxial tension test, heterogeneous deformation in the neck region can result in the localised generation of heat (Kuriyagawa and Nitta 2011). The necking mechanism in polymers is extremely complicated and the existence of nanofiller reinforcement increases this complexity. The effect of heat generation on polymer properties can be influenced by several factors, such as the polymer matrix (glassy or rubbery), molecular weight, spherulite size and boundaries, filler-matrix interfacial strength for filled polymer, filler type or shape and strain rate.

Conflicting results have been reported on the dependence of heat generation on strain rate in glassy polymer nanocomposites. McNally et al (2003) investigated heat generation during the uniaxial tensile testing of polyamide-12 and a polyamide-12/MAE synthetic clay nanocomposite. They found that the measured temperature was independent of strain rate in the range tested but highly dependent on the presence of the nanofiller. The presence of the synthetic clay in the polymer was seen to increase the temperature at failure and elongation at break by 47°C and 500% respectively. It was proposed that this was because the temperature increased above the glass transition temperature (T_g) in the polyamide-12/MAE (30°C), hence, changing the behaviour from glassy polymer to elastomeric. Shen et al. (2011), however, found that strain rate had some influence on the strain hardening behaviour of a PET (polyethylene terephthalate)-clay nanocomposite, which is a glassy polymer with T_g around 70°C. This was attributed to a possible increase in temperature at higher strain rates. The dependence of heat generation on strain rate, however, has not been investigated to date for rubbery polymer nanocomposites. This could potentially provide clear relationships between heat generation, strain rate and nanofiller due to the large strains to failure in these materials. Increases in temperature due to plastic heat generation can potentially affect the properties of polymer-based nanocomposites, reducing the plastic hardening and reducing the tensile strength at high strain rates. This is of significance when considering the use of these materials in applications involving high strain rates, such as impact protection.

On the other hand, various studies (Serban et al. 2013; Richeton et al. 2005; Wang et al. 2002) have reported that significant increases in the mechanical properties of some polymeric materials can be observed with increasing strain rate. In there studies, an increase in the elastic modulus and yield strength with increasing strain rate was observed for polyamide-12, polycarbonate and polyamide-6. There are, then complicity effect of strain rate, the overall effect being determined by the relative effects of strain rate dependence and thermal softening.

2.9.3 Temperature Effects

The ambient temperature is a crucial factor in the determination of the mechanical properties of polymers during tensile deformation (Serban et al. 2013; Cao et al. 2011; Shan et al. 2007; Merah et al. 2006; Richeton et al. 2005; Wang et al. 2002; Mahieux and Reifsnider 2001; Seguela et al. 1994, 1990). Seguela et al. (1994,

1990) indicated that the yielding behaviour of polyethylene can be affected by an increase in temperature. A sharp yield point was observed at room temperature, while a double yield point was seen at higher temperature. The behaviour has not been observed in the current work. Merah et al. (2006) evaluated the effect of temperature on the tensile properties of HDPE and found a linear reduction in the yield stress and modulus with temperature increase. Shan et al. (2007) pointed out that the stress-strain behaviour of a glassy polymer can display a rubber-like deformation at high temperatures and a linear temperature sensitivity can be observed for the first yield stress.

Studies on the effect of temperature on the tensile deformation of polymer-based nanocomposites, particularly these based on polyethylene are limited. The presence of the reinforcement in the polymer matrix can significantly affect the mechanical properties of the neat polymer or the blend, as discussed in the previous section. At elevated temperatures, the reinforcement materials, are generally temperature resistant and can retain their properties such strength and stiffness. On the other hand, most polymers, and particularly polyethylene, are highly sensitive to high temperatures. Increasing the temperature can lead to matrix softening, and consequently rapid reduction in the strength and stiffness. Therefore, at high temperatures, the effect of polymer softening and loss of the filler-matrix interaction can lead to significant degradation in the mechanical properties of the filled polymers (Cao et al. 2011).

2.10 Mechanical Deformation of Polymers

The mechanical deformation of polymers can be classified as time independent or time dependent. Depending on the response of the material after the deforming stress is removed, the time independent behaviour can be either elastic or plastic. Elastic behaviour is defined when the material returns to its original size and shape. Conversely, plastic behaviour occurs when the material does not return to its original dimensions when the deforming stress is released. Similarly, the time dependent behaviour can be either viscoelastic or viscoplastic. Viscoelastic deformation is a combination of elastic and viscous behaviour, while viscoplastic is a rate dependent plastic deformation. Viscoplastic deformation is a combination of permanent plastic deformation and creep, it is known also as viscoelastic-plastic deformation (Fischer-Cripps 2004)

2.10.1 Elastic Behaviour of Polymers

Nearly all materials exhibit elastic behaviour when subjected to low stress, and return to their original shape after the stress is removed. Many glasses, ceramics and thermosetting polymers exhibit this behaviour right up to fracture. The elastic modulus can be obtained from the slope of the elastic curve, which is described by Hooke's law ($\sigma = E\,\varepsilon$).

The basic mechanism of elastic deformation in polymers is an elongation of chains in the direction of the applied load. In semi-crystalline polymers, elastic behaviour occurs when the stress is applied to two adjacent chain-folded lamellae with an amorphous interlamellar phase between them. The material exhibits elongation of the tie chain and slide of the lamellas. The elastic modulus is obtained from the elastic properties of both crystal and amorphous phases. This deformation is reversible when the load is removed.

2.10.2 Plastic Deformation of Semi-Crystalline Polymers

Plastic deformation in semi-crystalline polymers is extremely complicated due to their multi-level hierarchical structure. To understand the plastic deformation in such polymers, the deformation mechanisms should be characterised at three different scale levels: micro, meso and macro-scale (Oleinik 2003). The deformation mechanisms include the micromechanism of deformation of crystalline and amorphous phases at the micro-level, the deformation of spherulites, bending, rotation and fragmentation of lamellar stacks at the meso-level and the overall polymer behaviour at the macro-level, which can be obtained using standard tests such as tensile and creep tests.

The macromolecular nature of the polymer is a key factor to determine its plasticity. For example, crystalline and amorphous layers in semi-crystalline polymers are connected by strong covalent bonds crossing the crystal-amorphous interface (tie molecules). Therefore, it is impossible to separate lamella from the adjacent amorphous layer. As a result, simultaneous and consistent deformation is occurring for lamellae and adjacent amorphous layers and the influence of each deformation on the other cannot be neglected, which increases the complexity of the deformation.

Verker et al. (2013) introduced a simple description of the deformation of a semi-crystalline polymer in two stress directions, towards the lamella side and towards the lamella surface, as seen in Figure 2.8. For the former, the figure shows two adjacent chain-folded lamellae with an amorphous interlamellar phase between them. When the stress is applied, elongation of the tie chain and stretch and slide of the lamellas occur, which is an elastic deformation, as seen in Figure 2.8-1B. At higher stress, plastic deformation begins with the unfolding of lamellas and separation of crystal block segments, as shown in Figure 2.8-1C. This is followed by the orientation of the segments and tie chains in the direction of the tensile stress, Figure 2.8-1D. Similar deformation occurs when the load is applied toward the lamella surface; however, in the elastic region the elongation of the tie chains is combined with contraction of the lamella segments, as seen in Figure 2.8-2B. The plastic deformation starts with separation of crystalline lamella block segments, as shown in Figure 2.8-2C. This is followed by elongation of crystalline lamella to form an aligned morphology, as seen in Figure 2.8-2D.

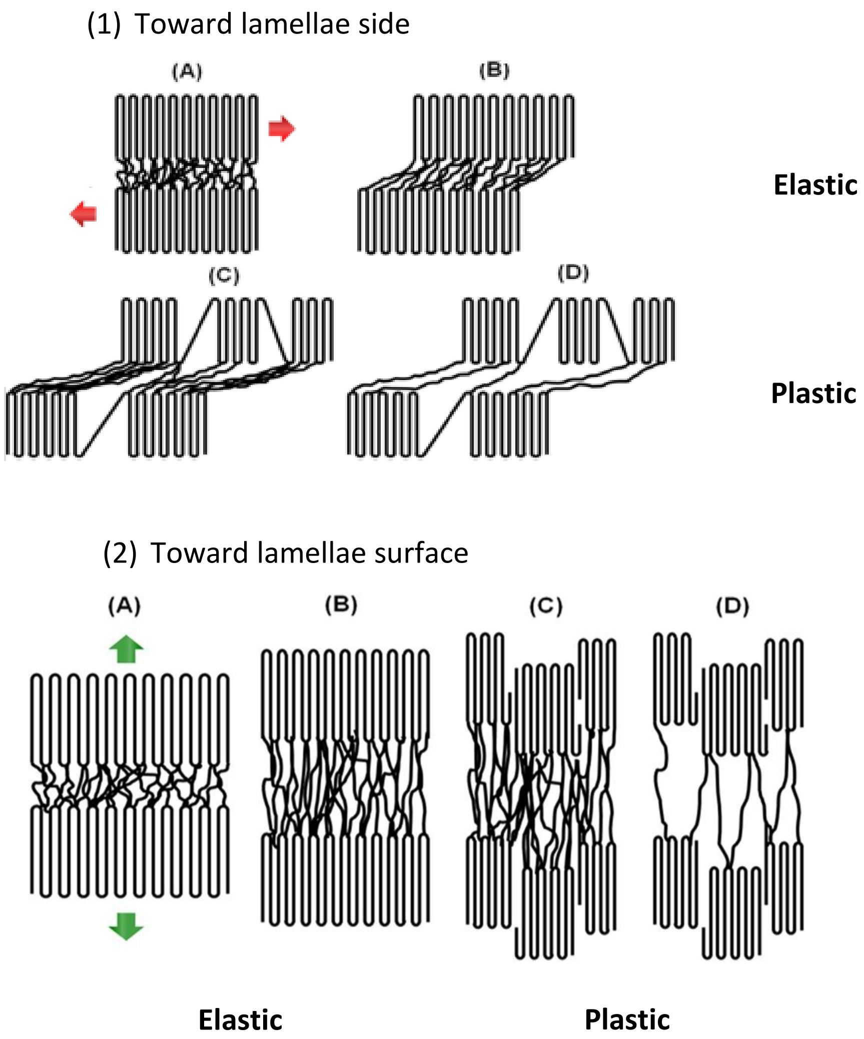

Figure 2.8: Schematic diagrams of the deformation in semi-crystalline polymers in different stress directions (Verker et al. 2013).

Although, various studies have been carried out to describe the plastic deformation of semi-crystalline polymers, a clear explanation has still not been achieved. The next section will describe in detail the most convincing interpretations of the deformation in semi-crystalline polymers, as agreed by many researchers (Bartczak and Galeski 2010; Pawlak et al. 2010; Thomas et al. 2009; Thomas et al. 2007; Oleinik 2003).

2.10.2.1 Deformation of Crystalline Phases

Bartczak and Galeski (2010) reported that two approaches can be used when considering the deformation of the crystalline phase. The adiabatic approach considers the simultaneous melting and recrystallization of polymers whereas the crystallographic approach considers dislocation nucleation and glide. The latter is considered to be more important according to several experimental studies (Bartczak et al. 1992; Lewis et al. 1972; Young et al. 1973). Unlike the plastic deformation of many materials, polymers exhibit large deformation accompanied with cavitation and voiding, which destroys the crystals.

The most important deformation in the crystallographic mechanism is the slipping of crystal blocks along a slip plane. The slip starts after a certain level of the critical resolved shear stress is reached. Crystallographic slip can be classified into chain slip or transverse slip, as seen in Figure 2.9. For chain slip, the dislocation glide occurs only along a plane that is parallel to the chain axis, while the glide direction is perpendicular to the chain axis in the transverse slip. In a tensile test, due to the slip between two crystals along a single plane between them, shear rotation of crystals can occur in the direction of the tensile axis. Similar to most crystalline materials, screw and edge dislocations can occur in semi-crystalline polymers, however, in polyethylene, the nucleation of screw dislocation is more likely to occur than edge dislocation, which then controls the rate of plasticity (Bartczak and Galeski 2010). Oleinik at al. (2012) concluded that the thermodynamic quantities of polyethylene are linearly dependent on the degree of crystallinity. Also, the work that is necessary to deform the crystalline phase is higher than the work necessary to deform the amorphous phase.

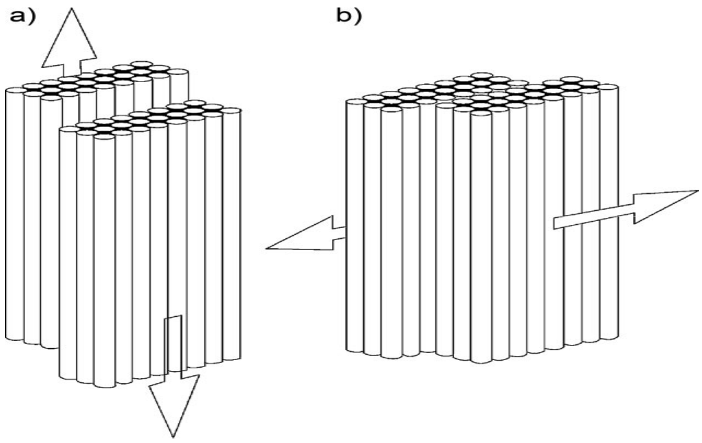

Figure 2.9: Two types of crystallographic slip of the polymer crystals: (a) chain slip (longitudinal) and (b) transverse slip (Bartczak and Galeski 2010).

2.10.2.2 Deformation of Amorphous Phases

There are three main deformation mechanisms for the deformation of the amorphous phase in semi-crystalline polymers. These are interlamellar shear, interlamellar separation and lamellae stack rotation, as shown in Figure 2.10 (Bartczak and Galeski 2010). Interlamellar shear occurs when the lamellae slip parallel to each other. It is considered to be an easy deformation mechanism for polymers tested above their glass transition temperature (T_g). This is an important mechanism in the deformation of semi-crystalline polymers with low Tg such as polyethylene (T_g ~ -120°C). Interlamellar separation occurs when a tensile stress is applied perpendicular to the lamellar surface. This deformation mechanism is responsible for the formation of the cavities that leads to the formation of voids or crazes, and is also responsible for the plastic flow of the amorphous phases. Lamellar stack rotation occurs when the lamellar stacks are surrounded by an amorphous region during the application of stress.

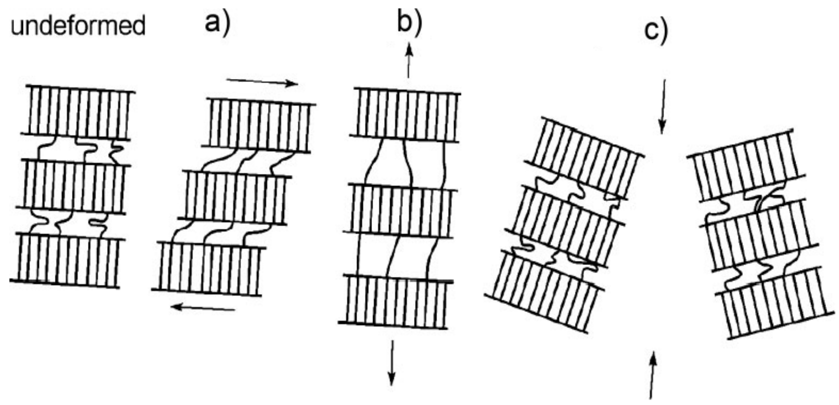

Figure 2.10: Deformation modes of the amorphous phases a) interlamellar shear, b) interlamellar separation, c) lamellar stack rotation (Bartczak 2010).

2.10.2.3 Deformation of Crystalline and Amorphous Phases

The amorphous and crystalline phases are connected strongly to each other by numerous molecular ties, thus deformation mechanism in semi-crystalline polymers is a combination of both crystalline and amorphous deformation mechanisms. The deformation sequence begins with a rapid increase in the stresses in the amorphous region. These stresses are then transferred to the crystalline region causing a plastic flow of the crystalline phase when the critical resolved shear stress is reached. This is followed by slip deformation of the crystalline phase, which controls the whole deformation at this stage. Later, the deformation is controlled by simultaneous deformation of both amorphous and crystalline phases until failure of the crystalline phase.

Hiss et al. (1999) developed a scheme to describe the tensile deformation mechanisms of polyethylene. This scheme can also be considered as a universal deformation scheme for semi-crystalline polymers (Bartczak 2010). It consists of four main points at various strains, as seen in Figure 2.11. These can be described as follows:

(A) The end of the elastic range (ε=0. 02).

(B) Yielding, where the crystallographic slip and interlamellar shear begins (ε=0. 1)

(C) A rapid increase in the stresses in the amorphous regions, which is transferred to the lamellae, resulting in slip, bending and fragmentation of the lamellae (ε=0. 6)

(D) Full stretch of the network of the amorphous phases, this dominates the deformation. Thus, it increases the applied stress on the crystals, which leads to fragmentation of the crystals to form the final fibrillar structure (ε=1).

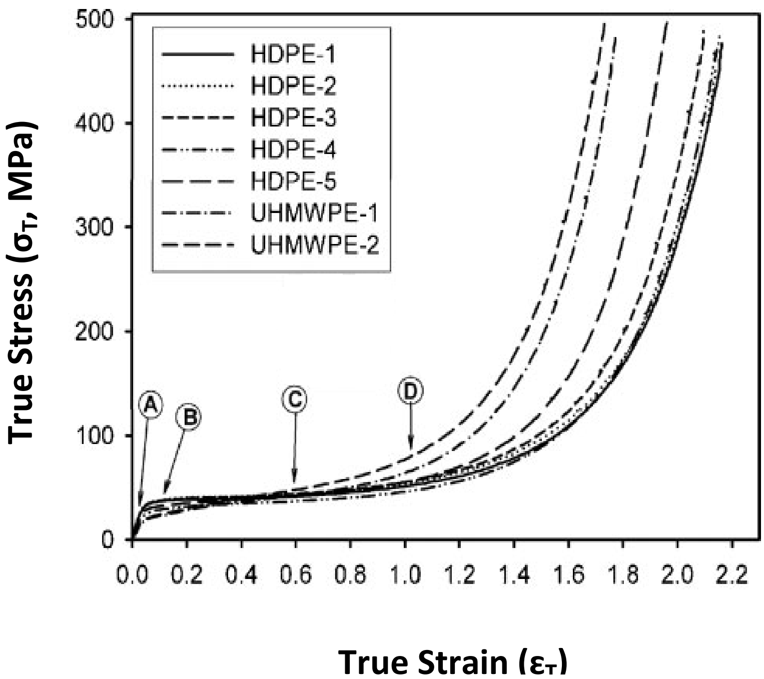

Figure 2.11: Critical points on the true stress-true strain curves of polyethylene samples (Bartczak 2010).

2.10.3 Fracture Behaviour of Polymers and Polymer Nanocomposites

Failure in polymers depends on the polymer properties. Brittle polymers show brittle fracture, where sudden disruption of the structure occurs. However, most polymers exhibit ductile failure, where gradual tearing leads more slowly to complete failure. The fracture surface of polymer-based nanocomposites can be used to analyse the interaction between the nanoparticle and the polymer matrix. Kim et al (2012) investigated the effect of surface modification of CNT on the adhesion with a PET matrix. They used the SEM image shown in Figure 2.12 as evidence of the improved CNT-matrix adhesion. It can be seen that there are pulled out CNTs while their ends still embedded in the polymer matrix, which indicates a good interaction between the CNT and the PET, at least in one end. Various studies have used images of embedded ends of CNTs or bridging of micro-cracks as evidence for good matrix-filler adhesion (Cho and Daniel 2008; Thostenson and Chou 2002).

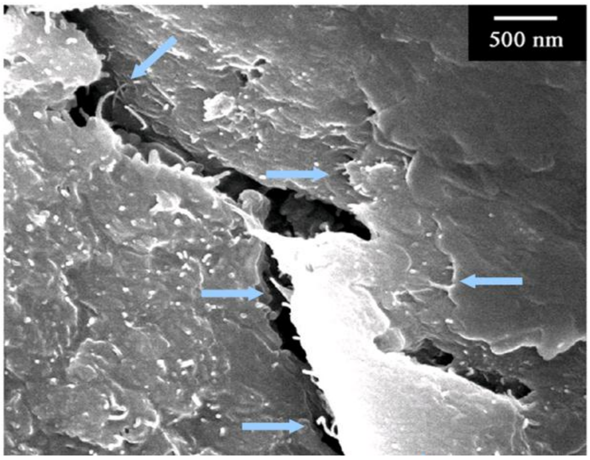

Figure 2.12: SEM image of the fracture surfaces of a PET nanocomposite containing 1.0 wt% of c-CNT, The arrows indicates that nanotubes were pulled out while their ends still embedded in the PET matrix or they were bridging the local micro-cracks in the nanocomposite (Kim et al 2012).

On the other hand, Lau et al. (2003) showed SEM images as evidence of poor adhesion between a polymer resin and CNTs. Pulled-out CNTs can be observed in

Figure 2.13a and the impression of pulled out CNTs can be seen in the matrix, Figure 2.13b. This indicates poor interaction between the polymer resin matrix and the CNT. This technique was used in the current study to evaluate the interaction between CNT, CB and clay nanoparticles and a polyethylene matrix. This is discussed further in Chapter 5.

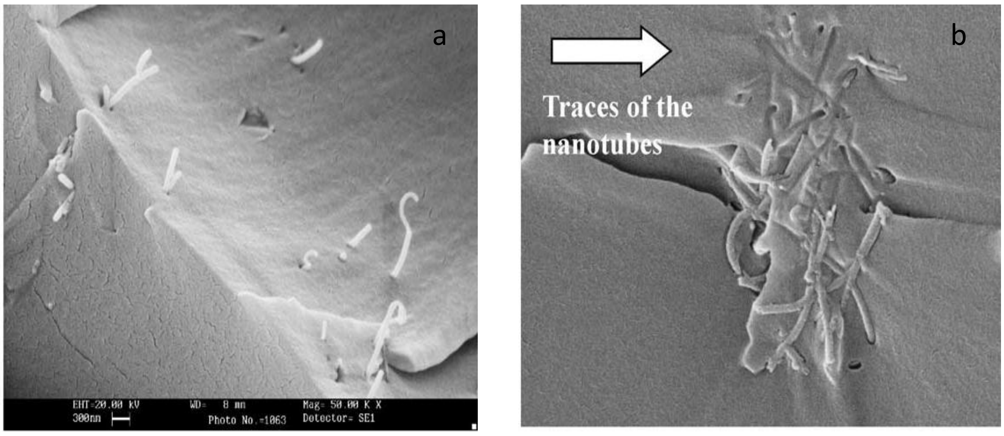

Figure 2.13: SEM images of fracture surfaces of polymer resin nanocomposites a) CNTs pulled-out from the matrix and b) impression of pulled out CNTs.

2.10.4 Creep Behaviour of Polymers

Creep is a time-dependent deformation that occurs in a solid material under the effect of a constant stress that is lower than the yield stress. Schematic curves of the creep behaviour of a material subjected to a constant stress are shown in Figure 2.14. Increasing the stress or temperature will increase the creep strain rate. The creep curve can be divided into three stages, primary or transient creep (stage I) where the strain rate decreases with increasing time, secondary or steady-state creep (stage II) where the strain rate remains essentially constant, and tertiary creep (stage III) where the strain rate increases rapidly to fracture (Shames et al. 1997).

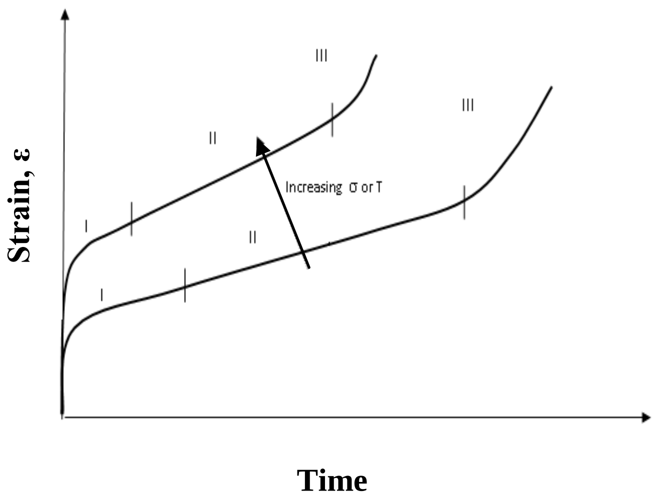

Figure 2.14: Strain versus time in a constant stress creep test.

In practice, the time periods that are spent in primary and tertiary stages are usually much shorter than that of steady-state. Therefore, most of the creep strain accumulates in steady state, and as a result creep experiments are usually correlated by studying the effect of stress (σ) and temperature (T) on the steady state creep rate ($\dot{\varepsilon}_s$). In Figure 2.15, a schematic plot of ln $\dot{\varepsilon}_s$ against ln σ; shows that at a constant stress, the steady state creep rate increases with increasing temperature. Furthermore, the steady state creep rate increases with increasing stress when the temperature remains constant. At constant temperature, a power law relationship between $\dot{\varepsilon}_s$ and σ can be written as

$$\dot{\varepsilon}_s = A\sigma^n \tag{2.3}$$

where, *A* is a constant and a function of temperature, and n is the stress exponent as represented by the slope of each line in Figure 2.15, which is independent of temperature.

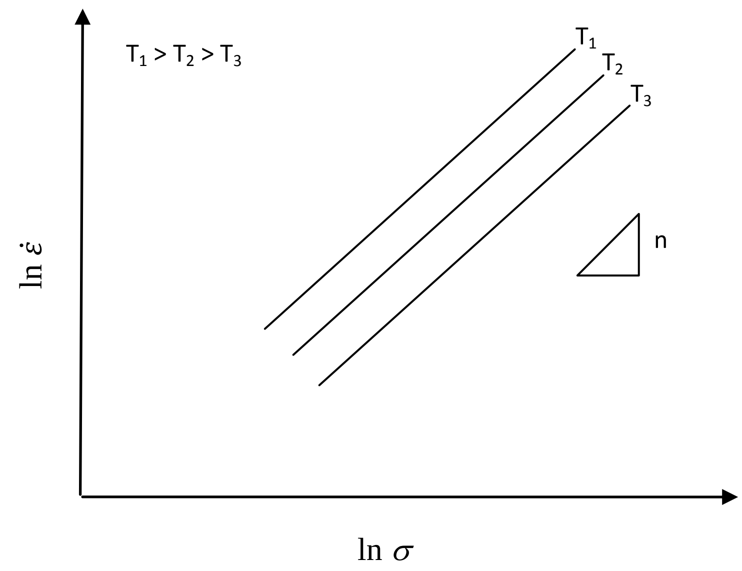

Figure 2.15: Stress and temperature dependence of steady state creep rate.

Viscoelastic materials exhibit both elastic (σ = E ε) and viscous ($\dot{\varepsilon} = \frac{\sigma}{\eta}$) behaviour when subjected to constant stress or strain. The viscoelastic behaviour of soft materials such as biomaterials, polymers and polymer nanocomposites is not fully understood; therefore finding a suitable test type and reasonable test parameters such as load, strain, load rate and strain rate is of significant scientific and practical interest.

Polymer based nanocomposites have more complex structures than bulk polymers or blends due to the existence of the additional strengthening nanoparticles. Various kinds of nanofiller have been utilised to enhance the mechanical properties of polymers such as elastic modulus, tensile strength, roughness, wear resistance, and viscoelastic properties, as discussed in Section 2.8.3. It is known that thermoplastic polymers have generally poor creep resistance, which can limit their application. Creep deformation is dependent on the mobility of polymer chains (Zhou et al. 2007; Vlasveld et al. 2005). The addition of nanoparticles can restrict the chain mobility, and consequently improve the dimensional stability and the lifetime of polymers (Yang et al. 2006). Various recent studies have reported that the creep resistance of thermoplastics can be significantly increased by the incorporation of small amounts of nanoparticles (Dai et al 2013; Jia et al. 2011; Zhou et al. 2007; Yang et al. 2007; Yang et al. 2006; Ranade et al. 2005; Zhang et al. 2004).

Various techniques can be used to determine the viscoelastic behaviour of polymers, such as tensile creep tests, dynamic mechanical thermal analysis (DMTA) and depth sensing indentation (Ward et al. 2004; Dub et al. 2008). All these techniques are used in the current study.

2.11 Constitutive Modelling of Creep Behaviour

Numerous constitutive models have been developed to describe the viscoelastic behaviour of polymers, composites and nanocomposites under various loading conditions (Dai et al 2013; Tang et al. 2012; Xianzhong and Jinping 2011; Jia et al. 2011; Jain and Nanda 2010; Yang et al. 2006; Ranade et al. 2005; Hasan and Boyce1995). Phenomenological models, consisting of combinations of elastic spring (obeying Hooke's law) and viscous dashpot (obeying Newton's law) elements can be used to represent a range of observed viscoelastic behaviour depending on the arrangement of the spring and dashpot elements. These models include the Maxwell model, Kelvin-Voigt model, Zener model, standard linear solid (SLS), Burger's model, generalized Maxwell model and generalized Kelvin-Voigt model, Figure 2.16. In the Maxwell model, Figure 2.16a, the elastic spring is connected in series with a viscous dashpot to describe the viscoelastic behaviour in a relaxation test. The Kelvin-Voigt model, Figure 2.16b, consists of spring and dashpot elements connected in parallel, which can be used to represent creep behaviour (Ward 1983; Randall and Consiglio 2000; Strojny and Gerberich 1998; VanLandingham et al. 2001; Findley et al. 1989; Peric and Dettmer 2003; Fischer-Cripps 2004; Shames and Cozzarelli 1997).

Creep modeling and analysis is important to characterize the time dependent deformation of polymeric materials. Burger's model, which is a combination of Kelvin-Voigt and Maxwell elements, Figure 2.16d, is the most commonly used model to describe the linear viscoelastic behaviour of composites (Dai et al 2013; Jia et al. 2011; David et al. 2011; Huang et al. 2011; Yang et al. 2006; Ranade et al. 2005). The total strain as a function of time can be obtained from Equation 2.4 (Ward 1983):

$$\varepsilon_B = \frac{\sigma}{E_M} + \frac{\sigma}{E_K}\left(1 - e^{-t/\tau}\right) + \frac{\sigma}{\eta_M} t \tag{2.4}$$

where E_M and η_M are the elastic modulus and viscosity of the spring and dashpot respectively in the Maxwell model. $\tau = \eta_K/E_K$ is the retardation time, which is the time for 63.2% or ($1-e^{-1}$) of the total deformation in the Kelvin unit to occur. η_K and E_K are the elastic modulus and viscosity of the spring and dashpot elements in the Kelvin - Voigt model, respectively. The Maxwell spring parameter, E_M represents the instantaneous strain that can be completely recovered after the load is removed. The Kelvin-Voigt spring parameter, E_k reflects the retardant elasticity or the stiffness of the amorphous phase. Both E_k and η_k can be used to describe the delayed viscoelastic deformation. The irrecoverable creep strain is represented by the viscous parameter of the Maxwell model, η_M. An increase in η_M can lead to lower flow of the dashpot and a reduction in the permanent deformation.

The creep rate of Burger's model ($\dot{\varepsilon}_B$) can be determined from the differentiation of Equation (2.4) as follows:

$$\dot{\varepsilon}_B = \frac{\sigma_0}{\eta_M} + \frac{\sigma_0}{\eta_K} e^{-t/\tau} \tag{2.5}$$

The creep rate can reach a constant value at long time scales of:

$$\dot{\varepsilon}_\infty = \frac{\sigma_0}{\eta_M} \tag{2.6}$$

Huang et al. (2011) stated that Burger's viscoelastic model was in good agreement with their transient creep data for a range of polymeric materials. David et al. (2011) employed various viscoelastic models (one-term generalized Maxwell model, two-term generalized Maxwell model and Burger's model) to study stress relaxation and to predict the long time response of a Twaron fabric/natural rubber composite.

They found that Burger's model gave the most accurate characterisation of the material response.

For polymer-based nanocomposites, Dai et al. (2013) studied the effect of orientation of polymer chains and nanotube alignment on the creep resistance of polycarbonate/CNT nanocomposites at elevated temperature using Burger's model. Jia et al. (2011) investigated the creep behaviour of polypropylene nanocomposites using Burger's model. Also, Ranade et al. (2005) used a modified Burger's model to study the non-linear time dependent creep of polyethylene/clay nanocomposites. The model was able to describe the viscoelastic behaviour of the material. Therefore, in this work, Burger's model was used to characterise the viscoelastic behaviour of the polyethylene nanocomposites.

In order to describe viscoplastic behaviour, a friction element can be combined with elastic and/or viscous elements to indicate plasticity, as shown in Figure 2.17. The viscoelastic-plastic model shown in Figure 2.17a represents a material that behaves like standard linear solid model below yielding and then acts as Burger's model after yield. The elasto-viscoplastic model shown in Figure 2.17b describes the behaviour of a material that act elastically until yielding and viscoelastic Maxwell behaviour after yielding. It can be seen that the incorporation of a friction element enable the modelling of material where there is a step change in the behaviour, such as when a new deformation is triggered. Further extension to these modules can be made by the insertion of non-linear elements (e.g. $\sigma = E\ \varepsilon^n$) or by combing elements in parallel to form a prony series representing variation in the retardation time due to variations in molecular chain length (e.g. the generalized Maxwell model). It can be seen that various types of behaviours can be represented by various combination of these basic elements and the model selected should be inferred by experimental test results.

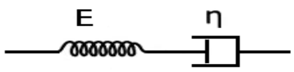

(a) Maxwell Model

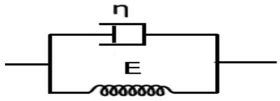

(b) Kelvin-Voigt Model

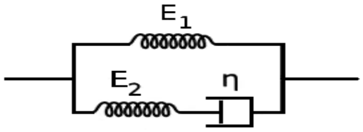

(c) Zener Model

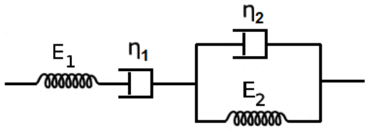

(d) Burger's Model

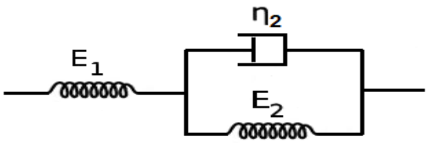

(e) Standard Linear Solid Model

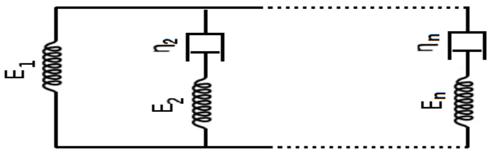

(f) Generalized Maxwell Model

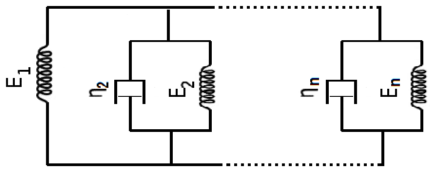

(g) Generalized Kelvin-Voigt Model

Figure 2.16: Some of the more common models which can be used to describe viscoelastic behaviour.

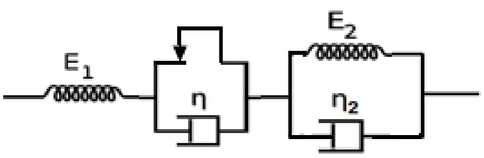

(a) Viscoelastic-Plastic Model

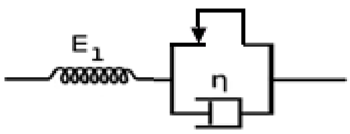

(b) Elasto-Viscoplastic Model

Figure 2.17: Examples of phenomenological models to describe viscoplastic behaviour

2.12 Depth Sensing Indentation of Polymers

Depth sensing indentation (DSI), instrumented indentation or nanoindentation tests have been widely used as a powerful way to evaluate the near surface properties of viscoelastic materials such as biological tissues, polymers and polymer nanocomposites in an extremely small area, using various loading and unloading pressures and loading and unloading rates (Shokrieh et al. 2013; Aldousiri et al. 2011; Olesiak et al. 2010; Wang et al. 2010; Yusoh et al. 2010; Hongbing et al. 2006; Dhakal et al. 2006; Shen et al. 2006; Cheng and Cheng 2005; Sun et al. 2005; Cai et al. 2004; Shen et al. 2004; Beake et al. 2002). The indentation hardness and elastic modulus are two important material properties that can be obtained using this technique (Oliver et al. 1992; Fischer-Cripps 2006). However, this technique has also been adopted to measure other mechanical properties such as creep (Huang et al. 2011; Tehrani et al. 2011; Zhang et al. 2004; Lucas and Oliver 1999; Lu et al. 2009), strain hardening (Yang et al. 2006), strain rate sensitivity (Fujisawa et al. 2008; Schwaiger et al. 2003), fracture behaviour of brittle materials (Pharr et al. 1993) and scratch properties (Yusoh et al. 2010; Wang et al. 2010).

The basic idea of the DSI test is the application of an indenter into the surface of a material whilst measuring force and displacement, with control over loading parameters and indenter shape. The force can be accurately applied down to a few milli-Newtons over an area in the micro to nanometre scale. Various indenter types can be used, such as a sharp triangular based pyramid indenter (Berkovich), flat-ended punch, conical and spherical indenters. Figure 2.18 shows schematic curves for a nanoindentation test using a Berkovich indenter. The load (P) is applied at a specific loading rate until it reaches the pre-defined maximum load at point (A). During the unloading part, the behaviour of the material can be classified as:

- Elastic, when the deformation is fully recovered (A-O).
- Elastic-Plastic (time independent) behaviour for the unloading curve (A-B).
- Viscoelastic (time dependent) behaviour for the unloading curve (A-C).
- Plastic behaviour for the unloading curve (A-D).

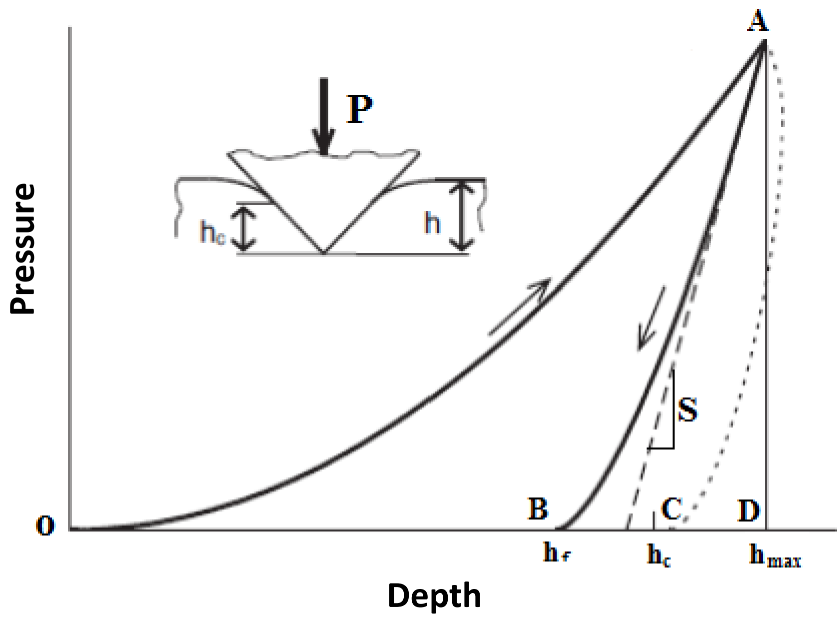

Figure 2.18: A schematic plot of load vs. depth curves of nanoindentation experiment, where h_{max} is the depth at the maximum load, h_f is the final depth after unloading, h_c is the contact depth and S is the stiffness (Menčík et al. 2011).

2.12.1 Standard Load-Unload Test for Polymers

The use of the DSI technique with polymers is a challenge due to the complex structure and deformation mechanisms involved. Both time independent and time dependent deformation can be seen in the indentation of polymers. The calculation of the indentation hardness and the indentation elastic modulus in the DSI technique depends on the assumption that the initial unloading part is elastic. The viscoelastic curve (A-C) that is shown in Figure 2.18 is the most common behaviour for polymers in nanoindentation tests (Altaf et al 2012; Briscoe et al. 1998; Ngan and Tang 2002; Cheng and Cheng 2005; Lu et al. 2009). This can lead to a negative slope (Oyen and Cook 2003), which invalidates the assumption of elastic unloading, and leads to a major error in the calculation of contact depth and contact stiffness. Therefore, applying appropriate loading and unloading rates and holding times at maximum load are important factors that should be considered to minimize the effect of viscoelastic behaviour in the unloading curve when testing polymers (Yang and Zhang 2004). Therefore, it is common practice to eliminate or minimize the creep effect through a rapid unloading rate (Cheng et al. 2005) or a long dwell/holding time at maximum load (Briscoe 1998; Chudoba and Richter 2001). In the current study, various loading and unloading and dwell periods were applied to find the optimum test parameters to obtain an initial elastic segment during the unloading. The viscoelastic behaviour was analysed from the response of the material to the applied load during holding. This will be discussed in detail in Chapter 7.

2.12.2 Analysis of DSI Data

Dorner and Nix (1986) and Oliver and Pharr (1992) developed methods to calculate the value of indentation hardness and indentation elastic modulus for elastic-plastic materials based on relationships developed by Sneddon (1965) for the penetration of an elastic half space by an axisymmetric punch. Dorner and Nix method assumes that the contact area remains constant when the indenter is initially unloaded. This method is only appropriate for a flat indenter. The Oliver and Pharr method fits the unloading curve to a power law with, exponents ranging from 1.2 to 1.6. This method has been widely used for the characterisation of the mechanical behaviour of polymer films (Strojny et al. 1998; Beake et al. 2002; Hodzic et al. 2000) and polymer nanocomposites (Shokrieh et al. 2013; Aldousiri et al. 2011; Olesiak et al. 2010; Wang et al. 2010; Yusoh et al. 2010; Hongbing et al. 2006; Dhakal et al. 2006; Shen et al. 2006; Cheng and Cheng 2005; Sun et al. 2005; Cai et al. 2004; Shen et al. 2004; Beake et al. 2002; Tehrani et al. 2010).

However, the ability to measure accurate properties using nanoindentation is limited by the viscoelastic behaviour of polymers. The Oliver and Pharr method assumes initial elastic behaviour during the unloading with no viscous deformation effect. Creep influences the maximum indentation depth and the gradient of the upper portion of the unloading curve, and then affects the results of stiffness and modulus. Therefore, the influence of creep should be eliminated before applying the Oliver and Pharr method to the unloading curve of a polymer. The creep behaviour in the nanoindentation test depends significantly on the loading and unloading rates as well as the creep rate of the material. In order to minimize the influence of creep on the measurements of the indentation hardness and indentation elastic modulus and make them more accurate, experimental parameters should be chosen carefully. Therefore, in this study, rapid unloading and a holding period at maximum load were applied to minimize the effect of creep of the polyethylene specimens.

2.12.3 DSI Creep Test

In DSI experiments, a creep test can be used to study the localised viscoelastic behaviour of materials. The depth vs. time curve is similar to that for bulk tests, which is discussed in Section 2.10.4. According to Mayo and Nix (1988), the indentation creep strain rate ($\dot{\varepsilon}_i$) can be calculated from the change in indentation depth with respect to time (dh/dt) using the following equation:

$$\dot{\varepsilon}_\mathrm{i} = \mathrm{k}\frac{\left(\mathrm{dh}/_{\mathrm{dt}}\right)}{\mathrm{h_p}} \tag{2.7}$$

where (k) is a dimensionless constant (≈1) and (hp) is the plastic depth of penetration. The mean pressure (P_m) under the indenter is obtained by dividing the load (P) by the projected contact area, which for a Berkovich indenter is:

$$\mathrm{P_m} = \frac{\mathrm{P}}{24.5\mathrm{h_p^2}} \tag{2.8}$$

The creep constants can then be calculated from log ($\dot{\varepsilon}_i$) vs. log (P_m) plots.

A number of studies have been carried out to investigate the creep behaviour of various materials using the nanoindentation technique (Li and Ngan 2004; Goodall and Clyne 2006; Alkorta et al. 2008; White et al. 2005; Abetkovskaia et al. 2010). However, Goodall and Clyne (2006) compared the creep parameters from the bulk creep test with the DSI creep parameters and no correlation was found. In this study, the relationship between the bulk creep behaviour and the nanoindentation creep behaviour is described in Chapters 6 and 7.

2.13 Summary

Polyethylene is a thermoplastic material with various types such as UHMWPE and HDPE. Each type has unique properties, for example UHMWPE possesses high toughness, high wear and chemical resistance. However, it is more prone to creep than HDPE, which exhibits a high creep resistance. Recently, blending techniques have been used to obtain desired material properties or to reduce a weak property in the neat polymer.

Due to the extremely high molecular weight of UHMWPE, and subsequent high viscosity, it is difficult to process using conventional techniques such as extrusion, injection or compression moulding. Various studies have been carried out to reduce the viscosity of UHMWPE, which can be achieved by blending with a lower molecular weight material. Improved material processability can be obtained by the addition of a polymer with lower viscosity such as HDPE, LDPE or LLDPE. However, this results in a reduction in the original properties of the UHMWPE such as wear resistance and toughness. This reduction can potentially be mitigated, whilst retaining the improved processability, by the addition of nano-reinforcement. Various nanoparticles can be incorporated into the blend matrix to enhance its properties. These nanoparticles can be classified according to their geometry into three categories, fibrous (1D), layered (2D) or particulate (3D). However, the effect of each type depends on several factors such as the host polymer, the nanoparticle geometry, the dispersion and the filler-matrix interaction. Novel material properties can be achieved by combining both an appropriate material selection (filler and matrix) and processing method.

Various processing techniques can be used to produce polymer-based nanocomposites, the choice mainly depending on the material viscosity. Common processing techniques for polymer-based nanocomposites are *in situ* polymerisation, melt and solvent processing. However, use of conventional processing techniques such as extrusion, injection or compression moulding can be a particular challenge for high viscosity polymers.

Polymer-based nanocomposites properties can be characterised from micro to macro scales using standard techniques. Microstructural features can be analysed using techniques such as SEM, TEM, AFM and XRD. The mechanical properties, rheology or tribology can be obtained using tensile test, rheometer, wear and scratch tests.

The deformation mechanisms of polymers are extremely complicated and the addition of nanoparticles can increase this complexity. The mechanical properties of polymer-based nanocomposites are dependent on the deformation mechanisms when subjected to an external load. The stress-strain behaviour of a material, which can be obtained from a tensile test is one of the most important material responses. It can reveal a number of the mechanical properties of the material such as elastic modulus, yield stress, failure strength, and strain at failure. Correlation between the material properties and testing conditions, such as temperature and strain rate, can also be determined using tensile tests.

The deformation mechanisms of semi-crystalline polymers, such as the polyethylene materials used in this investigation, are dependent on the deformation of the crystalline and amorphous phases. However, these phases are strongly connected together, and thus have a significant effect on each other during deformation, which increase the complexity of the deformation mechanism. The incorporation of nanoparticles can lead to significant changes in the microstructure, and consequently the deformation mechanism, which can be summarized in the following points:

- There is a large difference between the properties of the nanoparticle and the properties of the host matrix such as stiffness and strength, which can lead to variation in the response to deformation.
- The presence of the interface area acts as a new phase with different properties.
- Poor dispersion of nanoparticles can act as defects, which affects the distribution of stress and failure mechanism.

- Filler-matrix interaction can lead to a robust structure with strong bonding or a source of voids and cracks when the interaction is weak.

The deformation mechanism of polyethylene, as developed by Hiss et al. (1999), is considered a universal deformation scheme for semi-crystalline polymers. This scheme was used as a base to describe the deformation mechanism of the polyethylene-based nanocomposites used in this work. Analysis of the fracture surface after tensile failure has been used in various studies to evaluate the filler-matrix interaction and is also employed in this work.

Time-dependent deformation can occur when polymeric materials are subjected to constant load. This viscoelastic deformation is dependent on the mobility of the polymer chains. Mobility can be increased by increasing the temperature or restricted by the addition of reinforcement, such as the nanofiller used in this work. Various constitutive models can be used to describe the viscoelastic behaviour and provide an interpretation of the deformation mechanism.

The micro-scale properties of the viscoelastic material are important when the material is considered for specific applications such as total joint replacement and body armour protection. It is also important to investigate the temperature-dependent properties of certain materials at their in-service temperature to avoid unexpected behaviour or failure. DSI is a powerful technique that can be used to evaluate such properties. These include indentation hardness, indentation elastic modulus, elastic, viscoelastic and plastic behaviour. The relationships between the nanoindentation behaviour and various testing parameters such as temperature, load and depth rate can also be determined.

Conclusions

- Processing method parameters can significantly affect the morphology of the blend, and consequently the mechanical properties. According to the literature, the maximum temperature that has been used to mix UHMWPE with HDPE to date was 210°C (Xue et al. 2006; Abadi et al. 2010; Wood et al.

2010; Khasraghi and Rezaei 2013). This resulted in two distinct phases of UHMWPE and HDPE. Increasing the processing temperature may results in a more miscible blend and different mechanical properties than seen with the immiscible blends. The effect of processing method parameters on the blend properties and nanoparticle dispersion are investigated in Chapters 4 and 5, respectively.

- The dependence of heat generation during plastic deformation on strain rate, nanoparticle type and content, has not been investigated to date for rubbery polymer nanocomposites. This could potentially provide clear relationships between heat generation, strain rate and nanofiller due to the large strains to failure in these materials. Moreover, the effect of internal heat generation on the mechanical properties of polyethylene-based nanocomposites has not been investigated. These are some of the objectives of the current work, which will be discussed in Chapters 4, 6 and 8.
- To date, no work has been reported on the improvement of creep resistance in UHMWPE/HDPE blends by the incorporation of nanoparticles. Xue et al. (2006) found that the addition of CNT on UHMWPE/HDPE blend lead to lower creep resistance and proposed that this was due to the immiscible blend structure and the poor dispersion of the CNT. Thus, in the current work, two in-house processing methods were used to incorporate various nanoparticles into the UHMWPE/HDPE matrix to investigate the correlation between the morphology, the volume fraction of the filler, the ambient temperature and the creep resistance were investigated.
- To date, no work has been carried out to investigate the micro-scale properties of polyethylene-based nanocomposites at elevated temperatures by means of DSI. Therefore, in the current work, the dependence of the indentation properties of polyethylene-based nanocomposites on temperature was investigated.

Chapter 3
Experimental Methods

3.1 Introduction

Figure 3.1 provides an overview of the experimental methods used in this study. Materials were processed using two different methods, and compression moulded to form plaques. In order to characterise the mechanical properties of the polyethylene blends and their nanocomposites, several characterisation techniques were performed. These include bulk mechanical tests, microstructure analysis, thermal analysis and depth sensing indentation. Then, the results were analysed using various methods and software.

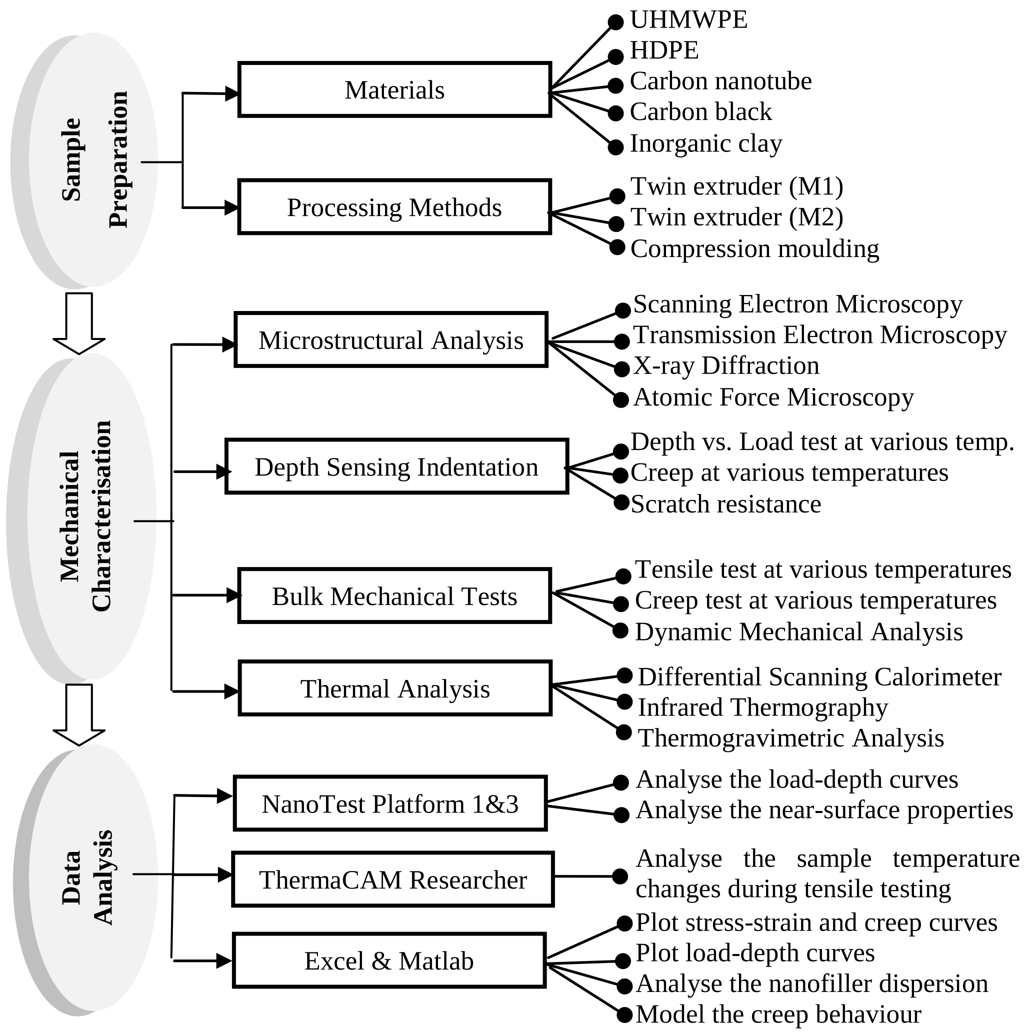

Figure 3.1: Experimental methods used in this study.

3.2 Sample Preparation

3.2.1 Materials

The materials tested in this study were UHMWPE/HDPE blended polymers with various nanofillers. Nascent UHMWPE powders (Sabic®UHMWPE3548) were purchased from SABIC (Sabic 2010) which had an average molecular weight of 3×10^{6} mol/g. HDPE powders (ExxonMobil ™ HDPE HMA014) were purchased from ICO Ltd (ExxonMobil Chemical Europe 2010). Carbon black (CB) powder with the commercial product name, black pearls ® 4040 (BP4040) and average particle diameter of 28 nm were provided by the Cabot Corporation, with density in the range of 1700-1900 kg/m^3 (Cabot Corporation 2007). Natural Hectorite nanoclay (BENTONE® HC Hectorite Clay) was supplied by Elementis Specialties Inc. in powder form, with an average particle size of less than 75µm and an average density of 2600kg/m^3 (Elementis Specialties Inc. 2010). Hectorite is a type of mineral clay that belongs to the Smectite group, formed from high silica content volcanic ash. The method by which the Hectorite Nanoclay is dispersed within the Polyethylene matrix is protected by patent WO/2010/106358 (Song et al. 2010). Multi-wall Nanotubes (NANOCYL™ NC7000) with an average outside diameter of 9.5nm and an average length of 1.5 µm, were provided by Nanocyl (Nanocyl 2009). Butylated hydroxytoluene and Tris (nonylphenyl) phosphate, supplied by Sigma-Aldrich (Sigma-Aldrich 2010), were used as primary and secondary antioxidants, to maintain the long term thermal stability and melt processing stability in processing method M2, respectively.

3.2.2 Processing

An in-house pre-mix technology was used to incorporate the nanofillers into the UHMWPE and HDPE powders. Nanoparticles were added to water, in a weight proportion of up to 3% for CNT and CB and up to 2% for clay. The pH was adjusted to pH 8.2 by adding aqueous sodium hydroxide solution. To ensure that the CNT and CB nanoparticles were dispersed and the clay nanoparticles were both exfoliated and dispersed, every mixture was then subjected to intense ultrasonic irradiation for 10 minutes. A 300 W ultrasonic horn at 20 kHz was used in this work. The suspension of dispersed nanoparticles was then mixed with twice the initial quantity of water, and polyethylene powder was added, such that the weight ratio of polyethylene powder to nanoparticle was 97 to 3 to form PE/3 wt. % nanoparticles. This mixture was stirred vigorously while being heated in a pressure vessel to 120°C at elevated pressure, and maintained at that temperature for 10 minutes with continuous stirring using a magnetic stirrer. During this period the nanoparticles adhere to the surfaces of the polyethylene powder, so there is no longer any nanoparticle in suspension. The mixture was then cooled to 5O°C. The water was separated from the polyethylene powder/nanoparticle using a filter, and the powder mixture was dried in an oven at 65°C for 12 hours. A twin-screw extruder, Figure 3.2 from Rondol Technology Ltd. (Staffordshire, UK) was then used to blend the UHMWPE and HDPE powders pre-mixed with CB, carbon nanotubes (CNT) or nanoclay to form nano-filled UHMWPE/HDPE blends with various nanoparticle contents, as shown in Table 3.1. A blend of 75 wt. % UHMWPE and 25 wt. % HDPE, abbreviated to U75H25, was used as the hybrid PE matrix to accommodate the nanofillers. Two processing methods (M1 and M2) were used and the mixing temperature was controlled using five zones from feeding port to die. The processing parameters are shown in Table 3.2.

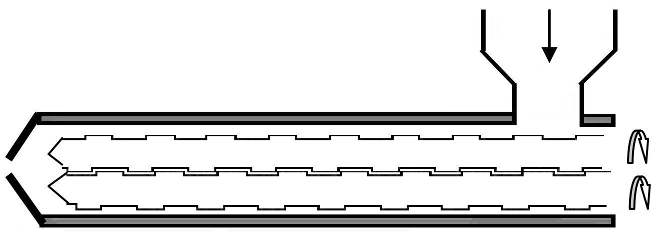

Figure 3.2: A twin-screw extruder.

Table 3.1: Nanofiller content.

Base Material	Filler	Filler Content (M1)	Filler Content (M2)
		wt. %	wt. %
U75H25	CB	0, 0.5, 1, 3	0, 0.5, 1, 3
U75H25	CNT	0, 0.5	0, 0.5, 1, 3
U75H25	clay	0, 0.5	0, 0.5, 1, 2

M1& M2 are two different processing methods

Table 3.2: Processing method parameters.

Processing Method	Extruder Speed (rpm)	Processing Temperature (°C)					
		Zone 1	Zone 2	Zone 3	Zone 4	Die	Cooling
M1	400	180	190	200	210	220	Water
M2	190	220	250	260	270	280	Water

Compression moulding, as illustrated in Figure 3.3, was used to mould the nanocomposite materials. The raw material was placed into a square mould (100 X 100 X 1.65 mm), and heated to 190°C, which is higher than the melting point of the composite (approximately 135°C). Various mould pressures (154, 232, 309, and 386 MPa) were investigated to optimise the properties of the material such as hardness and crystallinity. Various hold times at maximum pressure (10, 15 and 30 minutes) were also used to identify the most appropriate moulding parameters (Parasnis and Ramani 1998). The optimal moulding pressure and holding time were found to be 309 MPa and 15 minutes respectively, as indicated by the highest values of hardness and crystallinity. After compression moulding, the mould was cooled to room temperature using water cooling. The specimens were then cut from the plaques into dumbbell shape for tensile tests (this is shown in Section 3.5.1) using a die punch cutter and a square shape ($10mm^2$) for indentation tests.

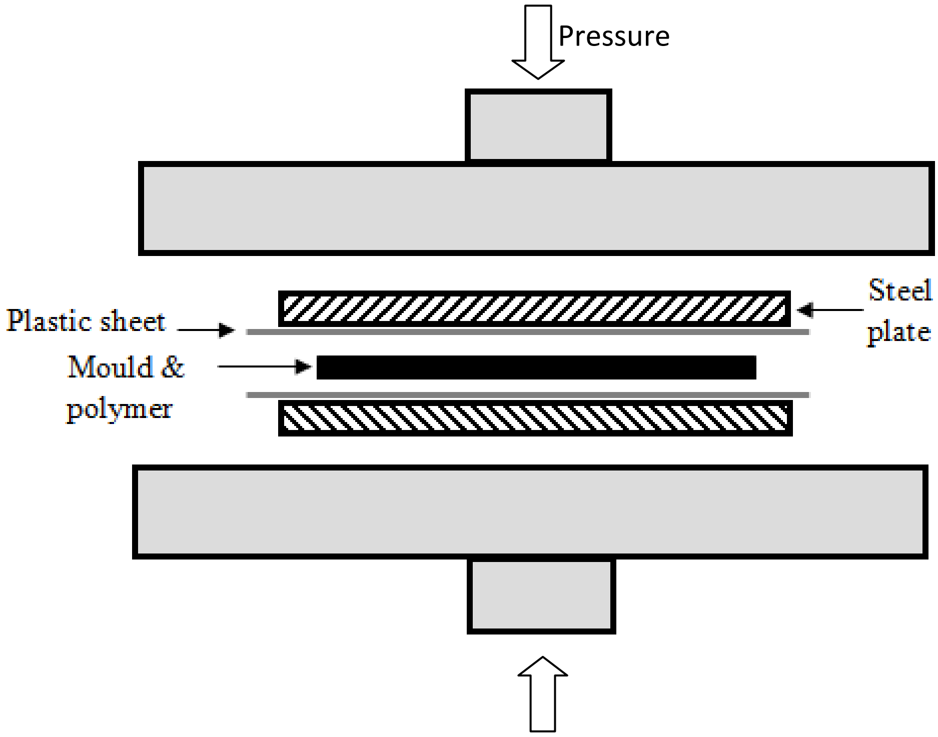

Figure 3.3: Schematic draw for a compression mould.

3.3 Characterisation of Nanoparticle Dispersion

3.3.1 Scanning Electron Microscopy (SEM)

The surface morphology was investigated using a LEO 440 Scanning Electron Microscopy (SEM) from Leo Electron Microscopy Ltd (Cambridge, UK) and a Philips XL30 ESEM-FEG from FEI Company (Eindhoven, The Netherlands). The dispersions of the CNT, CB and clay nanoparticles were studied after fracturing samples in liquid nitrogen, then coating them with platinum. In the analysis of the fracture surface after tensile testing, the fractured surface was cut from the rest of sample, mounted on an aluminium substrate and coated with platinum.

3.3.2 Transmission Electron Microscopy (TEM)

A JEOL 2000FX Transmission Electron Microscope (TEM) from JEOL Ltd. (Welwyn Garden, UK) was also used to analyse the dispersion of CB, CNT and clay nanoparticles in the blend matrix. A PC controlled ultra-microtome with a diamond knife from RMC products, Boeckeler instruments (Arizona, USA) was used for specimen cutting. The specimen and knife temperatures were set at -120 and -100^{o}C, respectively. The final section thickness was 90 nm using a 1mm/s cutting speed. The sectioned sample was mounted on a standard copper grid ring.

3.3.3 X-ray Diffraction (XRD)

X-ray Diffraction (XRD) patterns were obtained using a Philips X`Pert X-ray diffractometer (anode 40kV, filament current 35 mA) with Nickel-filtered Cu-Kα_1 (λ=0. 1542 nm) radiation at a scan speed of 1^{o}/min from the PANalytical company (Almelo, The Netherlands).

3.3.4 Atomic Force Microscopy (AFM)

A Dimension 3100 Atomic Force Microscopy from Veeco Instruments Inc. (Cambridge, UK) was used to analyse the surface roughness of the nanoindentation specimens. A sharp tip (in the range of 5-10 nm) attached to a cantilever was brought onto the specimen surface using tapping mode. The data were analysed using the Nanoscope software, which was also provided by Veeco Instruments Inc.

3.4 Depth Sensing Indentation (DSI)

The indentation experiments in this work were performed on 10 x 10 x 1.65 mm specimens using a NanoTest 600 from Micro Materials Ltd (Wrexham, UK). A Berkovich indenter, with a face angle of 65.3^{o}, was used to make indents with various maximum loads (5, 10, 20, 30, 40 mN). A 600s dwell period and 0.25, 0.5, 1, 1.5 and 2 mN/s loading and unloading rates, respectively were used and samples were tested at various controlled temperatures (25, 45 and 65^{o}C). The results were analysed using the Oliver and Pharr method (Oliver and Pharr 1992), and then plotted using Matlab software from MathWorks (Cambridge, UK) and Microsoft Excel.

3.4.1 The Nano Test 600 System

The NanoTest 600 system manufactured by Micro Materials Ltd (Wrexham, UK) was used for the DSI experiments. The system consists of three main parts, the high resolution microscopes, the sample stage that can move in three directions and the pendulum unit, Figure 3.4. All parts are placed on a steel platform that should be held in an equilibrium position using compressed air. The sample is mounted vertically on the sample stage and the load (0.1–500 mN) applied electromagnetically. The coil is attracted towards the permanent magnet which causes the pendulum to rotate on its frictionless pivot, producing motion of the probe towards the sample surface. The limit stop is used to define the operating orientation of the pendulum and to control the maximum movement of the indenter. The displacement of the indenter is measured with a parallel plate capacitor, with plates 0.3 to 0.5 mm apart when the system is at full sensitivity. The maximum measurement depth of the system is approximately 15-20 µm. In order to counter the mass of the coil and any indenter, a balance weight is located below the indenter holder.

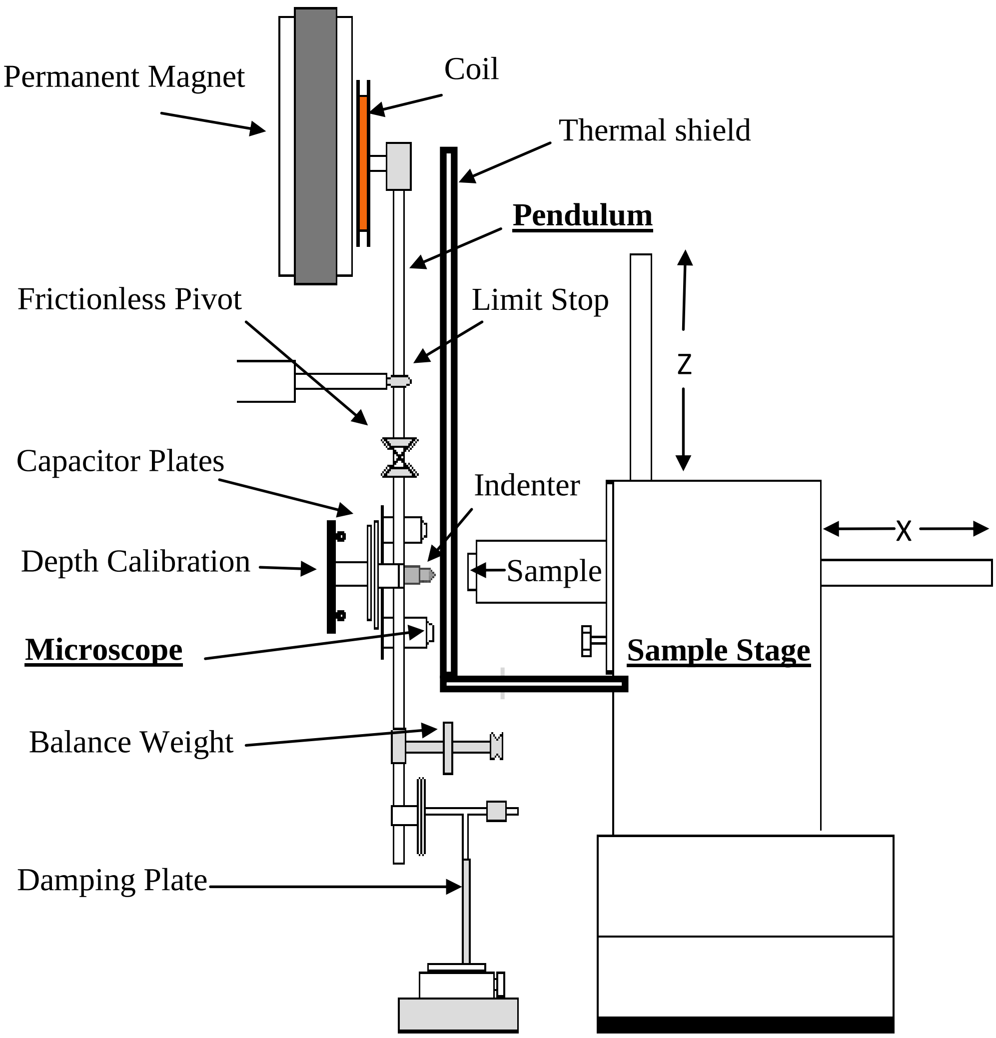

Figure 3.4: Schematic of NanoTest 600 system.

3.4.2 Factors Affecting DSI Results

In conventional indentation tests, the hardness and elastic modulus are usually calculated from the size of the residual impression after the load is removed. Although, the penetration depth can decrease significantly through elastic recovery, the residual penetration size is usually considered as identical to the contact area at maximum load. However, in DSI tests, the load and penetration depth can be measured directly during the loading and unloading of the indenter. This measurement can then be used to determine the projected area and to calculate the hardness and elastic modulus. However, various sources of errors are associated with the use of the DSI, these sources are (Fischer-Cripps 2011):

- **Thermal drift**

  Thermal drift results from a change in the dimensions of the instrument due to thermal expansion or contraction of the apparatus. This can be significant for small penetration depths made over a long period of time. In this study, experiments were carried out at controlled temperature. The specimen was kept at the selected temperature (25, 45 or 65^{o}C) for 30 minutes before starting the measurement, then the indenter was brought in contact with the sample surface using a low load (0.01 mN). The tip remained in contact for a period of time to equilibrate (5 minutes) before starting the measurement. A thermal shield was placed between the hot stage and the pendulum assembly, as seen in Figure 4.4. The maximum load was 40 mN, which resulted in displacements over 5µm. These factors ensured that thermal drift was not significant in the experimental measurements made in this work.

- **Creep**

  Creep can occur when polymer materials are indentation loaded. This can be most clearly seen when holding a constant indentation load as the indenter continues sinking into the specimen, increasing the depth readings. In this study, the effect of creep was minimised by selecting optimal values for parameters such as maximum load (40 mN), loading and unloading rate (2 mN/s) and the dwell period at maximum load (600 s).

- **Initial penetration depth**

  Before starting the indenter displacement measurements, which usually begin from the level of the sample free surface, it is necessary to make contact between the indenter and the specimen surface to determine a datum for the displacement measurements using a small initial contact load (P_i). This will cause an initial penetration depth (h_i), which can be added to the displacement measurements (h) to correct for the error of this initial depth. In this study, P_i was constant for all experiments at 0.01 mN, which caused a negligible value of h_i, < 5 nm compared to the measured contact depth, > 5 µm.

- **Instrument compliance**

  The total measured compliance is a combination of the contact compliance and the machine compliance. The contact compliance can be obtained from the addition of sample and indenter compliances. For a sample with high modulus value (small compliance), a small error in the machine compliance can significantly affect the accuracy of the sample modulus determination. Therefore, the machine compliance is one of the essential calibrations that need to be checked to ensure that the sample stiffness is determined accurately.

- **Indenter geometry**

  In DSI testing, the contact area, A_c is found from the geometry of the indenter at penetration depth h_c. For the Berkovich indenter, shown in Figure 3.5, used in this study:

$$A_c = 3\sqrt{3}\ \mathrm{h_c^2 tan^2\theta} \tag{3.1}$$

where, the semi-angle θ= 65.3° (Fischer-Cripps 2011).

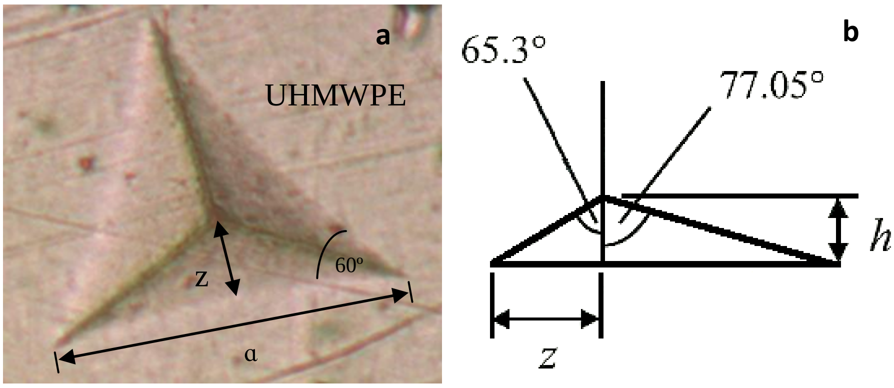

Figure 3.5: a) Typical indenter impression and b) Schematic geometry of Berkovich indenter

In practice, it is impossible to achieve the ideal geometry of the diamond indenter tip. Therefore, the diamond area function (DAF) was corrected using a reference sample (fused silica) with known hardness (8.8 GPa) and reduced modulus (69.6 GPa). The diamond area calibration relates the actual diamond contact area to the depth of penetration. Various loads were applied and the values of A_c were plotted as a function of h_c, which resulted in a range of data points that represented a smoothing equation. The equation fitting constants were used to account for any tip rounding of the indenter.

- **Piling-up and sinking-in**

The piling-up and sinking-in phenomena, shown in Figure 3.6, are the most significant materials-related factors that can affect the accurate determination of contact area and thus the values of indentation hardness and elastic modulus. Piling-up or sinking-in error can be quantified by two methods. The residual impression profile can be obtained by an optical surface profiler or atomic force microscope (AFM) (Menčik and Swain 1995; Randall and Julia-Schmutz 1998). In the second method, Pharr (1998) found that the ratio of the final indentation depth, h_f to the indentation depth at maximum load, h_{max} can be used to identify the indentation behaviour. When $h_f/h_{max} < 0.7$, very little piling-up or sinking-in occurs. Both of these methods were used in this study to determine the effect of piling-up and sinking-in errors. It was found from the residual impression profiles (an example is shown in Figure 3.7 for U75H25) using a Zygo instrument from ZygoLOT GmbH (Darmstadt, Germany) that the piling-up and sinking-in effects were insignificant. Also, the h_f/h_{max} ratio was < 0.7 for all materials investigated in this work. Therefore, the effects of piling-up and sinking-in could be ignored in the determination of indentation hardness and modulus in this work.

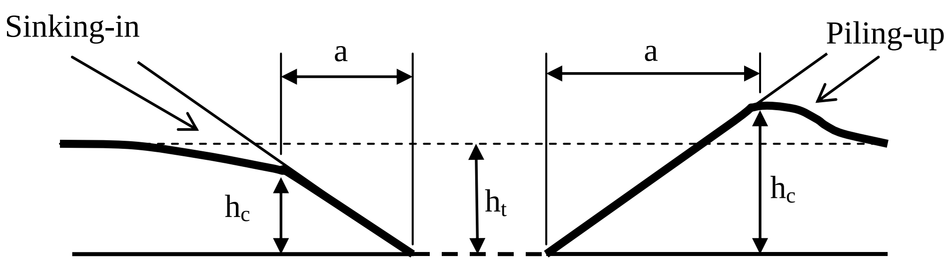

Figure 3.6: Schematic of piling-up and sinking-in.

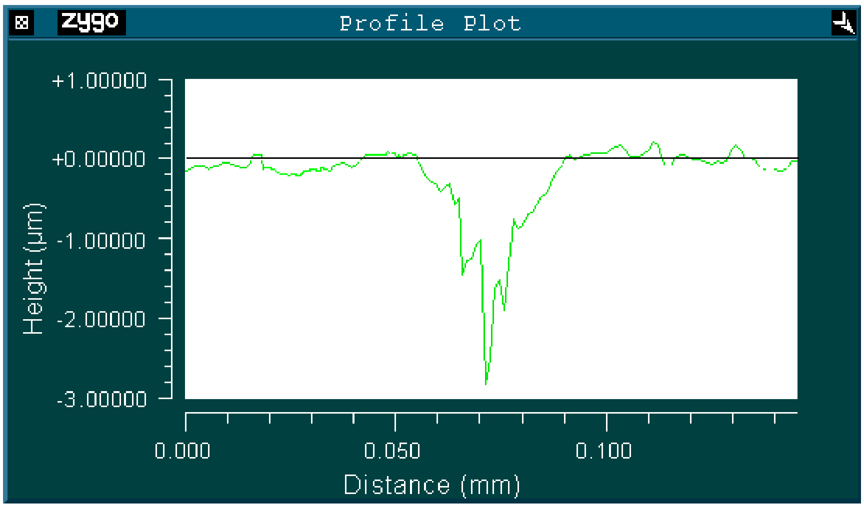

Figure 3.7: Indentation profile for U75H25.

- **Surface roughness**

Surface roughness is a very important factor when assessing nanoindentation results. Rough surfaces can lead to significant errors in the determination of the area of contact between the indenter and the sample. This effect increases for indentations with light loads or small depths. Therefore, specimen preparation is an important step to reduce the surface roughness. Specimen polishing can be used to improve the surface roughness for most materials, however, this can potentially affect the surface, therefore, in this work, the quality of the specimen surface was controlled during the compression moulding. Two 120 x120 mm square steel plates were polished to a mirror finish. Then, plastic sheets with higher melting point than polyethylene were placed between the mould and the steel plate, Figure 3.8. It can be seen from Figure 3.9 that this procedure results in low surface roughness of the materials investigated in this work and thus the factor of surface roughness was not considered in any calculations.

Figure 3.8: Schematic for the compression mould.

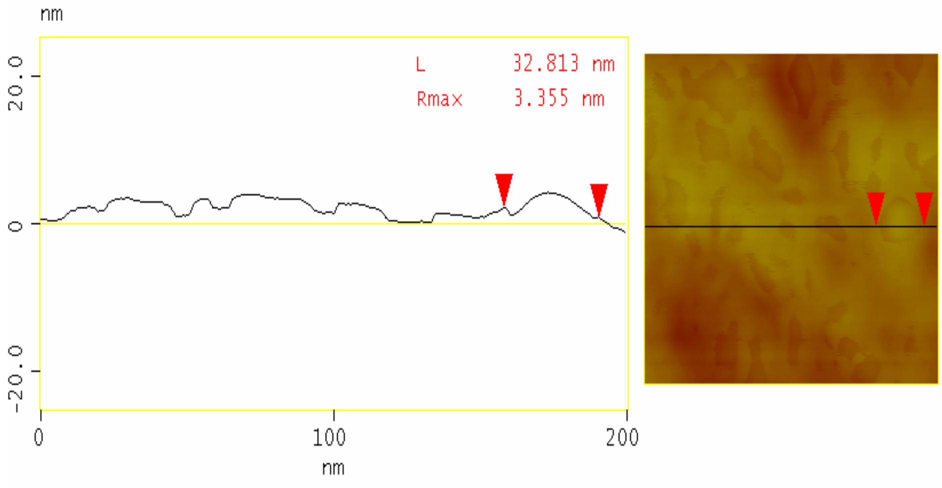

Figure 3.9: Section analysis of U75H25 nanocomposite.

3.4.3 Analysis of DSI Test Data

A Berkovich indenter is the most widely used indenter for DSI. It has a face angle of 65.3°, which gives the same projected area to depth ratio as a Vickers indenter (square based pyramid). Usually, the tip radius of a new indenter is in the range between 50 to 150nm (Ficher-Cripps 2006). The results can be analysed using the Oliver and Pharr method (Oliver and Pharr 1992). In this method, the initial portion of the unloading curve is described by the power law relation:

$$P = \alpha (h - h_r)^{m} \tag{3.2}$$

where P is the load, α and m are constants determined by curve fitting, h is penetration depth and h_r is the depth of the residual impression. The contact stiffness (S) can be obtained from the derivative of Equation (3.2) with respect to depth applied at the maximum loading point (h_{max}, P_{max}):

$$S = \frac{dP}{dh}(h = h_{max}) = m \propto (h_{max} - h_r)^{m-1} \tag{3.3}$$

The contact depth (h_c) at maximum load can be estimated using:

$$h_c = h_{max} - \varepsilon \frac{P_{max}}{S} \tag{3.4}$$

where ε is a constant related to the geometry of the indenter, which is 0.75 for the Berkovich indenter. Thus, the projected contact area (A_c) for an ideal geometry is determined from (h_c) using a specimen with known properties, such as fused silica by the following relation:

$$A_c \approx 24.5\, h_c^2 \tag{3.5}$$

and hence the indentation hardness (H) is:

$$H = \frac{P_{max}}{A_c} = \frac{P_{max}}{24.5 h_c^2} \tag{3.6}$$

The reduced modulus can be calculated from stiffness (S) using this relation:

$$S = \frac{dP}{dh} = \beta \frac{2}{\sqrt{\pi}}\, E_r \sqrt{A} \tag{3.7}$$

where, $A = 24.5{h_p}^2$, E_r is the reduced modulus and β is a correction factor which depends on the type of indenter (1.034 for Berkovich indenter). Consequently, the elastic modulus (E_s) for the specimen can be calculated using the following equation:

$$\frac{1}{E_r} = \frac{(1-\nu_s)^2}{E_s} + \frac{(1-\nu_i)^2}{E_i} \tag{3.8}$$

Where, E_s, ν_s and E_i, ν_i are the elastic modulus and the Poisson's ratios of the specimen and the indenter respectively, (E_i= 1141 GPa, $\nu_i = 0.07$).

3.4.4 Investigation of the Load Effect

In order to investigate the correlation between indentation properties and indentation load. The nanoindentation tests were performed at various loads 5, 10, 20, 30 and 40 mN with constant displacement rate (0.05 s^{-1}) and holding time at maximum load (600 s), as seen in Figure 3.10. A Berkovich indenter was used to make at least 10 indents. The experiments were carried out at a controlled chamber temperature (25^{o}C) and the test procedure for minimizing the effect of thermal drift was followed.

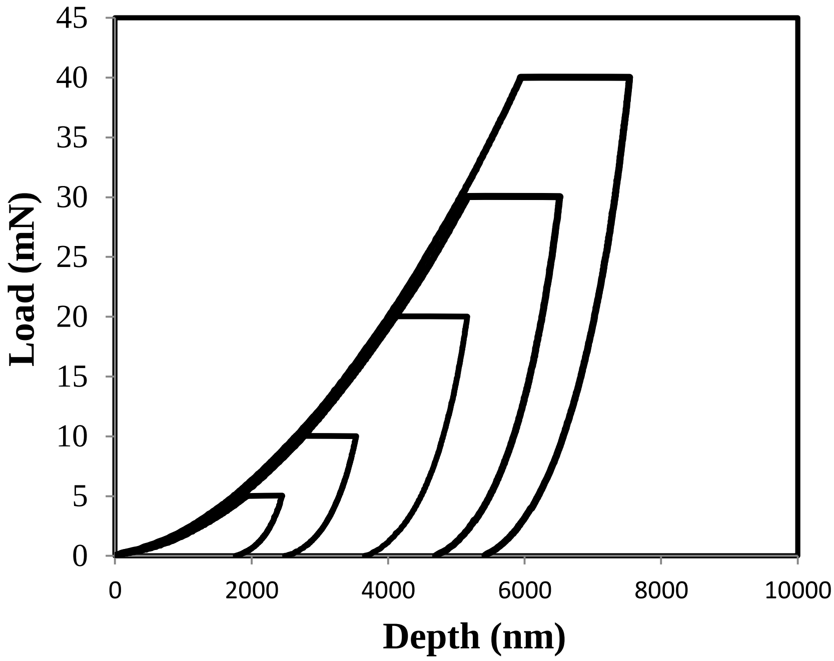

Figure 3.10: Typical diagram for indentation at various loads and constant dwell period.

3.4.5 Investigation of Nanoparticle Dispersion

In recent years, several experimental techniques have been used to analyse nanoparticle dispersion in nanocomposites at a micro or nano-scale. These include scanning electron microscopy (SEM), transmission electron microscopy (TEM) and wide angle X-ray diffraction (WAXD). However, enlarging the measurement scale can also provide useful information about nanoparticle dispersion, which is not achievable using the previous techniques. Therefore, in the current work a DSI method was used to investigate the spatially resolved properties of the nanocomposites at a micro-scale, in this case indentation hardness was measured over an area of approximately 1 mm^2. The variations in hardness value were used to evaluate the effect of the processing method on the blend morphology and the dispersion of nanoparticle in the blend matrix. A Berkovich indenter was used to make a grid of 10x10 indents, as shown in Figure 3.11 using 40 mN maximum load, 600s dwell period and 2 mN/s loading and unloading rates. The results were analysed using the Oliver and Pharr method (Oliver and Pharr 1992), and then plotted using Matlab software from MathWorks (Cambridge, UK).

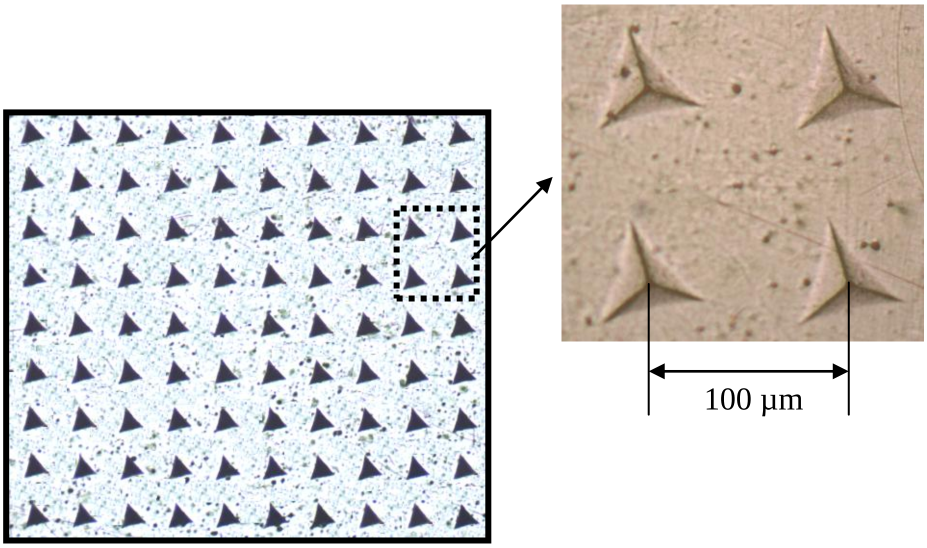

Figure 3.11: Image of 10x10 indents grid on U75H25 surface.

3.4.6 Investigation of the Creep Behaviour

The standard method of analysing nanoindentation data is based on the assumption that the initial portion of the unloading part is purely elastic. However, polyethylene is a thermoplastic polymer and known to exhibit viscoelastic behaviour (creep). A bulge or nose effect was found during the initial portion of unloading as a result of the creep behaviour of polyethylene, as seen in Figure 3.12 a. This can lead to errors in the calculation of contact stiffness (S) and contact depth (Cheng et al. 2005; Briscoe 1998). Therefore, it is common practice to eliminate the creep effect through a rapid unloading rate (Cheng et al. 2005) or a dwell/holding time at maximum load (Briscoe 1998). In the present work, the measuring cycle, as shown in Figure 3.12b consists of loading to a maximum load of 40 mN using 2 mN/s as loading and unloading rates, followed by a dwell period of 600 s at maximum load. The creep behaviour was obtained from the holding time at maximum load.

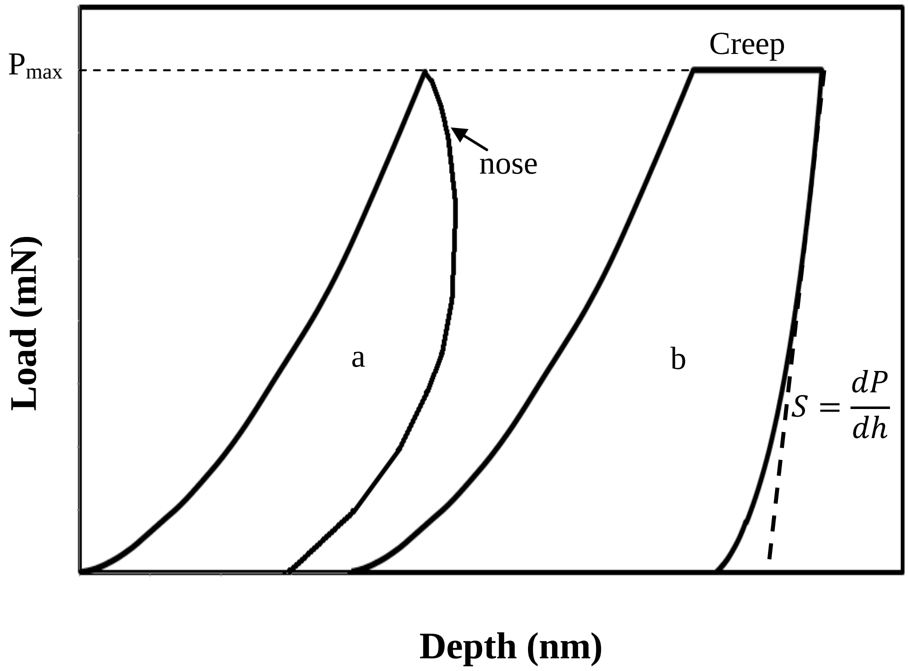

Figure 3.12: Creep effect on the load-depth curve of polyethylene.

3.4.7 Investigation of the Effect of High Temperature

The use of the nanoindentation technique at high temperature is limited due to several difficulties during the experimental procedure (Lu et al. 2010). These include the temperature equilibrium of the specimen and the indenter, thermal drift and sample oxidation. However, in this work, the experiments were carried out at only 45 and 65^{o}C and hence these problems were not significant. The specimen was heated to the selected temperatures and left for 30 minutes to one hour for equilibrium, the indenter was brought in contact with the specimen surface at low force (0.01 mN) and equilibrated at the temperature for 5 minutes. A thermal shield was used to minimise the heat effect on the instrument. The experiments were carried out with a controlled hot stage and chamber temperature using a loading rate of 2 mN/s to reach maximum load of 40 mN, and then the load was held at maximum for 600 s followed by unloading at 2 mN/s. The temperature dependent mechanical properties were analysed using the Oliver and Pharr method (Oliver and Pharr 1992).

3.5 Bulk Mechanical Characterization

3.5.1 Tensile Tests

Tensile tests were carried out using Instron 3366 and Instron 5985 tensile testing machines from Instron Corporation (Norwood, MA, USA) at various temperatures (25, 45 and 65^{o}C). Various strain rates were applied, 0.02, 0.04, 0.1, 0.2 and 0.3 s^{-1} and at least 5 samples were tested at each condition. Specimen preparation and testing methods were according to ASTM D638 (2010). The specimen dimensions are shown in Figure 3.13. A controlled chamber temperature was used to investigate the effect of various temperatures on the tensile properties. The samples were placed inside the chamber for five minutes before testing to reach temperature equilibrium.

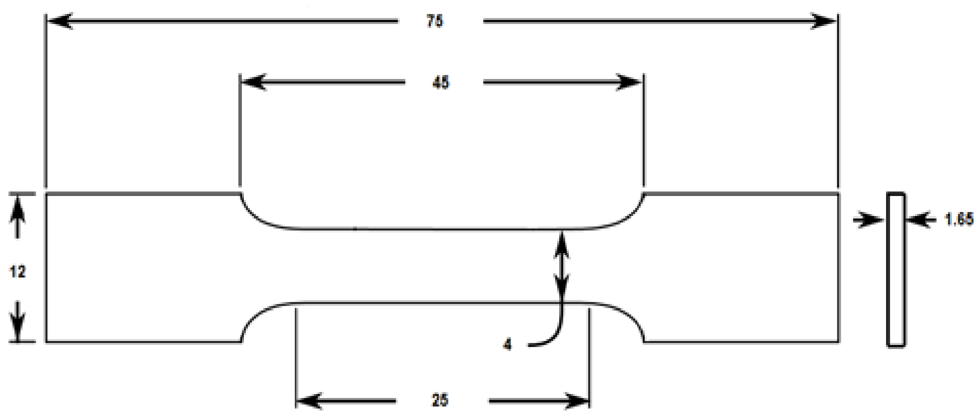

Figure 3.13: Tensile test sample dimensions (all dimensions in mm).

3.5.2 Creep Tests

Creep tests were carried out using an Instron 3366 tensile testing machine from Instron Corporation (Norwood, MA, USA) at room temperature (23 ± 2^{o}C). In order to define the linear viscoelastic regime for the polyethylene-based nanocomposites, various loads were applied 30, 40, 50, 60, 70, 90 and 100 N for a specific period of time (600s) and the isochronous stress-strain curves were plotted, as shown in Figure 3.14. Further tests were then performed to investigate the effect of nanoparticle type and volume fraction on the creep behaviour of polyethylene-based nanocomposites. For all comparisons, the samples were subjected to a constant load (60N), which was selected in the linear viscoelastic regime and held for a specific period of time (600s) and each test was repeated at least 5 times. The data were collected using an excel programme to plot the results. The data were fitted to the Burger’s model, all parameters being obtained by minimising the sum of the squared differences between the actual and calculated strains, using the solver in Excel.

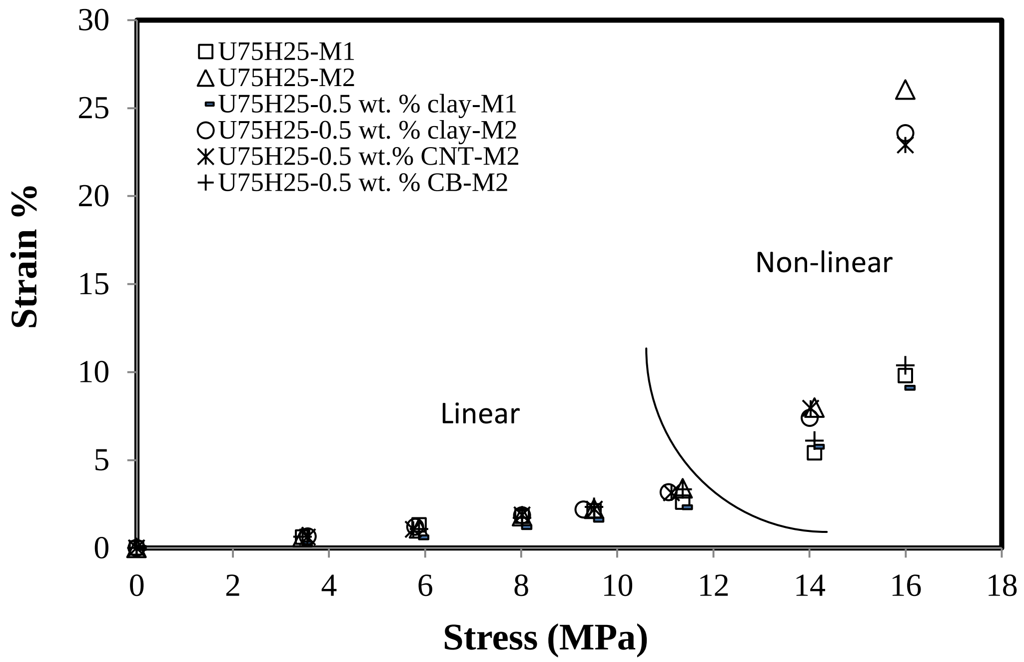

Figure 3.14: Isochronous plots showing transition from linear to non-linear stress-strain relationship.

3.6 Thermal Analysis

3.6.1 Differential Scanning Calorimetry (DSC)

Differential Scanning Calorimetry (DSC), (TA instruments, Shimadzu DSC60) was used to analyse the effects of compression moulding parameters and nanofiller content on the crystallinity of the blend and nanocomposites. Specimens, with average mass of 5 ± 0.2 mg, were sealed in aluminium pans and heated from 20 to 180^{o}C at a rate of 10°C per minute. The mass fraction degree of crystallinity was then determined by comparing the heat of fusion with that for fully crystalline polyethylene at the equilibrium melting point (290 J/g) (Humbert et al. 2009).

3.6.2 Thermogravimetric Analysis (TGA)

The Thermogravimetric Analysis (TGA) was undertaken using a machine from TA instruments, the SDT Q600 (Crawley, UK). This was used to analyse the thermal degradation behaviour of the polyethylene-based nanocomposites. The measurements were carried out in air at a heating rate of 40°C/min and an air flow of 100 ml/min for cooling. The sample was 16–17 mg and was placed in a platinum pan and heated to 600°C.

3.6.3 Infrared Thermography

Tensile tests are common experiments to measure the mechanical properties of materials; however, during plastic deformation, part of the mechanical work is converted to internal heat, which can significantly affect the measured mechanical properties. Figure 3.15 shows the equipment that was used to measure temperature changes during tensile tests. A thermal camera (FLIR SC3000) from FLIR systems AB (Danderyd, Sweden) was used to measure the surface temperature distribution of samples, with a temperature range from -20 to +150°C and accuracy of ± 1°C. 'FLIR ResearcherIR' software was used for the temperature analysis and an emissivity value equal to 0.9 was used. This value was determined by heating a sample in a controlled environment to 50 and 85°C, and then the sample's temperature was measured using the thermal camera. The emissivity setting was then adjusted until the correct value was reached. This equipment was used to create point, line and area profiles of temperature as a function of loading.

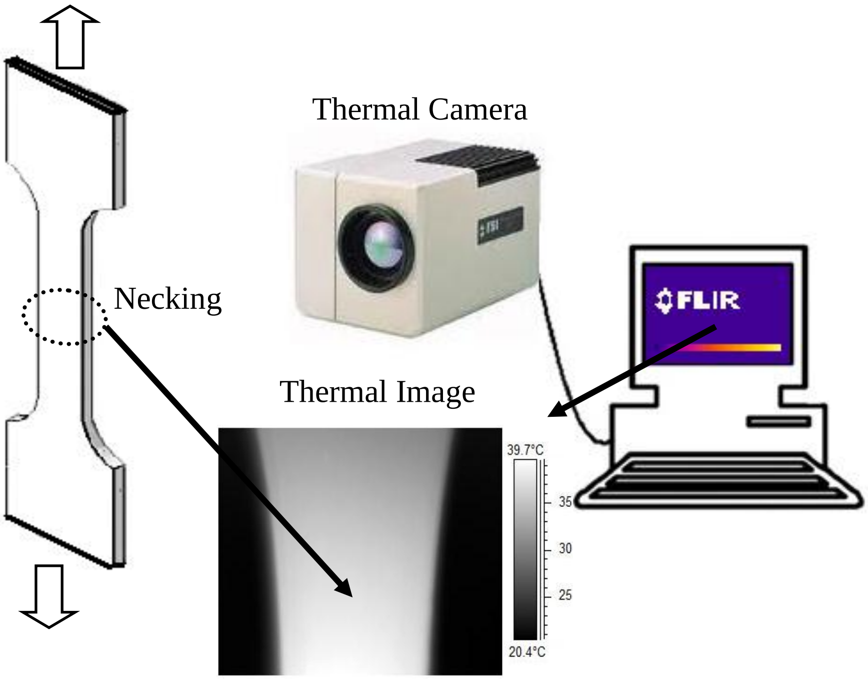

Figure 3.15: Temperature measurement during tensile test.

3.7 Summary

In order to characterise the mechanical properties of polyethylene-based nanocomposites, various experimental techniques were performed. The dispersion of the nanoparticles (CNT, CB and clay) in the polyethylene matrix is a key factor to achieve the desired properties. Therefore, two processing methods were used to mix the HDPE with the UHMWPE and the nanoparticles. The microstructures were investigated using DSC, TEM, SEM, XRD, AFM, optical microscopy and nanoindentation.

The nanoindentation tests were carried out to measure the spatially resolved properties of the polyethylene-based nanocomposites at various temperatures. These include the indentation hardness, indentation elastic modulus, temperature dependency and creep. The distribution of the nanofiller in the polymer matrix was evaluated through the spatial variation of the indentation hardness. Various loads were applied to obtain relationships between the indentation depth and the near surface properties. The creep effect was minimized by applying a dwell period at the maximum indentation load and a rapid unloading rate. The dwell period data were used to investigate the viscoelastic behaviour of the materials at various temperatures.

Bulk material properties were also studied, using tensile and creep tests. The tensile tests were applied to measure mechanical properties such as elastic modulus, yield strength, strength, fracture energy and plastic deformation. During the test, a high sensitivity thermal camera was applied simultaneously to find correlations between heat generation during plastic deformation, processing method, nanofiller type and volume fraction, filler-matrix interaction and the mechanical properties. The creep tests were performed to investigate the effect of the processing method, dispersion and the volume fraction on the creep behaviour of the polyethylene materials. A comparison between the creep behaviour from bulk tests and the creep behaviour from nanoindentation was also obtained. All samples and testing carried out in this work are summarised in Table 3.3.

Table 3.3: Summary of the experimental methods

Materials	Filler Content	Microstructural Analysis				Thermal Analysis			Bulk Tests				DSI Test	
									Tensile		Creep			
		SEM	TEM	AFM	XRD	DSC	TGA	IT	Room Temp.	High Temp.	Room Temp.	High Temp.	Room Temp.	High Temp.
UHMWPE	0	✓		✓		✓	✓	✓	✓	✓	✓	✓	✓	✓
HDPE	0	✓		✓		✓	✓	✓	✓	✓	✓	✓	✓	✓
U75H25-M1	0	✓		✓		✓		✓	✓		✓		✓	
U75H25-M2	0	✓				✓	✓	✓	✓	✓	✓	✓	✓	✓
U75H25-CB-M1	0.5	✓	✓	✓		✓		✓	✓		✓		✓	
	1	✓	✓	✓		✓		✓	✓		✓		✓	
	3	✓	✓	✓		✓		✓	✓		✓		✓	
U75H25-CB-M2	0.5	✓	✓			✓	✓	✓	✓	✓	✓	✓	✓	✓
	1	✓	✓			✓	✓	✓	✓	✓	✓	✓	✓	✓
	3	✓	✓			✓	✓	✓	✓	✓	✓	✓	✓	✓
H75H25-CNT-M1	0.5	✓	✓	✓		✓		✓	✓		✓		✓	
H75H25-CNT-M2	0.5	✓	✓			✓	✓	✓	✓	✓	✓	✓	✓	✓
	1	✓	✓			✓	✓	✓	✓	✓	✓	✓	✓	✓
	3	✓	✓			✓	✓	✓	✓	✓	✓	✓	✓	✓
U75H25-clay-M1	0.5	✓	✓	✓	✓	✓		✓	✓		✓		✓	
U75H25-clay-M2	0.5	✓	✓		✓	✓	✓	✓	✓	✓	✓	✓	✓	✓
	1	✓	✓		✓	✓	✓	✓	✓	✓	✓	✓	✓	✓
	2	✓	✓		✓	✓	✓	✓	✓	✓	✓	✓	✓	✓

Chapter 4

Morphology and Strain Rate Effects on the Mechanical Properties of the U75H25 Blends

4.1 Introduction

In this chapter, the effect of processing parameters and strain rate on the mechanical properties of U75H25 blends is investigated using tensile testing and DSI. The stress-strain behaviour of the U75H25 blends processed using methods M1 and M2 (see Section 3.2.2) are analysed and compared with the pure UHMWPE and HDPE. The phenomenon of internal heat generation during the plastic deformation of the U75H25 blends at high strain rates is investigated using a high sensitivity thermal camera, which is used to record the spatial and temporal temperature variations along with the stress-strain behaviour. The DSI technique is applied to evaluate the effect of processing methods on the micro-scale properties of the UHMWPE, HDPE and U75H25 blends.

4.2 Stress-Strain Behaviour

The effect of the processing method on the stress-strain behaviour of the U75H25 blend is shown in Figure 4.1. In this study, the effect of the degree of crystallinity is negligible, as no significant change in the crystallinity of the blends is observed, as seen in Table 4.1. The stress-strain behaviour, however, is strongly dependent on the processing method. Processing method M1 results in properties closer to the HDPE, whereas processing method M2 results in properties closer to that of the UHMWPE in the blended material. It is proposed that this can be attributed to the poor miscibility of UHMWPE and HDPE, which results in the formation of two different phases in U75H25-M1. This may be because the processing temperature was not sufficient for the UHMWPE to completely melt, resulting in UHMWPE phases surrounded by HDPE or a HDPE/UHMWPE blend material, as shown schematically in Figure 4.2a. In processing method M2, the temperature was increased (see Table 3.2), combined with the addition of anti-oxidant, to overcome the suspected incomplete melting of the UHMWPE. It can be seen in Figure 4.1 that the strain hardening behaviour of U75H25-M2 is similar to that of the UHMWPE. This indicates that the behaviour of the blend is UHMWPE dominated and that the UHMWPE is mixed well with the HDPE to form a new polymer microstructure, as illustrated in Figure 4.2b. No necking was observed for the UHMWPE, whilst clear neck formation was observed for the blends, as seen in Figure 4.3. The neck propagation, or cold drawing, of U75H25-M1 is longer than that for U75H25-M2. This can be attributed to two reasons. The poor miscibility of the blend can result in voids and cavitations in the microstructure, which ease chain mobility. The second reason is the increase in the internal heat during plastic deformation, which leads to a similar effect on chain mobility. This temperature increase is discussed further in Section 4.3.

Figure 4.4 indicates that the processing method has no significant effect on the yield strength and the elastic modulus of the U75H25 blends. Humbert et al. (2009) reported that the yield stress can increase with the degree of crystallinity in polyethylene. Therefore, the results are in agreement with that of crystallinity of the blends shown in Table 4.1.

Table 4.1: Mean values for crystallinity and melting point of base materials and blends

Material	Crystallinity %	Melting point (°C)
UHMWPE	49 ± 1.3	137 ± 0.5
HDPE	60.4 ±0.8	138.3 ±0.5
U75H25-M1	53.2 ± 2.1	137.6 ± 1
U75H25-M2	53.3 ± 2.7	138.3 ± 0.5

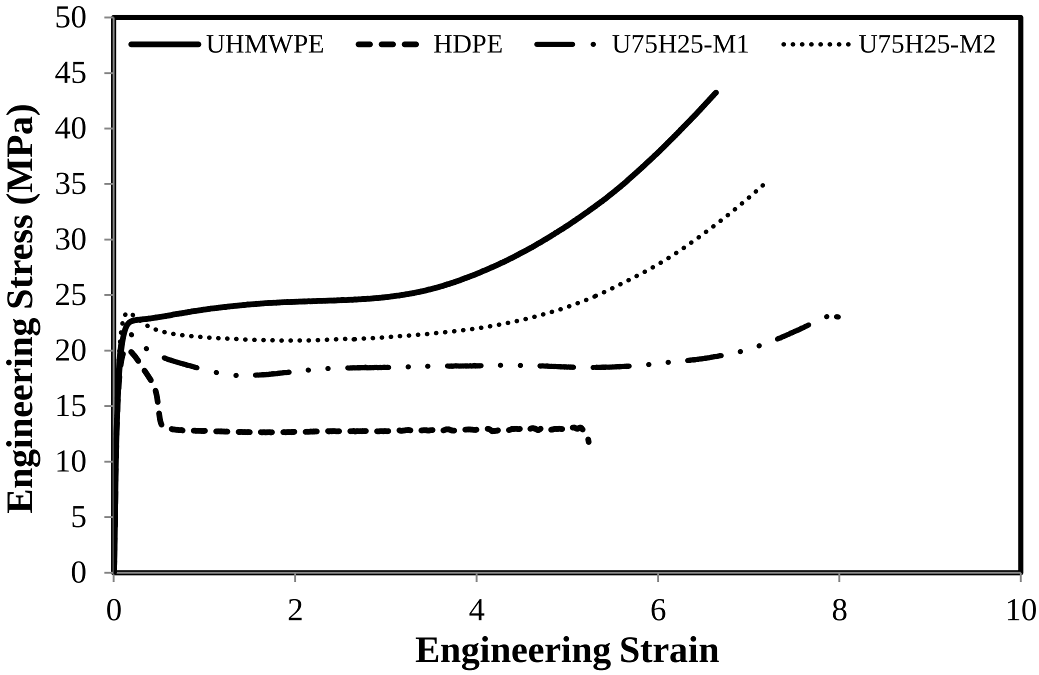

Figure 4.1: Effect of the processing method on the stress-strain behaviour of PE blends from tensile testing at 0.2 s^{-1} strain rate. (The tests were repeated at least 5 times and the mean plots are shown with error less than 5%).

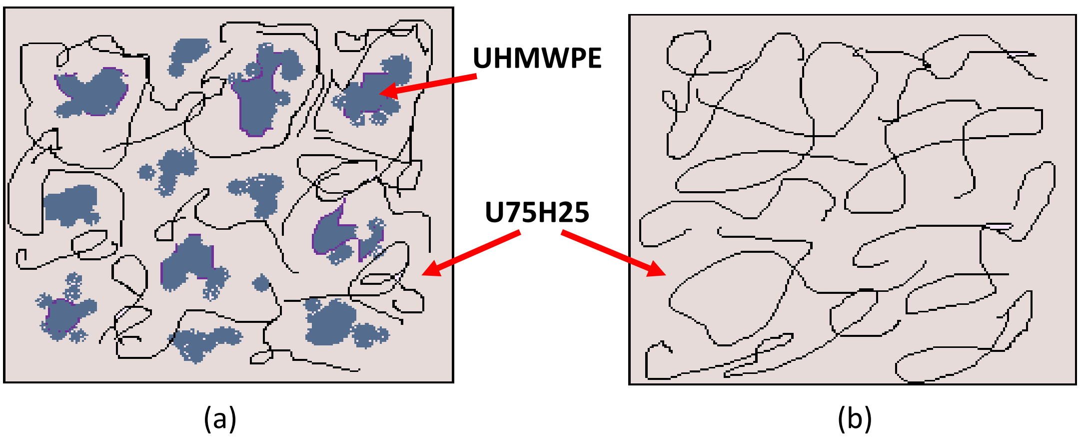

Figure 4.2: Schematic diagram for the microstructures of the blends processed using a) M1 and b) M2.

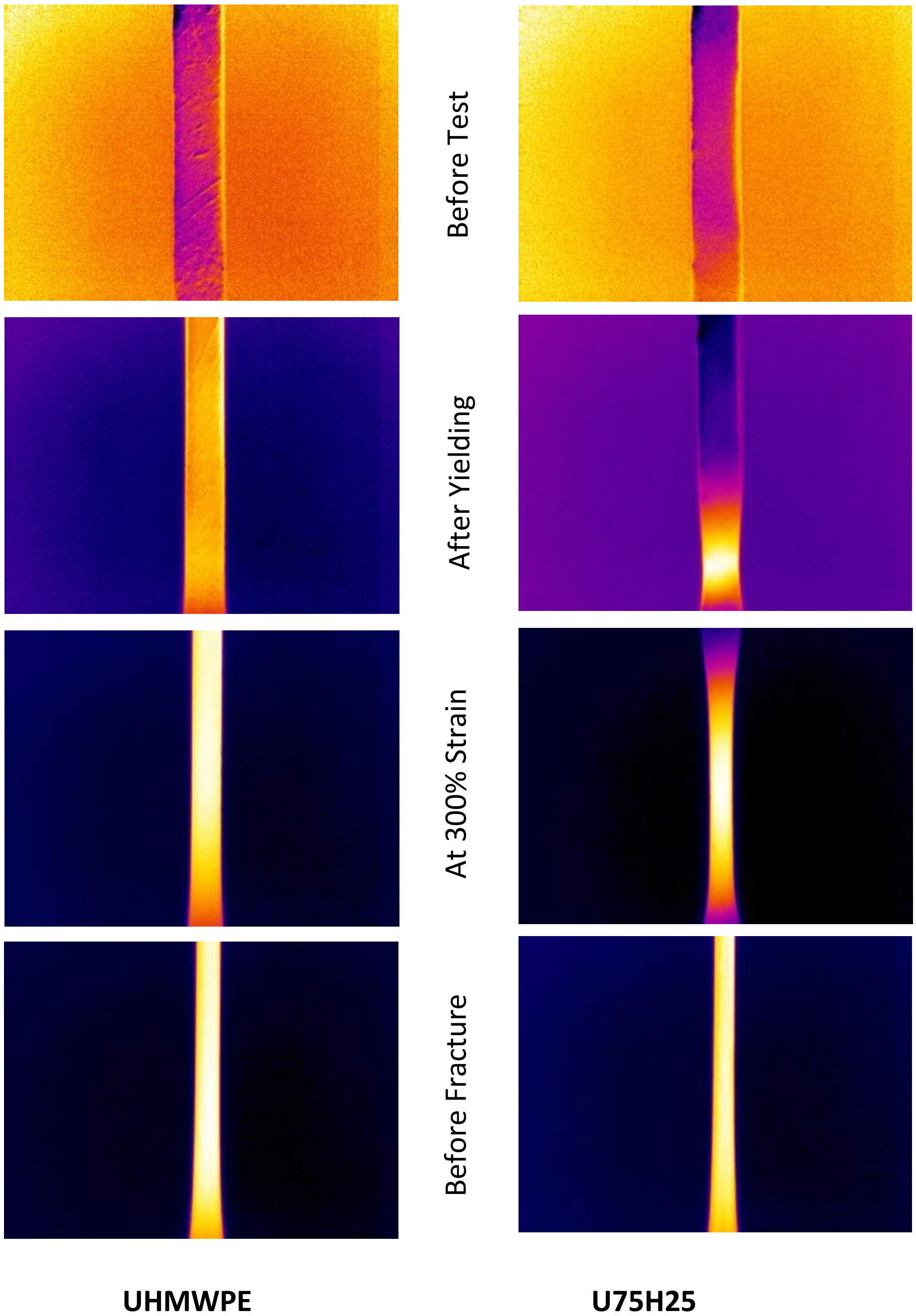

Figure 4.3: The changes in the sample shape during tensile test.

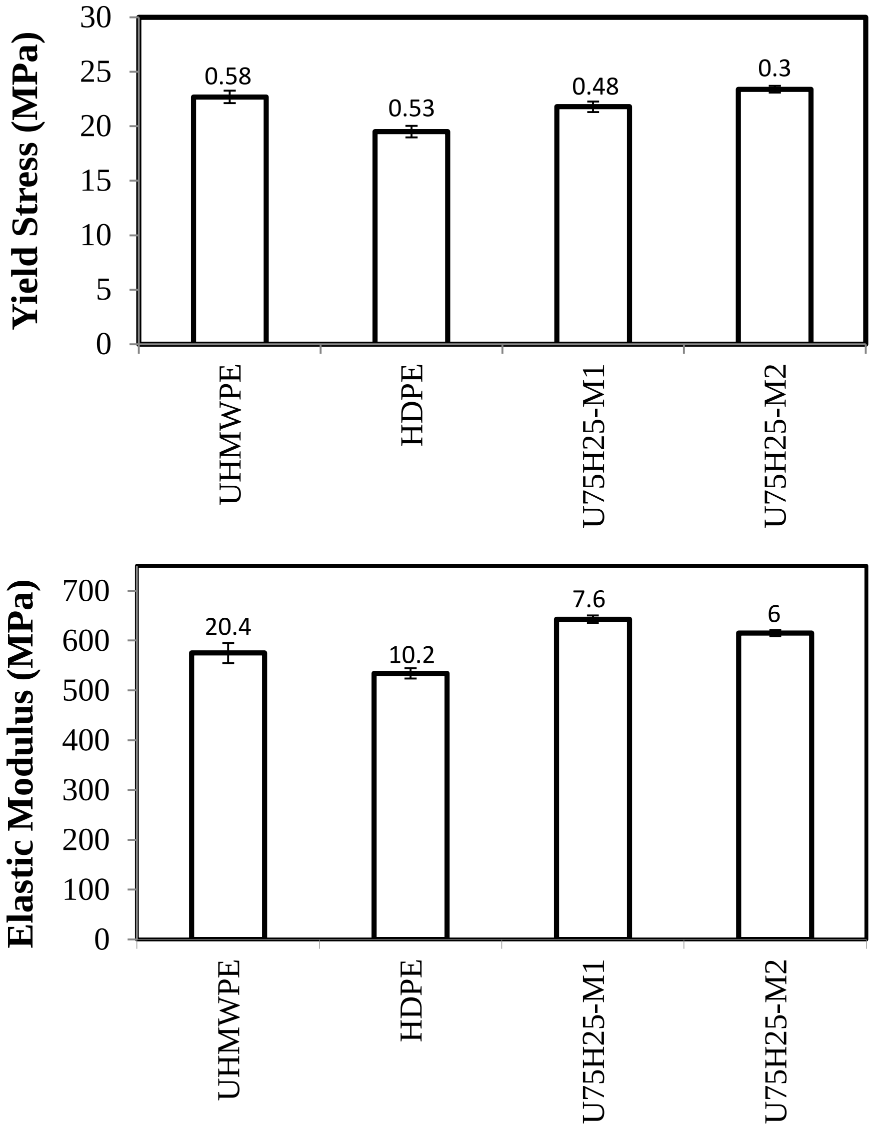

Figure 4.4: Yield stress and elastic modulus of polyethylene and blends processed using M1 and M2 (tested at 0.2 s^{-1} strain rate and room temperature, the values on the graph represent the standard deviation).

4.3 Strain Induced Temperature Measurements

In order to investigate the effect of strain rate and processing method on internal heat generation during the plastic deformation of polyethylene nanocomposites, a thermal camera (FLIR SC3000) was used to record the surface temperature during uniaxial tensile testing. Heat can be generated due to the friction between polymer chains during the transformation of a spherulitic structure to a fibril structure in the necking and also due to crystallographic mechanisms (slip of crystal blocks). During plastic deformation, molecules align towards the load direction through a complex mechanism which includes chain and transverse slip, bending, rotation and fragmentation of lamellar stacks in the crystalline phases and interlamellar shear and separation in the amorphous phases (see Section 2.10.2). The plastic work at high strain rates can be transformed partly into heat. This can lead to a significant temperature increase, which can contribute to thermal softening of the material.

The UHMWPE, U75H25-M2 and U75H25-M1 samples were tested at three different strain rates to study the effect of strain rate on heat generation. The results, shown in Figures 4.5 to 4.7 for UHMWPE, U75H25-M1 and U75H25-M2 respectively, indicate that the heat generated during plastic deformation is strongly dependent on the strain rate. A significant temperature increase in the UHMWPE, U75H25-M1 and U75H25-M2 samples can be seen at 0.2 s^{-1} strain rate, with a maximum temperature over 70°C in the U75H25-M1 blend and over 55°C in the U75H25-M2 blend. The temperature changes at high strain rate can be divided into five regions. Region 1 indicates that there is no significant increase in the temperature in the elastic region. Region 2 shows an increasing temperature following yielding of the material. Region 3 is an approximately constant stress region in which an approximate thermal equilibrium has been reached (45°C) as there is little change in the temperature. Strain hardening occurs in Region 4, and the temperature increases again until failure occurs. As a result of the temperature increase in Region 4, material softening appears in the strain hardening region for the specimens tested at 0.2 s^{-1} strain rate, and the ultimate tensile strength is reduced. The temperature increase in the U75H25-M1 blend is 15°C greater than that of the U75H25-M2 blend; therefore a more significant material softening and ultimate tensile strength reduction can be seen in the U75H25-M1 compared to U75H25-M2. In some of the curves an increase in temperature can be seen at failure, indicated as Region 5, which is associated with the heat of fracture (McNally et al. 2003; Shen et al. 2011).

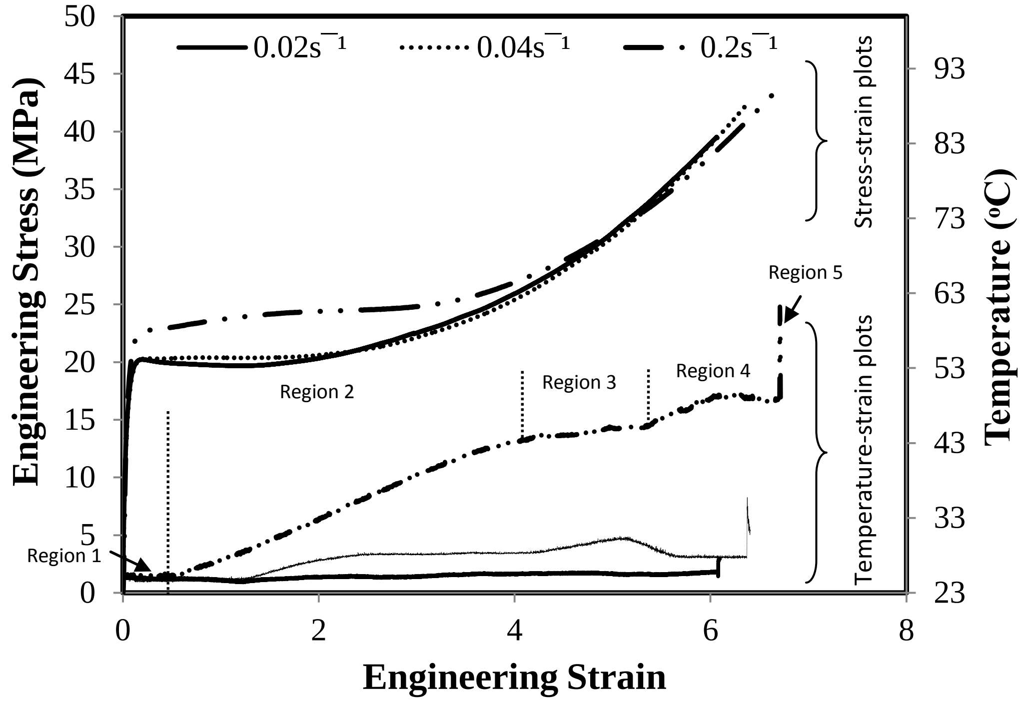

Figure 4.5: Temperature change for UHMWPE during tensile testing at various strain rates.

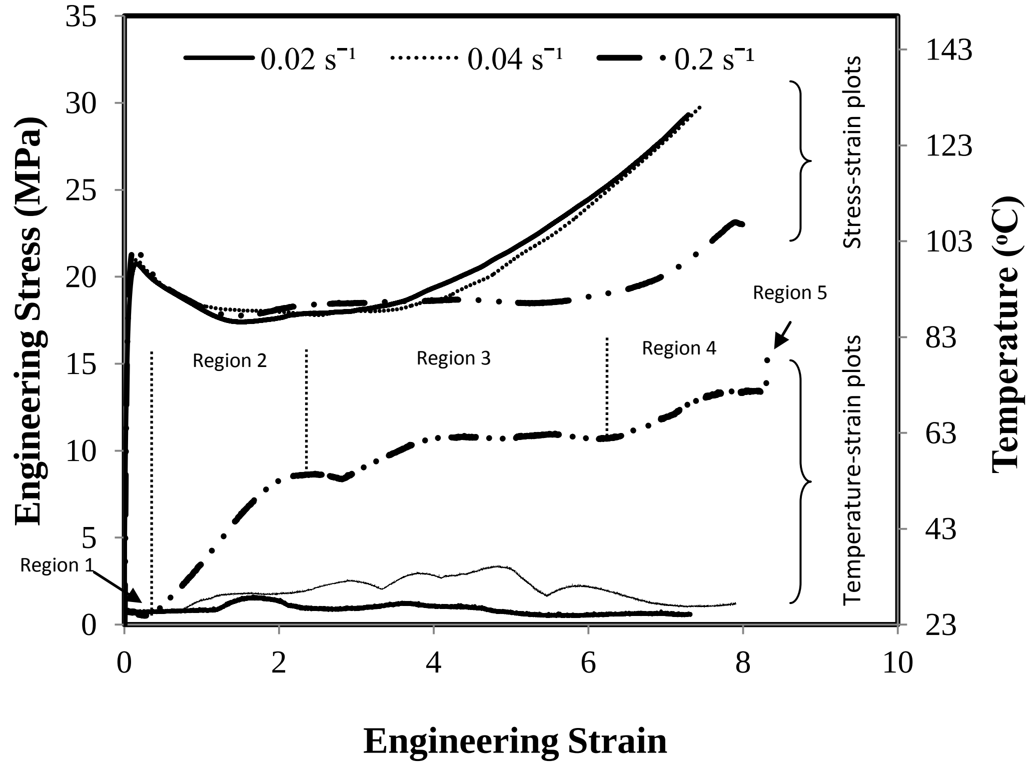

Figure 4.6: Temperature change for U75H25-M1 during tensile testing at various strain rates.

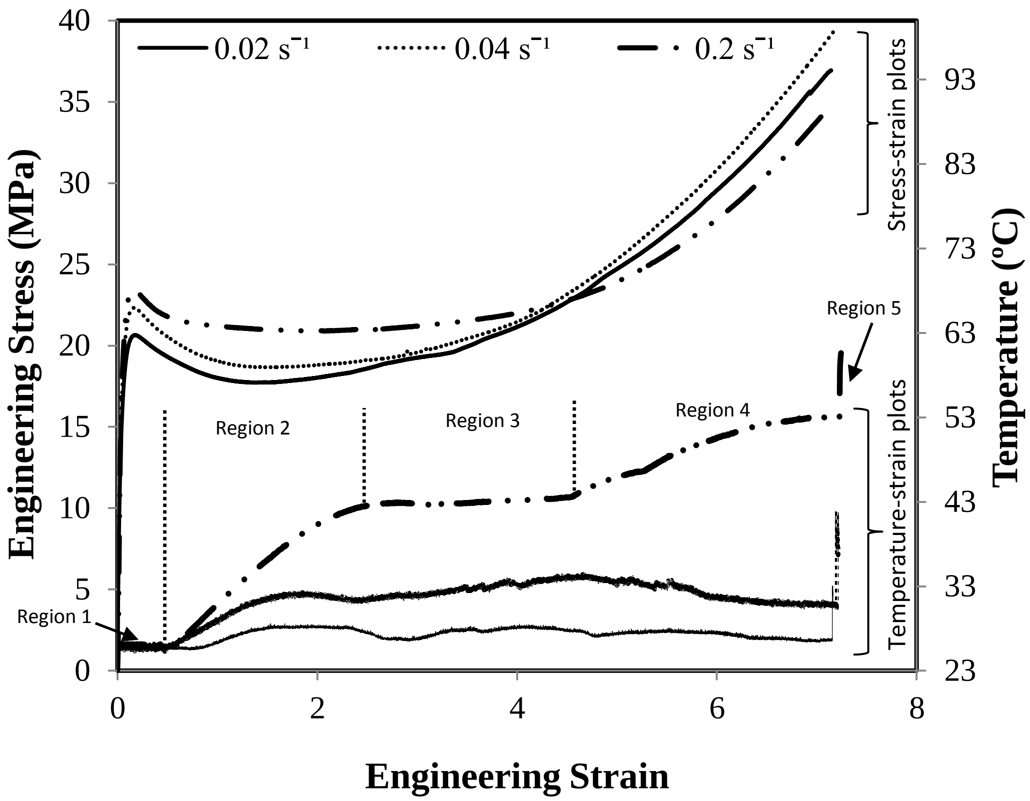

Figure 4.7: Temperature change for U75H25-M2 during tensile testing at various strain rates

Figure 4.8 summarizes the effects of processing method and strain rate on the temperature increase seen in tensile tests at 200 % strain. The maximum temperature increase in U75H25-M1 at high strain rates is considerably higher than that seen in the UHMWPE or U75H25-M2 materials. This is in agreement with our previous proposal of the more uniform mixing of the UHMWPE and HDPE chains at the higher processing temperature. The temperature difference can be attributed to the additional frictional heating from the two phase structure produced by M1. Incomplete mixing in the first processing method M1 to form different phases with weak bonding and microvoids between the phases would increases the internal friction area and also reduce the transfer of heat between the polymer crystallites. This temperature increase can cause significant thermal softening, which can be seen in the strain hardening behaviour in Figure 4.6.

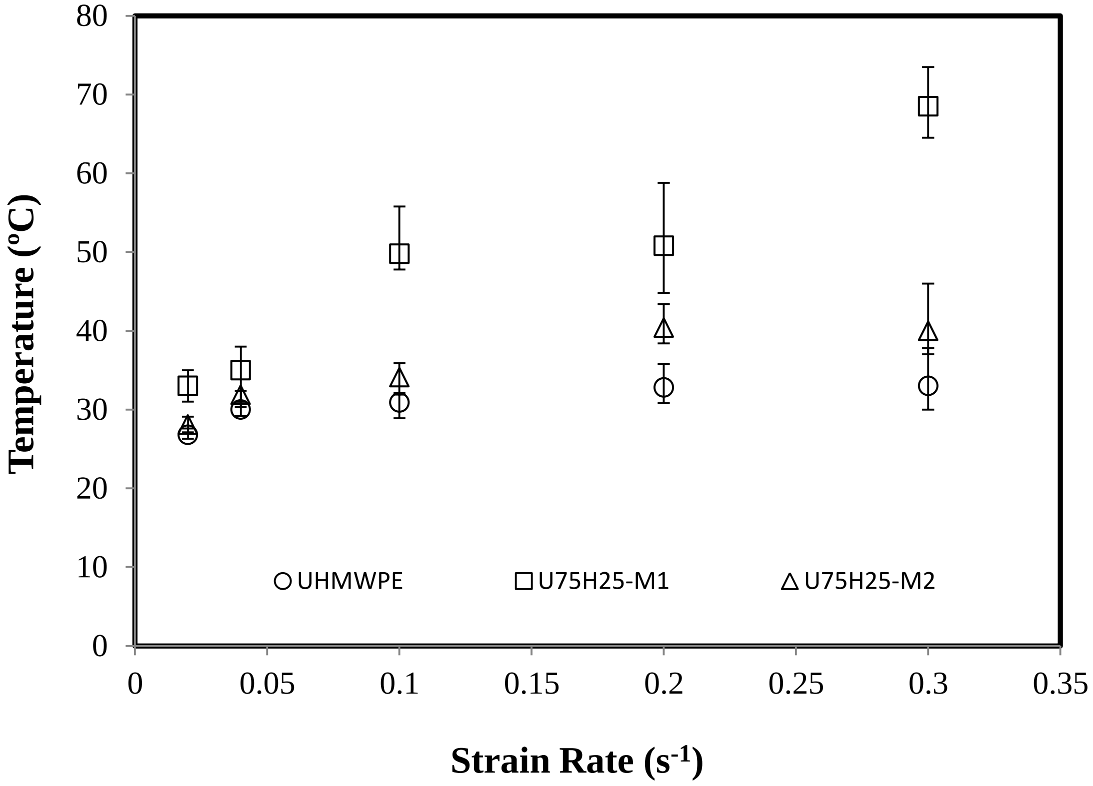

Figure 4.8: Strain rate and processing method effect on the temperature increase during tensile test of U75H25 blends at 200 % engineering strain

4.4 Creep Behaviour and Constitutive Modelling

4.4.1 Creep Behaviour

Figure 4.9 shows the effect of the addition of HDPE on the creep resistance of UHMWPE using the two different processing methods. A 9.3 MPa constant stress was applied for the creep tests as this was within the linear viscoelastic region (see Section 3.5.2). The primary and secondary creep stages can be clearly observed. As expected, the addition of HDPE to the UHMWPE resulted in an improvement in the creep resistance. However, it can be seen that blending the HDPE with the UHMWPE using processing method M1 increases the creep resistance by 32% after 600s compared to 10% using M2. These percentage values were calculated by comparing the values of creep strain at creep time of 600s. This can be explained by the improvement in the miscibility of the blend using processing method M2. As noted previously, in processing method M1, the temperature was not sufficient to melt the UHMWPE, which resulted in two different phases with different spherulite properties. The viscoelastic behaviour in semi-crystalline polymers such as UHMWPE and HDPE is a combination of crystalline and amorphous phase mobility and the changes in these microstructures can lead to significant variation in the polymer properties.

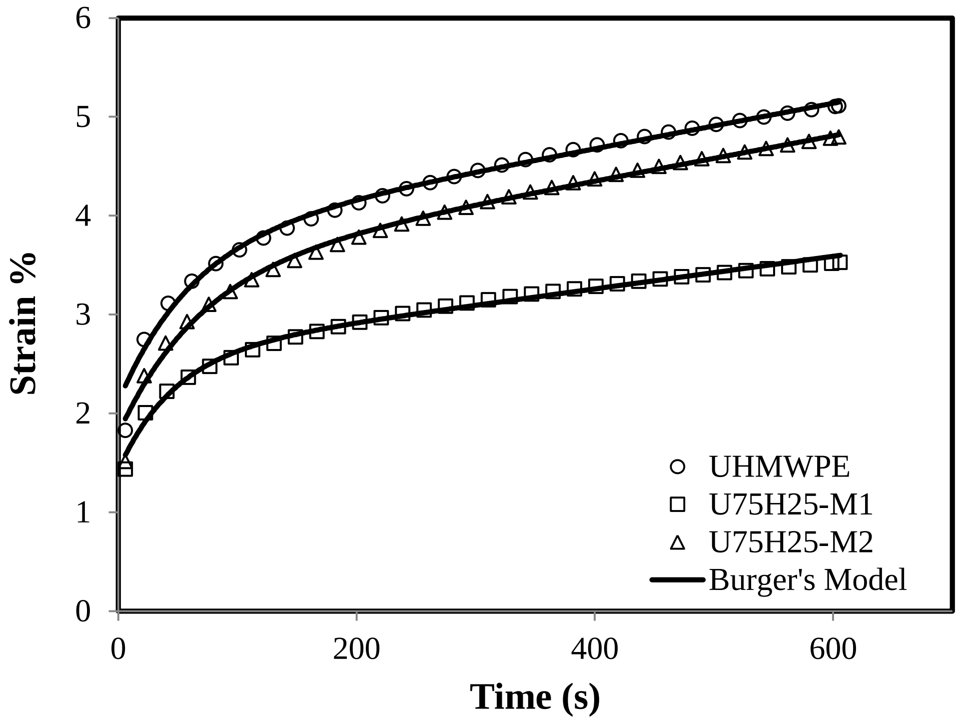

Figure 4.9: Comparison between the creep resistance of UHMWPE and the blends processed using M1 and M2 (9.3 MPa constant stress at room temperature).

4.4.2 Constitutive Modelling

Creep modeling and analysis is important in determining the time response of polymeric materials and can lead to a better understanding of the chain dynamics. Burger’s model, which is a combination of Kelvin-Voigt and Maxwell elements (see

Section 2.11), is a popular model to describe the linear viscoelastic behaviour of polymer composites. The total strain as a function of time can be obtained using Equation 2.4.

As shown in Figure 4.9, Burger's model results in an excellent fit to the experimental data. Table 4.2 shows the Burger's model fitting parameters. This indicates an increase in the elastic modulus of the spring with the addition of HDPE for both processing methods, (M1 and M2). The elasticity in the Maxwell element, E_M and the stiffness of the amorphous phase represented by the elasticity of the Kelvin spring, E_K, of the UHMWPE increases with the addition of the HDPE. The parameter η_M represents the irrecoverable creep strain, which also increases with the addition of HDPE using processing method M1. This indicates an increase in the resistance to permanent deformation in the M1 materials. This can be attributed to the poor miscibility of the U75H25 processed using M1, where HDPE can be found in separate phases. Retardation time, τ measures the delayed response to the applied stress and it can be seen that the retardation time for the U75H25-M1 is lower than the retardation time for UHMWPE and U75H25-M2.

Table 4.2: The parameters of Burger's model for creep tests.

Materials	E_M (MPa)	E_K (MPa)	η_M ($\times 10^3$ MPa.s)	τ (s)
UHMWPE	436	557	402	61.7
U75H25-M1	645	784	559	46.6
U75H25-M2	513	650	405	67.8

4.5 Depth Sensing Indentation Analysis

Depth sensing indentation (or nanoindentation) can be used to investigate the spatially resolved mechanical properties of materials. This technique is useful and directly applicable for materials with elastic-plastic response. However, polymers can exhibit time dependent behaviour which particularly affects the initial portion of unloading, and consequently the calculated contact depth and stiffness using standard methods. The creep displacement acts to reduce the apparent unloading stiffness, and in extreme case the creep displacement can be greater than the displacement recovery on initial unloading, resulting in a negative slope. This results in erroneous modulus value calculation. This effect can be reduced by using appropriate holding time at maximum load and a rapid unloading rate. In this study, the holding time at maximum load and the unloading rate were applied to minimise the effect of creep on the measured elastic modulus (see Section 3.4.6). Figure 4.10 shows the load-displacement curves for UHMWPE, HDPE, U75H25-M1 and U75H25-M2. 600s holding time at the maximum load (40mN) and an unloading rate of 2mN/s were used to minimise the effect of creep. This enabled unloading stiffness and contact area to be determined reliably, enabling the calculated modulus and indentation hardness to be used as measures of comparison between the different samples. It can be seen in Figure 4.10 that there is a significant difference between the unloading stiffness and indentation resistance of UHMWPE and HDPE, with HDPE being both stiffer and more resistant to plastic deformation. Intermediate results were achieved by mixing the HDPE with the UHMWPE. However, material processed using M1 shows higher stiffness and hardness than material processed using M2. This can be expected due to the presence of HDPE rich phases in the material processed by M1, while the behaviour of the material processed using M2 is dominated by the UHMWPE. These results are strongly in agreement with the stress-strain behaviour in tensile testing, as can be seen by comparison with Figure 4.1.

Table 4.3 summarises the average values of experimental data that were extracted from the load-displacement curves shown in Figure 4.10 using the Oliver and Pharr method described in Section 3.4.3. It can be seen that the elastic modulus and indentation hardness of HDPE are almost double those of UHMWPE. The material processed using M2 shows properties much closer to UHMWPE than the material processed using M1.

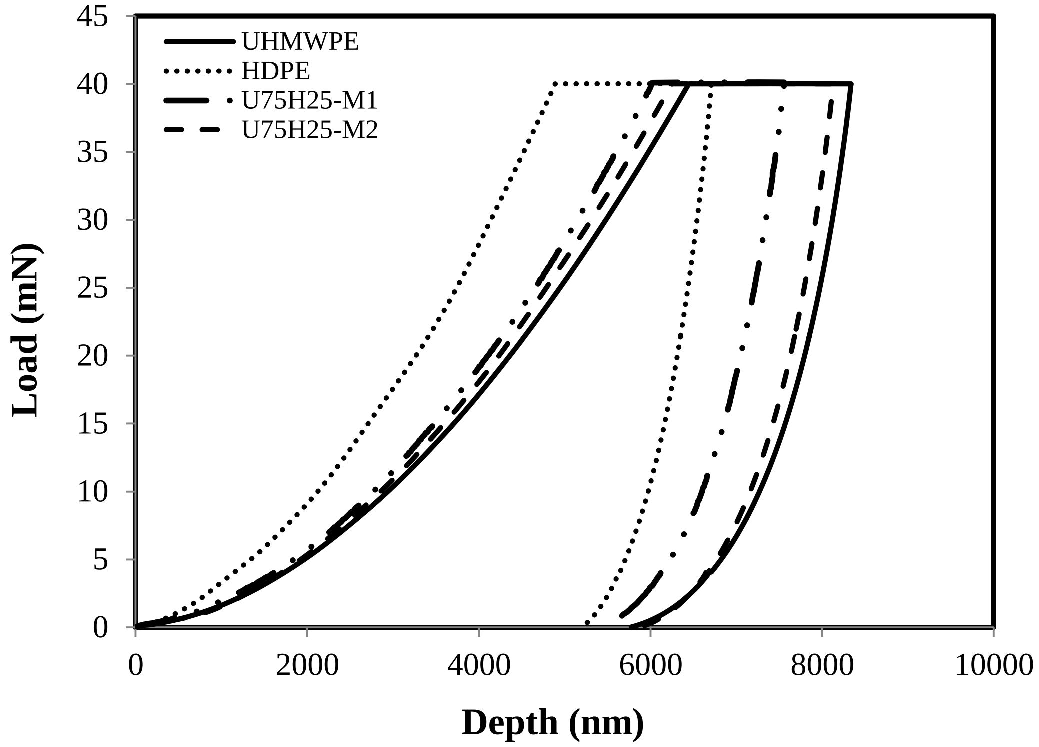

Figure 4.10: Comparison of the effect of processing method on the nanoindentation behaviour of polyethylene.

Table 4.3: Summary of nanoindentation test results.

Material	Elastic Modulus (MPa)	Hardness (MPa)	h_{max} (nm)	h_p (nm)	Δh (nm)
UHMWPE	720 ± 17	27.6 ± 1	8479 ± 97	7704 ± 89	1884 ± 12
HDPE	1432 ± 48	46 ± 1	6424 ± 104	5915 ± 110	1806 ± 9
U75H25-M1	979 ± 24	33.6 ± 3	7633 ± 140	6996 ± 141	1530 ± 14
U75H25-M2	830 ± 1	29.3 ± 2	8119 ± 142	7440 ± 138	1872 ± 10

Figure 4.11 shows the effect of processing method on the creep behaviour of the polyethylene blends at the micro-scale. This takes the time dependent deformation seen in the creep phase of the indentation curve and plots deformation against time at constant load. Unlike in a tensile test, the stress decreases with time in indentation creep as the contact area increases and hence the creep rate decreases, eventually becoming negligible. At this point unloading will result in mainly elastic recovery. It can be observed from the creep curves in Figure 4.11 and the change of depth during the dwell period values in Table 4.3 that the processing method can be an important factor in the creep behaviour. It can be seen from Table 4.3 that the change of depth during the dwell period for U75H25-M1 is 20% lower than that of UHMWPE. This indicates that the addition of HDPE to UHMWPE using processing method M1 can significantly affect the creep behaviour. On the other hand, it can be observed that there is no effect of the addition of HDPE to UHMWPE using processing method M2 on the creep resistance. This can be attributed to the improvement in the blend microstructure after increasing the processing temperature in processing method M2. These results are in excellent agreement with the bulk tensile creep results shown in Figure 4.9 and show the effectiveness of the DSI technique in investigating polymer material properties with high spatial resolution.

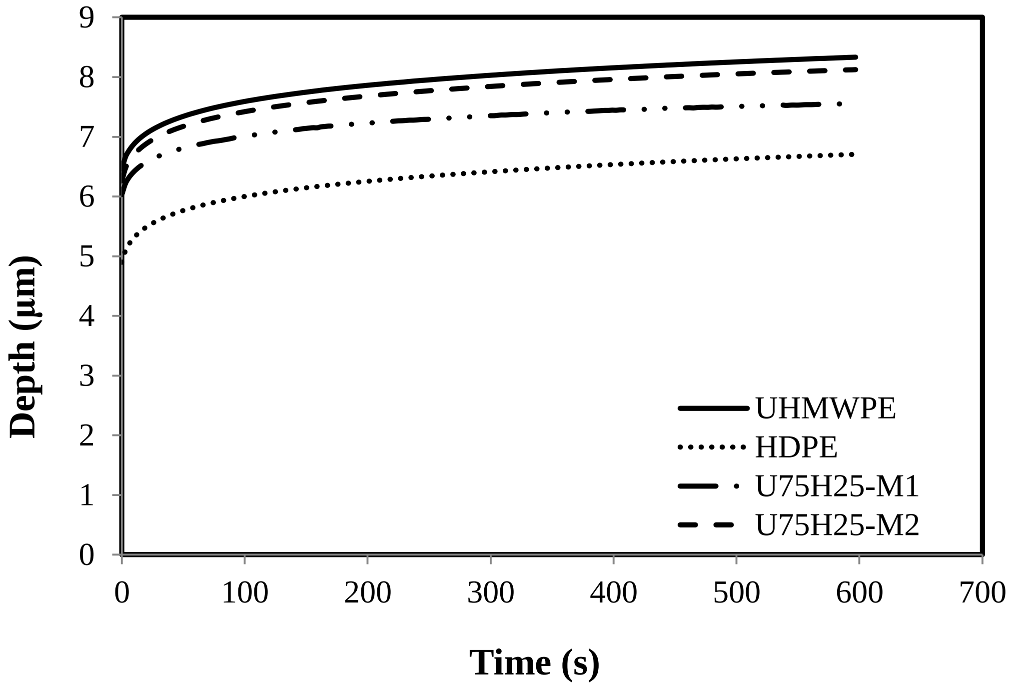

Figure 4.11: Effect of processing method on the creep resistance of U75H25 blends at a micro-scale (40 mN constant load at room temperature)

4.6 Summary

The results presented in this chapter showed the significant effects of processing method and strain rate on the polyethylene based material's properties. Two processing methods, M1 and M2, were used to prepare U75H25 blends. The effects of processing method on the mechanical properties of the blends were evaluated using various techniques such as tensile tests, creep tests, thermal imaging and depth sensing indentation. It was found that the processing method can significantly affect the toughness (area under the stress-strain curve) and the tensile strength. A significant reduction in these properties was observed for the U75H25 blend that was processed using method M1 compared to pure UHMWPE. This was attributed to the poor miscibility of HDPE and UHMWPE, which resulted in a microstructure with different phases such as pure UHMWPE, pure HDPE and blended material.

Material morphology and strain rate were found to be critical factors that affected heat generation during tensile testing, and consequently changed the mechanical behaviour. A significant temperature increase was observed after necking and continued until fracture. This temperature increase was detected using a high sensitivity thermal camera that was used simultaneously with the tensile test. Material processed using M1 showed higher heat generation during the plastic deformation compared to the material processed using M2. This was proposed to be due to the improvement in the miscibility of the second blend and the absence of voids and cavitation in the microstructure of the M2 material. The temperature increase during the plastic deformation increased with strain rate and caused thermal softening, which was observed in the strain hardening region.

The DSI results showed that the addition of HDPE using processing method M1 can increases the elastic modulus and stiffness of UHMWPE and reduce the permanent deformation. However, the material processed using M2 showed indentation properties much closer to UHMWPE.

Processing method was found to also be a critical factor in the creep behaviour of the blends at both micro and bulk scales. Blending 25 wt. % HDPE with 75 wt. % UHMWPE using M1 showed an increasing in the creep resistance of the blend. The addition of HDPE using M2 had no effect on the creep resistance of UHMWPE. Burger’s model was used to analyse the creep behaviour of the materials at bulk scale. The model was in a good agreement with the experimental data.

In summary then, it can be seen that by blending UHMWPE and HDPE, material properties between the two base materials can be obtained. Moreover, by varying processing parameters a range of blended polymer with different properties may be engineered. However, there are still limitations to the properties that can be attained by blending. These properties can potentially be enhanced with the addition of well dispersed nanofillers. Therefore, in Chapter 5, the effects of processing methods on the nanofiller dispersion will be discussed in details. Then, Chapter 6 shows how the addition of nanofiller can be used to further modify material properties.

Chapter 5
Processing Method Effect on the Dispersion of Nanoparticles

5.1 Introduction

Nanoparticle dispersion is an extremely important factor in the manufacture of nanocomposites that can affect both mechanical and rheological properties. In this chapter, scanning electron microscopy (SEM), transmission electron microscopy (TEM), X-ray diffraction (XRD) and depth sensing indentation are used to analyse nanoparticle dispersion in the U75H25 matrix using two processing methods M1 and M2. The effect of nanoparticle geometry on the formation of microcracks is also investigated.

5.2 Effect of Processing Method on the Blend Morphology

According to the results shown in Chapter 4, the processing temperature used in processing method M1 was not sufficient to completely melt the UHMWPE, which resulted in a pure UHMWPE phase immersed in a blend material. Increasing the processing temperature (see Section 3.2.2) resulted in a good mixed blend structure (see Section 4.2).

5.3 Microscopy Analysis of Nanoparticle Dispersion for Materials Processed using Method M1

The TEM and SEM images shown in Figures 5.1 to 5.4 show the dispersion of nanoparticles in the U75H25 matrix processed using processing method M1. Large aggregations of the CB nanoparticles can be seen in Figures 5.1 and 5.2. These aggregations of the CB nanoparticle reduce the surface to volume ratio, which is considered an important factor in the use of nanoparticles to improve material properties (Crosby and Lee 2007). Increasing the volume fraction of CB results in more aggregations, as shown in Figure 5.2, highlighted with the white circles. Large aggregation areas can be considered as defects in the microstructure of U75H25 due to the weak Van der Waals interaction between the CB nanoparticles.

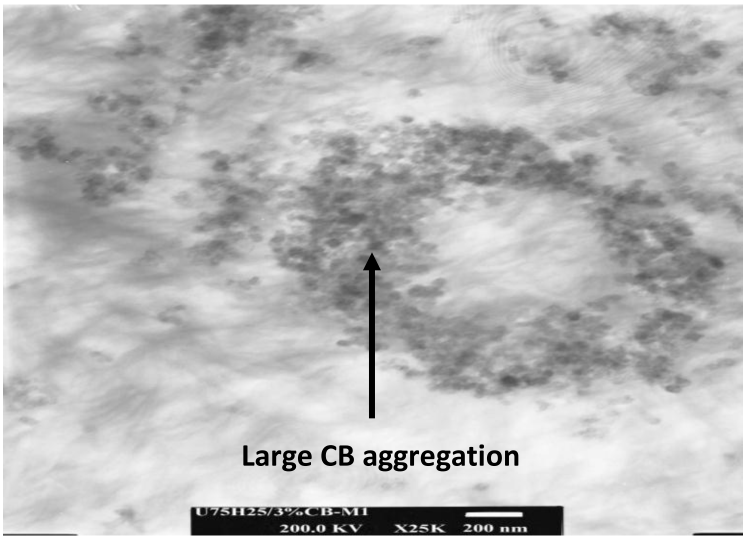

Figure 5.1: TEM image for 3 wt. % CB dispersion in U75H25 matrix using processing method M1.

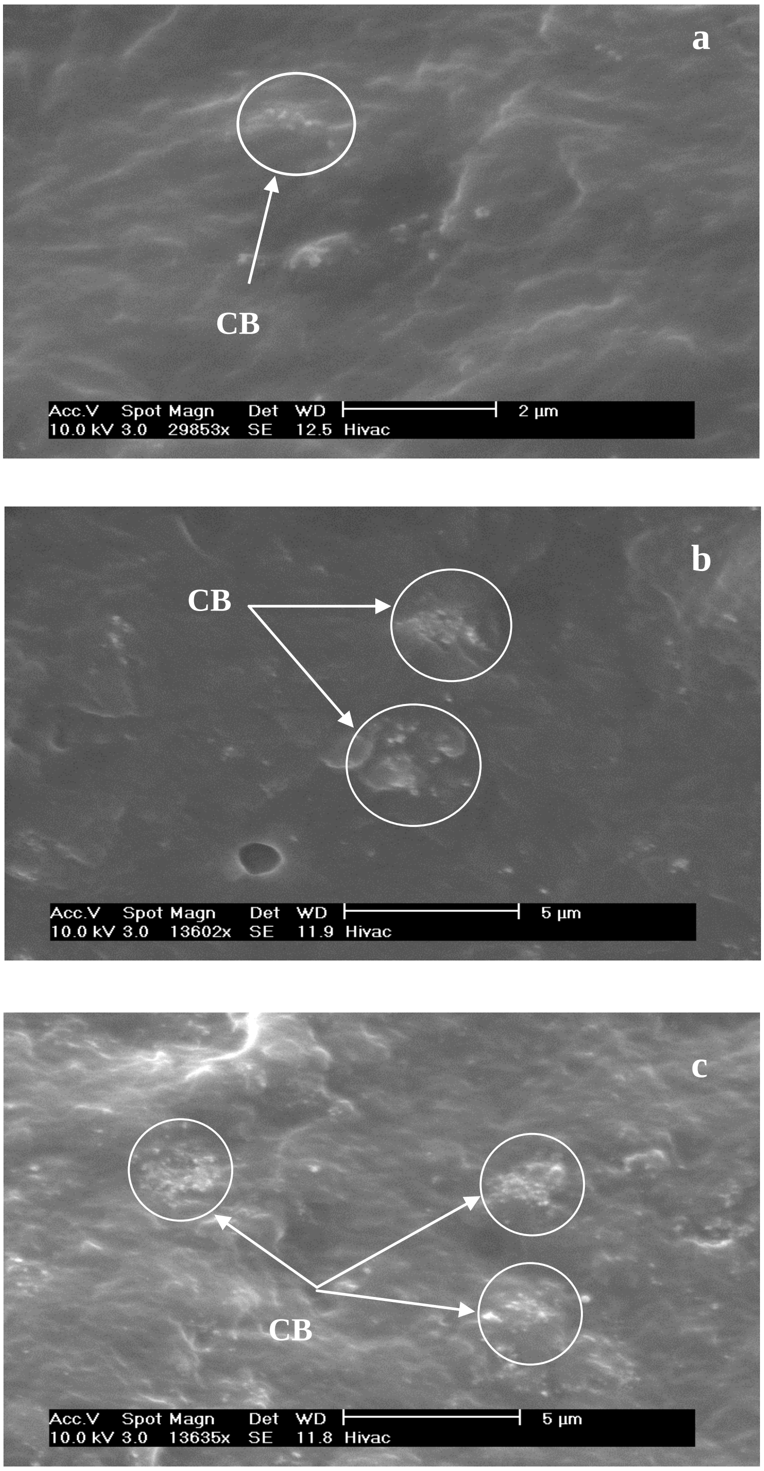

Figure 5.2: SEM images for CB dispersion in the U75H25 matrix using processing method M1: a) 0.5wt. % CB, b) 1 wt. % CB and c) 3 wt. % CB.

A reasonable dispersion of 0.5 wt. % CNT in the U75H25 matrix can be seen in the SEM image, Figure 5.3. CNTs are highlighted with the white circles and minor grouping of the nanotubes can be seen. Figure 5.4 is a TEM image of U75H25-0.5 wt. % clay processed using M1, which shows separate clay layers within the polymer matrix. The layers can be identified as the dark regions in the image, and this indicates good dispersion of the clay platelets in the polymer matrix.

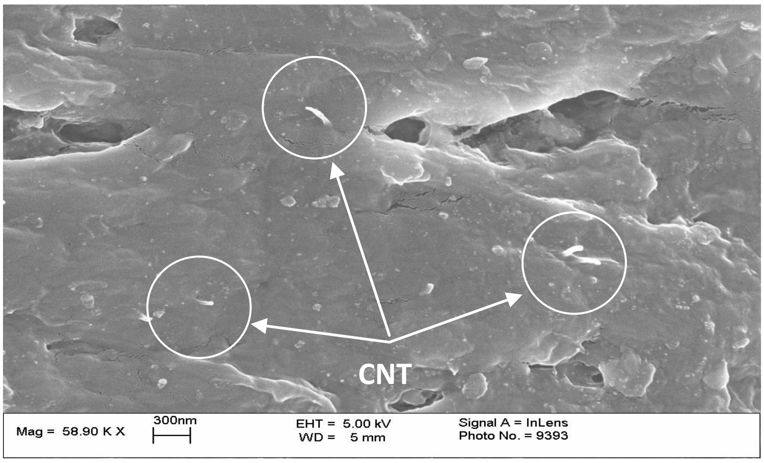

Figure 5.3: TEM image for the dispersion of 0.5 wt. % CNT in U75H25 matrix using processing method M1.

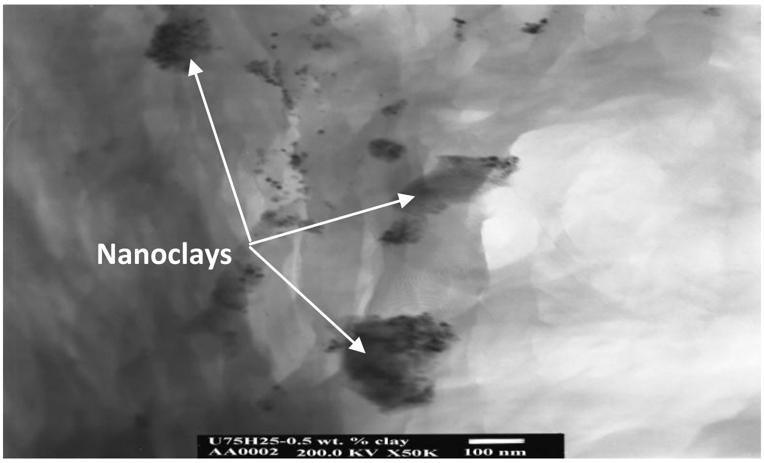

Figure 5.4: TEM image for the dispersion of 0.5 wt. % clay in U75H25 matrix using processing method M1.

5.4 Microscopy Analysis of Nanoparticle Dispersion for Materials Processed using Method M2

In processing method M2, the processing parameters were changed and the temperature was increased to a critical value to ensure full melting of the UHMWPE phase, as shown in Section 5.2. The M2 process provides a more homogeneous structure of the blend and the high processing temperature also enables the nanoparticle to disperse more effectively in the U75H25 matrix. Figure 5.5 shows an example of the improvement in CB dispersion using processing method M2 compared to M1 at the same volume fraction, as seen in Figure 5.1. From Figures 5.6 and 5.7 It can be seen that at low volume fraction (0.5 wt. %) of CB and CNT there are no large aggregates of nanoparticles. With increasing nanofiller content (1 wt. %), some small aggregations of CB can be observed, highlighted with the black arrows in Figure 5.6b, whereas no aggregation of CNTs are seen at a similar volume fraction, Figure 5.7b. For higher volume fractions (3 wt. %) of both CB and CNT, large aggregations can be seen in Figures 5.6c and 5.8c, which indicates that this volume fraction is greater than the maximum volume fraction of nanoparticles of the dispersion of CB and CNT into the U75H25 blend. Further evidence of the dispersion and aggregation of CNT and CB nanoparticles can be seen in the TEM images in Figure 5.8. These images provide further evidence for the large aggregations of both CB and CNTs at 3 wt. %.

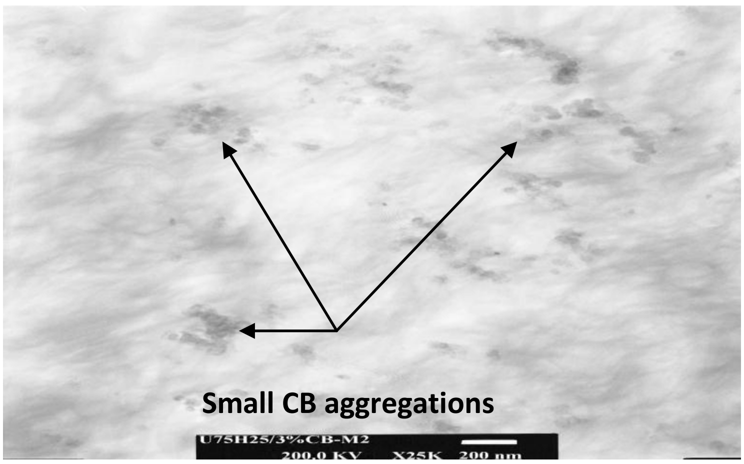

Figure 5.5: TEM images for the 3 wt. % CB dispersion in U75H25 matrix using processing method M2.

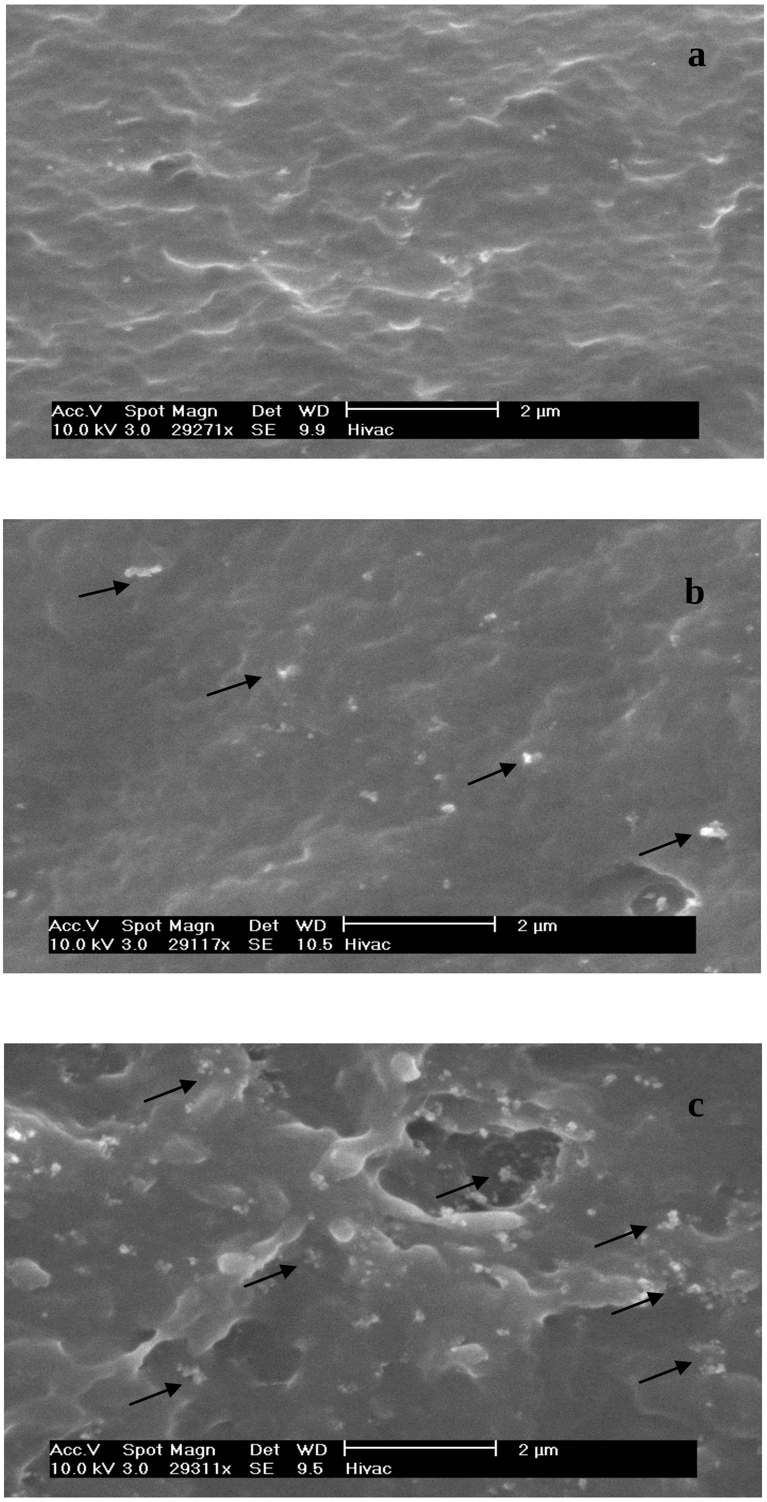

Figure 5.6: SEM images for the CB dispersion in U75H25 matrix: a) 0.5wt. % CB, b) 1 wt. % CB and c) 3 wt. % CB (arrows indicate the CB aggregations).

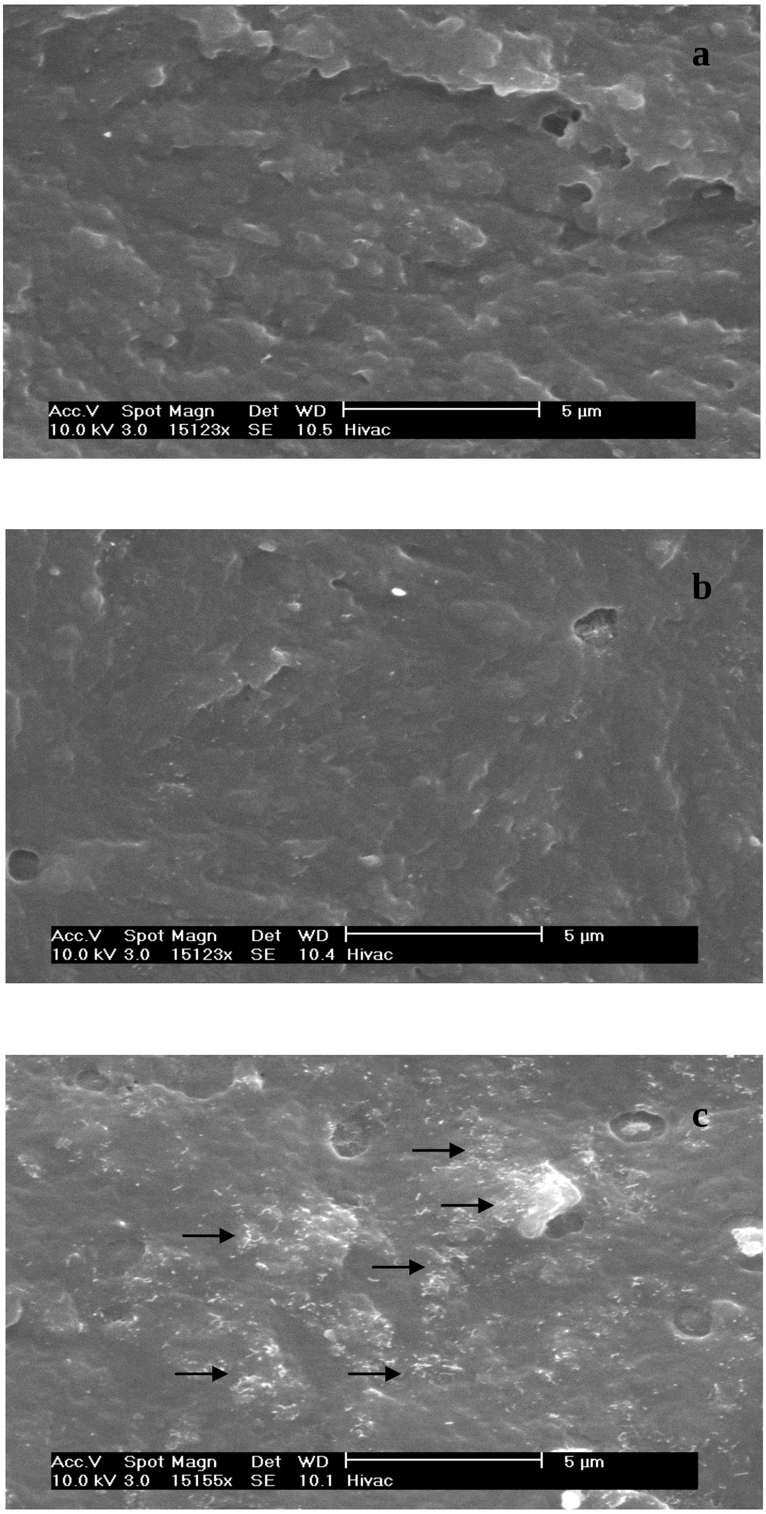

Figure 5.7: SEM images for the CNT dispersion in U75H25 matrix: a) 0.5wt. % CNT, b) 1 wt. % CNT and c) 3 wt. % CNT (arrows indicate the CNTs aggregations).

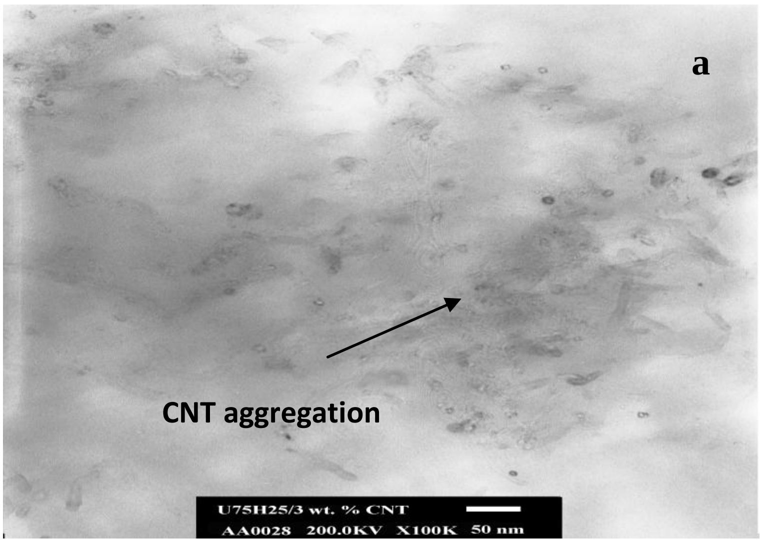

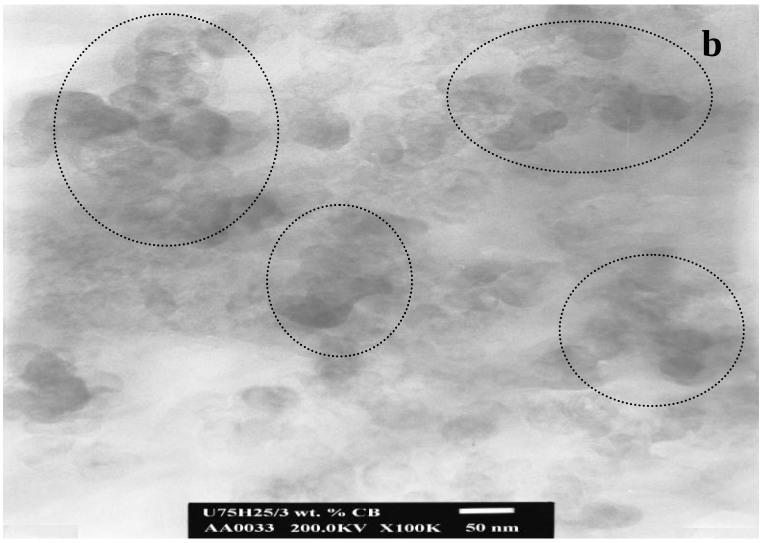

Figure 5.8: SEM images for the dispersion of nanofiller in U75H25 matrix: a) 3 wt. % CNT and b) 3 wt. % CB (circles indicate the CB aggregations).

Figure 5.9a shows an individual nanoclay layer in the M2 blend matrix, the clay being the dark region in the image. XRD experiments were also carried out to investigate nanoclay dispersion, with the results shown in Figure 5.9b. It can be seen from the XRD profiles that the peak seen with the original clay is not seen with the U75H25/clay nanocomposites, which is a typical feature of exfoliation. This supports the identification of single clay layers in the TEM investigation of the U75H25/clay nanocomposites.

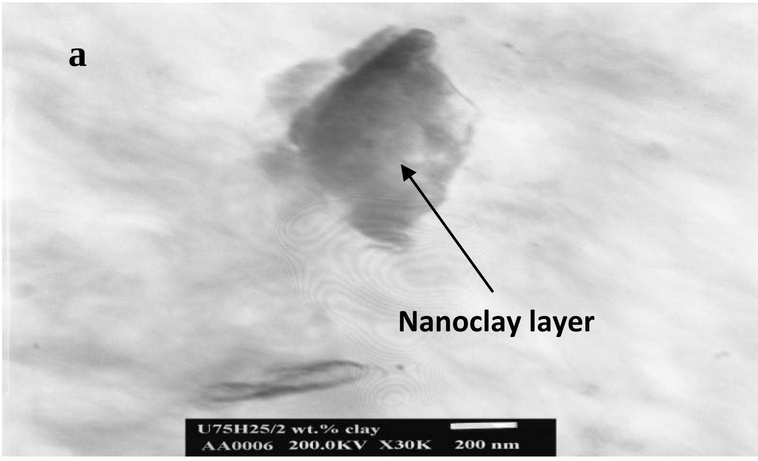

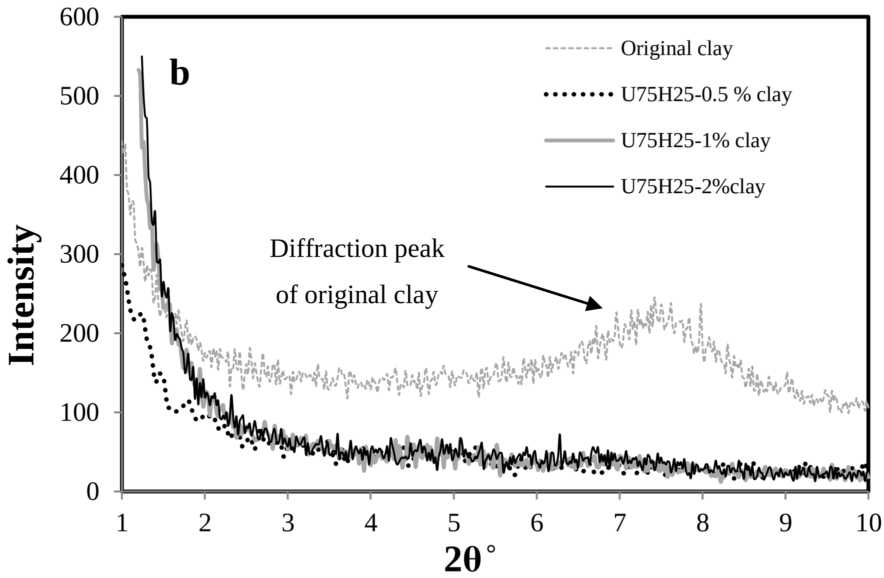

Figure 5.9: a) TEM image for the dispersion of clay into the blend matrix and b) XRD pattern.

5.5 Depth Sensing Indentation Results

5.5.1 Introduction

In recent years, several experimental techniques have been used to analyse nanoparticle dispersion at the micro or nano-scale. These include scanning electron microscopy (SEM), transmission electron microscopy (TEM) and X-ray diffraction (XRD), as discussed in the previous sections. However, enlarging the measurement scale can also provide information about nanoparticle dispersion, which is not achievable using the previous techniques. Therefore, in this work a DSI method was used to investigate the spatially resolved properties of the nanocomposites, in this case indentation hardness, over an area of approximately 1 mm^2. The variations in hardness value were used to evaluate the effect of the processing method on the blend morphology and the dispersion of CB, CNT and clay nanoparticles. This technique additionally gives information on the effect of nanoparticle dispersion on the spatially resolved mechanical properties.

5.5.2 The Properties of the Non-Reinforced Materials

The results are shown in Figures 5.10 to 5.15 for processing methods M1 and M2 compared with the pure UHMWPE and HDPE. In Figure 5.10, it can be seen that the influence of adding HDPE to the UHMWPE is to significantly increase the indentation hardness and the variation of hardness across the sample, which indicates poor mixing of the two polymer phases (UHMWPE and HDPE). In Figure 5.11, it can be seen that the hardness of the blend is similar to that of the UHMWPE and there is less variation in hardness than seen with M1. This indicates a better miscibility of the HDPE into the UHMWPE microstructure.

5.5.3 Dispersion of CB Nanoparticles

Looking now to the effect of adding CB to the blends, Figure 5.10 shows an increase in hardness and variation in hardness on the addition of CB. This indicates the formation of aggregations of CB nanoparticles during the preparation of the nanocomposites using M1. For the M2 processing method, there is less variation in hardness, which indicates that the CB appears to be more uniformly dispersed throughout the U75H25 matrix, particularly at 0.5 and 1 wt. %, as seen Figure 5.11. However, a greater difference in the indentation hardness values is observed at higher CB content, which, can be explained by the large aggregation of CB particles at high volume fraction, which is not unexpected. In terms of hardness for the materials processed using method M2, the blend with 0.5 wt. % CB has a similar low value to the unreinforced blend and the UHMWPE. The blends with higher CB black content have higher hardness values; however, these are still significantly lower than seen with the materials processed using method M1. These results are in agreement with the SEM and TEM images that were discussed in previous sections.

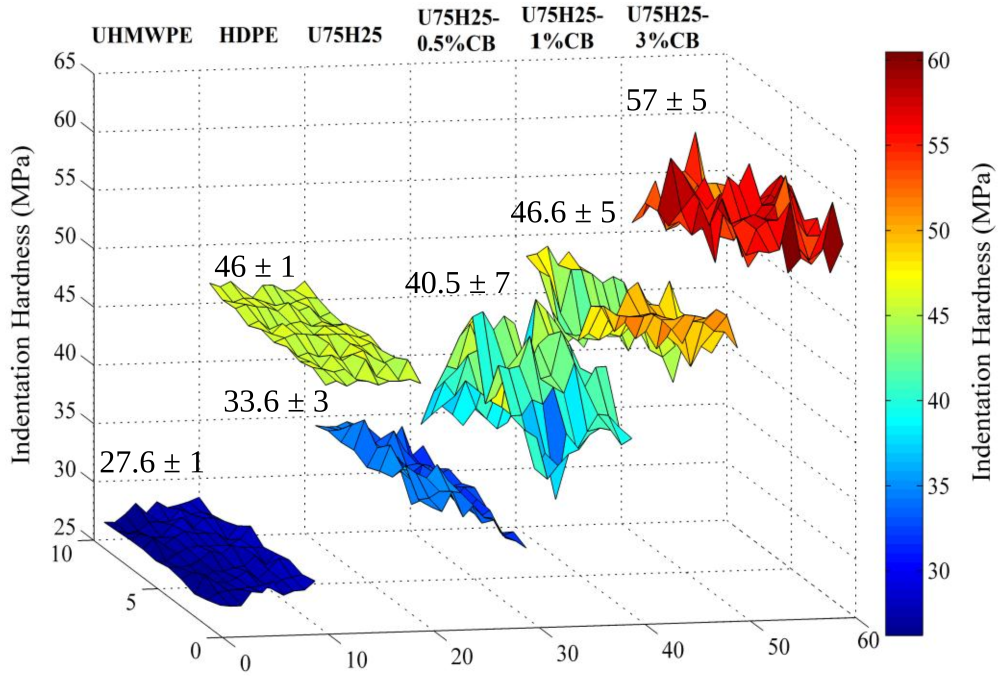

Figure 5.10: Indentation hardness for polyethylene & U75H25-CB nanocomposites using processing method M1, including mean and standard deviation values.

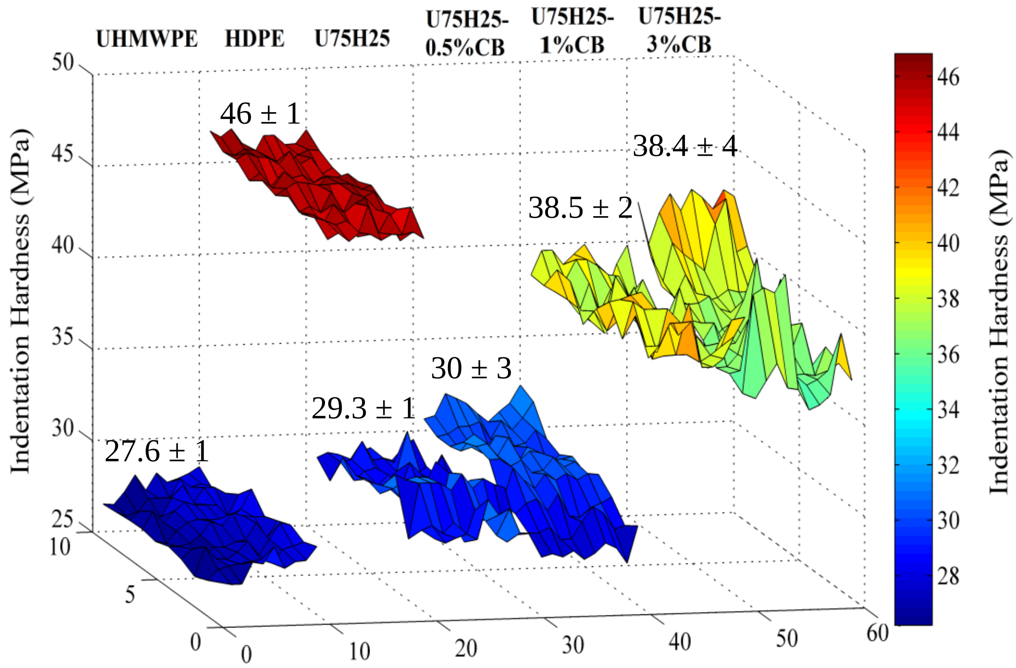

Figure 5.11: Indentation hardness for polyethylene & U75H25-CB nanocomposites using processing method M2, including mean and standard deviation values.

5.5.4 Dispersion of Clay Nanoparticles

Figures 5.12 and 5.13 show the effect of processing method on the dispersion of clay in the U75H25 matrix. An increase in the indentation hardness can be seen with the addition of 0.5 wt. % clay to the blend matrix. However, the results indicate a reasonably good distribution of the clay particles in the U75H25 blend. This is in agreement with the TEM image of the clay dispersion seen in Figure 5.4. The incorporation of clay particles using M2 shows a better distribution compared to material processed using M1, as seen in Figure 5.13. Additionally, no change in the indentation hardness is observed by the addition of 0.5 wt. % clay using processing method M2. Figure 5.14 indicates that the addition of 1 and 2 wt. % clay can lead to significant increases in the indentation hardness values. However, large variations in the indentation hardness can also be observed, which increase with clay volume fraction. This indicates the presence of intercalation of clay nanoparticles, which cannot be observed using XRD, as shown in Figure 5.9b. This can be used as evidence that an enlarged test area can lead to valuable information about the nanoparticle dispersion.

5.5.5 Dispersion of CNT Nanoparticles

Figure 5.12 shows that the addition of 0.5 wt. % CNT to the U75H25 using processing method M1 results in large variations in the indentation hardness values, which cannot be seen clearly using the SEM technique, as shown in Figure 5.3. This variation indicates the presence of CNT aggregations at low volume fractions. Adversely, the incorporation of 0.5 wt. % CNT using processing method M2 shows a significant increase in the indentation hardness with homogeneous distribution of the nanotubes, as shown in Figure 5.13. The addition of CNT using processing method M2 gives a better dispersion of the nanoparticle in the U75H25, therefore this method was used to process nanocomposites with higher volume fractions of CNT. In Figure 5.15, increasing the volume fraction to 1 wt. % CNT shows a similar effect on the indentation hardness as 0.5 wt. % CNT, with slight changes in the indentation hardness values. However, at 3 wt. % CNT, large variations in the indentation hardness values can be observed, which can be used as evidence of the existence of CNT aggregations. This is in agreement with the SEM and TEM images in Figures 5.7c and 5.8a, respectively.

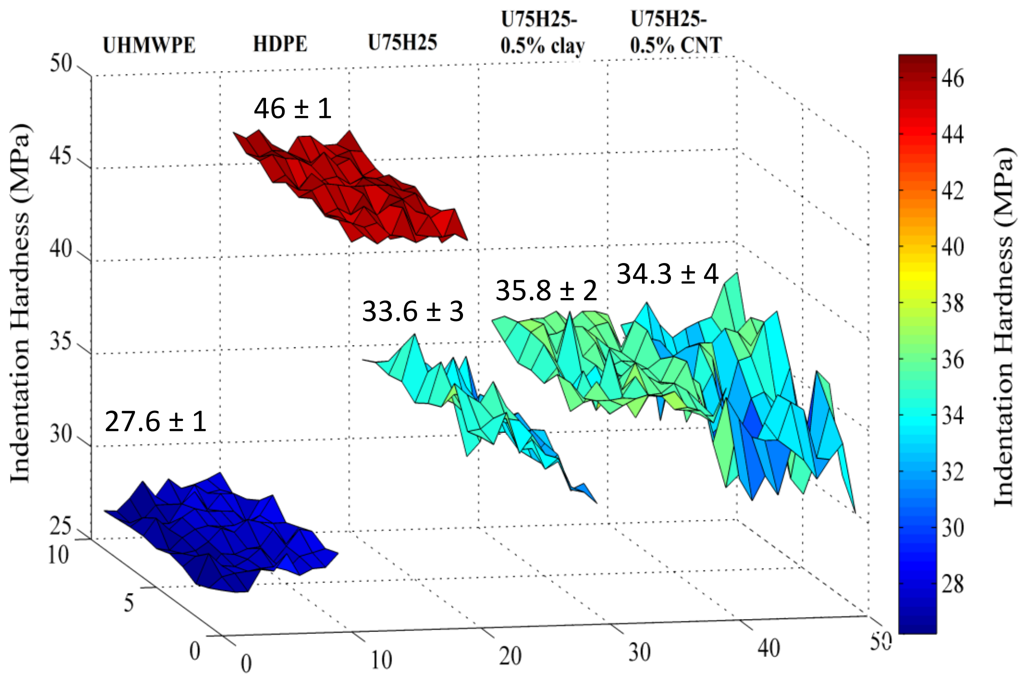

Figure 5.12: Indentation hardness for polyethylene blend & nanocomposites using processing method M1, including mean and standard deviation values.

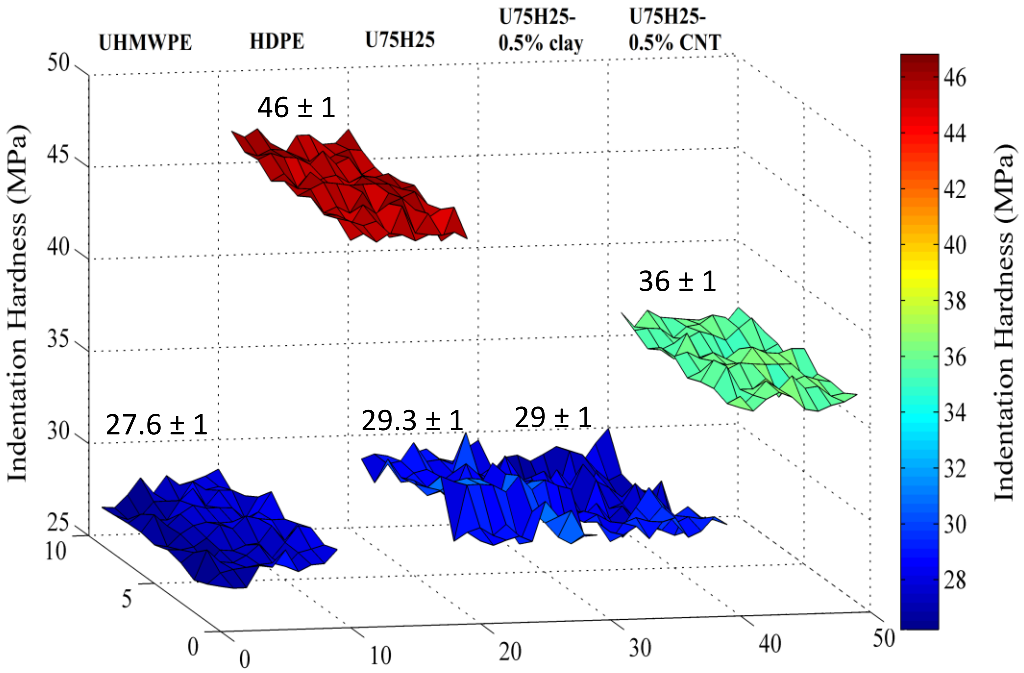

Figure 5.13: Indentation hardness for polyethylene blend & nanocomposites using processing method M2, including mean and standard deviation values.

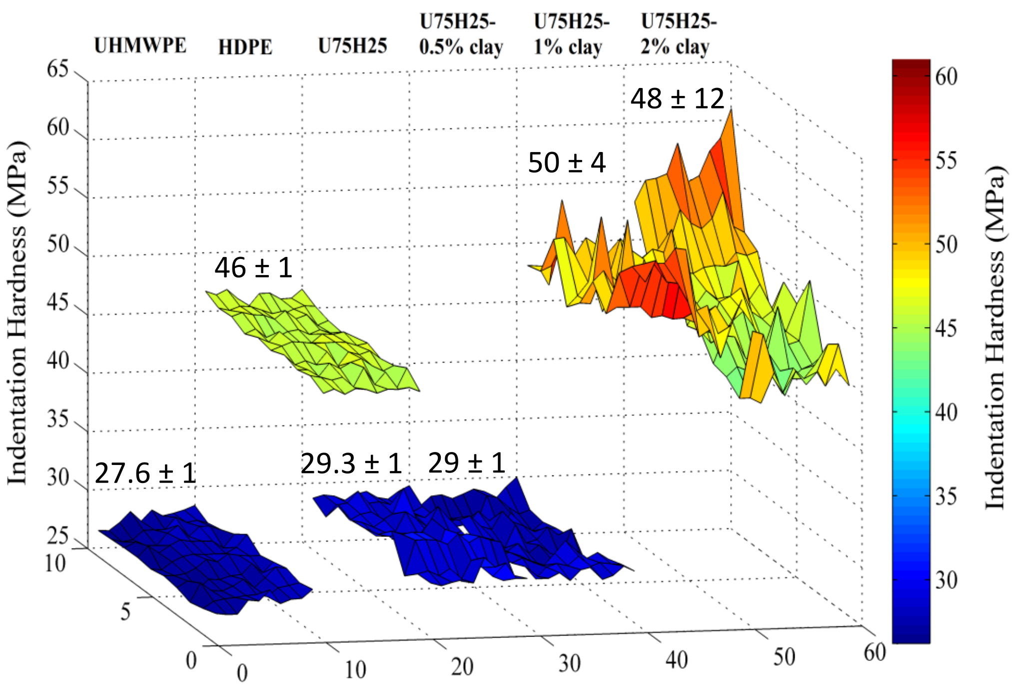

Figure 5.14: Indentation hardness for polyethylene & U75H25-clay nanocomposites using processing method M2, including mean and standard deviation values.

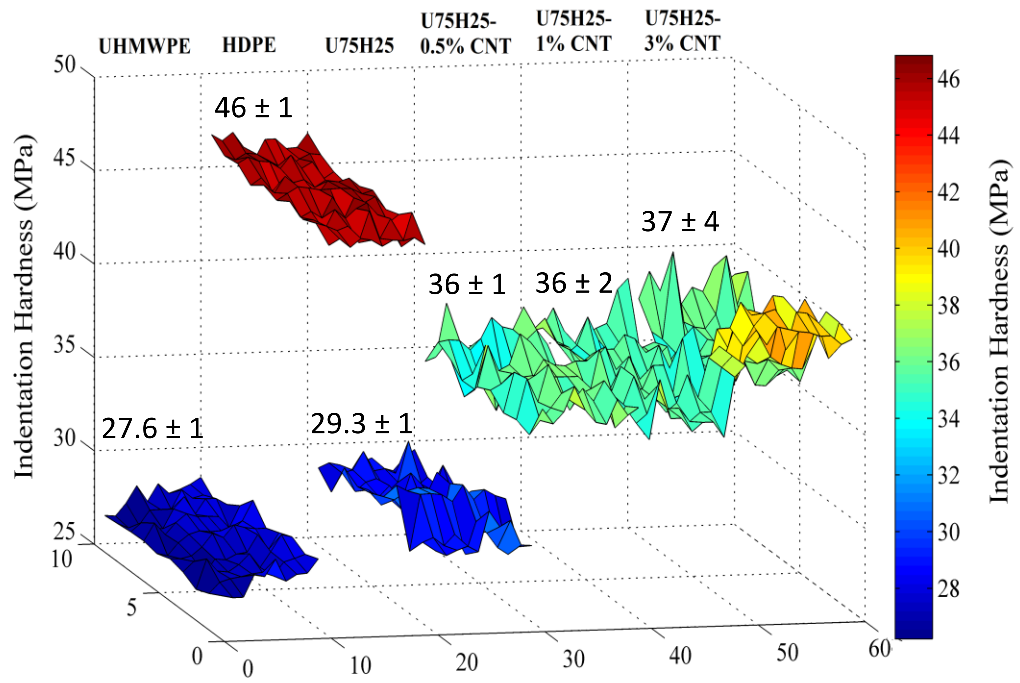

Figure 5.15: Indentation hardness for polyethylene & U75H25-CNT nanocomposites using processing method M2, including mean and standard deviation values.

5.6 Crystallinity of the Polyethylene-based Nanocomposites

Table 5.1 summarises the effect of processing method and the addition of nanoparticles on the crystallinity and melting temperature of the polyethylene nanocomposites. Universal Analysis software was used to calculate the crystallinity based upon 290 J/g for the 100 % crystalline material. It can be seen that there is a significant increase in the crystallinity when adding 0.5 wt. % clay using processing method M1, which affects the yield stress of the material (as will be discussed in Section 6.2). Owing to the small variations in the crystallinity values for all other materials, the crystallinity effect can be ignored as a major influence on the mechanical properties of the nanocomposites developed in this work.

Table 5.1: Mean values for the crystallinity and melting point of materials studied in this work.

Material	Crystallinity %	Melting point (°C)
U75H25-0.5 wt.% CB-M1	55.3 ± 1.6	137.3 ± 1
U75H25-0.5 wt.% CNT-M1	49 ± 2	138 ± 1
U75H25-0.5 wt.% clay-M1	70.1 ± 2.5	137.4 ± 1.2
U75H25-0.5 wt.% CB-M2	53 ± 3.5	138.1± 1.6
U75H25-0.5 wt.% CNT-M2	55 ± 1.6	139.3 ± 0.5
U75H25-0.5 wt.% clay-M2	56 ± 0.2	137.5 ± 1
U75H25-1 wt.% CB-M1	54.4 ± 0.7	138.4 ± 0.7
U75H25-1 wt.% CB-M2	54 ± 2.6	136.8 ± 0.2
U75H25-1 wt.% CNT-M2	53 ± 2.6	135 ± 0.5
U75H25-1 wt.% clay-M2	56 ± 0.4	138.7 ± 0.5
U75H25-3 wt.% CB-M1	54.6 ± 3.4	137 ± 1.4
U75H25-3 wt.% CB-M2	51.7 ± 1.3	137.3 ± 1.7
U75H25-3 wt.% CNT-M2	51.3 ± 3	134 ± 0.5
U75H25-2 wt.% clay-M2	57 ± 2	137 ± 1

5.7 Microcrack Formation in Samples Loaded in Tension

Figures 5.16 to 5.18 show SEM images of the surface features of polyethylene and polyethylene-based nanocomposite samples loaded in tension at 0.2 s^{-1} strain rate to 600 % strain. It can be seen in Figure 5.16a that no cracks formed on the surface of the stretched UHMWPE specimen. The effect of processing conditions on the microstructure of the U75H25 can be inferred from the SEM images shown in Figures 5.16b and 5.16c. Large numbers of micro-cracks are formed on the stretched surface of the blended polymer processed using M1, whereas only a small number of cracks are seen in the case of process M2. This indicates the formation of microvoids during the incomplete mixing in process M1 and the lack of interfacial strength between the two polymer phases. The addition of clay using processing method M1 causes more cracks compared to processing method M2, as seen in Figure 5.17. This can be attributed to the poor miscibility of the blend and the weak interaction between the nanoclay and the polymer matrix. However, the crack distribution indicates good distribution of the exfoliated clay, which is in agreement with the nanoindentation result shown in Figure 5.12.

Increasing the volume fraction of clay leads to more crack formation, as seen in Figure 5.18 for nanocomposites processed using M2. This can be used as further evidence of the weak interaction between the clay and the polymer matrix. The distribution of cracks that formed on the stretched surface of U75H25-1 wt. % clay can be used as evidence of the good distribution of the clay in the polymer matrix. However, for higher volume fraction of clay (2 wt. %), it can be seen that crack size is larger, which can be attributed to a poor distribution of clay and the existence of intercalation of the nanoclay layers, as shown in Figure 5.18b. For the U75H25-CB and U75H25-CNT materials processed using both M1 and M2, no significant crack formation was found, which can be considered to be evidence of better miscibility of the nanocomposites and better nanoparticle-matrix interactions. An example can be seen in Figure 5.19 for the nanocomposites processed using M1 and M2 with high volume fractions of CB and CNT, respectively.

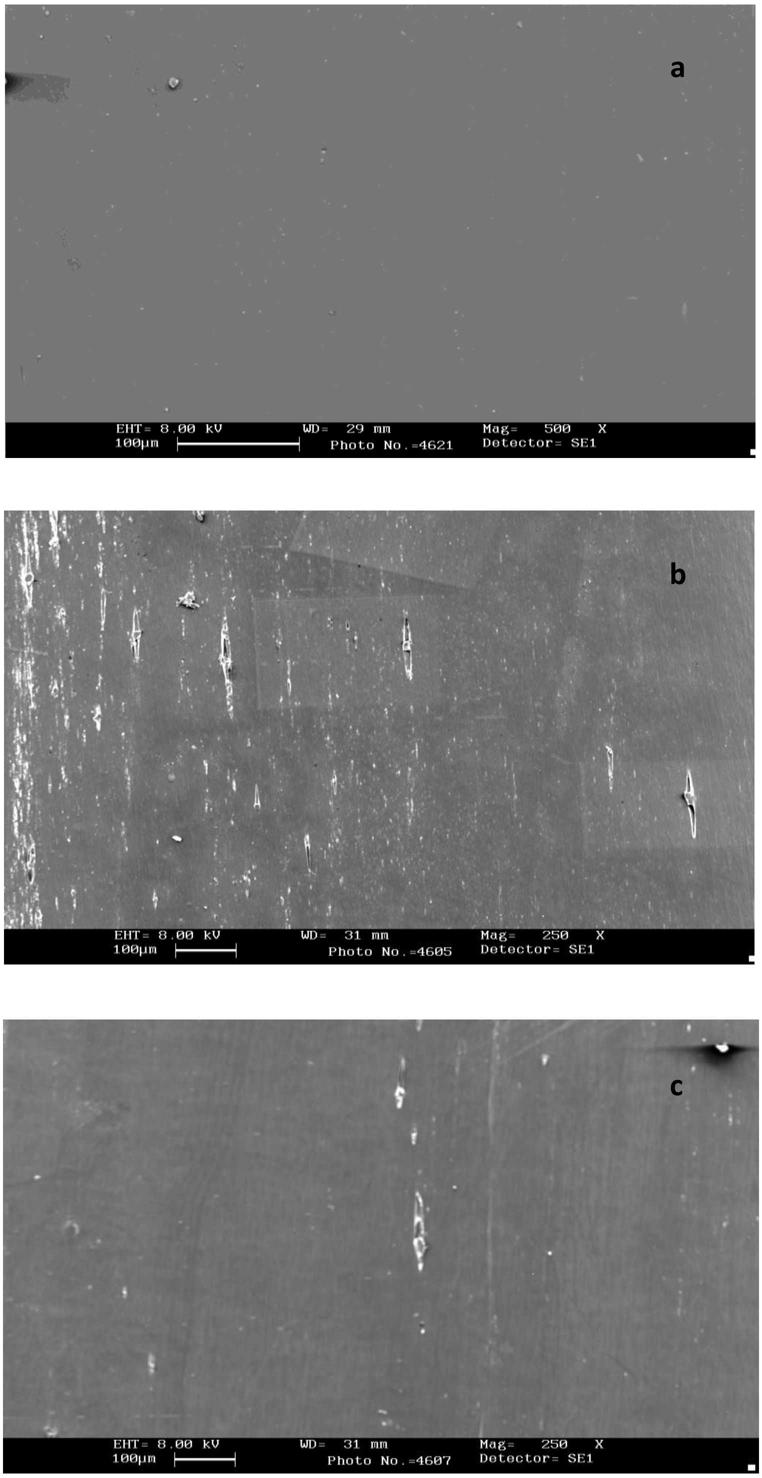

Figure 5.16: SEM images for samples stretched at 0.2 s^{-1} strain rate to 600 % strain: a) UHMWPE b) U75H25-M1 and c) U75H25-M2.

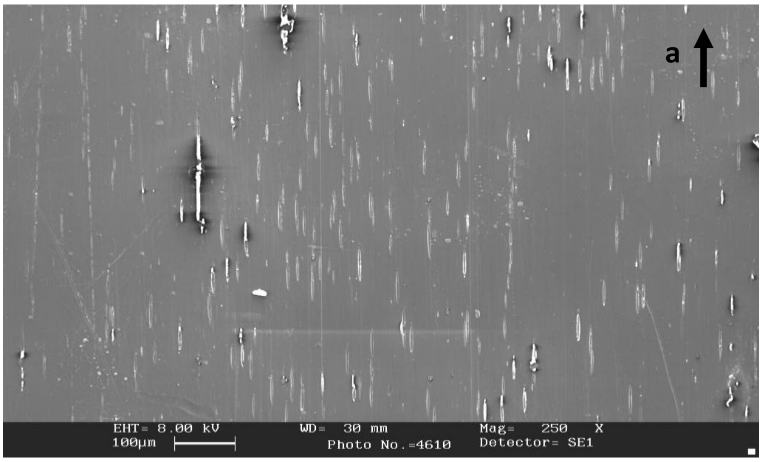

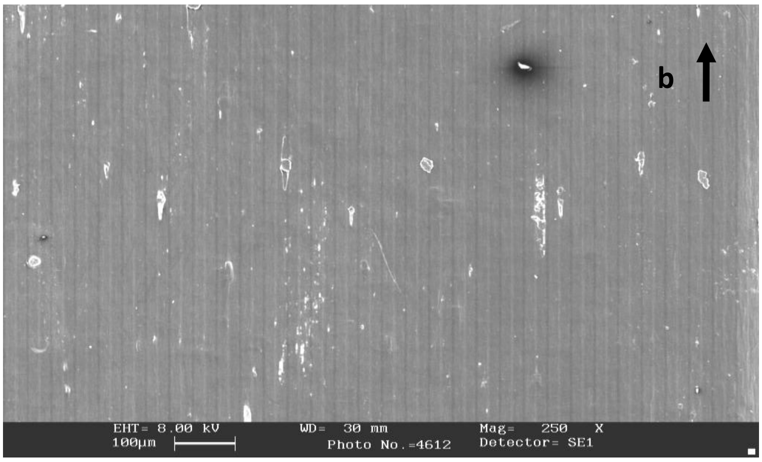

Figure 5.17: SEM images of the surface features of the stretched samples to 600 % strain: a) U75H25-0.5 wt. % clay-M1 and b) U75H25-0.5 wt. % clay-M2 (arrows indicate the direction of strain).

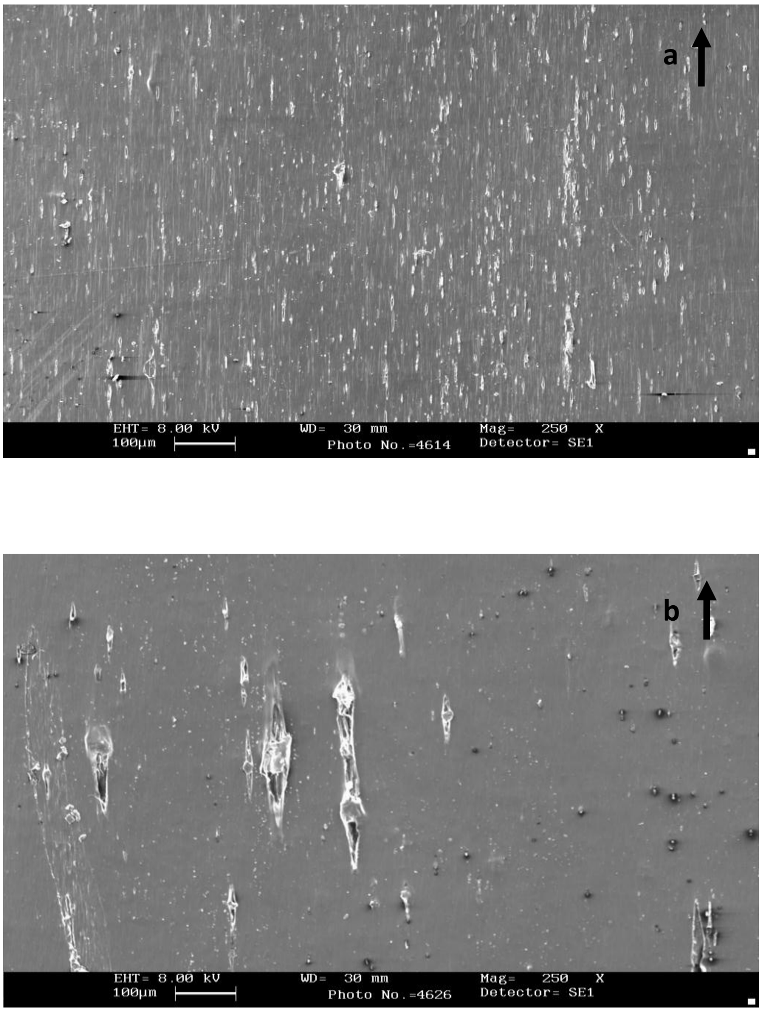

Figure 5.18: SEM images of the surface features of the stretched samples to 600 % strain: a) U75H25-1 wt. % clay-M2 and b) U75H25-2 wt. % clay-M2 (arrows indicate the direction of strain).

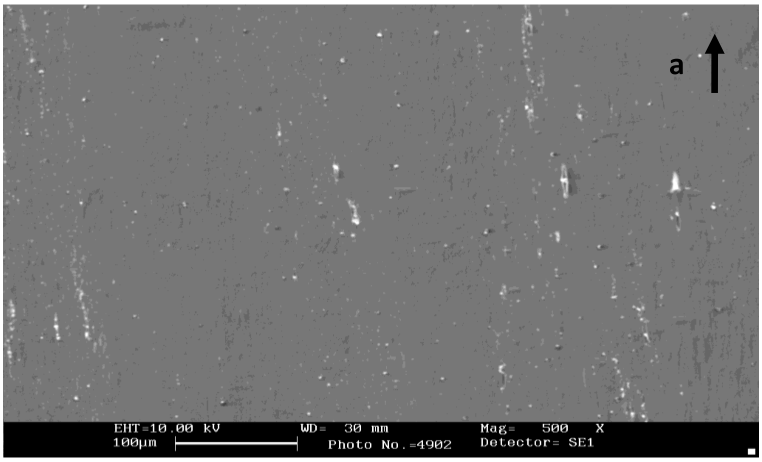

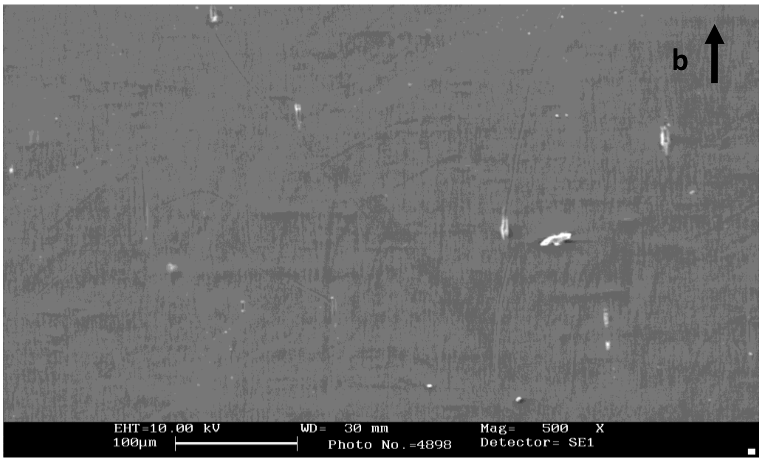

Figure 5.19: SEM images of the surface features of the stretched samples to 600 % strain: a) U75H25-3 wt. % CB-M1 and b) U75H25-3 wt. % CNT-M2 (arrows indicate the direction of strain).

5.8 Fracture Behaviour of the Polyethylene-based Nanocomposites

The fracture surfaces of the specimens after tensile testing were observed by SEM. Figures 5.20 to 5.24 show the micro-morphology of the fracture surfaces of UHMWPE, HDPE, blends and nanocomposites. In Figure 5.20a, the fracture surface of the UHMWPE indicates that no voids and fibrils were generated during elongation and a relatively smooth fracture surface results. The fracture surface features for HDPE are very different, as seen in Figure 5.20b. Large polymer flakes and fibrils can be seen in the matrix with large cavity formations. Also, there are numerous nodules, which are the actual separation areas (Brough et al. 2004; Sui et al. 2009). The presence of long fibrils can be considered as a feature of crazing or deformation areas in the HDPE, which can lead to the initiation of cracks and results in the absorption of fracture energy (Brough et al. 2004).

Figure 5.21 shows the effect of processing method on the fracture surface features of the U75H25 blends. There are obvious differences between the U75H25 blends processed using M1 and M2. In the fracture surface for U75H25-M1, shown in Figure 5.21a, large nodules can be seen, which has been proposed to contraction of polymer fibrils during fracture (Sui et al. 2009). Crazing and crack formation can found in the microstructure, as highlighted by white rings. These cracks can be attributed to the poor miscibility of the blend processed using M1, which produced material with two different phases (UHMWPE and HDPE). The presence of pure HDPE phases can lead to crazing and consequently cracking. In contrast, processing the U75H25 blend using processing method M2 results in a material with similar fracture surface features to the UHMWPE, as seen in Figure 5.21b.

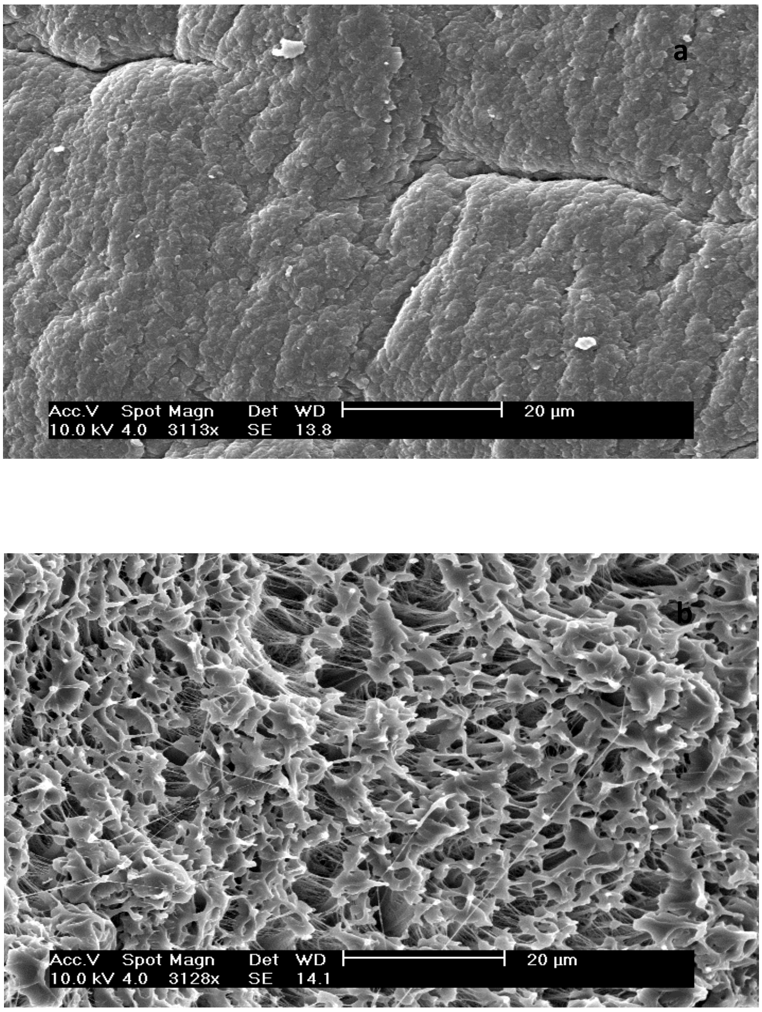

Figure 5.20: SEM images for the fracture surface of: a) UHMWPE and b) HDPE after tensile testing at 0.2 s^{-1} strain rate and 25°C room temperature.

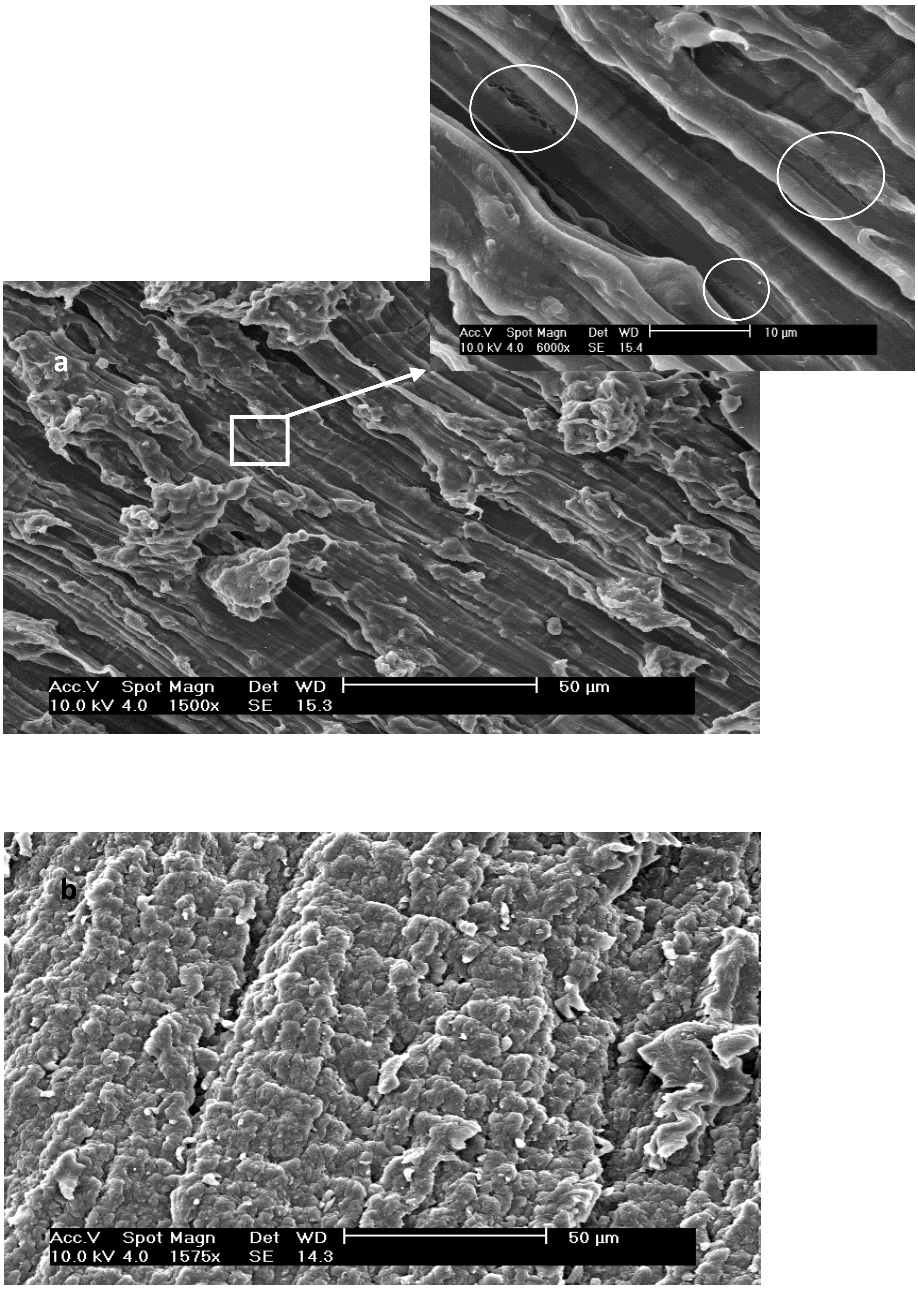

Figure 5.21: SEM images for the fracture surface of: a) U75H25-M1 (white rings indicate the microcracks) and b) U75H25-M2 after tensile testing at 0.2 s^{-1} strain rate and 25°C room temperature.

Figures 5.22 to 5.24 show the surface fracture features of the polyethylene-based nanocomposites. In Figure 5.22a, it can be seen that there is evidence of intercalated nanoclay layers at high volume fraction (2 wt. % clay). This is in agreement with the nanoindentation results shown in Figure 5.14. The poor interaction between the intercalated clay layer and the polymer matrix can lead to the formation of large microcracks as seen in Figure 5.18b. The presence of clay platelets can also enhance the formation of internal microvoids as seen in Figure 5.22b, which shows the existence of voids in the interior structure of the sample.

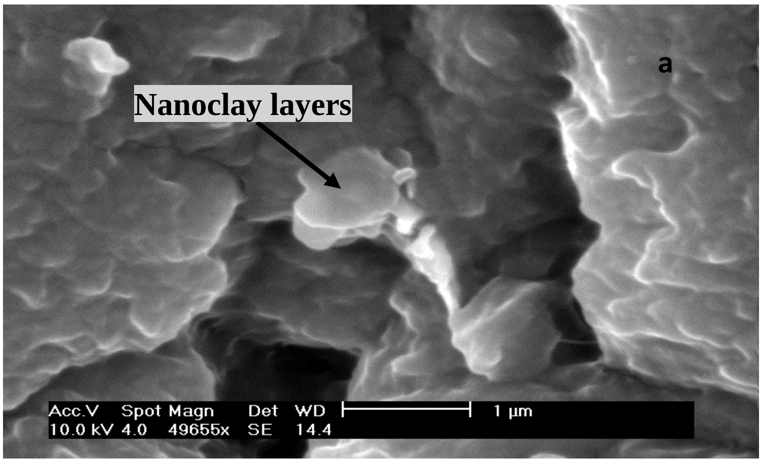

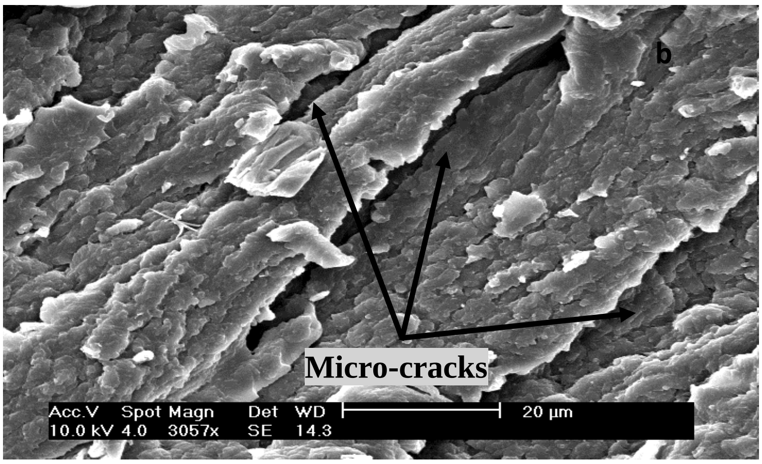

Figure 5.22: SEM images for the fracture surface of U75H25-2 wt. % clay.

Figures 5.23 and 5.24 show the fracture surfaces of U75H25-1 wt. % CNT and U75H25-3 wt. % CB, respectively. Similarly, in Figure 5.24, it can be seen that CB nanoparticles are still embedded in the polymer matrix after fracture which indicates the presence of good adhesion.

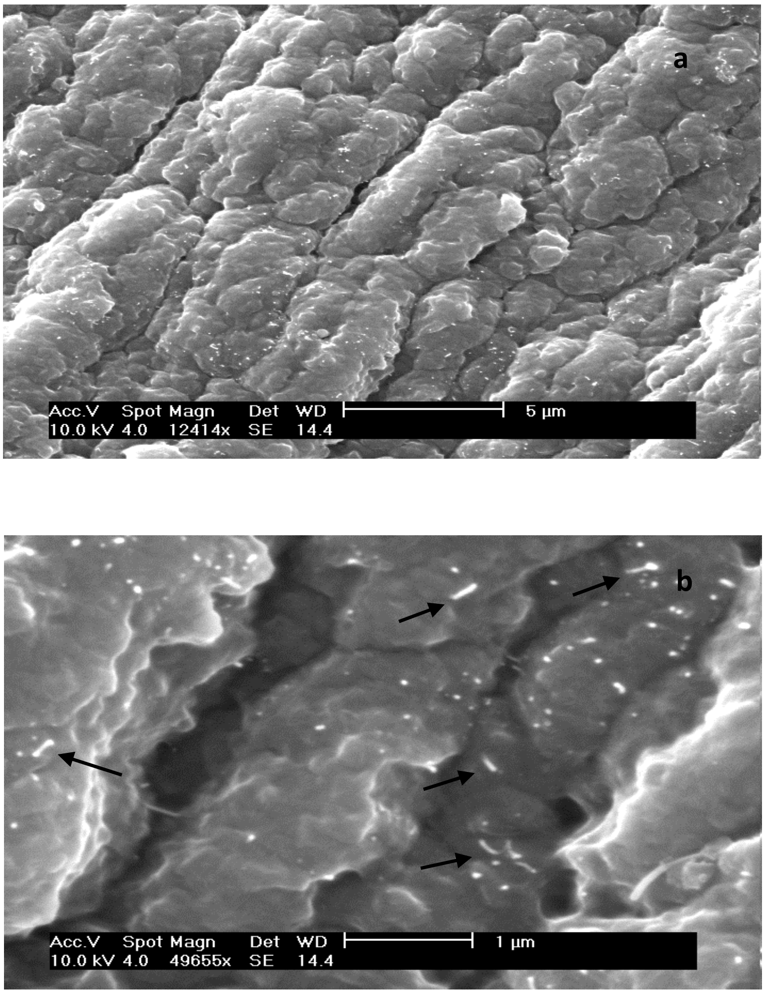

Figure 5.23: SEM images for the fracture surface of U75H25-1 wt. % CNT (arrows indicate the broken CNTs).

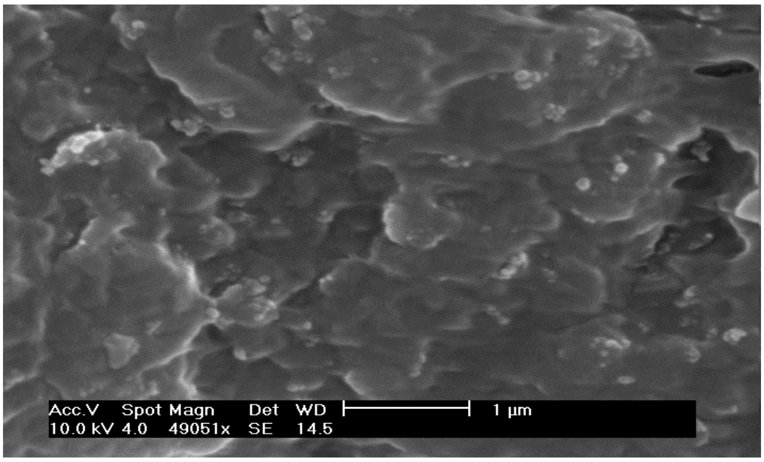

Figure 5.24: SEM images for the fracture surface of U75H25- 3 wt. % CB.

5.9 Summary

This is a key chapter to understand the effect of processing method, nanoparticle type and volume fraction, strain rate and temperature on the mechanical properties of the polyethylene-based nanocomposites, which will be discussed in Chapters 6, 7 and 8. The microstructures of the polyethylene and polyethylene-based nanocomposites were analysed using four techniques; SEM, TEM, XRD (for clay exfoliation and intercalation) and DSI. The results showed improvement in the nanoparticle dispersion using processing method M2. Enlarging the measurement scale by using the DSI in evaluating the nanoparticle dispersion resulted in valuable information about the nanoparticle distribution and correlation of the nanofiller type, volume fraction and dispersion with mechanical properties. At high volume fractions of nanoparticles, large aggregations of CB (M1 and M2), clay-M2 and CNT-M2 nanoparticles were found. This indicated that the maximum volume fraction is less than 3 wt. % for material filled CB or CNT and less than 2 wt. % for the material filled with clay nanoparticle.

Crack formation on the surface of tensile strained samples was used to analyse the effect of processing method on the blend miscibility and the nanoparticle-polymer matrix interaction. It was proposed that the blends with fewer cracks for a given strain could be considered as more miscible. It was then seen that the nanocomposites with fewer cracks, and hence better miscibility, had stronger nanoparticle-polymer matrix interaction. This was in agreement with observations from the fracture surfaces of samples tested to failure. Blending using processing method M1 resulted in a large number of cracks on both the stretched and fracture surfaces. The CNT and CB nanoparticles showed good adhesion with the matrix and no cracks were formed on the stretched or fractured surfaces for both processing methods.

Tables 5.2 and 5.3 summarise the results of the effect of processing method on the morphology, nanofiller dispersion and features of fracture surface. The effect of these parameters on the mechanical properties will be discussed in Chapters 6 and 7.

Table 5.2: Summary of the results of the materials processed using M1

Materials	Filler Content	Miscibility	Filler Dispersion	DSI Analysis	Fracture and Stretched Surfaces
U75H25	0	Poor	----	Properties closer to HDPE Large variations in the indentation hardness	Crazing and crack formation
U75H25-CB	0.5	Poor	Large aggregations	Large variations in the indentation hardness	No cracks Good particle-matrix adhesion
U75H25-CB	1	Poor	Large aggregations	Large variations in the indentation hardness	No cracks Good particle-matrix adhesion
U75H25-CB	3	Poor	Large aggregations	Large variations in the indentation hardness Indentation hardness higher than HDPE	No cracks Good particle-matrix adhesion
U75H25-CNT	0.5	Poor	Good	Large variations in the indentation hardness	No cracks Good particle-matrix adhesion
U75H25-clay	0.5	Very poor	Good	Small variations in the indentation hardness	Large number of cracks No particle-matrix adhesion

Table 5.3: Summary of the results of the materials processed using M2

Materials	Filler Content	Miscibility	Filler Dispersion	DSI Analysis	Fracture Surface
U75H25	0	Good	----	Properties closer to UHMWPE	Similar to UHMWPE No cracks
U75H25-CB	0.5	Good	Good	Good filler distribution Indentation hardness similar to U75H25-M2 blend	No cracks Good particle-matrix adhesion
U75H25-CB	1	Good	Small aggregations	Small variations in the indentation hardness	No cracks Good particle-matrix adhesion
U75H25-CB	3	Good	Large aggregations	Large variations in the indentation hardness	No cracks Good particle-matrix adhesion
U75H25-CNT	0.5	Good	Good	Good filler distribution An increase in indentation hardness	No cracks Good particle-matrix adhesion
U75H25-CNT	1	Good	Good	Small variations in the indentation hardness An increase in indentation hardness	No cracks Good particle-matrix adhesion
U75H25-CNT	3	Good	Large aggregations	Large variations in the indentation hardness An increase in indentation hardness	No cracks Good particle-matrix adhesion
U75H25-clay	0.5	Good	Good	Good filler distribution Indentation hardness similar to U75H25-M2 blend	No cracks on the stretched surface
U75H25-clay	1	Good	Poor	Large variations in the indentation hardness A significant increase in indentation hardness	Large number of cracks on the stretched surface
U75H25-clay	2	Good	Poor	Very large variations in the indentation hardness A significant increase in indentation hardness	Large size of cracks on the stretched and fracture surfaces

Chapter 6
Mechanical Properties of Polyethylene-based Nanocomposites (Bulk Properties)

6.1 Introduction

This chapter describes the effect of nanoparticle geometry and volume fraction on the mechanical behaviour of polyethylene-based nanocomposites manufactured using the two processing methods M1 and M2. Firstly, the effect of the processing method, nanoparticle type and volume fraction on the stress-strain behaviour of the polyethylene-based nanocomposites is discussed. During plastic deformation, mechanical work can be transformed partially into heat, which can cause thermal softening, which will consequently affect material properties. Therefore, the effects of the combination of the processing method, nanoparticle geometry and volume fraction and strain rate on heat generation during plastic deformation of the polyethylene-based nanocomposites are discussed.

The presence of stiff nanoparticles in the polyethylene microstructure can significantly affect the chain mobility during deformation, and therefore mechanical behaviour such as creep can be affected. The effects of the processing method, nanoparticle shape and volume fraction on the viscoelastic behaviour of polyethylene-based nanocomposites are, hence, also investigated. In order to better understand the chain dynamics during constant load application, Burger's model is used to fit and describe the experimental data.

6.2 Stress-Strain Behaviour

The effects of processing method and the incorporation of nanoparticles on the stress-strain behaviour and tensile properties of the nanocomposites were initially assessed using 0.2^{-1} strain rate at room temperature. In processing method M1, the inclusion of a small amount of the nanoparticles (0.5 wt. %) has significant effect on the tensile behaviour of the polyethylene blend, as seen in Figure 6.1. The presence of a small amount of clay in the polymer matrix results in a significant reduction in the elongation at break (approximately 75%). Also, the yield stress is increased by 2.6 MPa, which can be attributed to the increase in the degree of crystallinity, as shown previously in Table 5.1. The addition of CB and CNTs can be seen to increase the strain hardening, toughness and the tensile strength of the polymer in most cases. A major effect of the nanoparticles can be observed in the strain hardening region, where stretching of the network of amorphous phases occurs and dominates the deformation. During recrystallisation, the polymer chains can be densely packed around the nanoparticle, which then nucleates polymer entanglements that can increase the polymer toughness (Li et al. 2012). Increasing the volume fraction of the CB nanoparticles shows a reduction in the elongation at break by the addition of 1 wt. % CB. Fracture occurs at the start of the strain hardening, which is proposed to be due to the increase in temperature during plastic deformation, which will be discussed further in Section 6.3.1. In contrast, an improvement in the strain hardening behaviour can be observed with the inclusion of 3 wt. % CB. This can be related to a reduction in the heat generation during plastic deformation, at high wt. % CB, as discussed in more detail in Section 6.3.1.

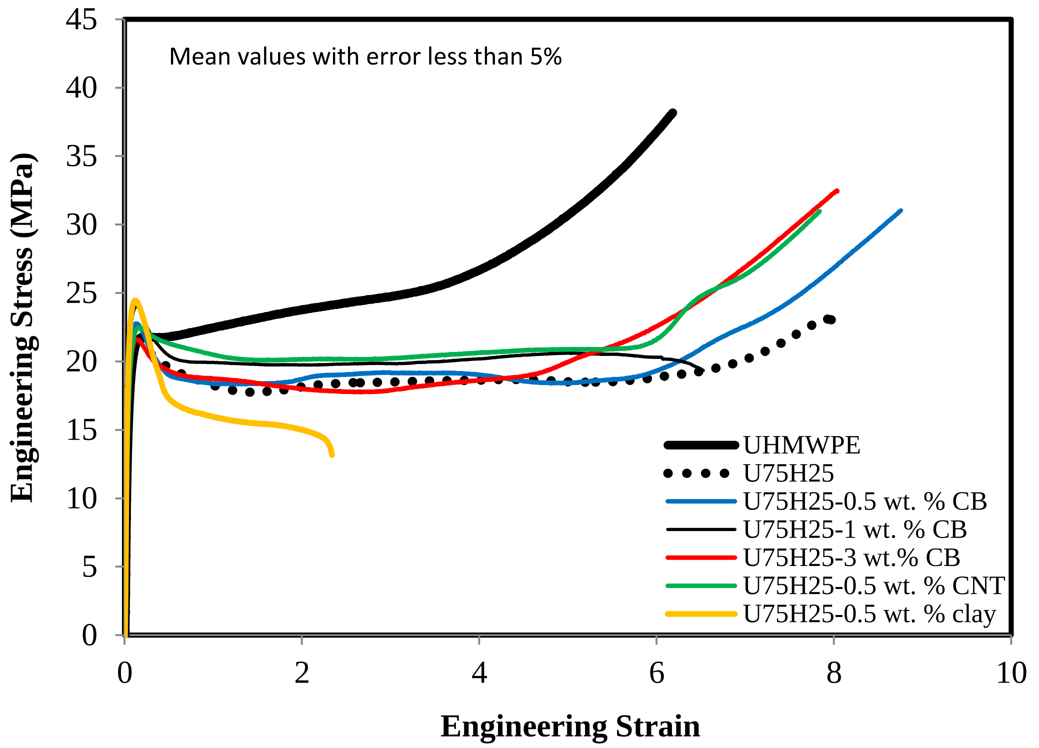

Figure 6.1: Effect of nanoparticle addition on the tensile behaviour of polyethylene nanocomposites-M1 using 0.2^{-1} strain rate.

Figures 6.2 to 6.4 show the effect of the addition of CB, CNT and clay nanoparticles on the tensile behaviour of polyethylene nanocomposites processed using M2. It can be seen that a slight improvement in tensile behaviour can be obtained by the incorporation of a small amount of the nanoparticle. However, at strain greater than 400%, a significant reduction in the tensile behaviour can be observed. This can be attributed to the thermal softening of the polymer at high strain rates, which can be because of the temperature increase during plastic deformation, which will be discussed later. It can also be seen that the inclusion of 0.5 wt. % nanofiller serves to increase the yield stress of the U75H25 blend. Generally, the results indicate that the incorporation of a small volume fraction of nanoparticles can be used to improve the tensile properties of the U75H25 blend.

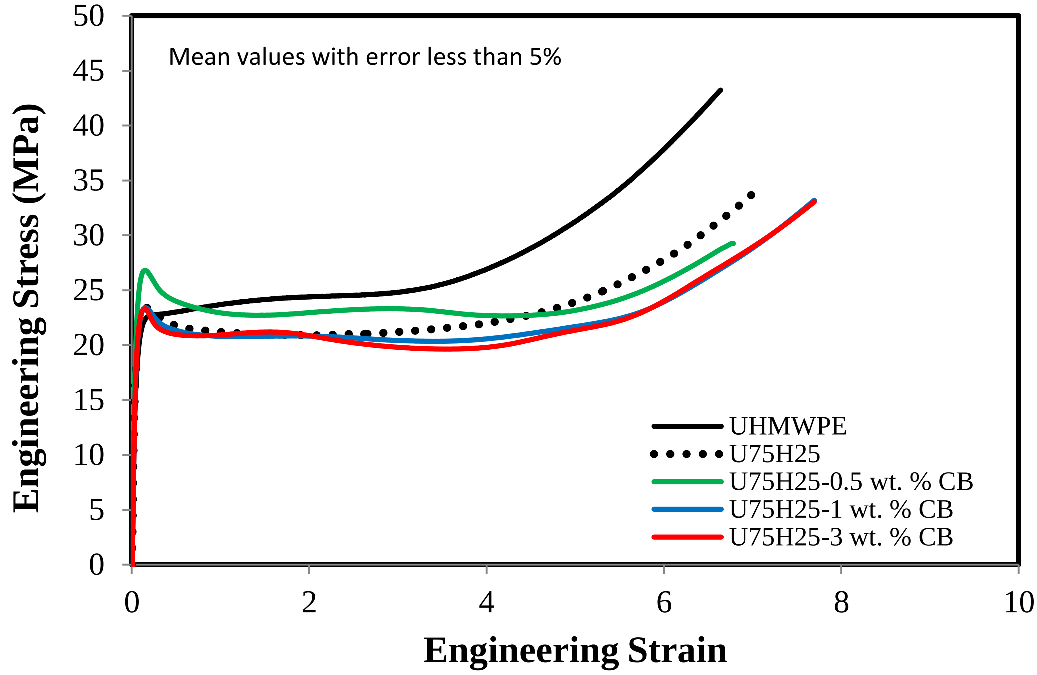

Figure 6.2: Effect of nanoparticle addition on the tensile behaviour of polyethylene-CB nanocomposites-M2 using 0.2^{-1} strain rate.

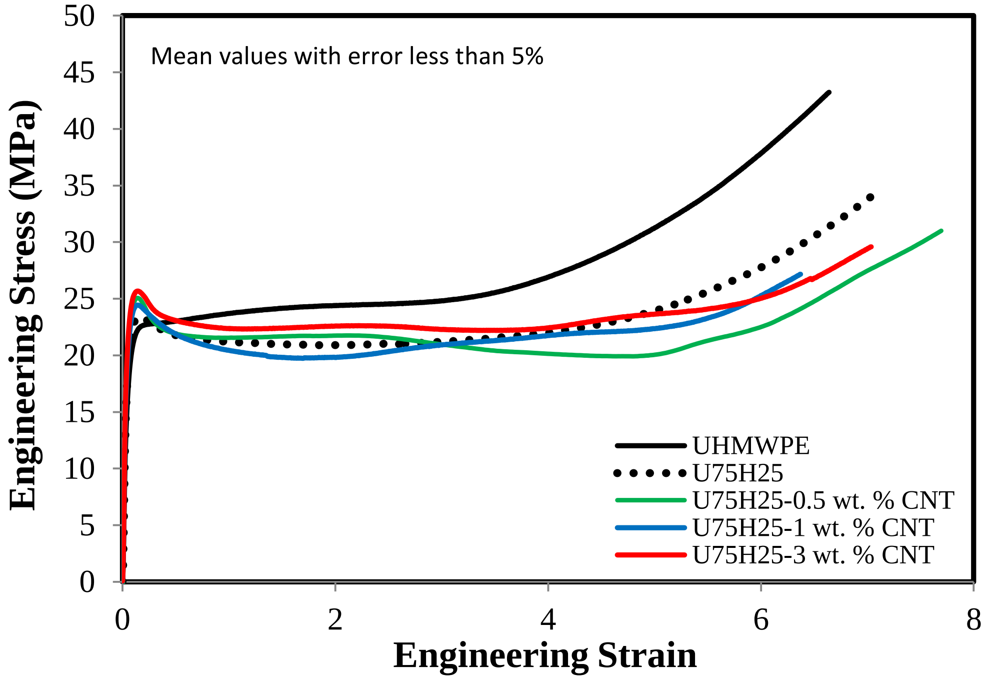

Figure 6.3: Effect of nanoparticle addition on the tensile behaviour of polyethylene-CNT nanocomposites-M2 using 0.2^{-1} strain rate.

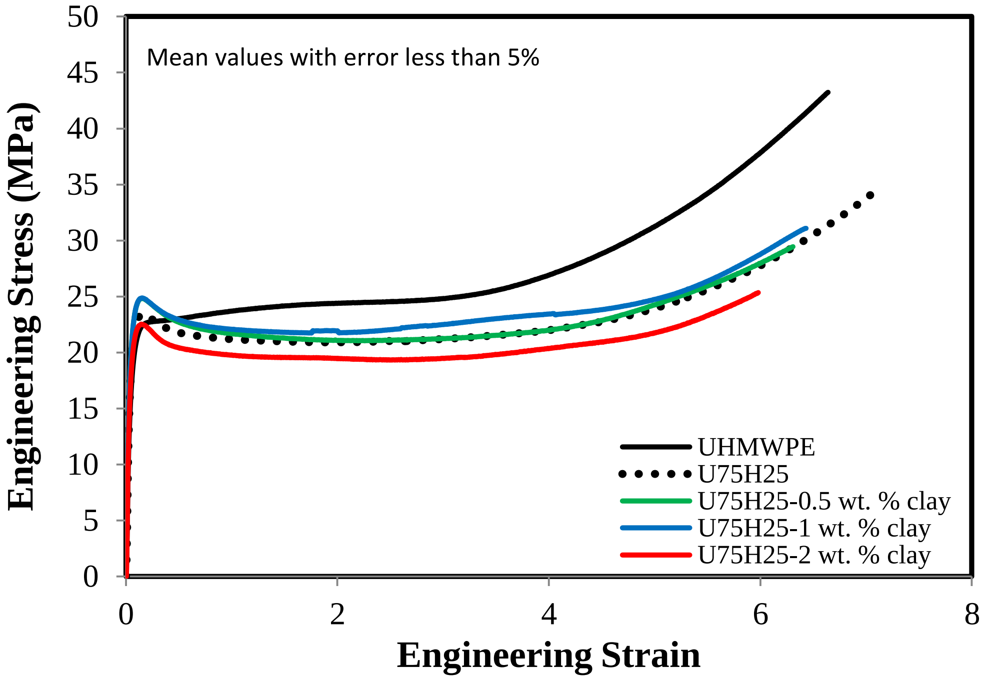

Figure 6.4: Effect of nanoparticle addition on the tensile behaviour of polyethylene-clay nanocomposites-M2 using 0.2^{-1} strain rate.

The effect of the nanoparticle type on the elastic modulus of the polyethylene nanocomposites using the two different processing methods is illustrated in Figure 6.5. The figure indicates that the nanoparticle type is an important factor in determining the material properties. The addition of a small volume fraction (0.5 wt. %) of CNT or clay nanoparticles to the U75H25 matrix can lead to improvements in the elastic modulus for both processing methods. A further increase in the elastic modulus can be obtained with an increase in the CNT content using processing method M2. However, increasing the volume fraction of clay nanoparticle using M2 can result in a reduction in the elastic modulus. The improvement in the elastic modulus at the small volume fraction can be attributed to the good dispersion of the nanoparticle at low filler loading, as discussed in Chapter 5, and the large difference in the stiffness value between the polymer and the nanoparticle. The 3D nanofiller (CB) generally results in a reduction in the elastic modulus value.

However, the addition of 0.5 wt. % CB using processing method M2 shows a slight increase in the elastic modulus, which can be attributed to the improvement in the matrix miscibility and the nanofiller dispersion.

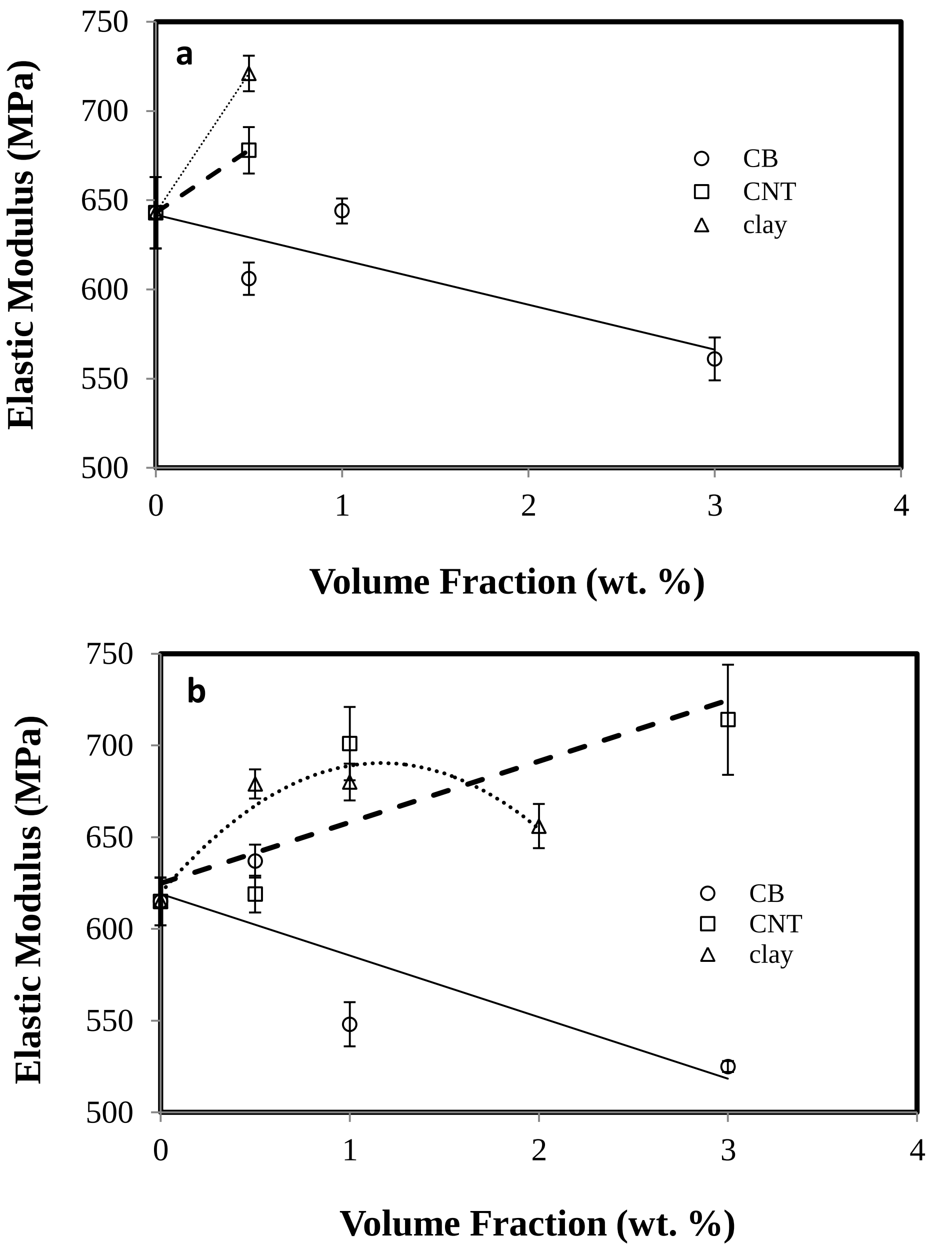

Figure 6.5: Effects of nanoparticle addition on the elastic modulus of polyethylene based nanocomposites using two processing methods: a) M1 and b) M2.

6.3 Strain Induced Temperature Measurements

In order to investigate the effect of the processing method, strain rate, nanoparticle type and loading on internal heat generation during the plastic deformation of polyethylene nanocomposites, a thermal camera (FLIR SC3000) was used to record the surface temperature during uniaxial tensile testing. Heat can be generated due to the friction between polymer chains during their rearrangement and the friction between the nanoparticles and U75H25 matrix in the case of nanocomposites. A significant temperature increase resulting from this internal heat generation can contribute to thermal softening of the material. Figure 6.6 shows an example of the stress-strain behaviour of the polyethylene nanocomposites at various strain rates and the temperature increase at each strain rate. The temperature changes at high strain rate can be divided into five regions. Region 1 indicates that there is no significant increase in the temperature in the elastic region. Region 2 shows an increasing temperature following yielding of the material. Region 3 is an approximately constant stress region in which an approximate thermal equilibrium has been reached as there is little change in the temperature. Strain hardening occurs in Region 4, and temperature increases again until failure occurs, with fracture in Region 5 being accompanied by a sharp increase in temperature.

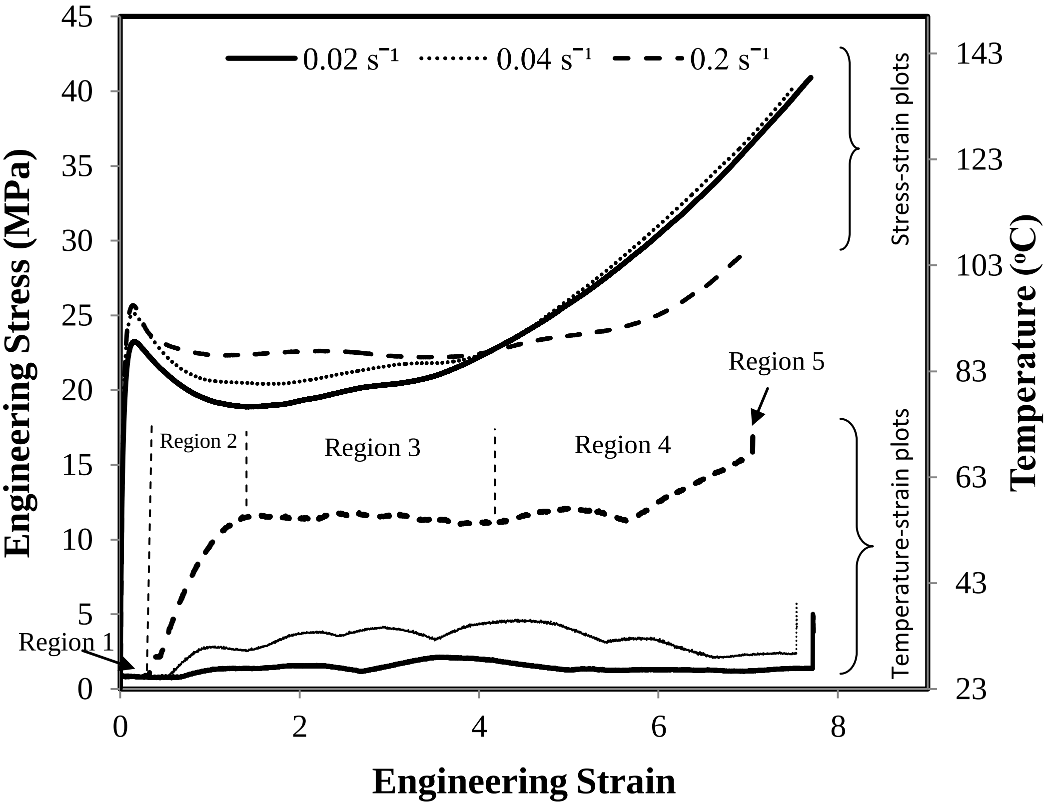

Figure 6.6: Temperature change for U75H25-3 wt. % CNT-M2 during tensile testing at various strain rates.

6.3.1 Processing Method Effects on Strain Induced Heating

Figures 6.7 to 6.9 summarise the effect of adding CB, CNT or clay nanoparticles to the U75H25 blend using processing methods M1 and M2 on the heat generation during the tensile tests. These figures indicate that the incorporation of nanoparticles into the blend matrix using M1 or M2 can increase the internal friction, and consequently generate more internal heat on straining. The amount of heat generation is dependent on the interfacial strength between the nanoparticle and U75H25 matrix, the morphology of the composite matrix and the dispersion of nanoparticle; however, this will also affect heat transfer in the sample, which will also affect the temperature increase. The poor miscibility of the blend and the formation of different phases in the material processed using M1 leads to void formation between the different phases and in the nanoparticle aggregation regions during material deformation, which will also affect the internal heat transfer. The complexity in the microstructure of the material manufactured using processing method M1 increases the difficulty of understanding the relation between the strain rate, the nanoparticle content and the internal heat generation during plastic deformation. In Figure 6.7, at strain rates over 0.04 s^{-1}, the heat generation is independent of the strain rate with the addition of 0.5 wt.% CB, however, temperature can be seen to increase with strain rate for materials with higher CB content (1 and 3 wt.%). It may be expected that the temperature would increase with CB content, however, this is not the case for the samples processed using method M1, as seen in Figure 6.7, as the two phase nature of the matrix and aggregation of the CB particles introduce further complicating effects. For example, the reason that the temperature for 3 wt. % CB is lower than that for 1 wt. % may be attributed to a number of effects including the reduction in surface to volume ratio caused by the large CB aggregations seen at this content, the improvement in internal heat transfer from these aggregations and the effect of the nanoparticles on void formation under straining. For the U75H25-CB nanocomposites processed with method M2, the relation between strain rate, CB content and internal heat increase is more clear as there is a general trend of increasing temperature with both strain rate and CB content. This can be related to the improvement in the CB nanoparticle dispersion as seen in the TEM and SEM images in Chapter 5, which provides a simpler relation between the number of particles and internal heat generation than seen with process M1.

The significant effect of processing method and consequently the quality of the miscibility on the heat generation during plastic deformation can be clearly seen in Figure 6.9. In this figure, it can be observed that the nanocomposites manufactured using M1 generate high temperatures compared to the materials processed using M2. For example, the U75H25-0.5 wt. % clay processed using M2 shows a reduction in temperature of 53% compared to a similar composition processed using M1. The large variation in the results of the materials processed using M1, which can be observed from the error bars, provides evidence for the poor miscibility of the blend and its nanocomposites. This is in agreement with the results presented and discussed in the previous chapter.

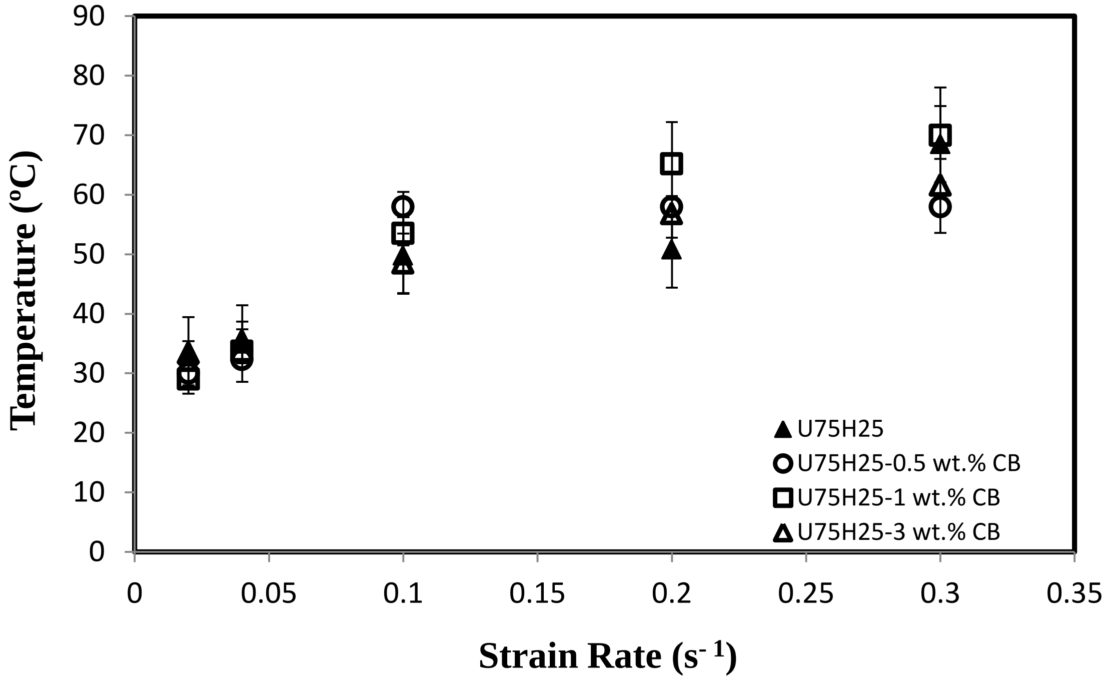

Figure 6.7: Strain rate effect on the temperature increase during tensile test of U75H25-CB nanocomposites processed with M1 at 200 % engineering strain.

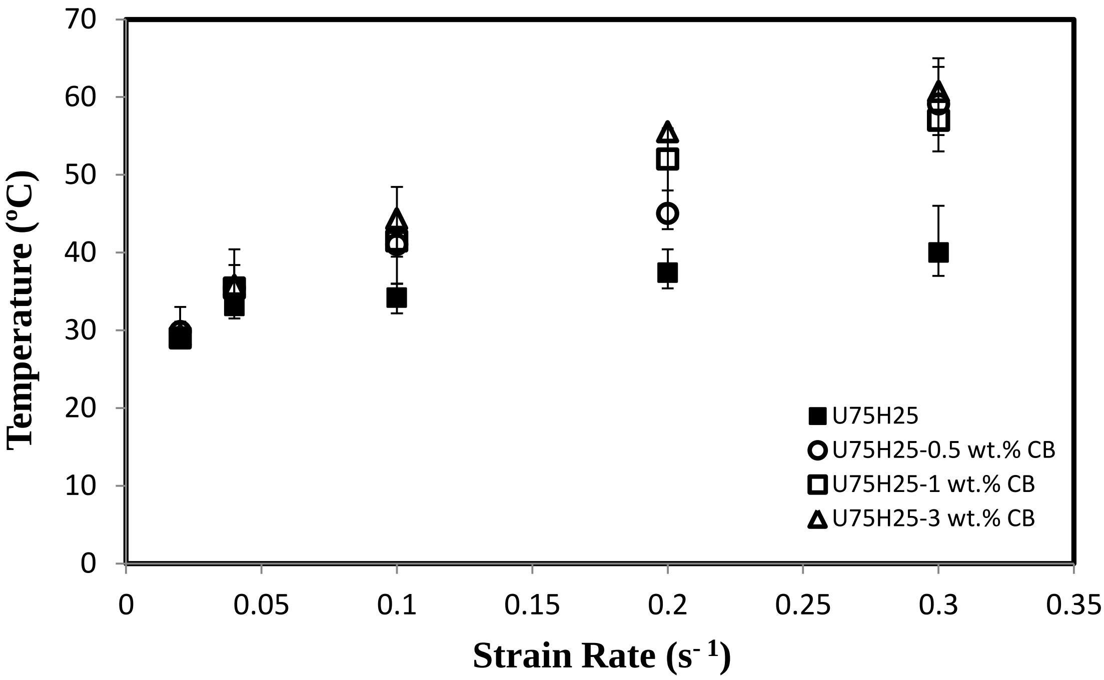

Figure 6.8: Strain rate effect on the temperature increase during tensile test of U75H25-CB nanocomposites processed with M2 at 200 % engineering strain.

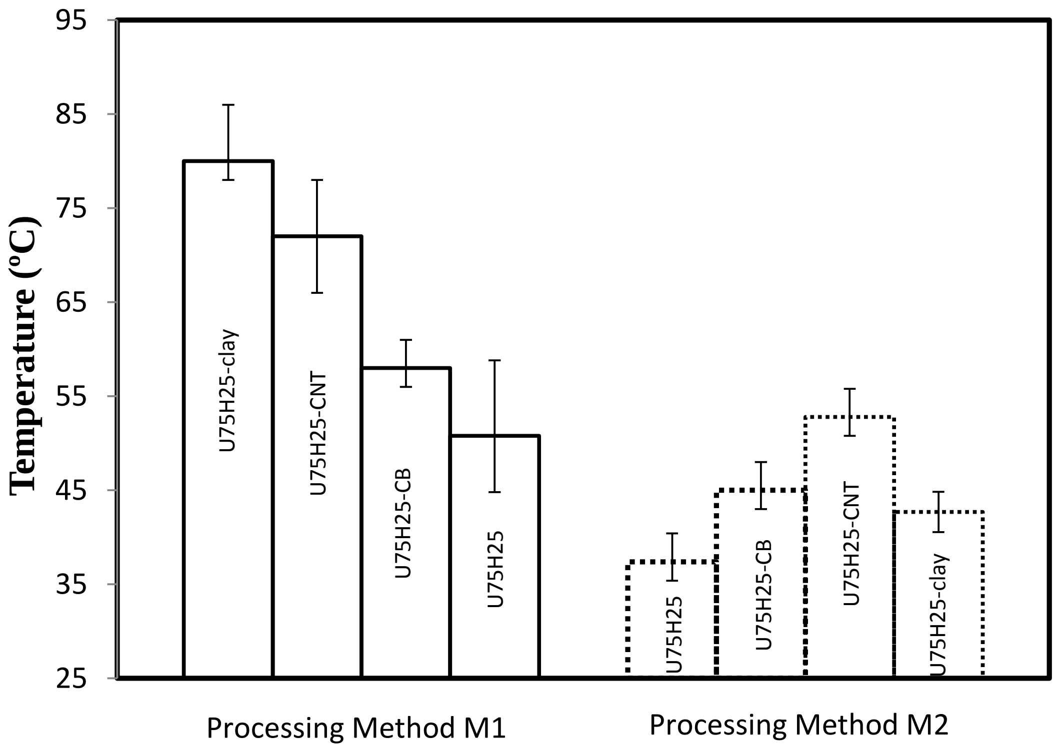

Figure 6.9: Effect of processing method on the heat generation during the tensile test at 200% strain, 0.2^{-1} strain rate and 0.5 wt. % nanofiller.

6.3.2 Nanoparticle Type Effects

Figures 6.10 to 6.12 show the correlations between nanoparticle type and weight percentage, strain rate and temperature at 200 % strain. Blending the HDPE with the UHMWPE results in a slight temperature increase in the blend material compared with the UHMWPE at strain rates over $0.1s^{-1}$. The incorporation of nanoparticles into the U75H25 matrix induces more significant temperature increases at higher strain rates. The deformation mechanisms of semi-crystalline polymers such as polyethylene can be ascribed to stretching of amorphous chains, shear yielding of crystallites, void formation, crazing and recrystallization with orientation. The presence of a third component such as CNT, CB or nanoclay in the U75H25 heterogeneous matrix can affect these mechanisms by introducing an interfacial area around the nanoparticle with high density and different bonding properties between the nanoparticle and the blend matrix, which can prevent the movement of the polymer chains (Li et al. 2012). The interaction between nanoparticle and polymer matrix, surface area to volume ratio, dispersion and orientation are all important factors to characterise the effect that the nanoparticles have on the mechanical deformation mechanisms and strain induced temperature increases.

There is very little or no interaction between non-polar polymers such as polyethylene and polar nanoparticles (Rahmat and Hubert 2011). This can increase the formation of microvoids and the friction during the movement of chains when nanoparticles are introduced. Since no chemical modification was used in the preparation of the nanoparticles used in this study, no interaction between the nanoparticle and the polymer matrix is likely to occur. However, non-covalent (mechanical) interaction can be obtained by embedding a small diameter CNT into polymers with higher molecular weight such as UHMWPE. This can increase the possibility of bridging, which happens when the long chains of UHMWPE interact with two or more CNTs at the same time and wrapping, which happens when a UHMWPE chain wraps around a CNT (Esfandiari and Nazokdast 2008; Haghighatpanah and Bolton 2013; Zheng et al. 2007). These two interaction mechanisms can be enhanced by increasing the CNT content. This can increase the frictional force between the CNT surface and polymer chains and explain the temperature increase in the polyethylene-CNT nanocomposites over the other two nanofillers (CB and nanoclay).

The second key factor that can affect temperature increase during plastic deformation is the surface area to volume ratio (A/V). The (A/V) ratio for CB, CNT and clay can be determined by:

$$\text{For CB,} \qquad \frac{\mathrm{A}}{\mathrm{V}} = \frac{6}{\mathrm{D}} \tag{6.1}$$

$$\text{For CNT,} \qquad \frac{\mathrm{A}}{\mathrm{V}} = \frac{2}{\mathrm{L}} + \frac{4}{\mathrm{D}} \approx \frac{4}{\mathrm{D}} \text{ (since L>D)} \tag{6.2}$$

$$\text{For clay,} \qquad \frac{A}{V} = \frac{4}{L} + \frac{2}{D} \approx \frac{2}{D} \text{(since L>D)} \tag{6.3}$$

where D is the diameter of CB and CNT and thickness of clay, L is the length of CNT and clay. The average diameter (D) for CB, CNT and nanoclay are 28, 9.5 and 40 nm, respectively, and thus CNT has the largest ratio and nanoclay has the smallest. This is in agreement with the results shown in Figures 6.10 and 6.11. The polyethylene-nanoclay nanocomposite generates less heat than the polyethylene-CNT nanocomposite at similar volume fraction. However, in Figure 6.12 the addition of CB shows slightly higher temperatures than CNT. This can be attributed to the large aggregations (poor dispersion effect) of CNT at higher volume fraction, which decreases the surface to volume ratio.

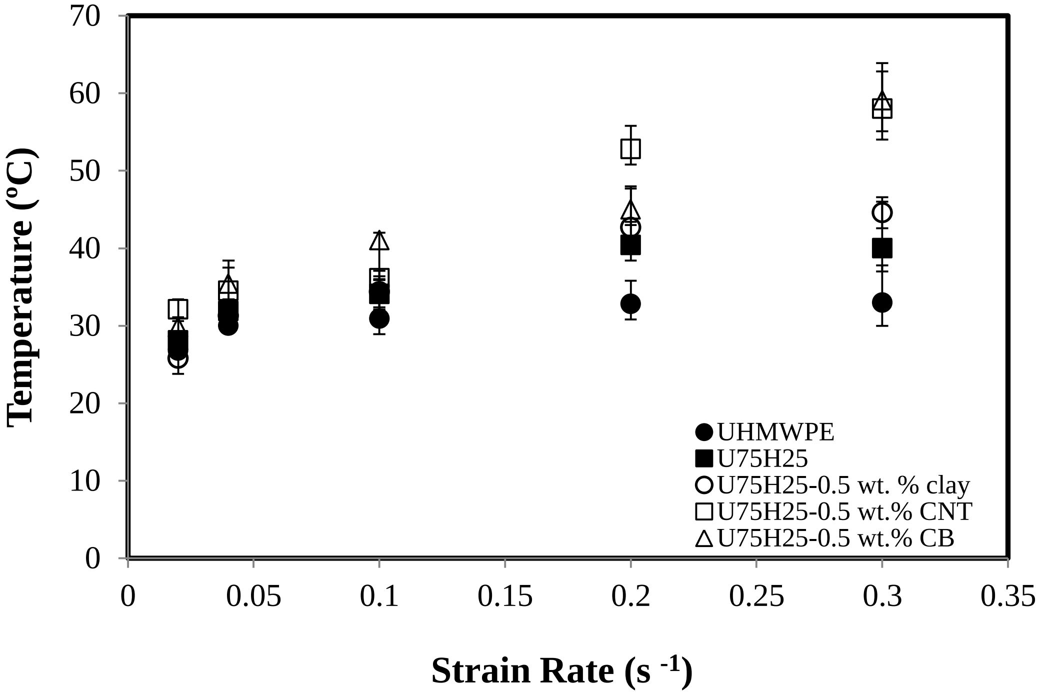

Figure 6.10: Effect of nanoparticle type on temperature increase during plastic deformation at different strain rates and 200 % strain, processed with M2.

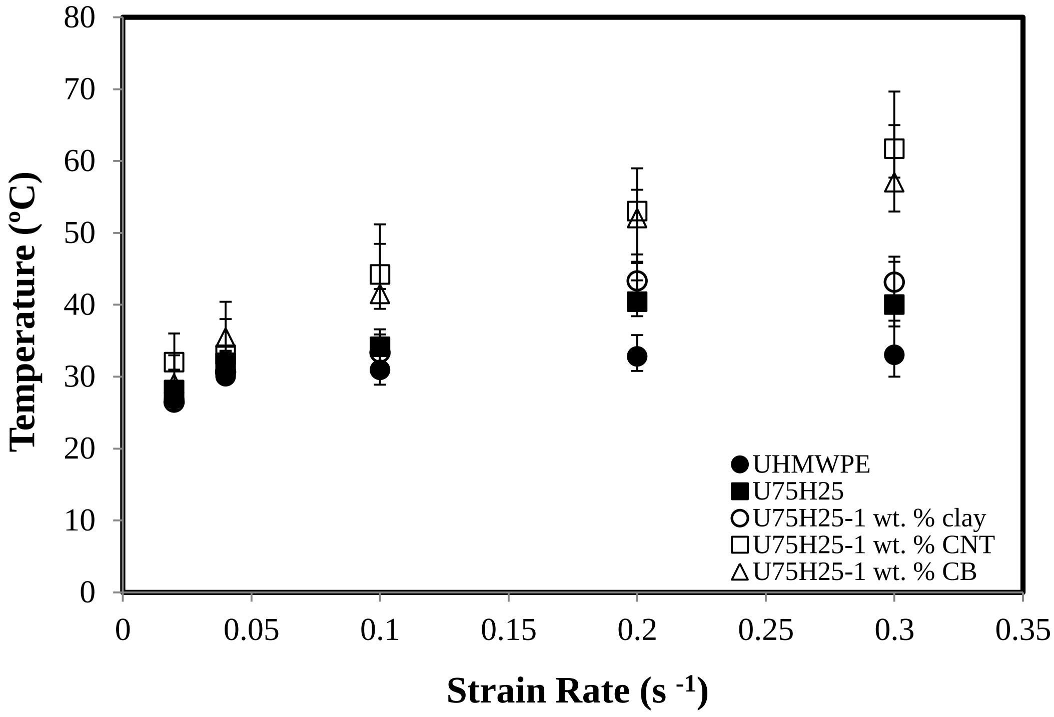

Figure 6.11: Effect of nanoparticle type on temperature increase during plastic deformation at different strain rates and 200 % strain, processed with M2.

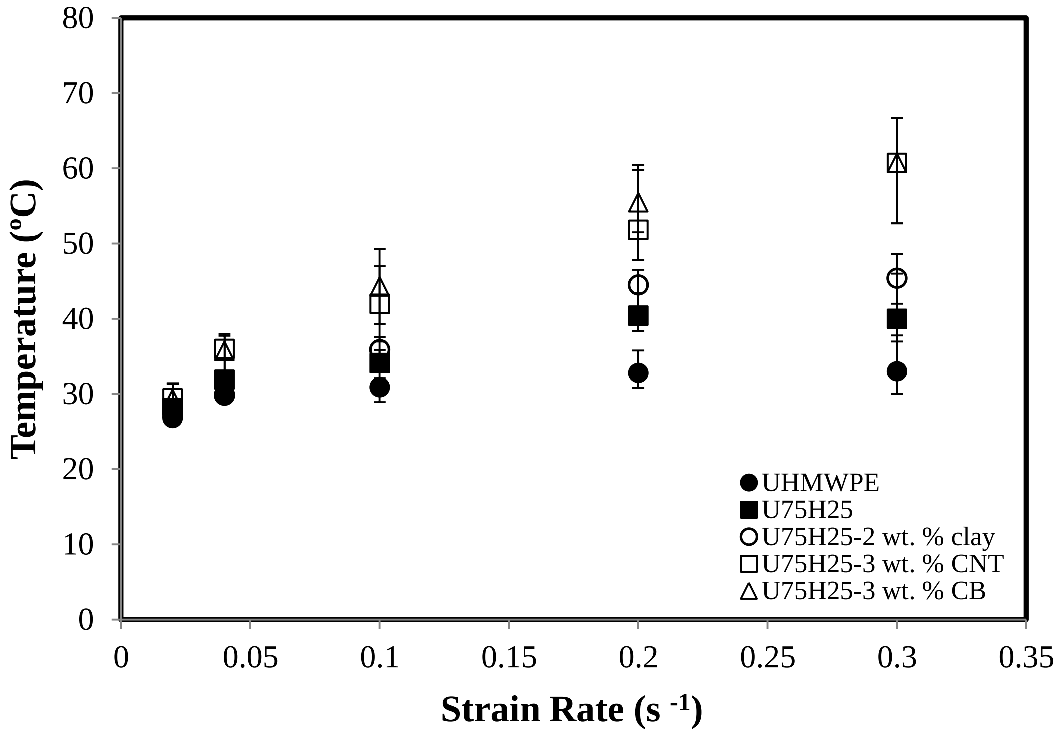

Figure 6.12: Effect of nanoparticle type on temperature increase during plastic deformation at different strain rates and 200 % strain, processed with M2.

6.3.3 Weight Fraction Effects

Figure 6.13 summarises the effects of nanoparticle structure and weight fraction on the temperature at 200 % strain when testing at 0.2 s^{-1} strain rate. The most important factors that influence the phenomenon of heat generation during plastic deformation of polymer nanocomposites are the interaction between nanoparticle and polymer matrix, dispersion, surface area to volume ratio and orientation. The effects of these factors were discussed previously at different strain rates. However, by analysing these effects at a specific strain rate ($0.2s^{-1}$), clear trends can be observed. It can be seen from Figure 6.13 that nanoclay generates less heat compared to CNT and CB. This can be attributed to three main reasons. The poor interaction between the clay platelet and polyethylene matrix, which can be observed from the formation of microcracks on the surface of stretched samples as shown in Figure 5.19. A confirmation of clay platelet exfoliation can be obtained from the distribution of small microcracks on the surface of stretched U75H25-1 wt. % clay, Figure 5.19a. However, at higher clay content a formation of large microcracks can be seen in Figure 5.19b, which may be attributed to the presence of intercalated clay layers as seen in Figure 5.22a. The presence of clay platelets can also enhance the formation of internal microvoids, as seen in Figure 5.22b. The third reason can be related to the lower ratio of the surface area to volume of the nanoclay compared to CNT and CB.

For CB and CNT nanoparticles, Figure 6.13 indicates that the temperature increase is dependent on the nanoparticle volume fraction. At low volume fraction, temperature increases with the amount of nanofiller. However, at a high content of CNT (3 wt. %), a reduction in temperature can be observed. This can be attributed to the formation of large aggregations, as shown in Figures 5.8c and 5.9a, which cause a reduction in the surface area to volume ratio, and consequently the frictional area. Also, the formation of large CNT networks can increase the heat dissipation due to an increase in the thermal conductivity. Similarly, the addition of higher CB content shows a reduction in the effect of increasing nanofiller content at high volume fraction, which can be attributed to the same reasons as discussed for CNTs. However, the transition point in the increasing trend starts at a lower volume fraction of CNTs than CB, 0.5 and 1 wt. %, respectively. This can be attributed to the difference in the surface to volume ratio between CNT and CB nanoparticles.

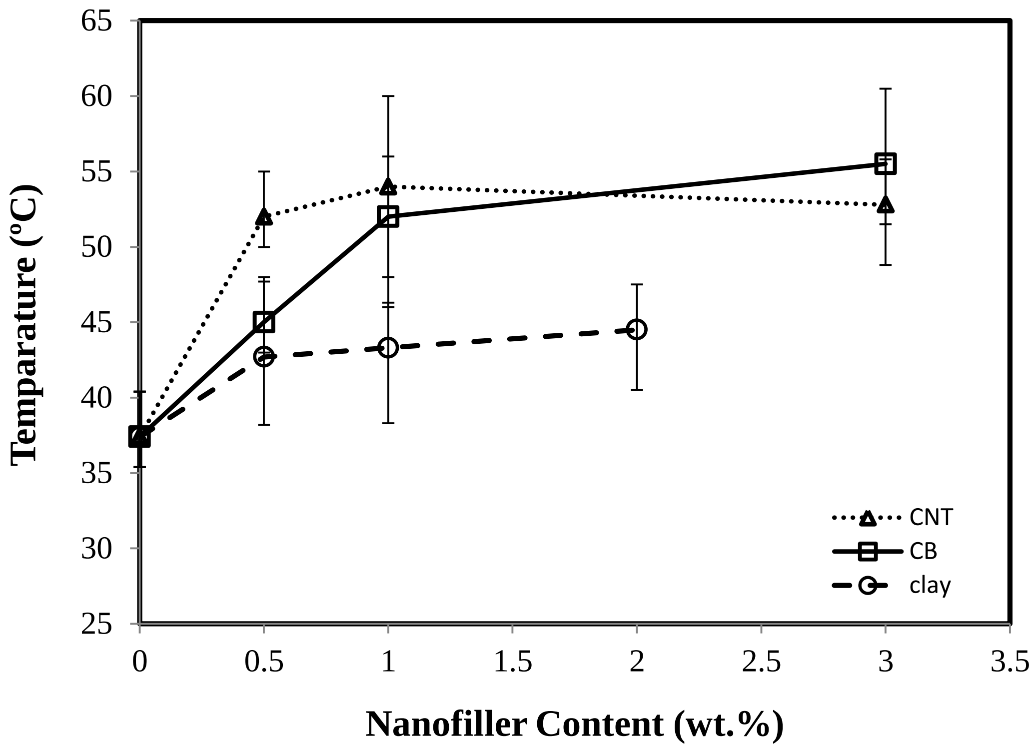

Figure 6.13: Effect of nanoparticle content on temperature increase during plastic deformation at 2 s^{-1} strain rate after 200 % strain of material processed with M2.

6.4 Thermal Softening at High Strain Rate

As discussed in the previous sections, the nanoparticle type showed a significant effect on the temperature increase during the tensile tests at high strain rates. This temperature increase can result in a significant effect on the stress-strain behaviour of the polyethylene nanocomposites, as seen in Figures 6.14 to 6.16. According to Figure 6.13, 1 wt. % CB, 0.5 wt. % CNT and 0.5 wt. % clay can be considered as transition volume fractions in the temperature-nanofiller and content relation, therefore the effect of nanoparticle type and temperature increase on the stress-strain behaviour was investigated at these specific volume fractions to avoid the effects of aggregations, voids and crack formation. The addition of CB and CNTs resulted in a significant increase in temperature compared to the addition of clay at strain rates over $0.04s^{-1}$, which can be attributed to the high frictional coefficient between nanoparticle and polymer matrix. This temperature increase results in a significant effect of a thermal softening in Region 4 of the stress-strain behaviour as seen in Figures 6.14 and 6.15. It can be observed from Figure 6.16 that the addition of 0.5 wt. % clay causes less thermal softening effects in the stress-strain behaviour in Region 4, which can be related to the reduction in heat generation at high strain rate with these particles.

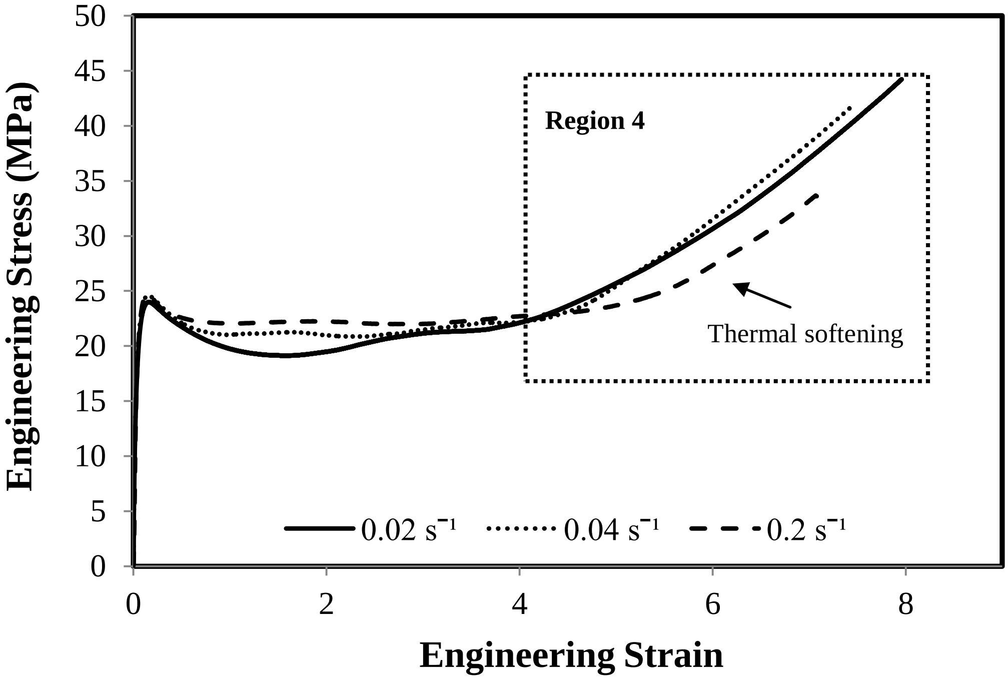

Figure 6.14: Thermal softening effect at high strain rate in the tensile testing of U75H25-1 wt. % CB processed with M2.

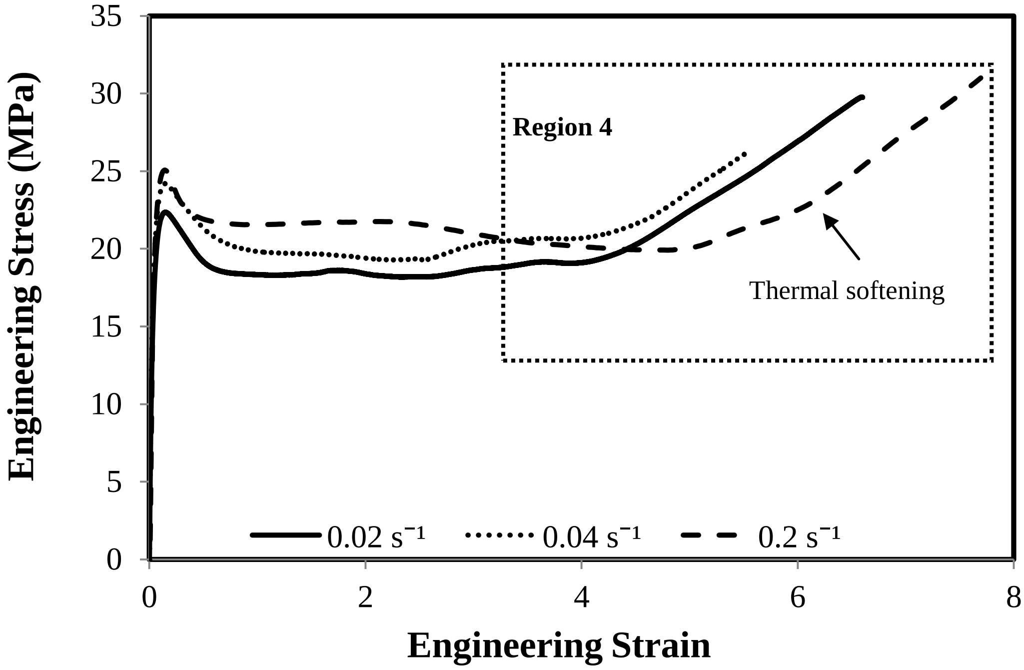

Figure 6.15: Thermal softening effect at high strain rate in the tensile testing of U75H25-0.5 wt. % CNT processed with M2.

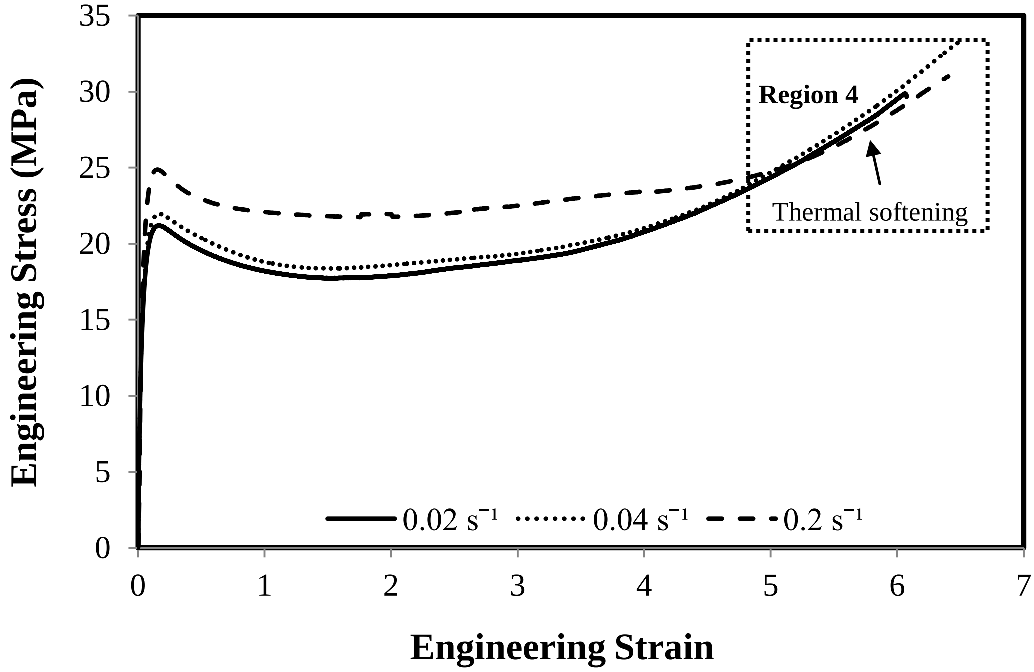

Figure 6.16: Thermal softening effect at high strain rate in the tensile testing of U75H25-0.5 wt. % clay processed with M2.

6.5 Tensile Creep Behaviour and Constitutive Modelling

6.5.1 Introduction

In addition to the tensile tests described in the previous section, creep measurements were carried out at room temperature, in which creep stress was selected in the linear viscoelastic region at 9.3 MPa. The creep strain versus time curves can be divided into two stages as shown in Figures 6.17 to 6.19, a primary creep stage, where the creep rate decreases rapidly with time due to the slippage and rearrangement of the polymer chains and secondary creep, where the creep rate reaches a steady-state value, which is normally for a longer period of time.

Thermoplastic polymers are considered as low creep resistant material, which reduces their applications. However, the addition of nanoparticles can potentially be used to restrict the polymer chain movement, and consequently increase the creep resistance. This is discussed in the following section.

6.5.2 Effect of Nanoparticles

It can be seen in Figures 6.17a and 6.18a that the addition of CB and CNT nanoparticles with processing method M1 causes a reduction in the creep resistance of the blend. This can be attributed to the poor miscibility of the blend, the poor dispersion of the nanoparticle, the large agglomeration and the poor filler-matrix interaction, which leads to a reduction in the surface area to volume ratio and acts as defects in the microstructure. Conversely, with processing method M2, the incorporation of the CB and CNT nanoparticle shows a significant improvement in the creep resistance, as shown in Figures 6.17b and 6.18b. The creep resistance generally increases with the addition of CB nanoparticles, however, at high volume fraction (3 wt. %) a reduction in the creep resistance can be observed, which can be related to the large aggregations of CB nanoparticles at this volume fraction. Unexpectedly, increasing the volume fraction of CNT with method M2 has no effect on the creep resistance, as seen in Figure 6.18b. The improvement of the creep resistance of the nanocomposites at low volume fraction can be attributed to the good dispersion of the nanoparticles, which can lead to polymer chain entanglements around the nanoparticles. Unlike the trends seen with the carbon fillers, the incorporation of clay nanoparticles using processing method M1 significantly reduces the creep strain, as seen in Figure 6.19a. This is most probably due to the increased crystallinity, as discussed in Section 5.6. However, there is only a slight improvement in the creep resistance using processing method M2, as shown in Figure 6.19b. These results can be used as evidence that processing method and nanoparticle type are key factors that affect the creep behaviour of polyethylene-based nanocomposites.

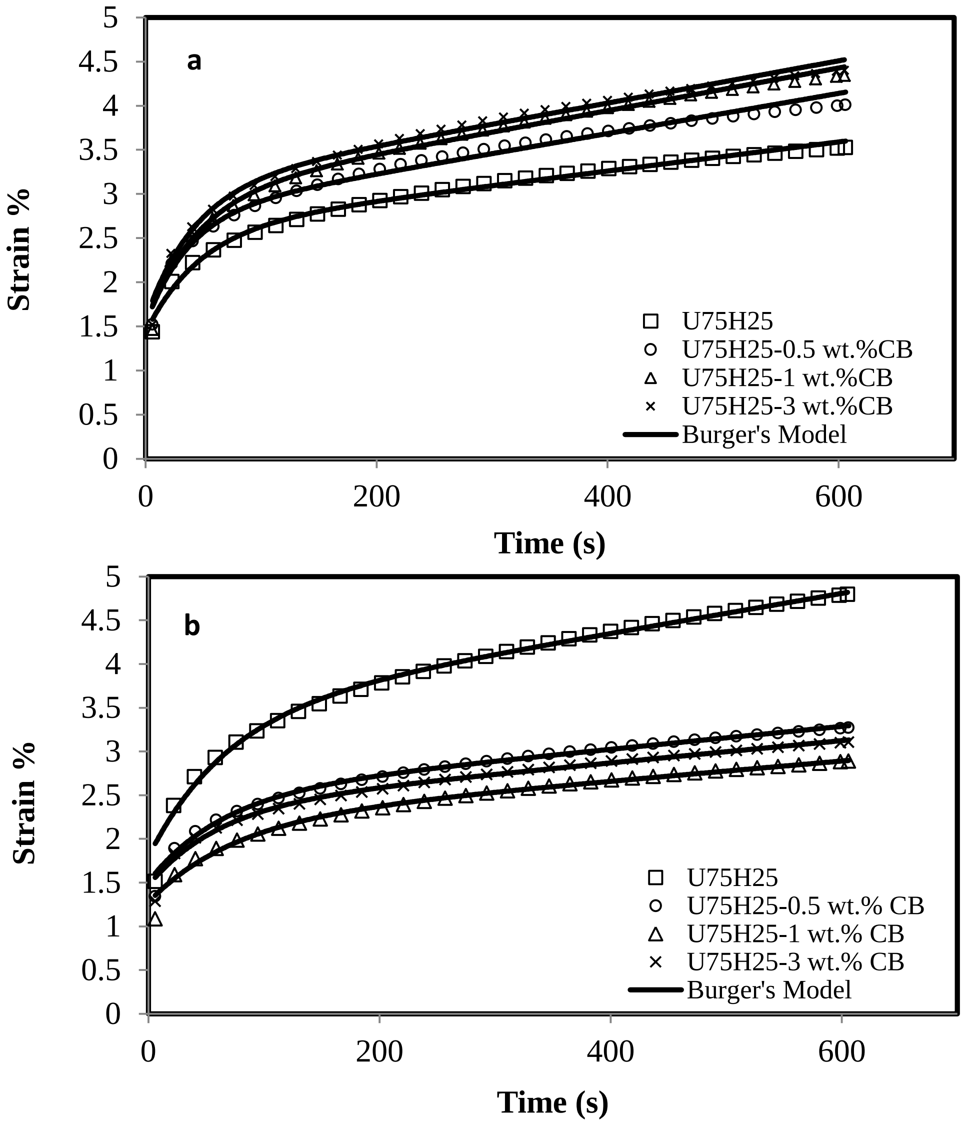

Figure 6.17: The effects of nanoparticles on the creep resistance of the blends processed using (a) M1 and (b) M2.

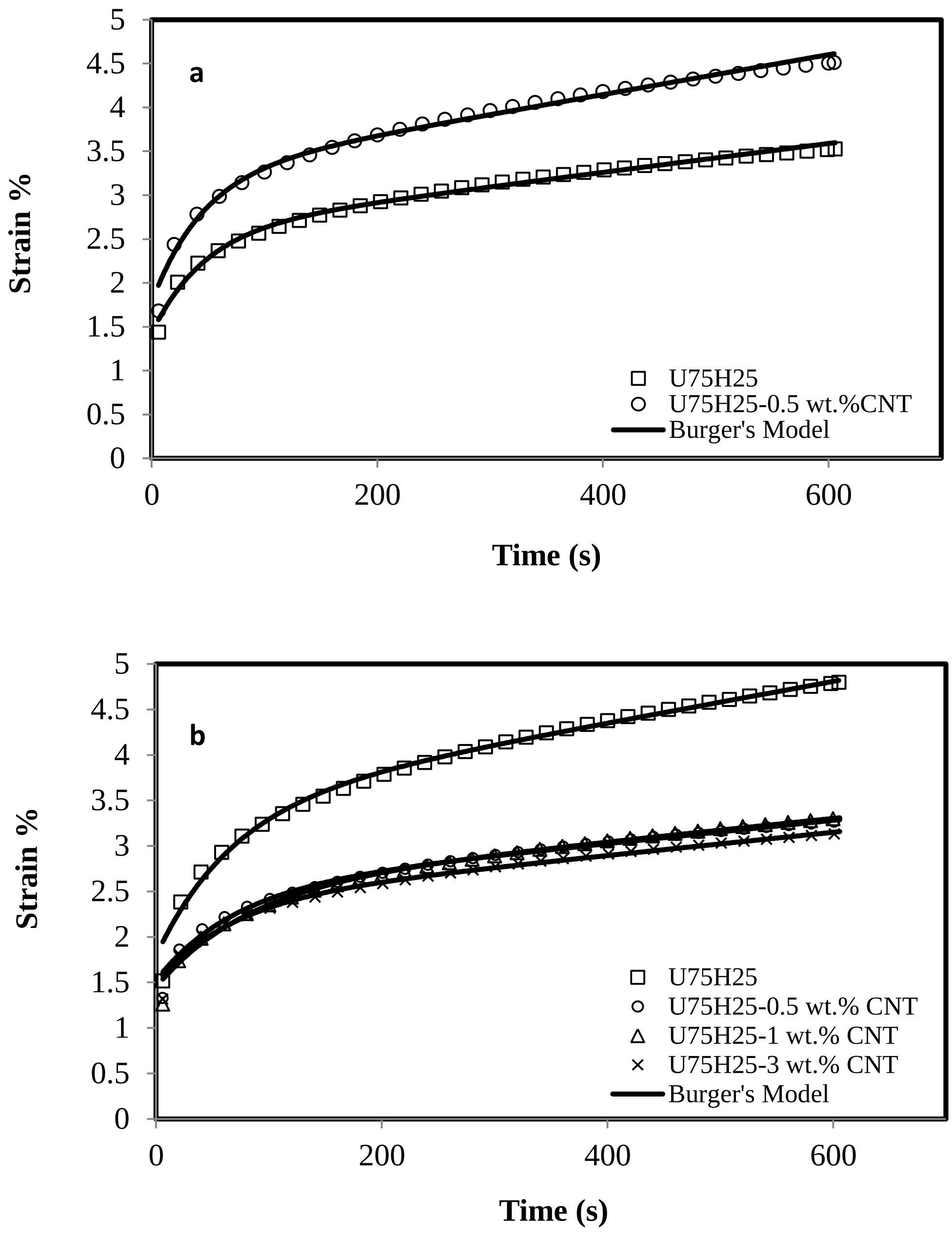

Figure 6.18: The effects of nanoparticles on the creep resistance of the blends processed using (a) M1 and (b) M2.

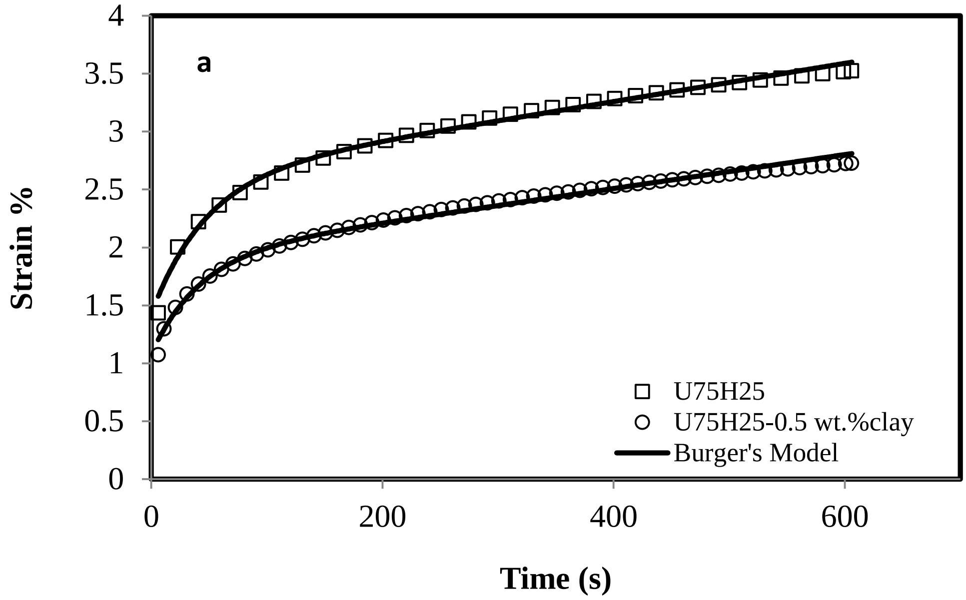

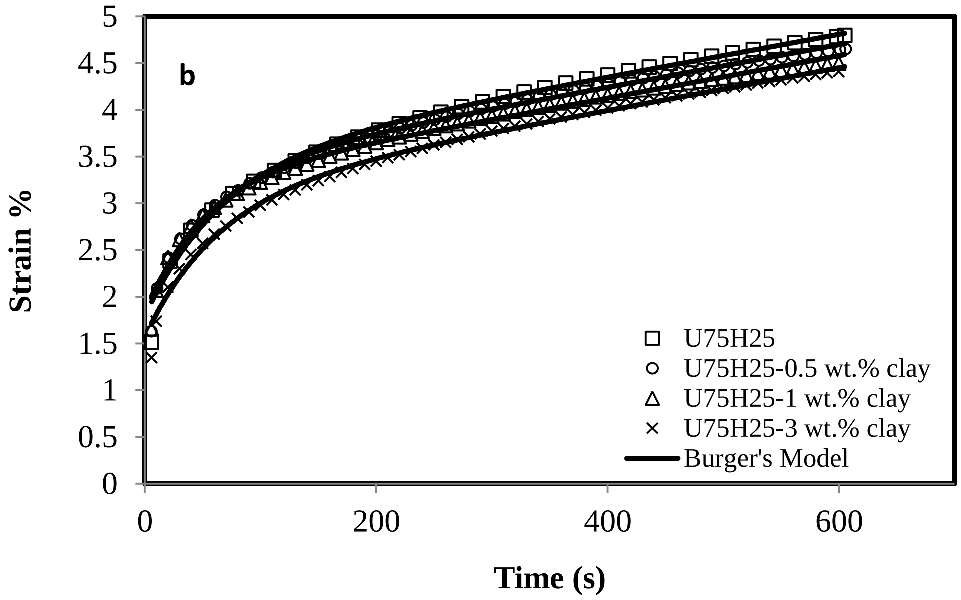

Figure 6.19: The effects of nanoparticles on the creep resistance of the blends processed using (a) M1 and (b) M2.

6.5.3 Constitutive Modelling of the Creep Behaviour

Creep modeling and analysis is important to determine the time response of polymers, which leads to a better understanding of chain dynamics. Burger's model, which is a combination of Kelvin-Voigt and Maxwell elements, is one of the most commonly used models to describe the linear viscoelastic behaviour of polymer composites (see Section 2.11). The total strain as a function of time can be obtained from Equation 2.4. Figures 6.17 to 6.19 show that curve fitting of this model to the creep experimental data results in very good agreement with the experimental data. Table 6.1 shows the Burger's model parameters. The table indicates a decreasing trend in Kelvin and Maxwell spring constants with the addition of CB or CNT nanoparticles using processing method M1 compared to an increasing trend for the materials processed using M2. However, at high volume fraction (3 wt. %) of CB or CNT processed using M2, a reduction in E_M can be observed, which can be attributed to the nanoparticle aggregation at high content, as discussed in Chapter 5. The elasticity E_M and the stiffness of the amorphous phase E_K of the blend can be increased by the addition of CB or CNT nanoparticles. The parameter η_M represents the irrecoverable creep strain, which also increases with the addition of CB. However, the addition of CNT has no significant effect on the irrecoverable creep strain. Retardation time, τ is the delayed response to the applied stress and it can be seen that the retardation time for the U75H25-CB nanocomposites is slightly less than that for the reinforced blend. Conversely, the addition of CB or CNT nanoparticles using processing method M1 shows a reduction in all parameters, which indicates a reduction in the stiffness and increase in the permanent deformation. It can also be seen also that there is no significant effect of the addition of nanoclay on the creep behaviour of the materials processed using M2.

Table 6.1: The simulated parameters of Burger's model for creep tests.

Materials	Filler content (wt. %)	E_M (MPa)	E_K (MPa)	η_M ($x10^3$ MPa.s)	τ (s)
U75H25-CB-M1	0	645	784	559	46.6
	0.5	604	734	405	37.2
	1	596	642	381	45.1
	3	583	617	365	42.1
U75H25-CB-M2	0	513	650	405	67.8
	0.5	610	924	705	63.3
	1	721	990	805	73.8
	3	627	1030	725	63.3
U75H25-CNT-M1	0	645	784	559	46.6
	0.5	518	630	405	45
U75H25-CNT-M2	0	513	650	405	67.8
	0.5	605	921	725	68.5
	1	635	941	725	80.5
	3	618	1020	725	65.5
U75H25-clay-M1	0	645	784	559	46.6
	0.5	851	1090	629	41.4
U75H25-clay-M2	0	513	650	405	67.8
	0.5	497	620	405	58
	1	510	652	405	48
	2	586	607	405	63.2

6.6 Summary

Correlations between processing method, nanoparticle type and geometry and the mechanical properties of a range of polyethylene-based nanocomposites were investigated in this chapter. It was found that careful selection of processing method and nanofiller can lead to significant improvement in the material's properties. These include toughness, tensile strength, yield stress, elastic modulus, hardness and creep resistance. The incorporation of a small volume fraction of the nanoparticles showed improvement in the tensile properties of the polyethylene-based nanocomposites. However, it was observed that at high strain rates a significant temperature increase occurred, which led to thermal softening, especially in the strain hardening region, and consequently a reduction in the failure stress. This temperature increase was attributed to heat generation due to the additional friction between the nanoparticle and the polymer chains during plastic deformation. The temperature increase was strongly dependent on the strain rate, processing method, nanoparticle type and volume fraction. Both processing method M2 and the presence of clay nanoparticles in the polymer matrix showed a reduction in the heat generation during plastic deformation of the polyethylene-based nanocomposites. This was proposed to be due to the improvement in the miscibility of the blend when processed using M2, the lower surface area to volume of the clay and the poor clay-matrix interaction, which led to the formation of voids and cracks in the microstructure.

The effect of processing method, nanoparticle type and volume fraction on the creep resistance of the U75H25 blend was investigated at room temperature. The creep resistance of the U75H25 blend was improved significantly by the addition of CB and CNT nanoparticles. This improvement was dependent on the CB volume fraction and independent on the CNT volume fraction, which indicated the significant effect of the nanoparticle geometry on the deformation mechanism.

Chapter 7
Mechanical Properties of Polyethylene-based Nanocomposites (Micro-Scale Properties)

7.1 Introduction

This Chapter presents the use of depth sensing indentation to determine the effect of the processing method, nanoparticle type and volume fraction on the micro-scale properties of the polyethylene-based nanocomposites. These include the elastic-plastic behaviour, viscoelastic behaviour, indentation hardness and elastic modulus.

7.2 Load-Depth Behaviour

Figures 7.1 to 7.3 show loading-hold-unloading curves for the U75H25 blend and its nanocomposites with different volume fractions of nanofiller processed using methods M1 and M2. These curves were obtained from DSI tests with a maximum load of 40mN, which was held for 600s to minimise the effect of the viscoelastic behaviour of the polyethylene, as discussed in Section 2.12.1. Generally, it can be observed from all figures that the incorporation of CB, CNT or clay nanoparticles, using both processing methods, results in a reduction in the penetration depth, which leads to an increase in the hardness values, as described in Section 5.5. The hardness values of the nanocomposites increase with increasing volume fraction of CB and CNT. This can be attributed to the presence of nanofillers with high hardness and surface area to volume ratio. It is expected that by increasing the volume fraction of the nanofiller the indenter interacts with more CB or CNTs, which results in more resistance to deformation. The addition of 2 wt. % clay nanoparticle displaced the curve to a higher penetration depth compared to 1 wt. % clay. This could be due to the intercalation of the clay platelets at high volume fraction and the poor distribution of clay nanoparticle in the U75H25 matrix, as discussed in Section 5.5.

The elastic modulus values were also calculated using Eq. (3.8) and the results are shown in Figure 7.4. The elastic modulus is a description of a material's tendency to deform elastically, which represents the overall stiffness of the polymer network. It can be seen that the elastic modulus increases with increasing volume fraction of nanofiller. Modulus and stiffness (slope of the unloading curve) have a direct relationship, as shown in Eq. (3.7). It is interesting to see transition values for the elastic modulus at 0.5 wt. % of the nanofiller. This value is obvious for the clay nanoparticle where a sharp increase in the modulus occurs. This can be attributed to the 2D geometry and large size of the clay platelets. These results can be used as evidence that nanoparticle geometry can significantly affect the indentation behaviour of polyethylene-based nanocomposites.

It can be observed that the addition of CB nanoparticles using both processing methods M1 and M2 resulted in a significant increase in the indentation elastic modulus. Conversely, in bulk tensile testing (see Section 6.2), a significant reduction in the elastic modulus was seen with the incorporation of CB nanoparticles using M1 and M2. This change in the CB nanoparticles effect on elastic modulus can be related to the differences in materials behaviour in tension and compression and the shape of CB particles. On the other hand, similar increasing trends of modulus at both macro and micro scales were obtained by the addition of CNT and clay nanoparticles using M1 and M2.

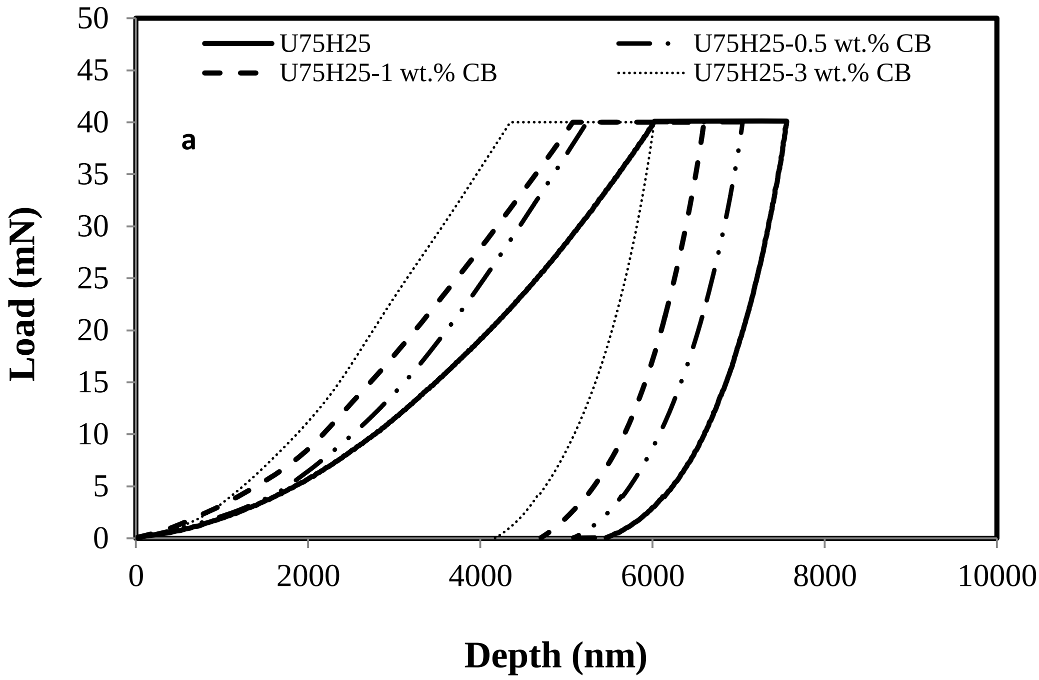

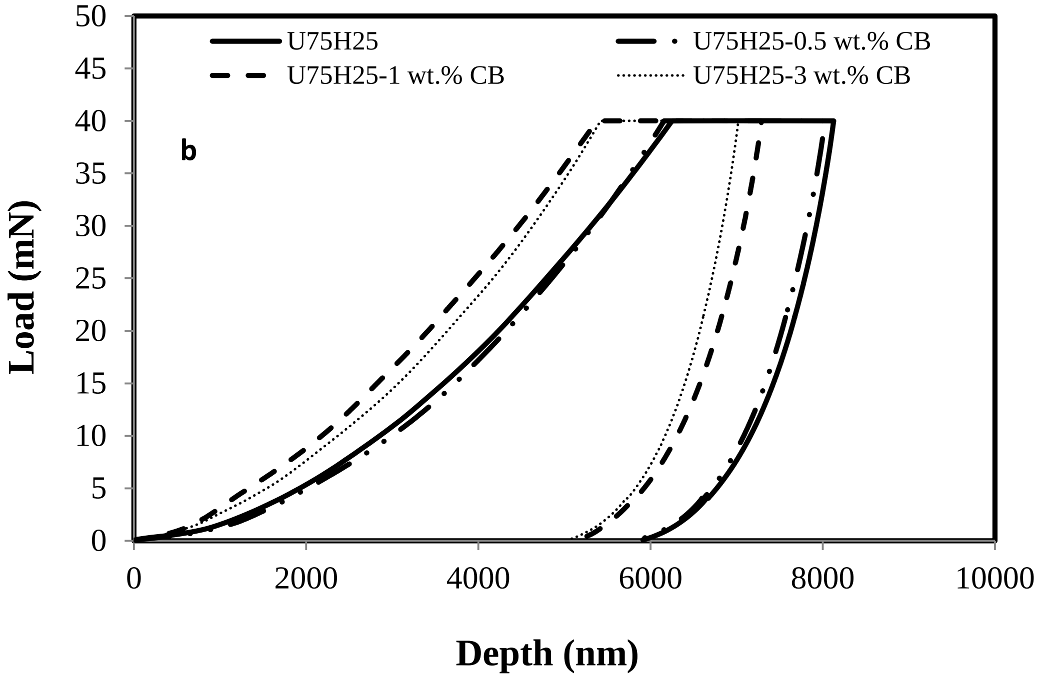

Figure 7.1: Nanoindentation behaviour of U75H25-CB nanocomposites processed using a) M1 and b) M2.

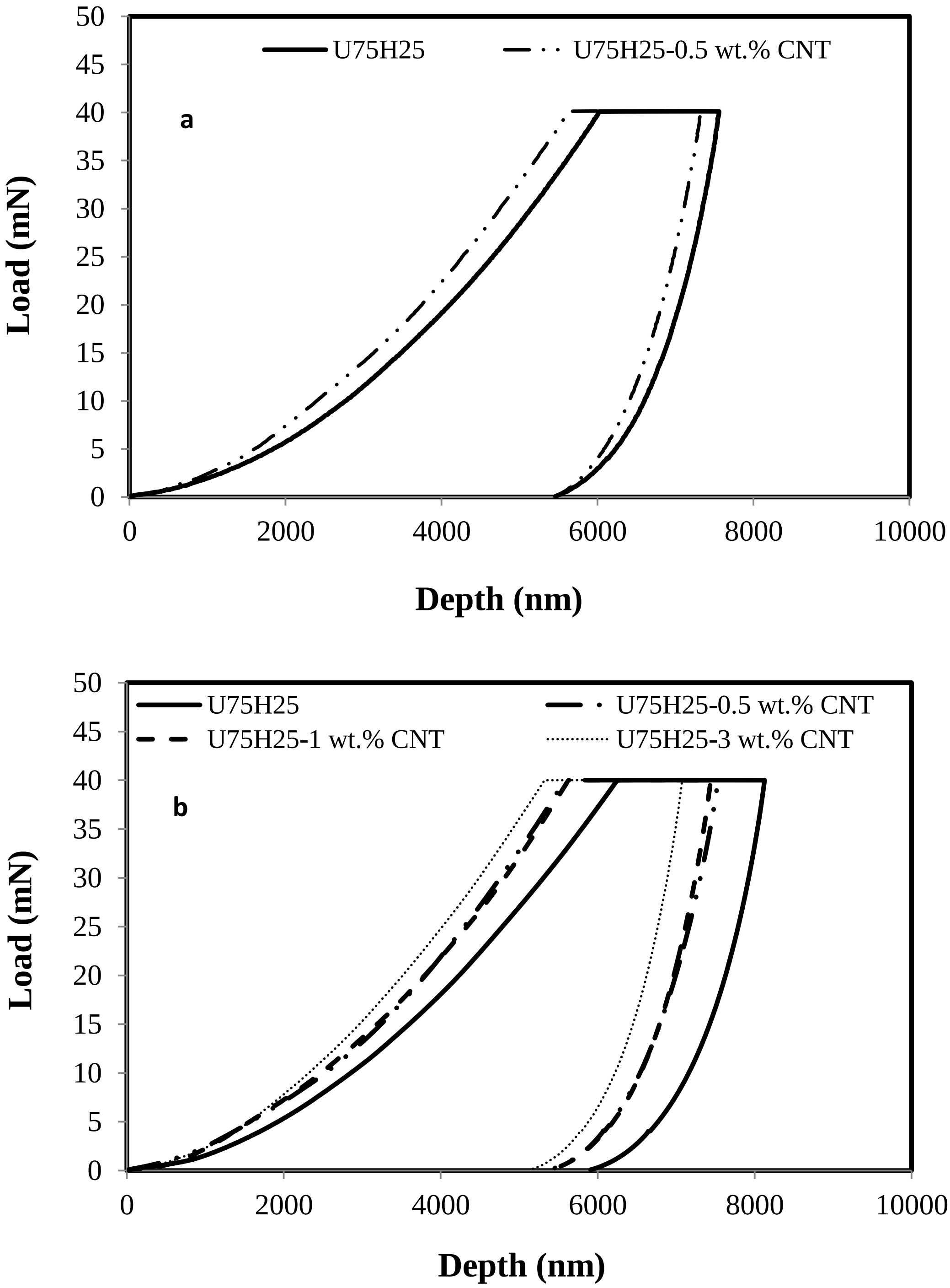

Figure 7.2: Nanoindentation behaviour of U75H25-CNT nanocomposites processed using a) M1 and b) M2.

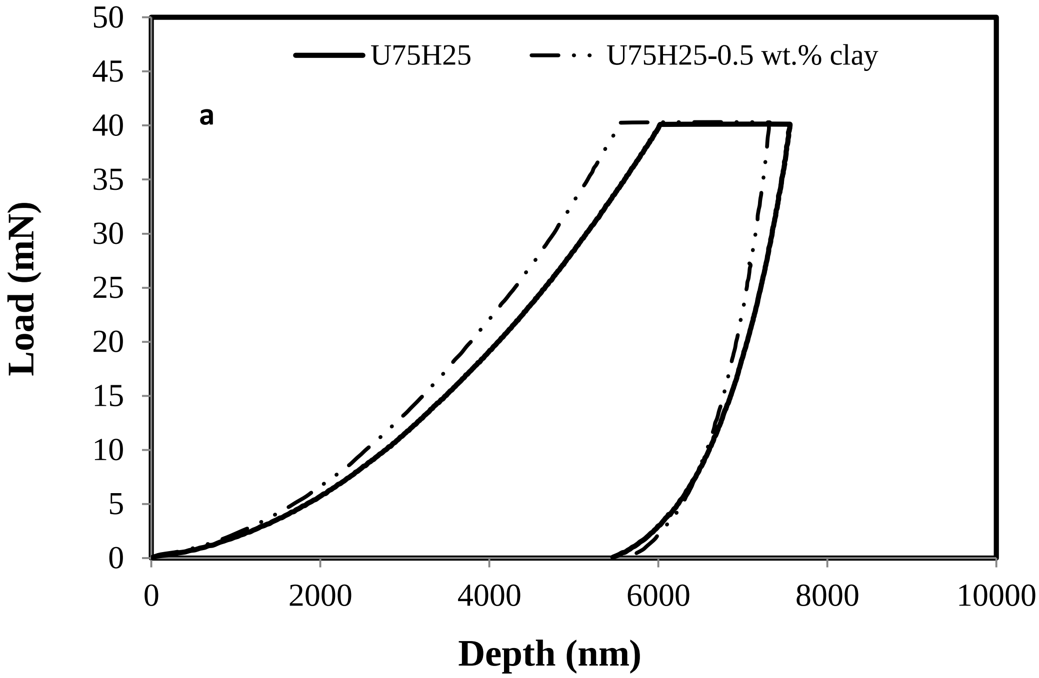

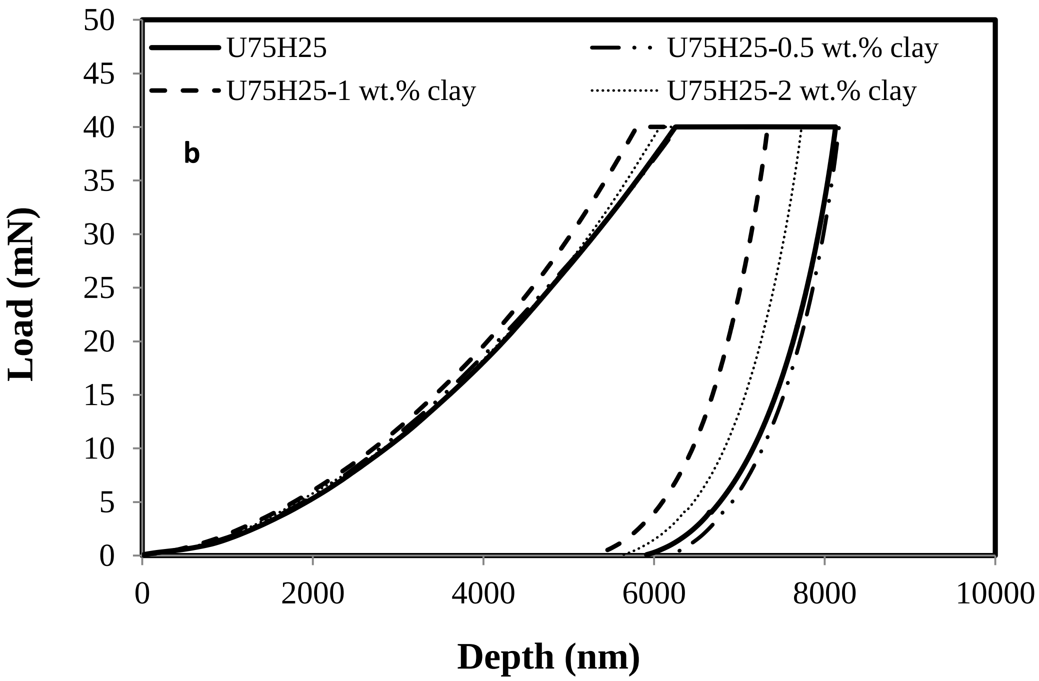

Figure 7.3: Nanoindentation behaviour of U75H25-clay nanocomposites processed using a) M1 and b) M2.

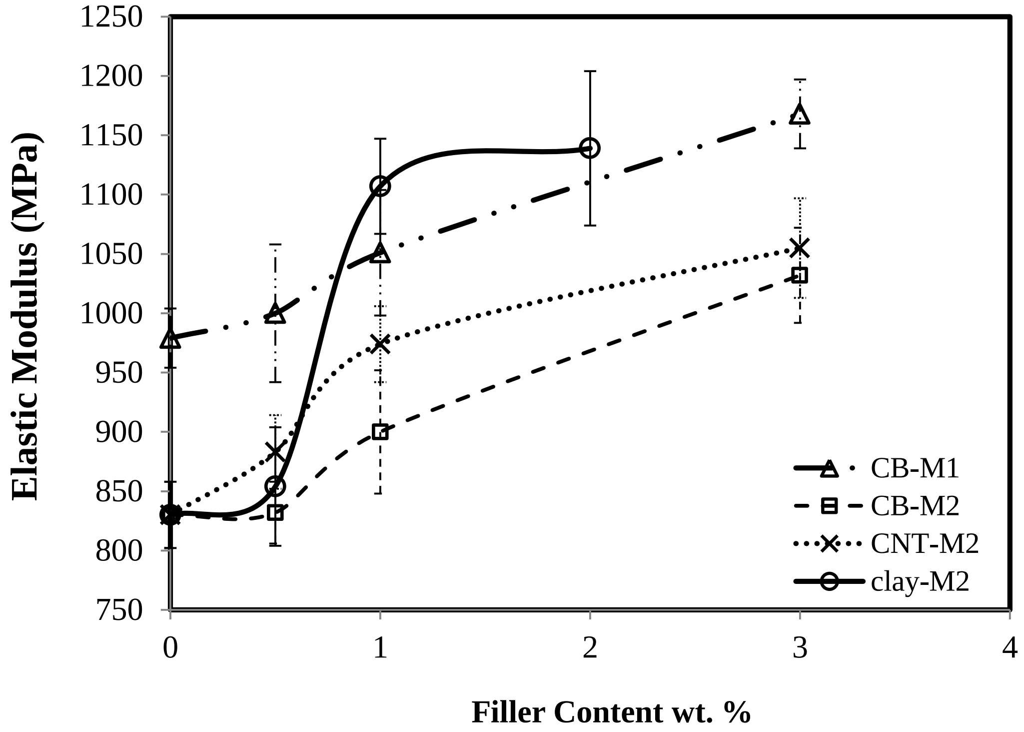

Figure 7.4: Effect of nanoparticle volume fraction on the elastic modulus of polyethylene-based nanocomposites measured by nanoindentation.

7.3 Micro-Creep Behaviour

There are a number of significant differences between standard tensile creep and indentation creep. Indentation creep is carried out using constant force, and the applied stress decreases during a creep experiment due to the increase in the contact area. In tensile creep, if a constant force is applied, the stress will increase as the sample creeps. A complex stress distribution occurs beneath an indenter, whereas a nominally uniform stress is seen in the gauge length of a sample in a tensile creep test and a localized creep occurs beneath the indenter and the surrounding material does not creep, whereas creep occurs across the whole gauge area in a tensile creep test. These differences should be considered when comparing creep data from the two tests.

Table 7.1 presents the effect of processing method and nanoparticle type on the creep behaviour of polyethylene-based nanocomposites at the micro-scale using the DSI technique. The incorporation of nanoparticles using processing method M2 improves the creep resistance of the U75H25 blend. This improvement increases with increasing volume fraction of the nanoparticles. The addition of nanoparticles using method M1 shows a reduction in the creep resistance compared to materials processed using M2. This can be attributed to the difference in the morphology of the materials, as discussed in Chapter 5.

The addition of 0.5 wt. % nanoparticles using processing method M1 results in a reduction in the creep resistance. In contrast, the addition of nanoparticles using processing method M2 shows no effect on the creep resistance of the U75H25 blend. This indicates the significant effect of processing method on the creep behaviour of polyethylene-based nanocomposites. However, increasing the volume fraction of the CB to 1 wt. % improves the creep resistance of materials processed using both M1 and M2. At high volume fractions of CB, the material processed using processing method M1 show a reduction in the creep resistance, which can be attributed to the formation of large aggregates of CB nanoparticles. Comparing this with the effect of CNT, it can be observed that the nanoparticle type has a significant effect on the indentation creep behaviour of polyethylene-based nanocomposites. The addition of high volume fraction of CNT shows a minor improvement in the creep resistance of the U75H25 blend.

The addition of 1 wt. % clay using processing method M2 shows significant effect on the creep resistance of the U75H25. However, increasing the volume fraction of clay to 2 wt. % resulted in a reduction in the creep resistance compared with 1 wt. % clay. This indicates a poor dispersion of the platelets at high volume fraction and the presence of intercalated clay layers.

Table 7.1: Change in the indentation depth during the dwell period.

Materials - M1	Δh (nm)	Materials - M2	Δh (nm)
U75H25	1530 ± 14	U75H25	1872 ± 10
U75H25-0.5 wt.% CB	1800 ± 6	U75H25-0.5 wt.% CB	1860 ± 15
U75H25-1 wt.% CB	1511 ± 12	U75H25-1 wt.% CB	1720 ± 11
U75H25-3 wt.% CB	1660 ± 16	U75H25-3 wt.% CB	1592 ± 17
U75H25-0.5 wt.% CNT	1771 ± 22	U75H25-0.5 wt.% CNT	1870 ± 12
		U75H25-1 wt.% CNT	1800 ± 15
		U75H25-3 wt.% CNT	1744 ± 9
U75H25-0.5 wt.% clay	1738 ± 13	U75H25-0.5 wt.% clay	1875 ± 11
		U75H25-1 wt.% clay	1524 ± 13
		U75H25-2 wt.% clay	1647 ± 21

7.4 Summary

The micro-scale properties of the polyethylene-based nanocomposites were evaluated by DSI. The effect of the incorporation of CB, CNT and clay on the indentation hardness, elastic modulus and creep were investigated. The results showed that the indentation hardness and elastic modulus increased significantly with increasing volume fraction of the nanofiller. The creep resistance improved with the addition of the nanoparticles processed using M2. It was encouraging to find similarity between the creep behaviour of the polyethylene-based nanocomposites at both macro and micro scales.

Chapter 8
Mechanical Properties of Polyethylene-based Nanocomposites at Elevated Temperatures

8.1 Introduction

In this chapter, the relationship between the temperature and the mechanical properties of the polyethylene-based nanocomposites is investigated. Firstly, the effect of the nanoparticles on the thermal degradation behaviour of the PE materials and nanocomposites are discussed. Then, the effect of the temperature on the stress-strain and creep behaviour is investigated. This includes the effect of temperature on material properties such as toughness, yield stress, tensile strength, elastic modulus and creep resistance. The dependence of the micro-scale properties of the polyethylene-based nanocomposites on temperature and nanofiller content is then explored using the DSI technique. This includes the dependency of the indentation hardness, elastic modulus and creep resistance on the temperature.

8.2 Thermal Degradation of Polyethylene-based Nanocomposites

Thermogravimetric analysis (TGA) curves for UHMWPE, HDPE, U75H25 and the polyethylene-based nanocomposites are shown in Figure 8.1. The thermal degradation starts at about 275°C and then completely breaks in the range of 475-575°C. It can be seen that the thermo-mechanical stability of the U75H25-CB and U75H25-CNT nanocomposites are higher than the UHMWPE and the U75H25 blend and this trend appears to increase as the CB and CNT volume fraction increase. For instance, the temperature at 20% mass loss of the U75H25-3 wt. % CB and U75H25-3 wt. % CNT materials are approximately 30 and 46°C higher than the U75H25 blend, respectively. This can possibly be explained by the formation of a thermally stable cross-linked carbonized layer on the nanoparticle surface during the thermal degradation, which tends to hinder diffusion. On the other hand, the addition of clay nanoparticles shows no effect on the thermal degradation of the blend, which indicates the significant effect of the nanoparticle type on the thermal properties of the polyethylene-based nanocomposites.

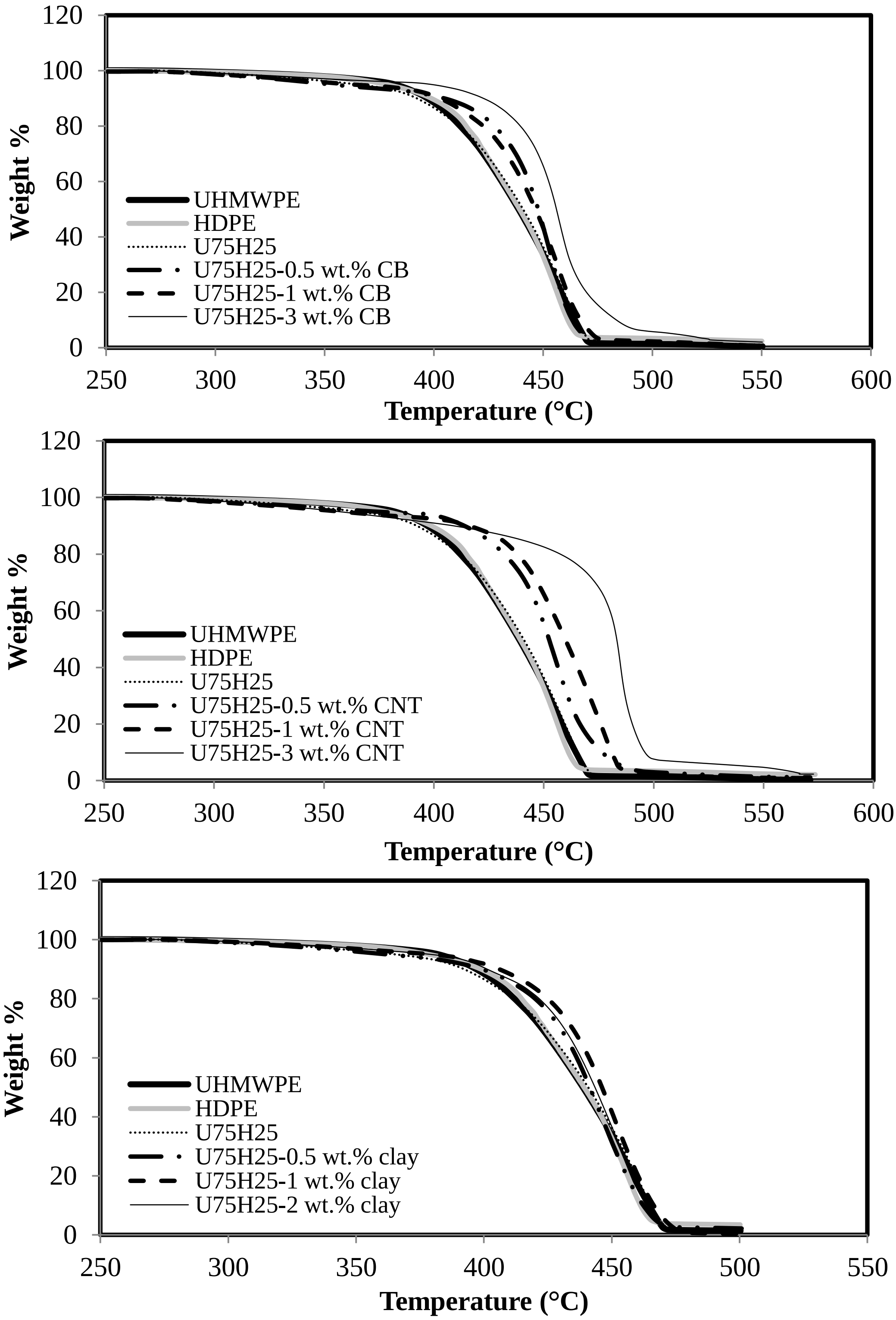

Figure 8.1: TGA results for UHMWPE, HDPE, U75H25 and polyethylene-based nanocomposites.

8.3 Tensile Properties of Polyethylene-based Nanocomposites

8.3.1 Stress-Strain Behaviour

During tensile testing at low strain rates, the test can be considered to be isothermal since no significant temperature increase occurs, as discussed in Section 2.9.2. However, at strain rates over 0.1^{-1} the deformation can be considered to be mostly adiabatic, with some loss of heat to the atmosphere, and the temperature effect increases with increasing strain rate, which leads to thermal softening in the strain hardening region, as shown in Figure 8.2 for the sample processed using method M2 and tested at room temperature. From this figure, 45°C can be considered as a critical value for the U75H25-M2, where thermal softening starts. Therefore, in this section the samples were tested at high temperatures (45 and 65°C) to eliminate the effect of the adiabatic heat, and investigates the dependence of the U75H25-M2 properties on the temperature and nanoparticle addition. It can be seen from Figure 8.2 that increasing the strain rate for the materials tested at high temperature leads to an increase in the yield stress and the tensile strength and no thermal softening occurs in the strain hardening region. Similar behaviour was observed for all the polyethylene-based nanocomposites manufactured using method M2.

Figures 8.3 and 8.4 show the effect of nanoparticle addition on the stress-strain behaviour of the U75H25-M2 at elevated temperatures. The experiments were carried out using 0.2^{-1} strain rate at 45 and 65°C sample temperatures. The addition of CB, clay and 0.5 wt. % CNT nanoparticles results in a reduction in the toughness and strength, which can be attributed to the poor filler-matrix interaction at high temperature. However, increasing the volume fraction of the CNT nanofiller shows a slight improvement in the toughness and yield stress of the U75H25-M2 blend. It is interesting to find that increasing the volume fraction of CB and Clay nanoparticles has no effect on the tensile behaviour of the nanocomposites at high temperature. This suggests that once temperature has exceeded the critical softening temperature, the nanoparticle performance is matrix dominated.

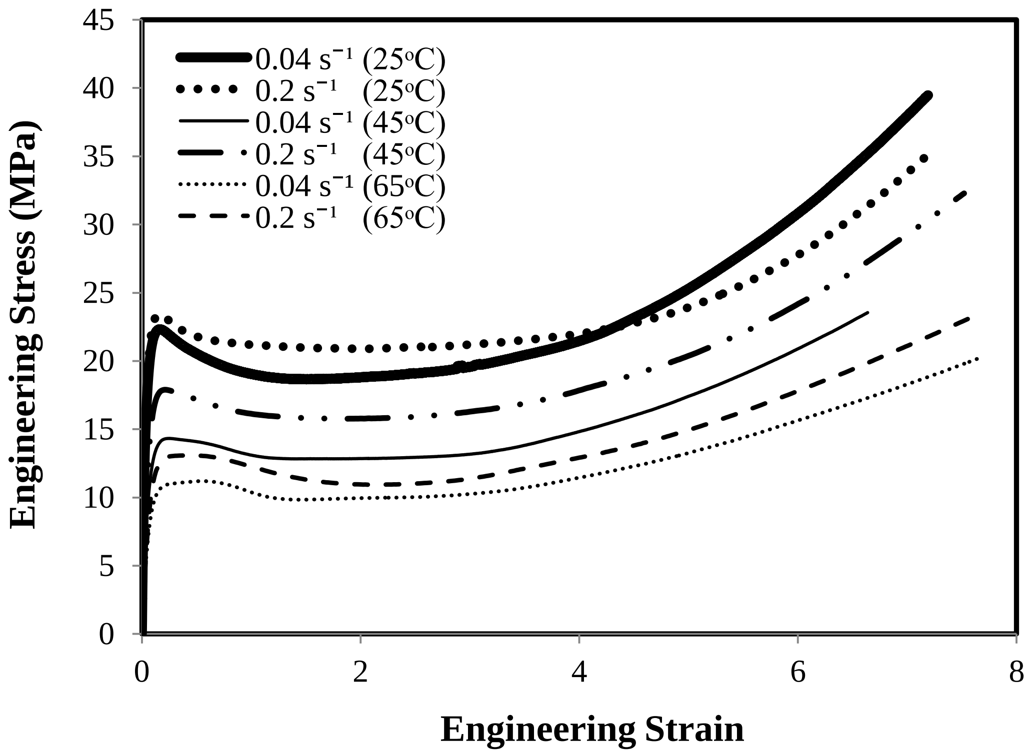

Figure 8.2: Effect of various temperatures on the stress-strain behaviour of the U75H25-M2 blend.

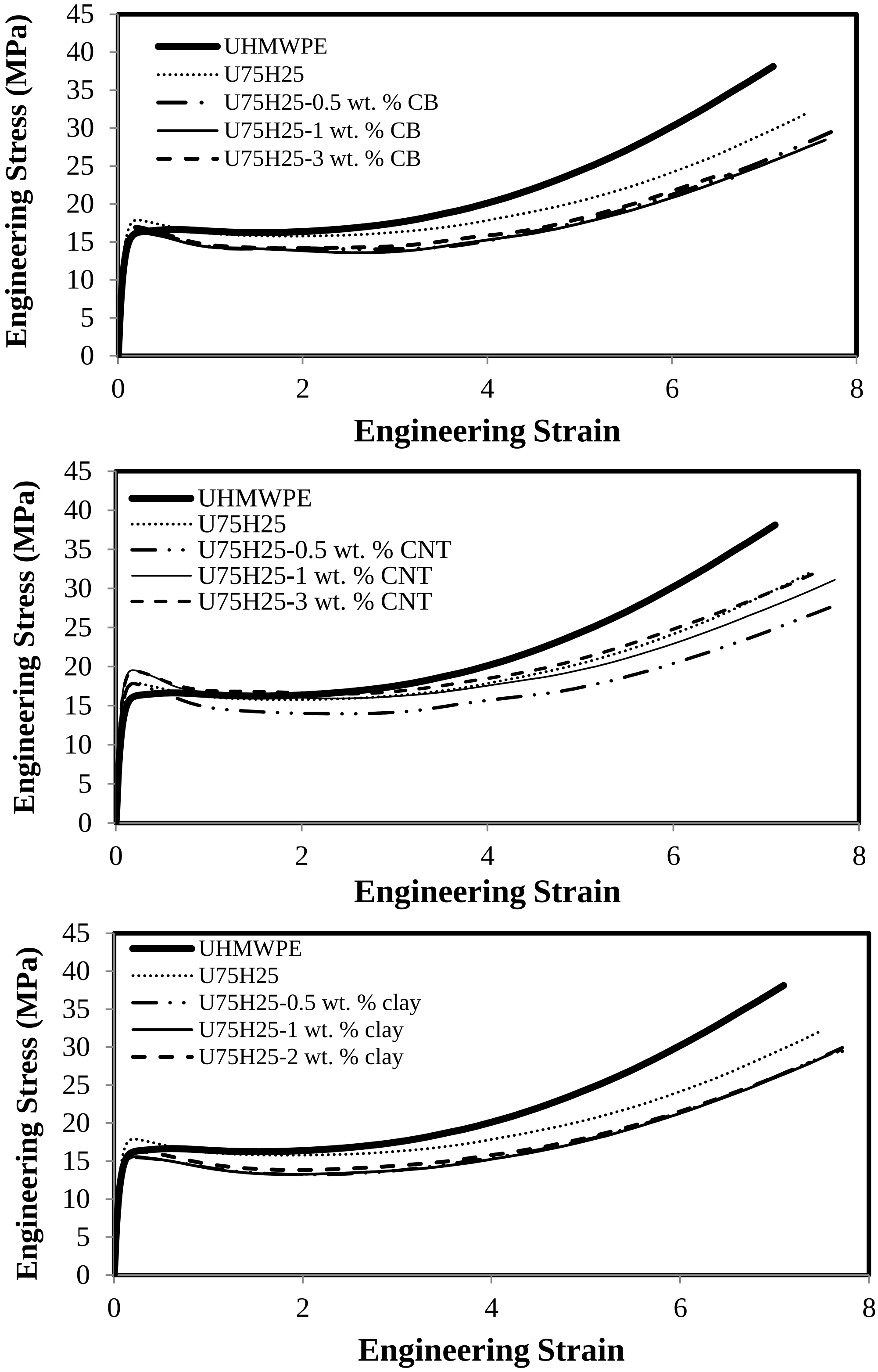

Figure 8.3: Effect of temperature on the stress-strain behaviour of the M2 nanocomposites at 0.2^{-1} strain rate and 45°C temperature.

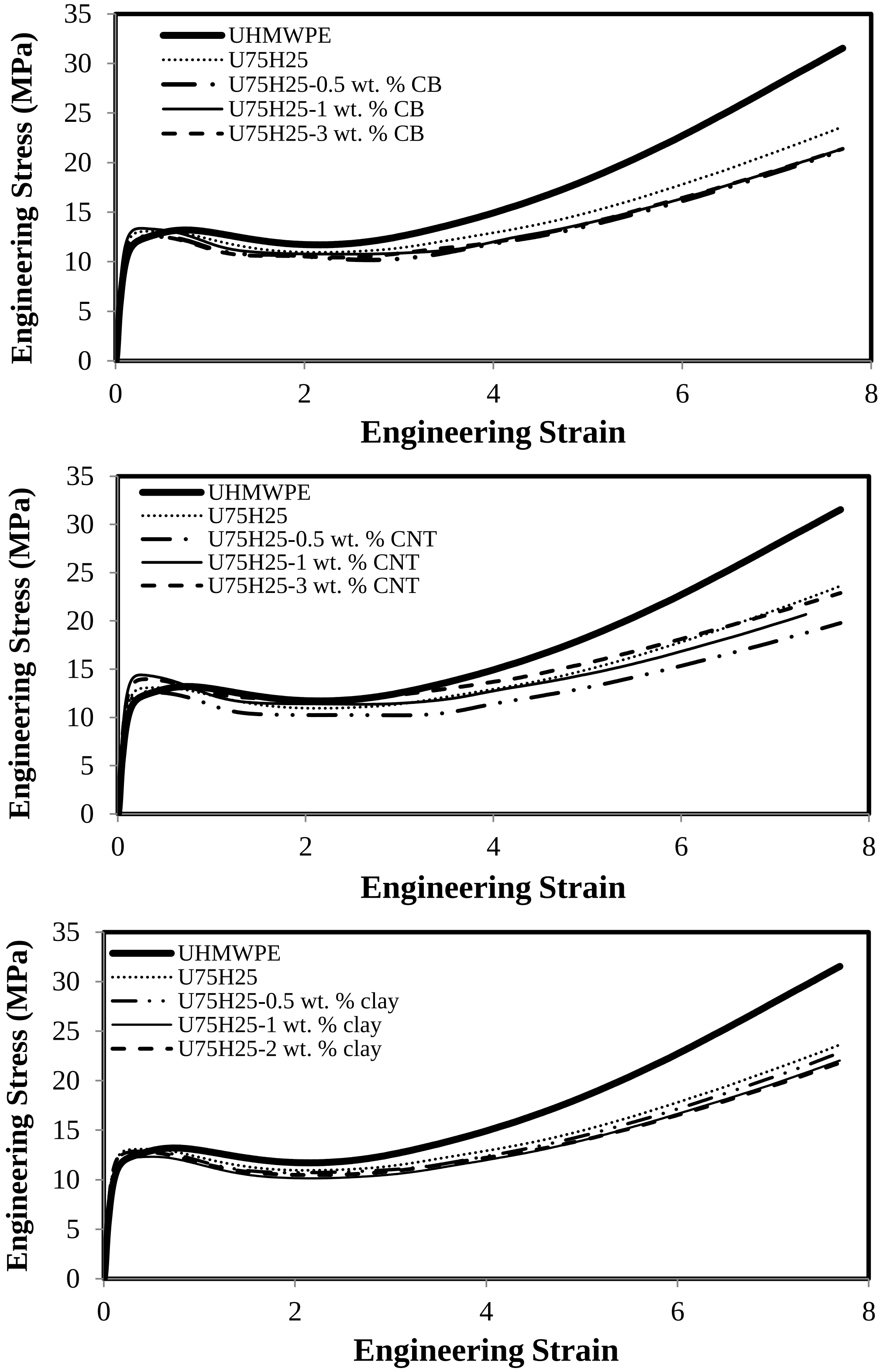

Figure 8.4: Effect of temperature on the stress-strain behaviour of the M2 nanocomposites at 0.2^{-1} strain rate and 65°C temperature.

8.3.2 Yield Stress and Elastic Modulus

The effects of ambient temperature on the yield stress and the elastic modulus of the polyethylene-based nanocomposites are shown in Figures 8.5 and 8.6, respectively. It can be observed that a significant reduction in the yield stress occurs for all materials at high temperatures. The increase in testing temperature leads to approximately 30 and 50% reduction in yield stress at 45 and 65°C, respectively. The incorporation of CB and CNT nanoparticles shows a slight improvement in the yield stress at high temperature. In contrast, the addition of clay decreases the yield stress compared to the unfilled U75H25. This can be attributed to the absence of interaction between clay and polyethylene matrix at elevated temperatures. Therefore, the presence of clay nanoparticles in the U75H25 matrix applied as defects in the microstructure. For the elastic modulus, it can be seen that an increase in temperature can lead to a significant reduction. The results show approximately 40 and 67% reduction in the elastic modulus at 45 and 65°C, respectively. This can be attributed to the increase in strain at high temperature, which reduces intermolecular forces and increases chain mobility. The addition of CB, CNT and clay nanoparticles leads to a slight increase in the modulus value at high temperature. However, it is interesting to find a reverse effect of the CB nanoparticles on the elastic modulus at high temperature compared to their effect at room temperature.

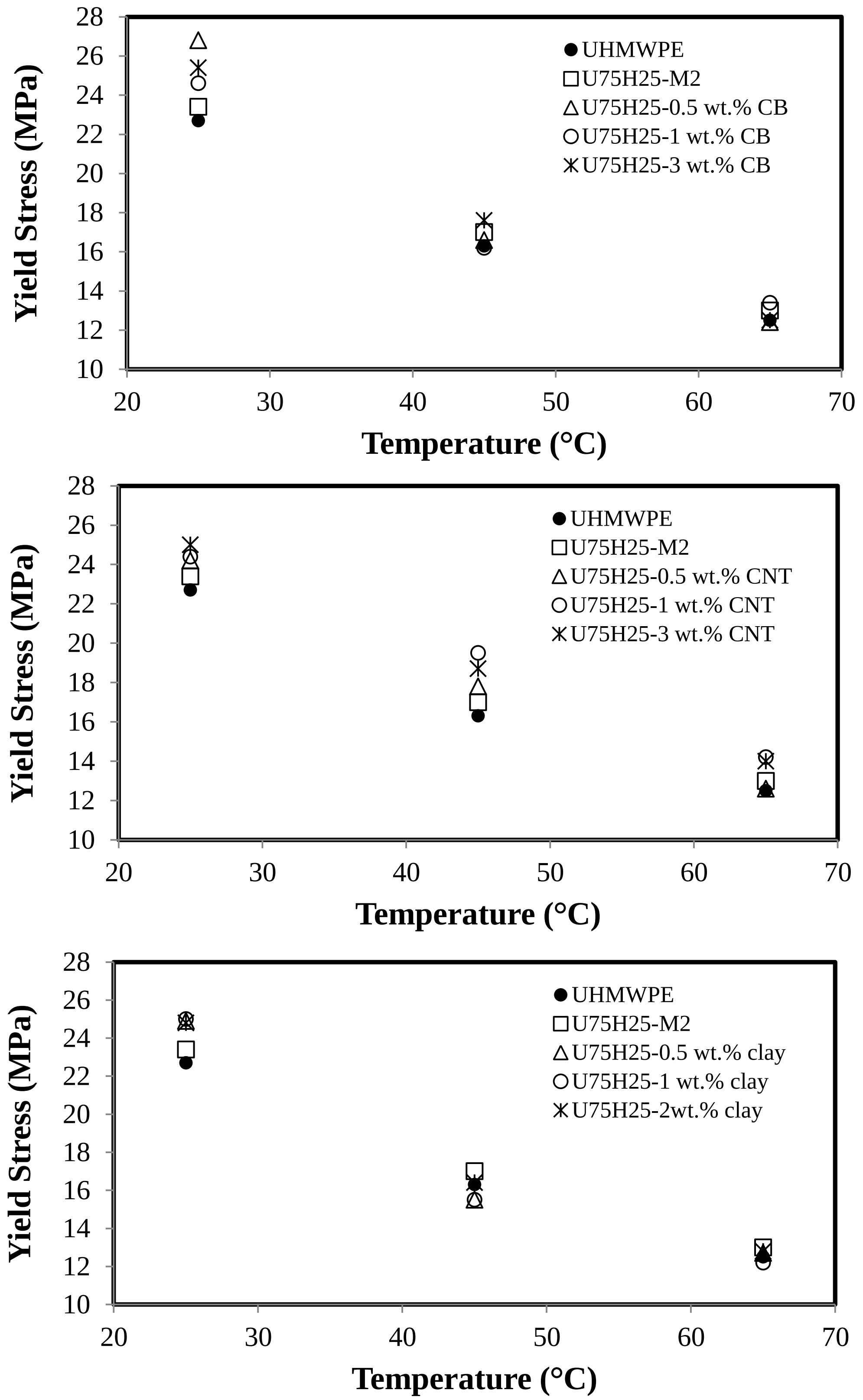

Figure 8.5: Dependence of average yield stress of the M2 nanocomposites on the ambient temperature.

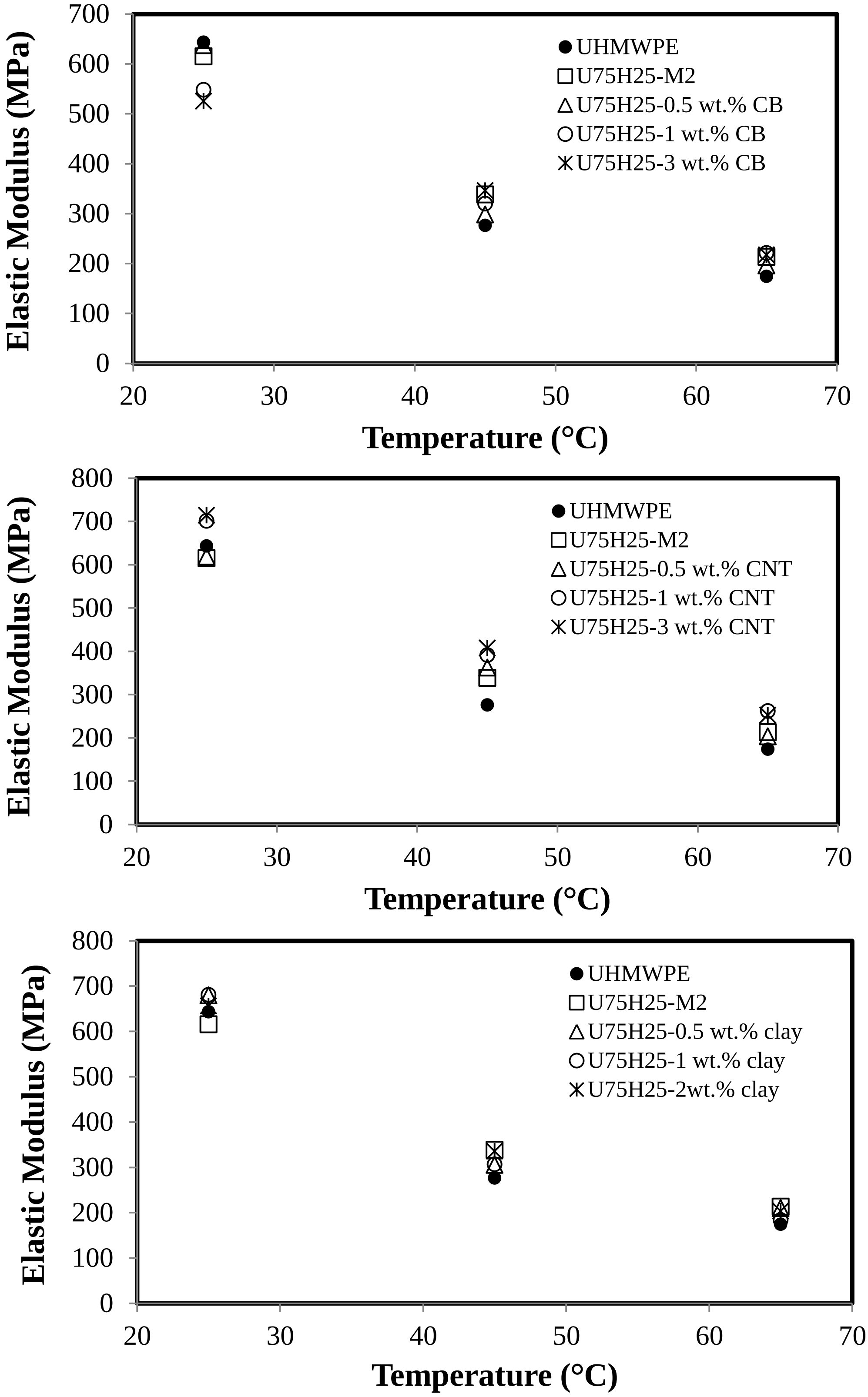

Figure 8.6: Dependence of average elastic modulus of the M2 nanocomposites on the ambient temperature.

8.4 Tensile Creep Behaviour

Tensile creep experiments were performed at various ambient temperatures using 3MPa constant stress to investigate the effect of temperature on the creep resistance of the M2 nanocomposites. The dependence of strain rate on temperature was evaluated after 600s creep time in the steady-state region. Generally, it can be observed from Figure 8.7 that there is a significant increase in the creep strain at high temperature, particularly at 65°C (up to 67%). Blending HDPE with UHMWPE results in an improvement in the creep resistance at all temperatures. Creep strain of U75H25 at 65°C is reduced by 10% compared with UHMWPE. Further increase in the creep resistance can be obtained by the incorporation of the nanoparticles. For example, the addition of 0.5 wt. % CB nanoparticles results in a reduction of 10% in creep strain at 65°C compared with U75H25.

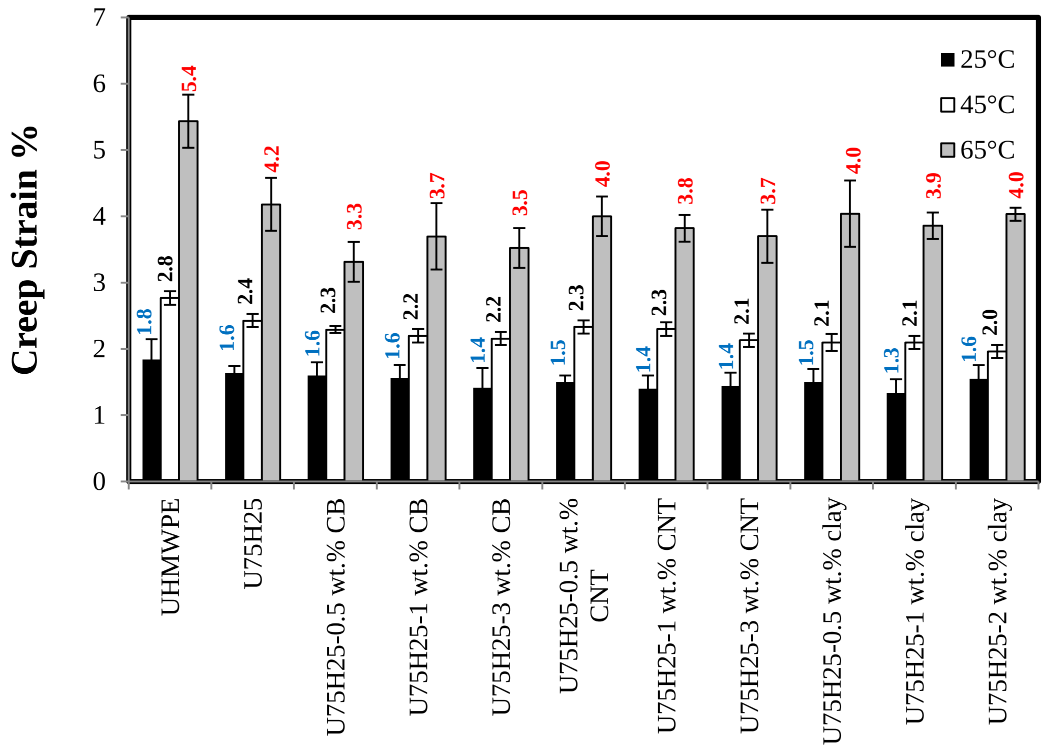

Figure 8.7: Creep strain of the M2 nanocomposites after 600s at various temperatures.

8.5 Depth Sensing Indentation Analysis

Figure 8.8 shows typical load-hold-unload curves for the U75H25-M2 blend at various temperatures. It can be seen that the blend become less stiff and the penetration depth increases as temperature increase and a similar trend was observed for the filled polymers. In order to investigate the effect of nanoparticle addition on the nanoindentation behaviour at various temperatures, a comparison of the effect of nanoparticles on the indentation depth is shown in Figure 8.9. The presence of the nanoparticles leads to a reduction in the penetration depth. The reduction in the penetration depth increases with increasing volume fraction of nanofiller. Increasing the temperature leads to a significant increase in the indentation penetration depth. For example, at 65°C the indentation penetration depths of the U75H25-1 wt. % CB, U75H25-1 wt. % CNT and U75H25-1 wt. % clay increase by 24, 18 and 21%, respectively compared to the indentation depths at room temperature.

The indentation hardness and elastic modulus were calculated following the same analysis discussed in Section 3.4.3. Figure 8.10 shows the indentation hardness and elastic modulus of the M2 nanocomposites at various temperatures (25, 45 and 65°C). It can be seen that increasing the temperature from 25 to 45°C causes a significant reduction in the indentation hardness of the polyethylene-based nanocomposites, in the range of 25 to 34%. However, only a small difference can be found between the indentation hardness values tested at 45 and 65°C, which supports the theory that 45°C is a critical softening temperature for the PE blends in the plastic region. Testing the materials at high temperatures also produces a significant effect on the elastic modulus. Increasing temperature by 20°C results in a significant reduction in the elastic modulus values, between 30 and 40%. Further reduction in the elastic modulus values (in the range of 4 to 21%) occurs by an additional temperature increase of 20°C. This indicates that the critical softening temperature referred to above is applicable to the plastic deformation region but not the elastic deformation region.

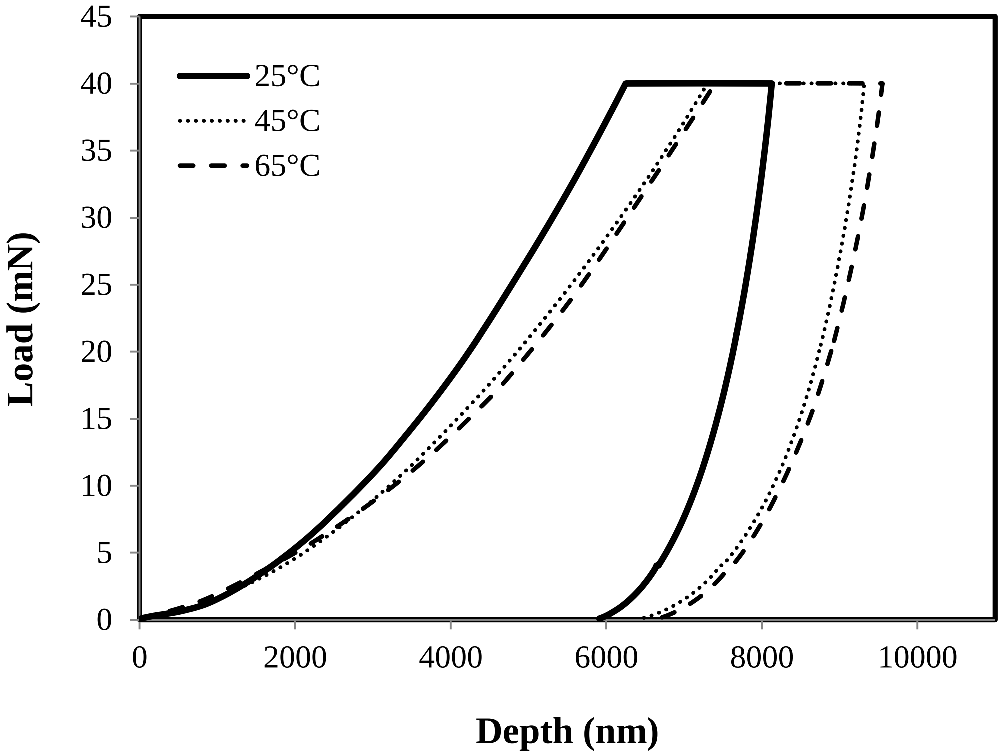

Figure 8.8: Load-depth curves of U75H25-M2 at various temperatures.

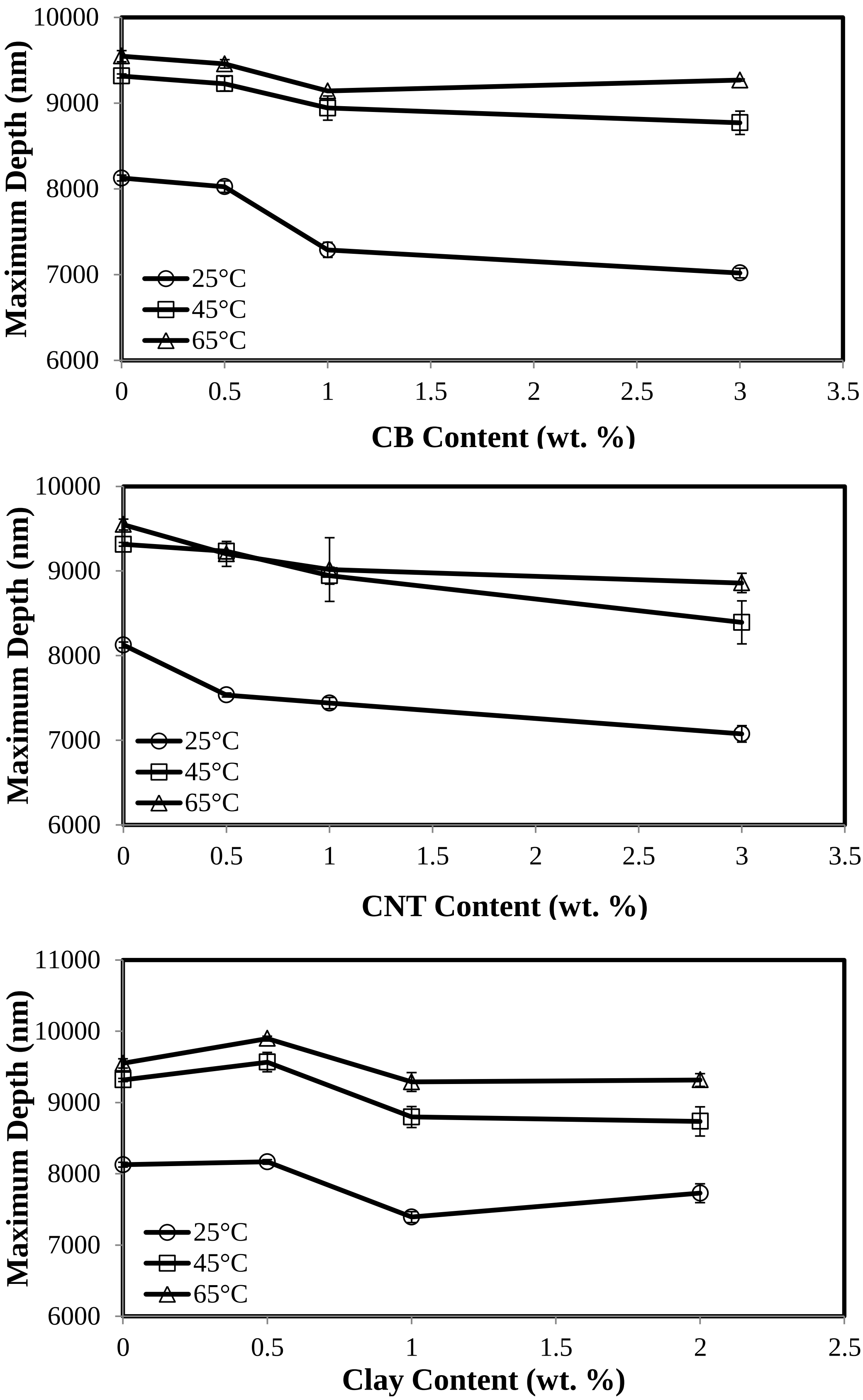

Figure 8.9: Dependency of maximum indentation depth on the nanoparticle loading and ambient temperature.

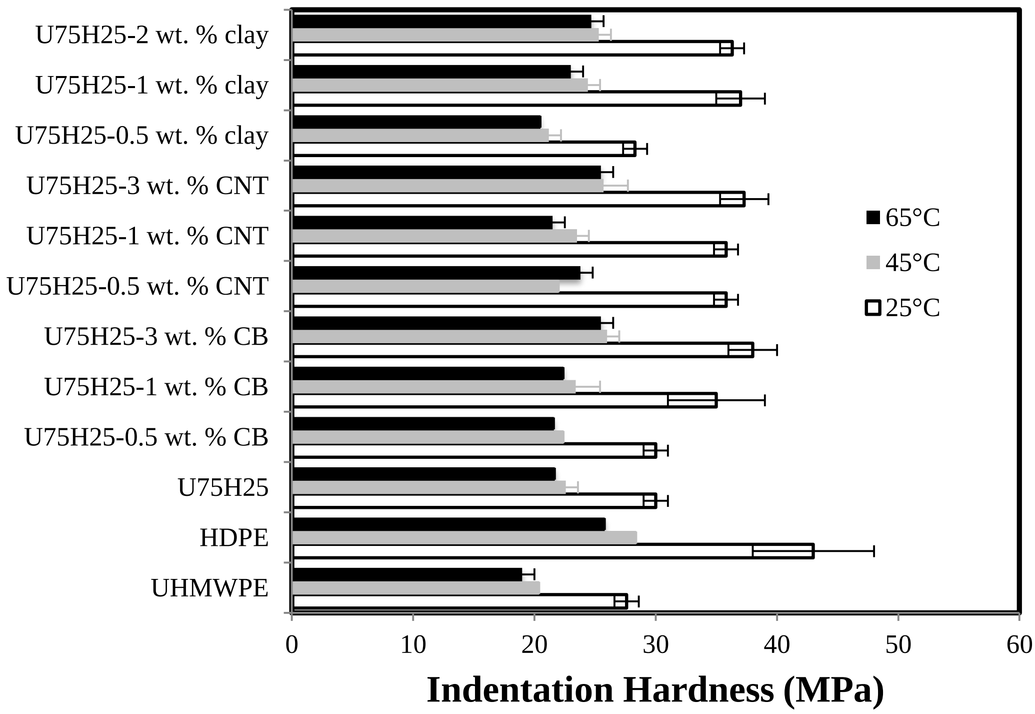

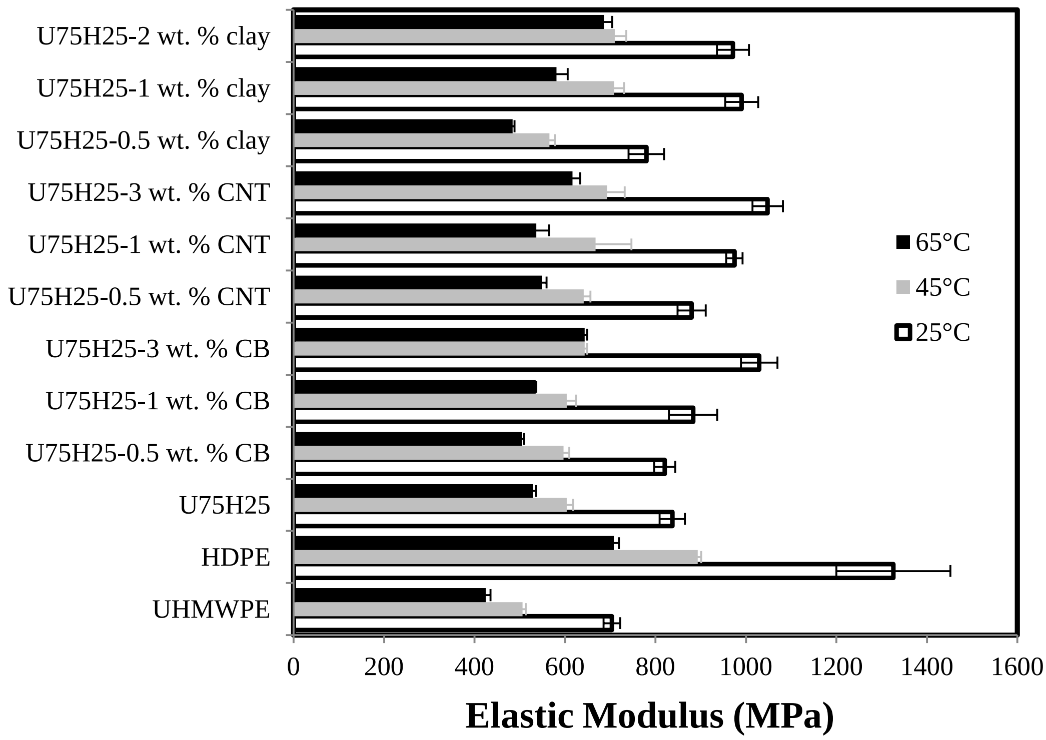

Figure 8.10: Effect of ambient temperature on the indentation hardness and elastic modulus.

8.6 Summary

The macro and micro mechanical properties of the polyethylene-based nanocomposites were evaluated at various temperatures. The results showed that the thermo-mechanical stability of the U75H25-M2 blend was improved with the addition of the CB and CNT nanoparticles, whereas no significant effect was observed with the incorporation of the clay nanoparticles. Testing the materials at elevated temperature resulted in significant effects on the stress-strain behaviour, and consequently the tensile properties such as toughness, elastic modulus, yield stress and strength. The difference in the toughness between the UHMWPE and the U75H25 tested at room temperature was reduced at high temperature with a slight increase in the yield stress. The yield stress and elastic modulus were significantly affected by the temperature. The results showed a significant reduction in the yield stress and elastic modulus when the temperature was increased from 25 to 65°C, up to 50 and 67%, respectively. The incorporation of a low volume fraction of nanoparticles resulted in a negative influence on the material toughness at elevated temperature. By increasing the loading of the CNT (1 and 3 wt. %), the nanocomposites showed similar strain hardening curves as the U75H25-M2 blend with improvement in the yield stress and elastic modulus.

The creep resistance of the polyethylene-based nanocomposites was highly affected by temperature with creep strain reduced by up to 66% by increasing the temperature from 25 to 65°C. The U75H25-M2 blend showed a greater creep resistance than the UHMWPE at all testing temperatures. The addition of the nanoparticles resulted in a positive effect on the creep resistance; the presence of the nanoparticles obstructed the polymer chain movement, which increased the creep resistance at all testing temperatures.

At the micro - scale, the spatially resolved properties were evaluated at various temperatures using DSI. Similar to the bulk tests, increasing the temperature led to significant reduction in material properties such as stiffness, hardness, elastic modulus and creep resistance. High temperatures caused material softening, which led to increasing penetration depth and consequently affected the hardness.

However, the presence of the nanoparticles resulted in an improvement in the hardness and the creep resistance at all testing temperatures. The elastic modulus was significantly affected by the temperature increase. Up to 60% reduction in the elastic modulus was obtained at elevated temperature.

Chapter 9
Discussion

9.1 Introduction

This chapter presents a discussion of the experimental results presented in the previous chapters. The discussion is divided into four parts, and starts with a discussion of the effect of processing method on the material morphology, heat generation during plastic deformation and mechanical properties. This is followed by a discussion of the effect of nanoparticle type and volume fraction on the heat generation during plastic deformation and the mechanical properties. Then, the dependency of heat generation during plastic deformation and mechanical properties on strain rate is discussed. Finally, the ambient temperature effects on the mechanical properties at macro and micro scales are discussed.

9.2 Processing Method Effects

The degree of nanofiller dispersion, and hence the morphology and mechanical properties, were highly dependent on the processing method. Two processing methods (M1 and M2) were used to prepare the materials, with nanofiller volume fraction up to 3 wt. %. Various types of nanoparticles (CNT, CB and inorganic clay) were blended separately with the U75H25 blend to obtain qualitative comparison based on morphology, nanoparticle geometry and volume fraction. The SEM and TEM images shown in Chapter 5 indicate that the processing parameters can significantly affect the dispersion of the nanoparticles. Large aggregations of CB nanoparticles were observed in the material processed using M1 at all volume fractions. Whilst, processing method M2 resulted in a uniform dispersion of CB nanoparticles at 0.5 and 1 wt. % CB and small aggregations at 3 wt. % CB. Both processing methods showed good dispersion of CNT and clay at low volume fraction (0.5 wt. %). However, large variations were observed in the mechanical properties, which can be related to the difference in the mechanical and physical properties of the nanoparticles and filler-matrix interaction.

The mechanical properties of the U75H25 blend such as tensile behaviour, creep resistance, elastic modulus and indentation resistance were strongly dependent on the processing method, as discussed in Chapter 4. Processing method M1 resulted in properties closer to the HDPE, whereas processing method M2 resulted in properties closer to that of the UHMWPE. This can be attributed to the poor miscibility of the UHMWPE and HDPE, which resulted in a formation of two different phases and voids in U75H25-M1. The processing temperature may have not been sufficient for the UHMWPE to completely melt, resulting in UHMWPE surrounded by HDPE, or a UHMWPE/HDPE blend material. This result is in agreement with a recent research for Khasraghi and Rezaei (2013), where they found two distinct phases of UHMWPE and HDPE in a blend processed using a brabender mixer at 210°C and 60 rpm. Therefore, in this study, the temperature was then increased by 60°C and an anti-oxidant added, to overcome the suspected incomplete melting phases. The new processing parameters and new blend morphology also resulted in an improvement in the nanofiller dispersion using processing method M2.

Further evidence for the poor miscibility of the materials blended using M1 were obtained from the surface features of the stretched samples (see Section 5.7). Large numbers of micro-cracks were formed in the stretched surface of the blend processed using M1. This indicated the formation of microvoids during the incomplete mixing and a lack of interfacial strength between the polymer spherulites. The effects of processing method on the microstructure of the blended materials were seen in fracture surface features, as seen in Section 5.8. Large nodules of polymer were formed in the fractured surface of U75H25-M1 blend, which is similar to that of the fractured surface of HDPE. Crazing and cracks were also formed in the microstructure of the U75H25-M1, which indicated the poor miscibility of the blend. On the other hand, the fractured surface features of the U75H25-M2 blend were similar to that of the UHMWPE, which were in agreement with the mechanical testing results.

The effects of processing method on the nanofiller dispersion were also investigated by means of DSI which provided information about the quality of nanoparticle distribution in the blend matrix (see Section5.5). The variations in the hardness values over an area of 1mm^2 were used to evaluate the effect of processing method on the blend morphology and the nanoparticle distribution. Mixing HDPE with UHMWPE using processing method M1 showed a significant increase in the indentation hardness and variations in the indentation hardness across the sample, which indicated the poor miscibility of the blend. Less variation in the indentation hardness was seen in the blend processed using M2, with indentation hardness values similar to that of the UHMWPE. This indicated a better miscibility of the blend processed using M2. The addition of CB and clay nanoparticles using M1 showed significant increase in the indentation hardness with large variations in the values, while the materials processed using M2 resulted in indentation hardness values similar to the blend material with less variations in the hardness values. At high volume fraction of the nanoparticles, large variations in the indentation hardness values were observed for the three nanoparticle types, which indicated the presence of large aggregations. This could not be observed in the XRD results for the clay exfoliation, which indicated that DSI is a valuable technique to investigate nanoparticle dispersion.

9.3 Nanoparticle Effects

Three different types of nanoparticle (CNT, CB and inorganic nanoclay) were embedded separately in the U75H25 blend to form nanocomposites using two different processing methods (M1 and M2). As discussed in Chapter 6, the addition of a small amount of the nanoparticles (0.5 wt. %) using processing method M1 showed a remarkable change in the stress-strain behaviour. Mechanical properties such as tensile strength and indentation resistance were increased with the incorporation of 0.5 wt. % CB and CNT, however, significant reduction in the creep resistance was observed. In contrast, the presence of a small amount of clay in the blend matrix resulted in a significant reduction in the elongation at break (approximately 75%) and a significant increase in the creep resistance. The addition of a small amount of nanoparticles using processing method M2 resulted in a slight improvement in the tensile behaviour. However, an effect of thermal softening was observed in the strain hardening region. The addition of CB and CNT resulted in a significant increase in the creep resistance of the nanocomposites. These variations in the mechanical properties indicated the dependency of the nanoparticle performance on the miscibility of the base blend. Table 9.1 shows the effect of nanoparticle addition on the mechanical properties of PE based nanocomposites processed using methods M1 and M2.

It is known that plastic work at high strain rates can be transformed partly into heat, which can lead to a significant temperature increase, and consequently affect the mechanical properties. The presence of nanoparticles resulted in a heterogeneous structure of the nanocomposites, which affected the deformation mechanism and increased the internal heat generation due to the additional friction between the nanoparticles and polymer chains. The poor interaction between the non-polar polyethylene and polar nanoparticles increased the possibility of microvoids formation and friction during the chain movement. The correlation between the nanoparticle type and heat generation during plastic deformation revealed that the nanoparticle geometry can significantly affect the internal temperature increase. The addition of CB and CNT nanoparticles generated more heat compared to nanoclay for the materials processed using M2. In addition, temperature increase was dependent on the nanoparticle volume fraction. However, at a high volume fraction of CNT and CB (3 wt. %) a reduction of temperature was observed. This can be attributed to the presence of large aggregations of nanoparticles, which resulted in a reduction in the surface area to volume ratio, and consequently the frictional area. Also, the formation of large CNT and CB networks increased the heat dissipation due to an increase in the thermal conductivity.

The micro-scale properties obtained from DSI technique were found to increase with the addition of nanoparticles, as discussed in Chapter 7. These include indentation hardness, elastic modulus, stiffness and creep resistance for all materials processed using M1 and M2. Generally, increasing the filler content resulted in an increase in the near-surface properties. The presence of nanofillers with high stiffness and surface area to volume ratio in a polymer matrix can lead to high resistance to deformation, which affected the indentation penetration depth.

Table 9.1: Mechanical properties of PE based nanocomposites.

			Micro-Scale Properties			Macro-Scale Properties		
Processing Method	**Material**	**Filler Content (wt. %)**	**H (MPa)**	**E (MPa)**	**Creep Resistance**	**E (MPa)**	**Yield Stress (MPa)**	**Creep Resistance**
	UHMWPE	----	27.6	700	Poor	640	23	Poor
M1	U75H25	----	33.6	979	Significant improvement	615	23.4	Significant improvement
	PE/CB	0.5	40.5	1000	Significant improvement	606	23	Significant reduction
		1	46.6	1051	Dependent on filler content	644	23.5	Dependent on filler content
		3	57	1168		561	23	
	PE/CNT	0.5	34.3	990	Reduced	678	23	Reduced
	PE/clay	0.5	35.8	1170	improved	721	24.5	Significant improvement
M2	U75H25	----	29.3	830	improved	643	23	Improved
	PE/CB	0.5	30	832	Improved	637	27	Significant improvement
		1	38.5	900	Dependent on filler content	540	25	Dependent on filler content
		3	38.4	1032		525	25	
	PE/CNT	0.5	36	883	Improved	619	24	Significant improvement
		1	36	974	Dependent on filler content	700	24	Independent on filler content
		3	37	1055		714	25	
	PE/clay	0.5	29	854	Improved	680	25	Improved
		1	50	1107	Dependent on filler content	680	25	
		2	48	1139		656	25	

9.4 Strain Rate Effects

In the uniaxial tension tests, heterogeneous deformation in the necking region resulted in the localised generation of heat. The necking mechanism in polymers is extremely complicated and the existence of nanofiller reinforcement increases this complexity and increased heat generation was seen with the incorporation of nanofillers. The additional heat can be generated from the friction between the nanoparticles and polymer chains during deformation. The effect of heat generation on polymer properties can be affected by several factors, such as the polymer matrix (glassy or rubbery), miscibility of blends, molecular weight, interfacial strength for filled polymer, filler type or shape and strain rate. Researchers have reported that the presence of nanoparticles in a polymer matrix can increase the heat generation at fracture in glassy polymers, as discussed in Section 2.9.2 (McNally et al. 2003; Shen et al. 2011). However, there is disagreement about the dependence of heat generation on strain rate in polymer nanocomposites. Therefore, questions were raised about the effect of strain rate on the heat generation during plastic deformation of rubbery polymers such as polyethylene-based nanocomposites and to what extent this heat can affect the mechanical properties. In order to investigate the effect of strain rate on internal heat generation during the plastic deformation of polyethylene nanocomposites, a thermal camera (FLIR SC3000) was used to record the spatial and temporal temperature variations during uniaxial tensile testing. The materials were tested at various strain rates from 0.05 to $0.3s^{-1}$ to establish relationship between the heat generation during plastic deformation and strain rate. The heat generation during plastic deformation was strongly dependent on a combination of strain rate, processing method, nanoparticle type and volume fraction. A significant temperature increase, up to 70°C, was obtained for the blend processed using M1 at $0.3s^{-1}$ strain rate compared to 40°C increase for the material processed using M2 at the same strain rate and after 200% strain. This temperature can be increased by 10°C at failure, as shown in Figure 9.1. This figure indicates the significant effect of processing method on heat generation at failure. Similarly, significant temperature increase, up to 85°C, was obtained for the nanocomposites processed using M1 at $0.2s^{-1}$ strain rate and after 200% strain, compared to a 55°C increase for the materials processed using M2. During the plastic deformation, molecules align towards the load direction through a complicated mechanism involving chain and transverse slip, bending, rotation and fragmentation of lamellar stacks in the crystalline phases and interlamellar shear and separation in the amorphous phases (Hiss et al. 1999; Bartczak and Galeski 2010). The presence of a third component such as CNT, CB or nanoclay in the U75H25 heterogeneous matrix can affect these mechanisms by introducing an interfacial area around the nanoparticle with high density and different bonding properties between the nanoparticle and the blend matrix, which can prevent the movement of the polymer chains and causes additional friction. Plastic work at high strain rates can be transformed partly into heat, which led to a significant temperature increase, which then contributed to thermal softening of the material. Therefore, in applications that involve plastic deformation and high strain rate it is important to consider the temperature increase during plastic work.

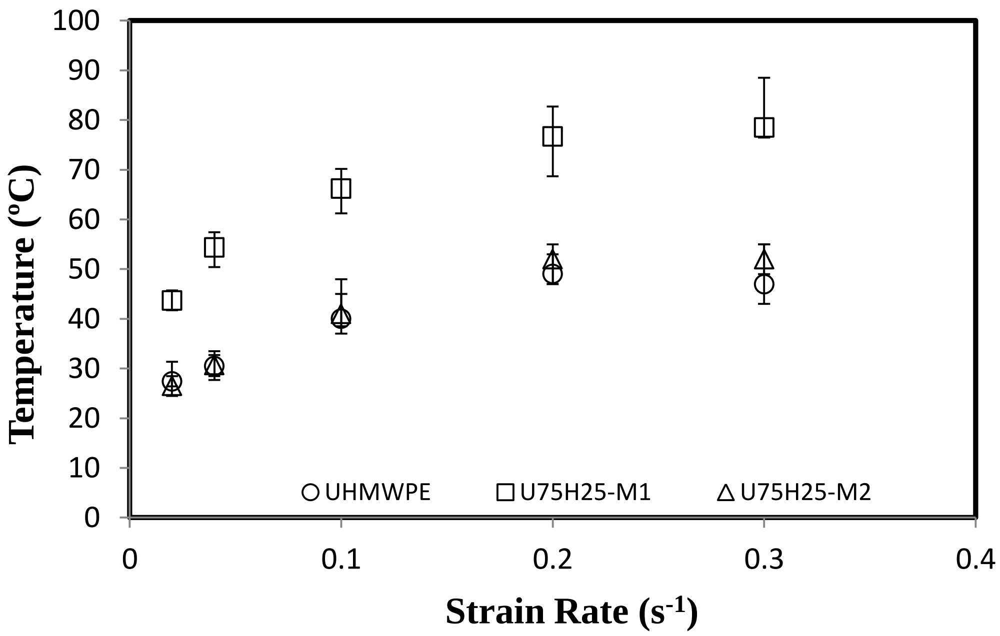

Figure 9.1: Strain rate and processing method effect on the temperature increase during tensile test of U75H25 blends at failure.

9.5 Temperature Effects

The temperature effects discussed in this work can be divided into two parts. First, the effect of the internal temperature increase during plastic deformation. As discussed previously, heat generation during plastic deformation was highly dependent on processing method, strain rate and nanoparticle type and volume fraction. Significant temperature increase was observed during plastic deformation of the U75H25-M1 and its nanocomposites. However, the poor miscibility of the blend and the formation of different phases in the material processed using M1 led to large voids formed between the different phases and in the nanoparticle aggregation regions during material deformation, which affected the internal heat transfer. The complexity in the microstructure of the material manufactured using processing method M1 increased the difficulty of understanding the relation between the strain rate, the nanoparticle volume fraction and the internal heat generation during plastic deformation. Therefore, the materials processed using M1 were not considered for further investigation of the temperature effects. The U75H25 blend processed using M2 showed mechanical properties closer to the UHMWPE and less heat generation was observed at high strain rate. The incorporation of nanoparticle resulted in more heat generation due to the additional friction between the nanoparticles and polyethylene chains. The volume fractions 1 wt. % CB, 0.5 wt. % CNT and 0.5 wt. % clay were considered as transition volume fractions in the temperature-nanofiller and content relation, therefore the effect of nanoparticle type and temperature increase on the stress-strain behaviour was investigated at these specific volume fractions to avoid the effects of aggregations. The addition of CB and CNT resulted in a significant increase in temperature compared to the addition of clay at strain rates over $0.04s^{-1}$, which can be attributed to the high frictional coefficient between nanoparticle and polymer matrix. This temperature increase resulted in a significant effect of a thermal softening in Region 4 of the stress-strain behaviour, which caused a reduction in the toughness and tensile strength (see Section 6.4). Also, a combination of nanoparticles and strain rate can result in a significant temperature increase at failure, as seen in Figure 9.2. Therefore, this temperature effect should be considered carefully when investigating or testing PE based nanocomposites at high strain rates. The critical softening temperature was considered to be around 45°C. The second investigation studied the effect of ambient temperature on the mechanical properties of the M2 nanocomposites (see Section 8.3). The rubbery polyethylene is highly sensitive to ambient temperature due to the low T_g (-120°C) and melting temperature (~134°C). In this study, the materials were tested at the critical softening temperature seen in the high strain rate test at 25°C (45°C) in order to evaluate the mechanical properties in Region 4 during plastic deformation. Also, this temperature is a reasonable high ambient temperature for many polymer applications.

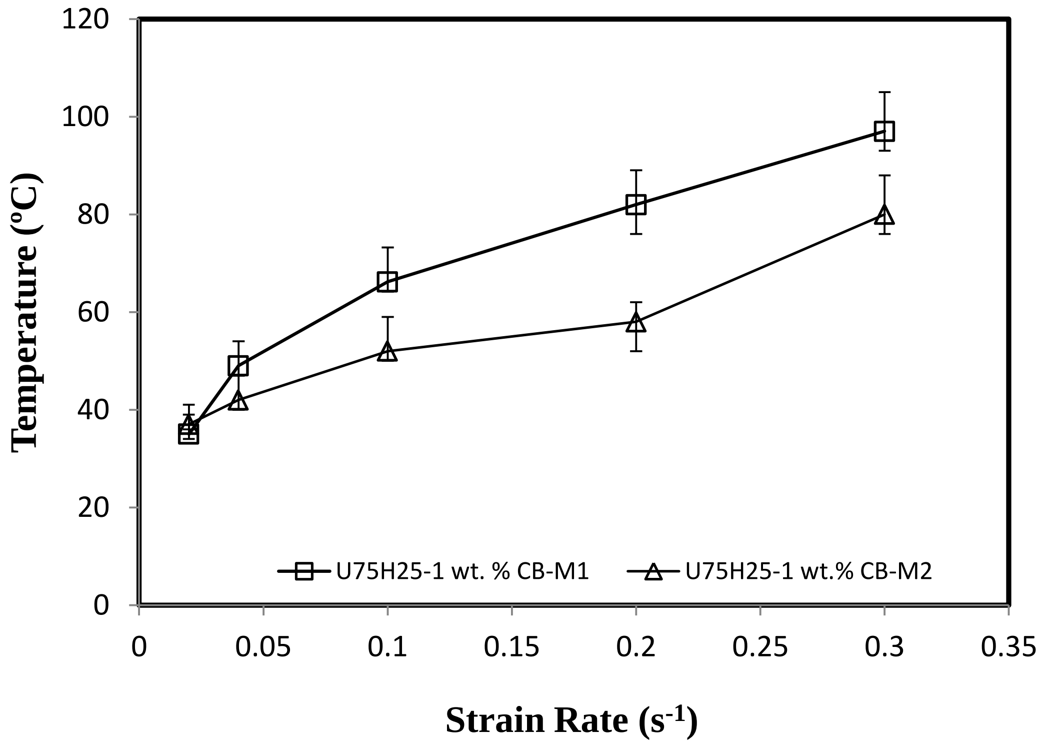

Figure 9.2: Strain rate, processing method and nanoparticle effect on the temperature increase during tensile test of U75H25-1 wt. % CB at failure.

At elevated temperatures, the yield stress and tensile strength increased as strain rate increased and no thermal softening effect was observed for all materials. However, the addition of the CB, clay and 0.5 wt. % CNT nanoparticles resulted in an unexpected reduction in the tensile behaviour at high temperatures, which can be attributed to the weak interaction effects at high temperature. Slight improvement in the blend behaviour was obtained with the addition of a high volume fraction of CNT. The yield stress, elastic modulus and creep resistance were highly affected by temperature increase. Significant reductions of up to 50, 67 and 60% were observed in the yield stress, elastic modulus and creep resistance at high temperature, respectively for the blend material and slight improvements were seen with the incorporation of nanoparticles.

The micro-scale properties were also found to be strongly dependent on the ambient temperature. Increasing the temperature resulted in a significant reduction in the indentation hardness, elastic modulus and creep resistance, by values up to 44, 60 and 24 %, respectively. However, the presence of nanoparticle resulted in improvements in all these properties.

9.6 Summary

The mechanical properties of polyethylene–based nanocomposites are greatly influenced by various factors, including processing method parameters, nanoparticle type and volume fraction, strain rate and ambient temperature. Two processing methods were used and the results indicated that increasing processing temperature led to better miscibility of the blended materials and better dispersion of nanoparticles. This also led to less heat generation during plastic deformation and mechanical properties closer to the UHMWPE. Nanoparticle geometry and volume fraction showed significant effects on the mechanical properties of the materials. The creep resistance and near-surface properties were improved significantly with the incorporation of CNT and CB. The temperature increase during plastic deformation was an important factor that affected the behaviour of the polyethylene-based nanocomposites. Relationships were obtained between heat generation during plastic deformation, strain rate, processing method and nanoparticle addition. Heat generation during plastic deformation can be increased significantly with increasing strain rate and the addition of nanoparticles. Also, the heterogeneous structure of the immiscible material can significantly increase localization of heat generation during plastic deformation. It was found that ambient temperature increase can significantly reduce the mechanical properties of polyethylene-based nanocomposites such as toughness, yield stress, elastic modulus and creep and indentation resistance.

Most of materials presented in the current study can be used in various applications such as:

- Ropes and lines owing to their close properties to UHMWPE and the significant improvement in the creep resistance.
- Nets for fishing, gloves, ice hockey, sail and swimming clothes.

Chapter 10
Conclusions and Future Work

10.1 Introduction

The main aims and objectives of this research have been achieved and the findings were broadly discussed in the previous chapter. The final conclusions of this research and the recommendation for future study are presented in this chapter.

10.2 Conclusions

The main conclusions of this research are as follows:

1. A range of polyethylene-based nanocomposites have been developed to obtain near UHMWPE properties with easier processing and low cost or to enhance material properties such as creep resistance, yield stress, stiffness, elastic modulus, thermal degradation and indentation resistance. Two processing methods M1 and M2 were used to prepare the U75H25 blends and the nanocomposites. The microstructure of polyethylene blends and polyethylene-based nanocomposites was analysed using SEM, TEM, XRD for clay exfoliation and intercalation and DSI. The results showed improvement in the nanoparticle dispersion using processing method M2. In processing method M2, the temperature was increased 60°C compared to M1, which was sufficient to melt the UHMWPE and improve the miscibility of the material and the dispersion of nanoparticles.
2. Using the DSI technique to evaluate the nanoparticle dispersion and processing method resulted in valuable information about the nanoparticle distribution and more understanding of the quality of the blend and its nanocomposites. The results showed that the blend processed using M2 has properties similar to that of the UHMWPE, and less variations in the indentation hardness over the area tested. This indicated an improvement of the blend miscibility compared to that of the blend processed using M1. At high volume fractions of nanoparticles, large aggregations of CB and CNT nanoparticles were

found, which indicated that the maximum volume fraction of nanoparticles is less than 3 wt. %. In addition, large aggregations were found at 2 wt. % clay, which could not be observed using XRD. This indicates that the DSI can provide more information compared to the standard techniques.

3. Crack formation on the surface of stretched samples was used to analyse the effect of processing method on the blend miscibility and the filler-matrix interaction. It was proposed that the blend with fewer cracks formation can be considered as more miscible. Also, the materials with fewer cracks have better filler-matrix interactions. This was in agreement with the fracture surface analysis. The blend processed using method M1 showed the formation of a large number of cracks on both stretched and fractured surfaces, while few cracks were formed in the materials manufactured using processing method M2. The CNT and CB nanoparticles showed good adhesion with the matrix and no cracks was formed on the stretched or fractured surfaces, which indicates good filler-matrix interaction.

4. Properties have been shown to be strongly dependent on the processing method. The processing method can significantly affect the toughness and tensile strength of the material. A significant reduction in these properties was observed for the U75H25 blend processed using M1. This was attributed to the poor miscibility of HDPE and UHMWPE, which resulted in a microstructure with different phases such as pure UHMWPE, pure HDPE and blend.

5. Correlations between the processing method, nanoparticle type and geometry and mechanical properties of polyethylene-based nanocomposites were investigated. It was found that careful selection of the processing method and the nanofillers can lead to significant improvement in the material properties. These include toughness, tensile strength, yield stress, elastic modulus, hardness and creep resistance.

6. The creep resistance of the U75H25 blend manufactured using processing method M2 improved significantly with the addition of CB and CNT nanoparticles. This improvement was dependent on the CB volume fraction and independent of the CNT volume fraction. The addition of clay nanoparticles showed only a slight

increase in the creep resistance compared to CNT and CB. Burger's model was used to analyse the creep behaviour of the materials. The curve fitting was in a good agreement with the experimental data.

7. Processing method, nanoparticle geometry, content of nanofiller and strain rate were found to be critical factors that affected heat generation during plastic deformation, and consequently affected the mechanical behaviour. A significant temperature increase was observed after necking and continued until fracture. The material processed using M1 showed greater heat generation during the plastic deformation compared to the material processed using M2. This was attributed to the improvement in the miscibility of the second blend and the absence of voids and cavitation in the microstructure. The temperature increase during the plastic deformation increased with strain rate and caused considerable thermal softening at high strain rates, which was observed in the strain hardening region. Further temperature increase was observed with the addition of nanoparticles, especially CNT and CB. This temperature increase was attributed to heat generation due to the additional friction between the nanoparticles and polymer chains during plastic deformation. This temperature increase was strongly dependent on the strain rate, processing method and nanoparticle type and volume fraction. Both processing method M2 and the presence of clay nanoparticle in the polymer matrix resulted in a reduction in the heat generation during plastic deformation compared to processing method M1 and the addition of CB and CNT. This was attributed to the improvement in the miscibility of the blend processed using M2, the lower surface area to volume of the clay and the poor clay-matrix interaction, which led to the formation of voids and cracks in the microstructure.

8. The DSI results showed that the addition of HDPE using processing method M1 can increase the indentation hardness, elastic modulus and stiffness of UHMWPE and reduce the permanent deformation. However, the material processed using M2 showed indentation properties much closer to UHMWPE.

9. Indentation hardness and elastic modulus increased significantly with increasing volume fraction of nanofiller. Creep resistance at the micro-scale

improved significantly with the addition of CB and CNTs processed using M2. It was interesting to find similarity between the creep behaviour of the polyethylene-based nanocomposites at both macro and micro scales.

10. According to the TGA, the thermal stability of the U75H25-M2 blend improved with the addition of CB and CNT nanoparticles, whereas no significant effect was observed with the incorporation of the clay nanoparticles.

11. The tensile properties of the PE based nanocomposites were highly dependent on the ambient temperature. A significant reduction was found in the yield stress and elastic modulus as temperature increase. The incorporation of a low volume fraction of nanoparticles resulted in a negative influence on the material toughness at elevated temperature. With increasing volume fraction of the CNT (1 and 3 wt. %), the nanocomposites showed similar stress-strain curves as the U75H25-M2 blend with improvement in the yield stress and elastic modulus.

12. The creep resistance of the polyethylene-based nanocomposites was significantly affected by temperature. The creep strain reduced by 66% when the temperature increased from 25 to 65°C. The U75H25-M2 blend showed better creep resistance than the UHMWPE at all testing temperatures. The addition of the nanoparticles resulted in a positive effect on the creep resistance; the presence of the nanoparticles obstructed the polymer chain movement, which increased the creep resistance at all testing temperatures.

13. At the micro - scale, the near surface properties were evaluated at various temperatures using the DSI. Similar to the bulk tests, increasing the temperature led to significant reduction in the material properties such as stiffness, hardness, elastic modulus and creep resistance. The high temperature caused material softening, which led to an increase in the penetration depth and consequently affected the hardness. However, the presence of the nanoparticles resulted in an improvement in the hardness and creep resistance at all testing temperatures. The elastic modulus was significantly affected by the temperature increase with up to 60% reduction at elevated temperature.

10.3 Future Work

For further investigations on the work described in this thesis, it would be beneficial to:

- Process an expanded range of blended materials using processing method M2. For example, 80:20, 70:30 and 60:40 wt. % of UHMWPE and HDPE, respectively. The mechanical properties of the blends may introduce further evidence of the capability of this processing method to produce miscible blends. The addition of various nanoparticles on these blends may show a relationship between the blend composition, the nanofiller type and content and the mechanical properties.
- Investigate the effect of various blend compositions on the heat generation during plastic deformation. A correlation may be obtained between blends, nanofiller content and internal temperature increase.
- Investigate the effect of the addition of another 2D nanoparticle such as Graphene sheet on the heat generation during plastic deformation of U75H25 blend and the mechanical properties. Compare that with the results of the U75H25/clay nanocomposites presented in this thesis may distinguish between the effect of the physical and chemical properties effects.
- Investigate the effect of nanoparticle addition on the internal temperature increase during dynamic tests.
- Investigate the effect of interface enhancement on the heat generation during plastic deformation. Non-polar polymers such as polyethylene are difficult matrix materials to obtain ideal filler-matrix interactions. The formation of a crystalline layer around CNTs by thermal treatment and the formation of a chemical interface between CB and polyethylene may improve the interaction, and reduce the heat generation during plastic deformation, and consequently affect the material properties.
- Investigate the mechanical properties of fibres of the polyethylene-based nanocomposites presented in the current study.

References

Abadi, M.B.; Ghasemi, I.; Khavandi, A.; Shokrgozar, M.A.; Farokhi, M.; Homaeigohar, S.S. & Eslamifar, A. (2010) "Synthesis of nano b-TCP and the effects on the mechanical and biological properties of b-TCP/HDPE/UHMWPE nanocomposites", *polymer composites*, Vol.31, pp. 1745-1753.

Abetkovskaiaa, S.O.; Chizhika, S.A.; Rudnitskyb, V.A. and Krenb, A.P. (2010) "Evaluation of viscoelastic properties of materials by nanoindentation", *Journal of Friction and Wear*, Vol.31, pp. 180–183.

Advani, S. (2007) "Processing and properties of nanocomposites", USA: World Scientific Publishing Co. Pte. Ltd..

Ajayan, P.M.; Schadler, L.S.; Braaun, P.V. (2003), "Nanocomposite science and technology", Germany: Wiley-VCH.

Akovali, G. (2001) "Handbook of composite fabrication", Exeter: Rapra Technology Ltd.

Alamo, R. G. Graessley, W. W. ; Krishnamoorti, R. ; Lohse, D. J. ; Londono, J. D. ; Mandelkern, L. ; Stehling, F. C. & Wignall, G. D. (1997) "Small angle neutron scattering investigations of melt miscibility and phase segregation in blends of linear and branched polyethylenes as a function of the branch content", *Macromolecules*, Vol.30, 561-566.

Aldousiri, B., Dhakal, H.N., Onuh, S., Zhang, Z.Y. & Bennett, N. (2011) "Nanoindentation behaviour of layered silicate filled spent polyamide-12 nanocomposites", *Polymer Testing*, Vol.30, pp. 688-692.

Alexandre, M. and Dubois, P. (2000) "Polymer-layered silicate nanocomposites: preparation, properties", *Materials Science and Engineering*, 28:15, pp. 1-63.

Alexandre, M.; Dubois, P.; Sun, T.; Garces, J.M. & Jérôme, R. (2002) "Polyethylene layered silicate prepared by polymerisation-filling techniques: synthesis and mechanical properties", *Polymer*, Vol.43, pp. 2123-2132.

Alkorta, J., Martinez-esnaola, J.M. & Gil Sevillano, J. (2008) "Critical examination of strain-rate sensitivity measurement by nanoindentation methods: Application to severely deformed niobium", *Acta Materialia*, Vol.56, pp. 884-893.

Allcock H.; Lampe, F. and Mark, J. (2003) "Contemporary polymer chemistry", 3^{ed}, pp.546.

Altaf, K.; Ashcroft, Ian A. & Hague, R. (2012) "Modelling the effect of moisture on the depth sensing indentation response of a stereolithography polymer", *Computational Materials Science*, Vol.52, p.112-118.

Anderson, J. (1982) "High density and ultra-high molecular weight polyethylenes: their wear properties and bearing applications", *Tribol Int.*, Vol.15, pp. 43-47.

Baker, D. A.; Hasting, R. S. & Pruitt, L. (2000) “Compression and tension fatigue resistance of medical grade ultra high molecular weight polyethylene: the effect of morphology, sterilization, aging and temperature”, *Polymer*, Vol.41, pp. 795-808.

Balazs, A. C.; Emrick, T. & Russell, T. P. (2006) “Nanoparticle polymer composites: Where two small worlds meet”, *Science*, Vol.314, pp.1107–1110.

Bartczak, Z. & Galeski, A. (2010) “Plasticity of semicrystalline polymers”, *Macromol. Symp*, Vol.294-I, pp. 67–90.

Bartczak, Z.; Argon, A.S. & Cohen, R.E. (1992) “Deformation mechanisms and plastic resistance in single-crystal-textured high-density polyethylene”, *Macromolecules*, Vol.25, pp. 5036–5053.

Beake, B. D.; Zheng, S. & Alexander, M. R. (2002) “Nanoindentation testing of plasma-polymerised hexane films”, *J.Mater.Sci.*, Vol.37, pp. 3821-3826.

Beake, B.D.; Chen, S.; Hull, J.B. and Gao, F. (2002) “Nanoindentation behaviour of clay/poly(ethylene oxide) nanocomposites”, *J. Nanosci. Nanotechnol.*, Vol.7, pp. 73–79.

Bin, Y.Z.; Ma, L.; Adachi, R.; Kurosu, H. & Matsuo, M. (2001) “Ultra drawing of low molecular weight polyethylene- ultra high molecular weight polyethylene blend films prepared by gelation/ crystallization from semi dilute solution”, *Polymer*, Vol.42, pp. 8125-8135.

Bogue, R. (2011) “Nanocomposites: a review of technology and applications”, *Assembly Automation*, Vol.31, pp. 106-112.

Briscoe, B.J.; Fiori, L. & Pelillo, E. (1998) “Nano-indentation of polymeric surfaces”, *J. Phys. D, Appl. Phys*. Vol.31, pp. 2394-2405.

Brough, I.; Haward, R.; Healey, G. & Wood, A. (2004) “Scanning electron micrographs of high density polyethylene fracture surfaces”, *Polymer*, Vol.45, pp. 3115–3123.

Cabot corporation, USA, 2007, http://www.cabot-corp.com.

Cai, G.; Yuan, A.; Zhang, L.; You, X.; Ting X. & Sheng, G. (2004) “Nanomechanic Properties of polymer-based nanocomposites with nanosilica by nanoindentation”, *Journal of reinforced plastics and composites*, Vol.23, pp. 1365-1372.

Cao, S.; Wang, X. & Wu, Z. (2011) “Evaluation and prediction of temperature dependent tensile strength of unidirectional carbon fiber-reinforced polymer composites”, *Journal of Reinforced Plastics and Composites*, Vol.30, pp.779-807.

Chang, T.E. ; Jensen, L.R. ; Kisliuk, A. ; Pipes, R.B. ; Pyrz, R. & Sokolov, A.P. (2005) “Microscopic mechanism of reinforcement in single-wall carbon nanotube/polypropylene nanocomposite”, *Polymer*, Vol.46, pp.439.

Chen, J.; Yang, W.; Yu, G.P.; Wang, M.; Ni, H.Y. & Shen, K.Z. (2008) “Continuous extrusion and tensile strength of self-reinforced HDPE/UHMWPE sheet”, *J. Mater Process Technol*, Vol.202, pp. 165–169.

Chen, Y.; Zou, H.; Liang, M. & Liu, P. (2013) “Rheological, thermal, and morphological properties of low-density polyethylene/ultra-high-molecular-weight polyethylene and linear low-density polyethylene/ultra-high-molecular-weight polyethylene blends”, *J. Appl. Polym. Sci.*, Vol.29, pp. 945-953.

Chen,Y.; Qi, Y.; Tai, Z.; Yan, X.; Zhu, F. & Xue, Q. (2012) “Preparation, mechanical properties and biocompatibility of graphene oxide/ultrahigh molecular weight polyethylene composites”, *European Polymer Journal*, Vol.48, pp. 1026-1033.

Cheng, L.; Xia, X.; Scriven, L.E. and Gerberich,W.W. (2005) “Spherical-tip indentation of viscoelastic material”, *Mechanics of Materials*, Vol.37, pp.213–226.

Cheng, Y. T. & Cheng, C. M. (2004) “Scaling, dimensional analysis, and indentation measurements”, *Materials Science and Engineering R*, Vol.44, pp. 91–149.

Cheng, Y.T. & Chen, C.M. (2005) “Relationships between initial unloading slope, contact depth, and mechanical properties for conical indentation in linear viscoelastic solids”, *Journal of Materials Research*, Vol.20, pp. 1046-1053.

Cheng, Y.T.; Ni, W.Y. & Cheng, C.M. (2005) “Determining the instantaneous modulus of viscoelastic solid using instrumented indentation measurement”, *J. Mater. Res.,* Vol.20, pp. 3061-3071.

Cho, J. & Daniel, I. (2008) “Reinforcement of carbon/epoxy composites with multi-wall carbon nanotubes and dispersion enhancing block copolymers”, *Scripta Materialia*, Vol.58, pp.533–536.

Chudoba, T. & Richter, F. (2001) “Investigation of creep behaviour under load during indentation experiments and its influence on hardness and modulus results”, *Surface and Coatings Technology*, Vol.148, pp. 191–198.

Cotten, G.R. & Boonstra, B.B. (1967) *Rubber Chem. Tech.*, Vol.40, pp.829.

Crosby, A.J. & Lee, J-Y. (2007) “Polymer Nanocomposites: The “Nano” Effect on Mechanical Properties”, *Polymer Reviews*, Vol.47, pp.217–229.

Dai, Z.; Gao, Y.; Liu, L.; Pötschke, P.; Yang, J. & Zhang, Z. (2013) “Creep-resistant behavior of MWCNT-polycarbonate melt spun nanocomposite fibers at elevated temperature”, *Polymer*, pp.1-7.

David, N.V.; Gao, X.L. & Zheng, J.Q. (2011) “Stress relaxation of Twaron/Natural Rubber composite”, *Journal of Engineering Materials and Technology*, Vol.133.

Deng, M.; Latour, R.A.; Drews, M.J. & Shalaby, S.W. (1996) “Effects of gamma irradiation, irradiation environment, and postirradiation aging on thermal and tensile properties of ultrahigh molecular weight polyethylene fibers”, *J. Appl. Polym. Sci.*, Vol.61, pp. 2075.

Deshmane, C.; Yuan, Q,; Perkins, R. & Misra R. (2007) “On striking variation in impact toughness of polyethylene–clay and polypropylene–clay nanocomposite systems: The effect of clay–polymer interaction”, *Mater. Sci. Eng. A*, Vol.458, pp.150–157.

Dhakal, H.N.; Zhang, Z.Y. & Richardson, M.O.W (2006) "Nanoindentation behaviour of layered silicate reinforced unsaturated polyester nanocomposites", *Polymer Testing*, Vol.25, pp. 846–852.

Doerner, M. F. & Nix, W. D. (1986) "A method for interpreting the data from depth-sensing indentation instruments", *J. Mater. Res.*, Vol.1, pp. 601-609.

Donnet, J.B. & Voet, A. (1976) "Carbon Black: physics, chemistry and elastomer reinforcement", New York : Marcel Dekker, INC.

Dresselhaus, MS.; Dresselhaus, G. & Eklund, PC. (1996) "Science of fullerenes and carbon nanotubes", New York: Academic Press.

Dub, S. N. & Trunov, M. L. (2008) "Determination of viscoelastic material parameters by step-loading nanoindentation", *J. Phys. D: Appl. Phys.*, Vol.41, 074024.

Durmus, A.; Kasgöz, A. & Macosko, C.W. (2008) "Mechanical Properties of Linear Low-density Polyethylene (LLDPE)/clay Nanocomposites: Estimation of Aspect Ratio and Interfacial Strength by Composite Models", *J. Macromol. Sci. Part B Phys.*, Vol.47, pp.608–619.

Durmus, A.; Kasgoz, A. & Macosko, C.W. (2007) "Linear low density polyethylene (LLDPE)/clay nanocomposites. Part I: Structural characterization and quantifying clay dispersion by melt rheology", *Polymer*, Vol.48, pp. 4492-4502.

Dusunceli, N. & Colak, O.U. (2008) "Modelling effects of degree of crystallinity on mechanical behaviour of semicrystalline polymers", *International Journal of Plasticity*, Vol.24, pp. 1224-1242.

Ehrenstein, G. (2001) "Polymeric Materials", Munich : Carl Hanser Verlag.

Elementis Specialties, USA, 2010, http://www.elementis-specialties.com.

Esfandiari, A. & Nazokdast, H. (2008) "Review of polymer-organoclay nanocomposites", *Journal of Applied Science*, Vol.8, pp. 545-561.

ExxonMobil Chem. Europe, Belgium, 2010, http://www.exxonmobilchemical.com.

Findley, W. N.; Lai, J. S. & Onaran, K. (1989) "Creep and relaxation of nonlinear viscoelastic materials: with an introduction to linear viscoelasticity". New York: Dover Publications, Inc.

Fischer-Cripps, A.C. (2004) "A simple phenomenological approach to nanoindentation creep", *Materials Science and Engineering A*, Vol.385, pp. 74–82.

Fischer-Cripps, A.C. (2006) "Critical review of analysis and interpretation of nanoindentation test data", *Surface & Coatings Technology*, Vol.200, pp. 4153 – 4165.

Fischer-Cripps, A.C. (2011) Nanoindentation, 3rd edition, New York: Springer.

Fouad, H. & Elleithy, R. (2011) "High density polyethylene/graphite nano-composites for total hip joint replacements: Processing and in vitro characterization", *J. Mech. Behav. Biomed. Mater.,* Vol.4, pp.1376-1383.

Friedrich, K.; Fakirov, S. & Zhang, Z. (2005) “Polymer composite from nano-to macro-scale”, USA: Springer Science + Business Media Inc.

Fujisawa, N. & Swain, M.V. (2008) “Nanoindentation-derived elastic modulus of an amorphous polymer and its sensitivity to load-hold period and unloading strain rate”, *J. Mater. Res.*, Vol.23, pp. 637-641.

Fulcher, J.T.; Lu, Y.; Tandon, G.P. & Foster, D.C. (2010) “Thermomechanical characterization of shape memory polymers using high temperature nanoindentation”, *Polymer Testing*, Vol.29, pp. 544-552.

Galetz, M.C.; T. Bla, T.; Ruckdäschel, H.; Sandler, J. K. W.; Altstädt, V. & Glatzel, U. (2007) “Carbon nanofibre-reinforced ultrahigh molecular weight polyethylene for tribological applications”, *J. Appl. Polym. Sci.*, Vol.104, pp. 4173.

Gellert, E.P.; Pattie, S.D. & Woodward, R.L. (1998) “Energy transfer in ballistic perforation of fibre reinforced composites”, *J. Mater. Sci.*, Vol.33, pp. 1845.

Goodall, R.C. & Clyne, T.W. (2006) “A critical appraisal of the extraction of creep parameters from nanoindentation data obtained at room temperature”, *Acta Materialia*, Vol.54, pp. 5489-5500.

Guermazi, N.; Elleuch, K.; Ayedi, H.; Fridrici, V. & Kapsa, P. (2009), *Mater Des.*, Vol.30, pp. 3094

Haghighatpanah, S. & Bolton, K. (2013) “Molecular-level computational studies of single wall carbon nanotube-polyethylene composites”, *Computational Materials Science*, Vol.69, pp. 443-454.

Hameed T. & Hussein, I.A. (2002) “Rheological study of the influence of Mw and comonomer type on the miscibility of m-LLDPE and LDPE blends”, *Polymer*, Vol.43, pp. 6911-6929.

Hameed, T. & Hussein, V. (2004) “Effect of short chain branching of LDPE on its miscibility with linear HDPE”, *Macromol. Mater. Eng.*, Vol.289, pp. 198-203.

Harris, PJF. (1999) “Carbon nanotubes and related structures: new materials for the twenty-first century”. Cambridge: Cambridge University Press, pp. 279

Hasan, O.A. & Boyce, M.C. (1995) “A constitutive model for the nonlinear viscoelastic viscoplastic behavior of glassy polymers”, *Polymer Engineering and Science*, Vol.35, pp. 331-344.

Havelin, L.I. ; Fenstad, A. M. ; Salomonsson, R. ; Mehnert, F. ; Furnes, O. ; Overgaard, S. ; Pedersen, A.B. ; Herberts, P. ; Kärrholm, J. & Garellick, G. (2009) “The Nordic arthroplasty register association: A unique collaboration between 3 national hip arthroplasty registries with 280,201 THRs”, Acta Orthopaedica, Vol.80, pp.393-401.

Hill, M. J.; Barham, P. J. & Keller, A. (1992) “Phase segregation in blends of linear with branched polyethylene: The effect of varying the molecular weight of the linear polymer”, *Polymer*, Vol.33, pp. 2530-2541.

Hill, M. J.; Barham, P. J. & Ruiten, J.V. (1993) “Liquid-liquid phase segregation in blends of a linear polyethylene with a series of octene copolymers of differing branch content”, *Polymer*, Vol.34, pp. 2975-2980.

Hill, M.J.; Morgan, R.L. & Barham, P.J. (1997) “Minimum branch content for detection of liquid-liquid phase separation, using indirect techniques, in blends of polyethylene with ethylene-octene and ethylene-butene copolymers”, *Polymer*, Vol.38, pp. 3003-3009.

Hillmansen, S. ; Hobeika, S. ; Haward, R. N. & Leevers, P. S. (2000) “The effect of strain rate, temperature, and molecular mass on the tensile deformation of polyethylene”, *Polymer Engineering and Science*, Vol.40, p.481.

Hiss, R.; Hobeika, S.; Lynn, C. & Strobl, G. (1999) “Network stretching, slip processes, and fragmentation of crystallites during uniaxial drawing of polyethylene and related copolymers. A comparative study”, *Macromolecules*, Vol.32, pp. 4390-4403.

Ho, S. P.; Riester, L.; Drews, M.; Boland, T. & Laberge, M. (2003) “Nanoindentation properties of compression-moulded ultra-high molecular weight polyethylene”, *Proc. Instn Mech. Engrs. Part H: J. Engineering in Medicine*, Vol.217, pp.357-366.

Hodzic, A.; Stachurski, Z. H. & Kim, J. K. (2000) “Nano-indentation of polymer-glass interfaces: Part I. Experimental and mechanical analysis”, *Polymer*, Vol.41, pp. 6895-6905.

Hongbing, L.; Huang, G.; Wang, B.; Mamedov, A. & Gupta, S. (2006) “Characterization of the linear viscoelastic behavior of single-wall carbon nanotube/polyelectrolyte multilayer nanocomposite film using nanoindentation”, *Thin Solid Films*, Vol.500, pp. 197 – 202.

Huang, C.C.; Wei, M.K. & Sanboh Lee (2011) “Transient and steady-state nanoindentation creep of polymeric materials”, *International Journal of Plasticity*, Vol.27, pp.1093-1102

Huang, J.C. (2002) “Carbon black filled conducting polymers and polymer blends”, *Advance in polymer Technology*, Vol.21, pp. 299-313.

Humbert, S.; Lame, O. & Vigier, G. (2009) “Polyethylene yielding behaviour: What is behind the correlation between yield stress and crystallinity?”, *Polymer*, Vol.50, pp.3755-3761.

Hussain, F.; Hojjati, m.; Okamoto, M. & Gorga, R.E. (2006) “Review article: Polymer-matrix Nanocomposites, Processing, Manufacturing, and Application: An Overview”, *Journal of Composite Materials*, Vol.40, pp. 1511-1575.

Hussein, I.A. (2003) “Influence of composition distribution and branch content on the miscibility of m-LLDPE and HDPE blends: rheological investigation”, *Macromolecules*, Vol.36, pp. 2024-2031.

Hussein, I.A. & Williams, M.C. (2004) “Rheological study of the influence of branch content on the miscibility of octene m-LLDPE and ZN-LLDPE in LDPE”, *Polymer Eng. Sci.*, Vol.44, pp. 660-672.

Hussain, F.; Hojjati, M.; Okamoto, M. & Gorga, R.E. (2006) " Review article: Polymer-matrix nanocomposites, processing, manufacturing, and application: An overview", *Journal of Composite Materials*, Vol.40, pp. 1511-1575.

Iijima, S. (1991) "Helical microtubules of graphitic carbon", *Nature*, Vol.354, pp.56.

Jain, S.K. & Nanda, A. (2010) "A constitutive model for creep rupture", *Mechanics of Advanced Materials and Structures*, Vol.17, pp. 459–466.

Jia, Y.; Peng, K.; Gong, X-L. & Zhang, Z. (2011) "Creep and recovery of polypropylene/carbon nanotube composites", *International Journal of Plasticity*, Vol.27, pp.1239–1251.

Jordan, J.; Jacob, K I.; Tannenbaum, R.; Sharaf, M.A. & Jasiuk, I. (2005) "Experimental trends in polymer nanocomposites-a review", *Materials Science and Engineering A*, Vol.393, pp. 1-11.

Jouni, M.; Boiteux, G. & Massardier, V. (2013) "New melt mixing polyethylene multiwalled carbon nanotube nanocomposites with very low electrical percolation threshold", *Polymer Adv. Technol.*, Vol.24, pp. 909–915.

Kanagaraj, S.; Varanda, F.R.; Zhiltsova, T.V.; Oliveira, M.S.A. & Simoes, J.A.O (2007) "Mechanical properties of high density polyethylene/carbon nanotube composites", *Compos. Sci. Technol.*, Vol.67, pp. 3071–3077.

Kelly, J.M. (2002) "Ultra-high molecular weight polyethylene", *Journal of Macromolecular Science, Part C: Polymer Reviews*, Vol.42, pp.355-371.

Khare, A.R.; Westphal, S.P.; Ling, M.T.K.; Qin, C. & Woo, L. (2000) "Thermal and dynamic mechanical analysis on metallocene ULDPE/PP blends to optimize impact properties", *Thermochemica Acta*, Vol.357–358, pp. 155–160.

Khasraghi, S.S. & Rezaei, M. (2013) "preparation and characterisation of UHMWPE/HDPE/MWCNT melt-blended nanocomposites", *Journal of Thermoplastic Composites Materials*, pp. 1-22.

Kim, J.Y. & Kim, S.H. (2012) "High performance PET/carbon nanotube nanocomposites: preparation, characterization, properties and applications", *Nanocomposites - New Trends and Developments*, Ebrahimi, F. (Ed.), ISBN: 978-953-51-0762-0, In Tech, DOI: 10.5772/50413.

Koenen, J.A. (1992) "Observation of the heat exchange during deformation using an infra-red camera", *Polymer*, Vol.33, pp. 4732-4736.

Kontou, E. & Niaounakis (2006) "Thermo-mechanical properties of LLDPE/SiO 2 nanocomposites", *Polymer*, Vol.47, pp. 1267-1280.

Kraus, G. (1970) "Thermal expansion, free volume, and molecular mobility in a carbon black-filled elastomer", *J. of polymer Science*, A2, Vol.8, pp. 571.

Kuriyagawa, M. & Nitta, K. (2011) "Structural explanation on natural draw ratio of metallocene-catalyzed high density polyethylene", *Polymer*, Vol.52, pp. 3469-3477.

Kurtz, S. M. (2004) “The UHMWPE Handbook: ultra high molecular weight polyethylene in total joint replacement”, London: Elsevier Academic press.

Laine, R.M.; Choi, J. & Lee, I. (2001) “Organic-inorganic nanocomposites with completely defined interfacial interactions”, Adv. Mater. , Vol.13, pp. 800-803.

Lau, K.T. (2003) “Interfacial bonding characteristics of nanotube/polymer composites”, *Chemical Physics Letters*, Vol.370, pp. 399–405.

Lau, K.T.; Shi, S.Q. & Cheng, H.M. (2003) “Micro-mechanical properties and morphological observation on fracture surfaces of carbon nanotube composites pre-treated at different temperatures”, *Composites Science and Technology*, Vol.63, pp. 1161–1164

Leblance, J. (2010) “Filled Polymers : Science and Industrial Application”, USA: Taylor and Francis Group, LLC.

Lee, L.; Changchum, C.; Han, X.; Jiong, S. & Guojun, X. (2005) *Polymer Nano Composite Foams*, Vol.65, pp. 2344-2363.

Lewis, D.; Whiller, E.J.; Maddams, W.F. & Preedy, J.E. (1972) “Comparison of twinning produced by rolling and annealing in high- and low-density polyethylene”, *Journal of Polymer Science Part A-2: Polymer Physics*, Vol.10, pp. 369–373.

Li, H. & Ngan, A.H.W. (2004) “Size effects of nanoindentation creep”, *Journal of Materials Research*, Vol.19, pp. 513-522.

Li, Y.; Liu, Y.; Peng, X.; Yan, C.; Liu, S. & Hu, N. (2011) “Pull-out simulations on interfacial properties of carbon nanotube-reinforced polymer nanocomposites”, *Computational Materials Science*, Vol.50, pp. 1854–1860.

Li, Y.; Martin Kröger, M. & Liu, W.K. (2012) “Nanoparticle Geometrical Effect on Structure, Dynamics and Anisotropic Viscosity of Polyethylene Nanocomposites”, *Macromolecules*, Vol.45, pp. 2099−2112.

Liang, J.Z. & Yang, Q.Q. (2009) “Mechanical Properties of Carbon Black-Filled High-Density Polyethylene Antistatic Composites”, *Journal of reinforced plastic and composite*, Vol.28, pp. 295-304.

Liang, S.; Wang, K.; Chen, D.; Zhang, Q.; Du, R. & Fu, Q. (2008) “Shear enhanced interfacial interaction between carbon nanotubes and polyethylene and formation of nanohybrid shish–kebabs”, *Polymer*, Vol.49, pp. 4925–4929.

Lim, K.L.K.; Mohd Ishak, Z.A.; Ishiaku, U.S.; Fuad, A.M.Y.; Yusof, A.H.; Czigany, T.; Pukanszky, B. & Ogunniyi, D.S. (2005) “High-density polyethylene/ultrahigh-molecular-weight polyethylene blend. I. The processing, thermal, and mechanical properties”, *J. Appl. Polym. Sci.*, Vol.97, pp. 413-425.

Longère, P. & Dragon, A. (2008) “Plastic work induced heating evaluation under dynamic conditions: critical assessment”, *Mechanics Research Communication*, Vol.35, pp. 135-141.

Lordi, V. & Yao, N. (2000) “Molecular mechanics of binding in carbon-nanotube-polymer composite”, *Journal of Materials Research*, Vol.15, pp. 2770-2779.

Lu, Y.C.; Jones, D.C.; Tandon, G.P.; Putthanarat, S. & Schoeppner, G.A. (2010) “High temperature nanoindentation of PMR-15 polyimide”, *Experimental Mechanics*, Vol.50, pp. 491–499.

Lu, Y.C.; Tandon, G.P. ; Jones, D.C. & Schoeppner, G.A. (2009) “Elastic and viscoelastic characterization of thermally-oxidized polymer resin using nanoindentation”, *Mech Time-Depend Mater*, Vol.13, PP. 245–260.

Lucas, A. A. ; Ambrósio, J. D. ; Otaguro, H. ; Costa, L. C. & Agnelli, J.A.M., (2011) “Abrasive wear of HDPE/UHMWPE blends”, *Wear*, Vol.270, pp.576-583.

Lucas, B. N. and Oliver, W. C. (1999) “Indentation power-law creep of high-purity indium”, *Metallurgical and Materials Transactions A*, Vol.30, pp. 601-610.

Mahieux, C.A. & Reifsnider, K.L. (2001) “Property modeling across transition temperatures in polymers: A robust stiffness - Temperature model”, *Polymer*, Vol.42, pp. 3281-3291.

Malpass, D.B. (2010) “Introduction to industrial polyethylene: properties, catalysts and processes”, Canada: Scrivener publishing LLC.

Mamunya, Y. (2001) “Polymer Blends Filled with Carbon Black: Structure and Electrical Properties”, *Macromolecular Symposia*, Vol.170, pp. 257–264.

Mason, J.J.; Rosakis, A.J. & Ravichandran, G. (1994) “On the strain and strain rate dependence of the fraction of plastic work converted to heat: an experimental study using high speed infrared detectors and the Kolsky bar”, *Mechanics of Materials*, Vol.17, pp. 135-145.

Mayes, A. M. (2005) “Nanocomposites-softer at the boundary”, *Nature Materials*, Vol.4, pp.651–652.

Mayo, M.J. & Nix, W.D. (1988) “A micro-indentation study of superplasticity in Pb, Sn, and Sn-38 wt% Pb”, *Acta Metallurgica*, Vol.36, pp. 2183-2192.

McNally, T.; Murphy, T.W.; Lew, C.Y.; Turner, R.J. & Brennan, G.P. (2003) “Polyamide-12 layered silicate nanocomposites by melt blending”, *Polymer*, Vol.44, pp. 2761–2772

McNally, T.; Potschke, P.; Halley, P.; Murphy, M.; Martin, D.; Bell, Steven; Brennan, Gerard; Bein, D.; Lemoine, P. & Quinn, J.P. (2005) “Polyethylene multiwalled carbon nanotube composites”, *Polymer*, Vol.46, pp. 8222–8232.

Mencik, J. & Swain, M.V. (1995) “Errors associated with depth-sensing microindentation tests”, *Journal of Materials Research*, Vol.10, pp. 1491-1501.

Menčík, J.; He, L.H. & Němeček, J. (2011) “Characterization of viscoelastic-plastic properties of solid polymers by instrumented indentation”, *Polymer Testing*, Vol.30, pp. 101–109.

Merah, N.; Saghir, F.; Khan, Z. & Bazoune, A. (2006) “Effect of temperature on tensile properties of HDPE pipe material”, *Plastics, Rubber and Composites*, Vol.35, pp. 226-230.

Mittal, V. (2012) “Characterization techniques for polymer nanocomposites”, USA: Wiley-VCH.

Morgan, R.L.; Hill, M.J. & Barham, P.J. (1999) “Morphology, melting behaviour and co-crystallization in polyethylene blends: the effect of cooling rate on two homogeneously mixed blends”, *Polymer*, Vol.40, pp. 337-348.

Nanocyl, Belgium, (2009), http://www.nanocyl.com.

Ngan, A.H.W. & Tang, B. (2002) “Viscoelastic effects during unloading in depth-sensing indentation”, *Journal of Materials Research*, Vol.17, pp. 2604-2610.

Nwabunma, D. & Kyu, T. (2008) “Polyolefin blends”, USA: John Wiley & Sons, Inc.

Oleinik, E. (2003) “Plasticity of semicrystalline flexible-chain polymers at the microscopic and mesoscopic levels”, *Polymer Science Series C*, Vol.45, pp. 17- 117.

Oleinik, E. ; Salamatina, O. ; Rudnev, S. ; Bartczak, Z. ; Galeski, A. & Galeski, A. (2012) “Plasticity of semicrystalline polyethylenes viewed through the prism of thermodynamics”, *Journal of Applied Polymer Science*, Vol.125, pp.4169-4176.

Olesiak, S.E., Oyen, M.L. & Ferguson, V.L. (2010) “Viscous-elastic-plastic behavior of bone using Berkovich nanoindentation”, *Mechanics of Time-Dependent Materials*, Vol.14, pp. 111-124.

Oliver, W. C. & Pharr, G. M. (1992) “An improved technique for determining hardness and elastic modulus using load and displacement sensing indentation experiments”, *J.Mater.Res*, Vol.7, pp. 1564-1583.

Oliver, W. C. & Pharr, G. M. (2004) “Measurement of hardness and elastic modulus by instrumented indentation: Advances in understanding and refinements to methodology”, *J. Mater. Res.*, Vol.19, pp.3-20.

Parasnis, N. C. & Ramani, K. (1998) “Analysis of the effect of pressure on compression moulding of UHMWPE”, *Journal of Materials Science: Materials in Medicine*, Vol.9, pp. 165-172.

Paul, D.R. & Robeson L.M. (2008) “Polymer nanotechnology: nanocomposites”, *Polymer*, Vol.49, pp. 3187-3204.

Pawlak, A. & Galeski, A. (2013) “Cavitation during tensile drawing of annealed high density polyethylene”, *Polymer*, Vol.51, pp. 5771-5779.

Payne, A.R. (1965) “in reinforcement of elastomers”, New York : Interscience, pp.69.

Peacock, A.J. (2000) “Handbook of polyethylene: structure, properties and application”, USA: Marcel Dekker, Inc.

Peng-Cheng, M.; Siddiqui, N.A.; Marom, G. & Jang-Kyo Kim (2010) “Dispersion and functionalization of carbon nanotubes for polymer-based nanocomposites: A review”, *Composites: Part A*, Vol.41, pp.1345–1367.

Peric, D. & Dettmer, W. (2003) “A computational model for generalized inelastic materials at finite strains combining elastic, viscoelastic and plastic material behaviour”, *Eng. Comput.*, Vol.20, pp. 768.

Pharr, G.M. (1998) "Measurement of mechanical properties ultra-low load indentation", *Materials Science and Engineering A*, Vol.253, pp. 151-159.

Pharr, G.M., Harding, D.S. & Oliver, W.C. (1993) "In: Nastasi, M., Parkin, D. M. and Gleiter, H., (ed.); Mechanical properties and deformation behavior of materials having ultra-fine microstructures", *Netherland: Kluwer Academic Press*, pp. 449-461.

Prevorsek, D.C.; Know, Y.D. & Chin, H.B. (1994) "Analysis of the temperature rise in the projectile and extended chain polyethylene fiber composite armor during ballistic impact and penetration", *Polymer Eng. Sci.*, Vol.34, pp. 141.

Pöllänen, M.; Suihkonen, R.; Nevalainen, K.; Koistinen, A.P.; Suvanto, M.; Vuorinen, J. & Pakkanen, T.T. (2013) "Morphological, mechanical, tribological, and thermal expansion properties of organoclay reinforced polyethylene composites", *Polymer Engineering & Science*, Vol.53, pp.1279-1286.

Qian, D.; Dickey, E.C.; Andrews, R. & Rantell, T. (2000) "Load transfer and deformation mechanisms in carbon nanotube– polystyrene composites", *Appl. Phys. Letter*, Vol.76, pp.2868.

Qian, D.; Liu, WK. & Ruoff, RS. (2003) "Load transfer mechanism in carbon nanotube ropes", *Composite Science and Technology*, Vol.63, pp. 1561.

Qian, D.; Wagner, G.J.; Liu, W.K.; Yu, M.F. & Ruoff, R.S. (2002) "Mechanics of carbon nanotubes", *Appl. Mech. Rev.*, Vol.55, pp. 495–533.

Rahmat, M. & Hubert, P. (2011) "Carbon nanotube-polymer interactions in nanocomposites: a review", *Composites Science and Technology*, Vol.72, pp. 72-84.

Ramanathan, M.; Seth B. & Darling, M.S. (2011) "Mesoscale morphologies in polymer thin films", *Progress in Polymer Science*, Vol.36, pp. 793–812.

Ranade, A.; Nayak, K.; Fairbrother, D. & D'Souza, N. (2005) "Maleated and non-maleated polyethylene–montmorillonite layered silicate blown films: creep, dispersion and crystallinity", *Polymer*, Vol.46, pp. 7323–7333.

Randall, N. X. & Consiglio, R. (2000) "Nanoscratch tester for thin film mechanical properties characterization", *Rev. Sci. Instrum.*, Vol.71, pp. 2796.

Randall, N.X & Julia-Schmutz, C. (1998) "Evolution of contact area and pile-up during the nanoindentation of soft coating on hard substrates", *J. Material Res.*, Vol.13, pp. 21-26.

Ray, S.S. & Okamoto, M. (2003) "Polymer/layered silicate nanocomposites: a review from preparation to processing", *Prog. Polym. Sci.*, Vol.28, pp. 1539–1641.

Ren, P.G.; Di, Y.Y.; Zhang, Q.; Li, L.; Pang, H. & Li, Z.M. (2012) "Composites of ultrahigh-molecular-weight polyethylene with graphene sheets and/or MWCNTs with segregated network structure: Sreparation and properties", *Macromolecular Materials and Engineering*, Vol.297, pp.437-443.

Richeton, J.; Schlatter, G.; Vecchio, K.S. Re´mond, Y. & Ahzi, S. (2005) "A unified model for stiffness modulus of amorphous polymers across transition temperatures and strain rates", *Polymer*, Vol.46, pp.194-201.

Rittel, D. (1999) “On the conversion of plastic work to heat during high strain rate deformation of glassy polymer”, *Mechanics of Materials*, Vol.31, pp. 131-139.

Robenson, L.M. (2007) “Polymer blends: A comprehensive review”, USA: Hanser Gardner Publication Inc., pp. 1-7.

Sabic, Saudi Arabia, (2010), http://www.sabic.com.

Sahebian, S.; Zebarjad, S.; Sajjadi, S.; Sherafat, Z. & Lazzeri, A. (2007) *J. Appl. Polym. Sci.*, Vol.104, pp.3688

Saito, R.; Dresselhaus, G. & Dresselhaus, M.S. (1998) “Physical properties of carbon nanotubes”, Imperial College Press.

Schmidt, D.; Shah, D. & Giannelis, E.P. (2002) “New advances in polymer/layered silicate nanocomposites”, *Current Opinions in Solid State and Materials Science*, Vol.6, pp. 205-212.

Schwaiger, R.; Moser, B.; Dao, M.; Chollacoop, N. & Suresh, S. (2003) “Some critical experiments on the strain-rate sensitivity of nanocrystalline nickel”, *Acta materialia.*, Vol.51, PP. 5159-5172.

Seguela, R. & Darras, O. (1994) “Phenomenological aspects of the double yield of polyethylene and related copolymers under tensile loading”, *J. Mater. Sci*., Vol.29, pp.5342-5352.

Seguela, R. & Rietsch, F. (1990) “Double yield point in polyethylene under tensile loading”, *J. Mater. Sci. Letter*, Vol.9, pp.46-47.

Seltzer, R.; Kimb, J.K. & Mai, Y.W. (2011) “Elevated temperature nanoindentation behaviour of polyamide 6”, *Polymer International*, Vol.60, pp. 1753-1761.

Serban, D.A.; Weber, G.; Marsavina, L.; Silberschmidt, V.V. & Hufenbach, W. (2013) “Tensile properties of semi-crystalline thermoplastic polymers: Effects of temperature and strain rates”, *Polymer Testing*, Vol.32, pp.413–425.

Shames, I. H. & Cozzarelli, F. A. (1997) “Elastic and Inelastic Stress Analysis, UK: Taylor & Francis Ltd.

Shan, G.F.; Yang, W.; Yang, M.; Xie, B.; Feng, J. & Fu, Q. (2007) “Effect of temperature and strain rate on the tensile deformation of polyamide 6”, *Polymer*, Vol.48, pp.2958-2968.

Shen, L.; Phang, I.Y.; Liu, T. & Zeng, K. (2004) “Nanoindentation and morphological studies on nylon 66/organoclay nanocomposites: II. Effect of strain rate”, *Polymer*, Vol.45, pp. 8221–8229.

Shen, L.; Phang, I.Y; Chen, L.; Liu, T. & Zeng, K. (2004) “Nanoindentation and morphological studies on nylon 66 nanocomposites. I. Effect of clay loading”, *Polymer*, Vol.45, pp. 3341–3349.

Shen, L.; Tjiu, W.C. & Liu, T. (2005) “Nanoindentation and morphological studieson injection-molded nylon-6 nanocomposites”, *Polymer*, Vol.46, pp. 11969-11977.

Shen, Y.; Harkin-Jones, E.; Hornsby, P.; McNally, T. & Abu-Zurayk, R. (2011) “The effect of temperature and strain rate on the deformation behaviour, structure development and properties of biaxially stretched PET–clay nanocomposites”, *Composites Science and Technology*, Vol.71, pp. 758–764.

Shokrieh, M.M.; Hosseinkhani, M.R.; Naimi-Jamal, M.R. & Tourani, H. (2013) “Nanoindentation and nanoscratch investigations on graphene-based Nanocomposites”, *Polymer Testing*, Vol.32, pp. 45–51.

Sigma-Aldrich, UK, (2010), www.sigmaaldrich.com.

Singh, S. P.; Smith, J. F. & Singh, R. P. (2008) “Characterization of the damping behavior of a nanoindentation instrument for carrying out dynamic experiments”, *Experimental Mechanics*, Vol.48, pp. 571–583.

Sneddon, I. N. (1965) “The relation between load and penetration in the axisymmetric boussinesq problem for a punch of arbitrary profile”, *Int. J. Eng. Sci.*, Vol.3, pp. 47-57.

Song, M.; Cai, D. & Jin, J. (2010) “Loaded polymer”, *WIPO*, PTC/GB2010/106358.

Sreekanth, P.S.R. & Kanagaraj, S. (2013) “Assessment of bulk and surface properties of medical grade UHMWPE based nanocomposites using Nanoindentation and microtensile testing”, *Journal of the Mechanical Behavior of Biomedical Materials*, Vol.18, pp. 140-151.

Stoeffler, K.; Lafleur, P.G.; Florence, P.S.; Bureau, M.N. & Denault, (2011) “Micro-mechanisms of deformation in polyethylene/clay micro- and nanocomposites”, *J. Composites: part A*, Vol.42, pp.916-927.

Strojny, A. & Gerberich, W. W. (1998) “Experimental analysis of viscoelastic behavior in nanoindentation”, *Materials Research Society*, Vol.522, pp. 660–668.

Strojny, A.; Xia, X.; Tsou, A. & Gerberich, W. W. (1998) “Techniques and considerations for nanoindentation measurements of polymer thin film constitutive properties”, *J. Adhes. Sci. Technol.*, Vol.12, pp. 1299-1321.

Sui, G.; Zhong, W.H.; Ren, X.; Wang, X.Q. & Yang, X.P. (2009) “Structure, mechanical properties and friction behavior of UHMWPE/HDPE/carbon nanofibers”, *Materials Chemistry and Physics*, Vol.115, pp. 404–412.

Sun, J.; Francis, L.F. & Gerberich, W.W. (2005) “Mechanical properties of polymer-ceramic nanocomposite coatings by depth-sensing indentation”, *Polymer Engineering and Science: Society of Plastics Engineers*.

Swallowe, G.M. (1999) “Mechanical properties and testing of polymers”, Dordrecht, The Netherlands: Kluwer Academic Publisher.

Tang, C.; Xie, X.; Wu, X.; Li, R. & Mai, Y. (2002) “Enhanced wear performance of ultra high molecular weight polyethylene crosslinked by organosilane”, *J. Mater Sci: Mater Med.*, Vol.13, pp.1065-1069.

Tang, W.; Santare, M.H. & Advani, S.G. (2003) “Melt processing and mechanical property characterization of multi-walled carbon nanotube/high density polyethylene (MWNT/HDPE) composite films”, *Carbon*, Vol.41, pp. 79–85.

Tang, X-G; Hou, M.; Zou, J.; Truss, R.; Zhu, Z. (2012) “The creep behaviour of poly (vinylidene fluoride)/‘‘bud-branched’’ nanotubes nanocomposites”, *Composites Science and Technology*, Vol.72, pp. 1656–1664.

Tehrani, M., Safdari, M. & Al-Haik, M. S. (2011) “Nanocharacterization of creep behavior of multiwall carbon nanotubes/epoxy nanocomposite”, *International Journal of Plasticity*, Vol.27, pp.887-901.

Thomas, C.; Ferreiro, V.; Coulon, G. & Seguela, R. (2007) “In situ AFM investigation of crazing in polybutene spherulites under tensile drawing”, *Polymer*, Vol.48, pp.6041-6048.

Thomas, C.; Seguela, R.; Detrez, F.; Miri, V. & Vanmansart, C. (2009) “Plastic deformation of spherulitic semi-crystalline polymers: An in situ AFM study of polybutene under tensile drawing”, *Polymer*, Vol.50, pp.3714-3723.

Thomas, E.T. (2007) “Introduction to nanocomposite materials: properties, processing, characterization”, USA: DES tech publications Inc.

Thomas, S.; Kuruvilla, J.; Malhotra, S.K.; Koichi, G. & Sreekala, M.S. (2012) *Polymer composites: macro and microcomposites*, Vol.1, USA: Wiley-VCH.

Thostenson, E.T. & Chew, T.W. (2002) “Aligned multi-walled carbon nanotubes reinforced composite: processing and mechanical characterization”, *Journal of physics D – applied physics*, Vol.35, pp. L77-L80.

Tjong, S. C. (2006) “Structural and mechanical properties of polymer nanocomposites”, *Materials Science & Engineering R-Reports*, Vol.53, pp.73–197.

Tjong, S.C.; Meng, Y.Z. & Xu, Y. (2002) “Structure and properties of polyamide 6/vermiculite nanocomposites prepared by direct melt compounding”, *J. Polym. Sci. Part B: Polym. Phys.*, Vol.40, pp. 2860-2870.

Todorov, L.; Martins, C. & Viana, J. (2009) “Characterization of PET nanocomposites with different nanofillers”, *Solid State Phenomena*, Vol.151, pp. 113-117.

Tulsyan, K.; Toshniwal, S.; Dorairaju, G.; Schmidt, D.F. & Reynaud, E. (2010) “Thermomechanical assessment of plastic deformation in model amorphous polyamide/clay nanocomposites”, *Journal of Nanomaterials*, dio: 10.1155 /2010 /679786.

Valdes, S.S.; Vargas, E.R.; Valle, L.F.R.; Nonell, J.M.; Colunga, J.G.M.; Villarreal, M.H.G.; Quintanilla, M.L.; Adame, M.S. & Garcia, D.M. (2013) “Effect of functionalized polyethylenes on clay dispersion in high density polyethylene nanocomposites”, *Polym. Bull.*, Vol.70, pp. 535-547.

VanLandingham, M. R.; Villarrubia, J. S.; Guthrie, W. F. & Meyers, G. F. (2001) “Nanoindentation of polymers: An overview”, *Macromolecular Symposia*, Vol.167, pp. 15-44.

Verker, R.; Atar, N.; Quero, F.; Eichhorn, S.J & Grossman, E. (2013) "Tensile stress effect on the macromolecular orientation and erosion mechanism of an atomic oxygen irradiated polyimide", *Polymer Degradation and Stability*, Vol.98, pp. 997-1005.

Vlasveld, D.P.N.; Bersee, H.E.N. & Picken, S.J. (2005) "Creep and physical aging behaviour of PA6 nanocomposites", *Polymer*, Vol.46, pp.12539–12545.

Wang, Z.; Zhou, Y. & Mallick, P. (2002) "Effects of temperature and strain rate on the tensile behavior of short fiber reinforced polyamide-6", *Polymer Composites*, Vol.23, pp.58-71.

Wang, M.; Liao, Y. & Chen, D. (2010) "Study of the necking phenomenon in fiber drawing by infrared thermography", *Polymer Testing*, Vol.29, pp. 674–678.

Wang, M.; Liao, Y. & Chen, D. (2013) "Determination of linear thermal expansion coefficient of polymeric materials by infrared thermography", *Polymer Testing*, Vol.32, pp. 175–178.

Wang, Z.; Gua, P. & Zhang, Z. (2010) "Indentation and scratch behavior of nano-SiO2/polycarbonate composite coating at the micro/nano-scale", *Wear*, Vol.269, pp. 21–25.

Ward, IM. (1983) "Mechanical properties of solid polymers", Weinheim: John Wiley and Sons Ltd.

Ward, I.M. & Sweeney, J. (2004) "An introduction to the mechanical properties of solid polymers, 2nd edition, England: John Wily & Sons Ltd.

Westby, M.D. & Backman, C.L. (2010) "Patient and health professional views on rehabilitation practices and outcomes following total hip and knee arthroplasty for osteoarthritis: a focus group study", *BMC Health Service Res.*, Vol.10, pp.119

White, C.; Vanlandingham, M.; Drzal, P.; Chang, N. & Chang, S. (2005) "Viscoelastic characterization of polymers using instrumented indentation. II. Dynamic testing", *J. Polymer Sci. B: Polymer Phys*, Vol.43, pp.1812–1824.

Wignall, G. D. Alamo, R. G. ; Londono, J. D. ; Mandelkern, L. ; Kim, M. H. ; Lin, J. S. & Brown, G. M. (2000) "Morphology of blends of linear and short-chain branched polyethylenes in the solid state by small-angle neutron and X-ray scattering, differential scanning calorimetry, and transmission electron microscopy", *Macromolecules*, Vol.33, pp. 551-561.

Wignall, G.D.; Londono, J.D.; Lin, J.S.; Alamo, R.G.; Galante, M.J. & Mandelkern, L. (1995) "Morphology of blends of linear and long-chain-branched polyethylenes in the solid state: A study by SANS, SAXS, and DSC", *Macromolecules*, Vol.28, pp.3156-3167.

Wood, W.; Li, B. & Zhong, W. (2010) "Influence of phase morphology on the sliding wear of polyethylene blends filled with carbon nanofibers", *Polymer Engineering & Science*, Vol.50, pp. 613-623.

Wu, C.; Zhang, M.; Rong, M. & Friedrich, K. (2002) *Composite Sci. and Technology*, Vol.62, pp. 1327.

Xianzhong, X. & Jinping, H. (2011) "A stress relaxation model for the viscoelastic solids based on the steady-state creep equation", *Mech. Time-Depend Mater.*, Vol.15, pp. 29–39.

Xu, Y.; Ray, G. & Abdel-Magid, B. (2006) "Thermal behavior of single-walled carbon nanotube polymer–matrix composites", *Compos. Part A: Appl. Sci. Manuf*., Vol.37, pp.114.

Xu, S. & Tangpong, X. (2013) "Review: tribological behaviour of polyethylene-based nanocomposites", *Journal of Material Science*, Vol.48, pp. 578-597.

Xue, Y.; Wu, W.; Jacobs, O. & Schädel, B. (2006) "Tribological behaviour of UHMWPE/HDPE blends reinforced with multi-wall carbon nanotubes", *Polymer Test*ing, Vol.25, pp. 221-229.

Yang, B.; Riester, L. & Nieh, T. G. (2006) "Strain hardening and recovery in a bulk metallic glass under nanoindentation", *Scr. Mater.*, Vol.54, pp. 1277-1280.

Yang, H.; Chen, Y.; Liu, Y.; Cai, W.S. & Li, Z.S. (2007) "Molecular dynamics simulation of polyethylene on single wall carbon nanotube", *The Journal of Chemical Physics,* Vol.127, pp. 094902.

Yang, J.; Zhang, Z.; Friedrich, K. & Schlarb, A. (2007) "Creep resistant polymer nanocomposites reinforced with multiwalled carbon nanotubes*", Macromol. Rapid Commun.*, Vol.28, pp. 955–961.

Yang, J-L.; Zhang, Z.; Schlarb, A.K. & Friedrich, K. (2006) "On the characterization of tensile creep resistance of polyamide 66 nanocomposites. Part II: Modeling and prediction of long-term performance", *Polymer*, Vol.47, pp. 6745-6758.

Yang, S.; Zhang, Y. W. & Zeng, K. (2004) "Analysis of nanoindentation creep for polymeric materials", *J. Appl. Phys.*, Vol.95, pp. 3655-3666.

Young, R.J.; Bowden, P.B.; Ritchie, J. & Rider, J.G. (1973) "Deformation mechanisms in oriented high-density polyethylene", *J. of Mater. Sci.*, Vol.8, pp. 23–36.

Yu M-F; Yakobson, B.I. and Ruoff, R.S. (2000) "Controlled sliding and pullout of nested shells in individual multiwalled carbon nanotubes", *J. Phys. Chem. B*, Vol.104, pp 8764.

Yuan, Q.; Bateman, S.A. & Dongyang, W. (2010) "Mechanical and conductive properties of carbon black-filled high-density polyethylene, low-density polyethylene, and linear low-density polyethylene", *Journal of Thermoplastic Composite Materials*, Vol.23, pp. 459-471.

Yuen, S-M; Ma, C-C M.; Wu, H-H.; Kuan,H-C; Chen, W-J; Liao, S-H.; Chia-Wen Hsu, C-W. & Wu, H-L. (2007) "Preparation and thermal, electrical, and morphological properties of multiwalled carbon nanotube and epoxy composites", *J. Appl. Polym. Sci.*, Vol.103, pp.1272.

Yusoh, K.; Jin, J. & Song, M. (2010) "Subsurface mechanical properties of polyurethane/organoclay nanocomposite thin films studied by nanoindentation", *Progress in Organic Coatings*, Vol.67, pp. 220-224.

Zhang, Z.; Jing-Lei Yang & Friedrich, K. (2004) "Creep resistant polymeric nanocomposites", *Polymer*, Vol.45, pp. 3481–3485.

Zhang, Z.; Yang, J.L. & Friedrich, K. (2004) "Creep resistant polymeric nanocomposites", *Polymer*, Vol.45, pp. 3481-3485.

Zheng, Q.; Xue, Q.; Yan, K.; Hao, L.; Li, Q. & Gao, X. (2007) "Investigation of molecular interactions between SWNT and polyethylene/polypropylene /polystyrene /polyaniline molecules", *J. Phys. Chem. C*, Vol.111, pp. 4628–4635.

Zhenhua, L. & Yunxuan, L. (2012) "Mechanical and tribological behaviour of UHMWPE/HDPE blends reinforced with SBS", *Polymer-Plastic Tech. & Eng.*, Vol.51, pp. 750-753.

Zhou, T.H.; Ruan, W.H.; Yang, J.L.; Rong, M.Z.; Zhang, M.Q. & Zhang, Z. (2007) "A novel route for improving creep resistance of polymers using nanoparticles", *Composites Science and Technology*, Vol.67, pp. 2297–2302.

Zois, H.; Apekis L. & Omastova M. (2001) "Electrical Properties of Carbon Black-filled Polymer Composites", *Macromolecular Symposia*, Vol.170, pp. 249–256.

Zoo, Y.S.; An, J.W.; Lim, D.P. & Lim, D.S. (2004) "Effect of Carbon Nanotube Addition on Tribological Behavior of UHMWPE", *Tribology Letters*, Vol.16, pp. 305-309.